Molecular determinants of morphology and function of microvilliated sensory cells in zebrafish

Laura Desban

Sorbonne Université

Ecole doctorale « Cerveau, Cognition, Comportement »

Thèse de doctorat de Neurosciences intitulée

Molecular determinants of morphology and function of microvilliated sensory cells in zebrafish

réalisée à l'Institut du Cerveau et de la Moelle épinière

par **Laura Desban**

et dirigée par Pierre-Luc Bardet & Claire Wyart

Présentée et soutenue publiquement le 06 septembre 2018 devant un jury composé de :

Rapportrice	Katie KINDT, acting chief (NIH/Bethesda)
Rapportrice	Nadine PEYRIERAS, DR (UPMC/Paris)
Examinatrice	Juliette AZIMZADEH, CR (Univ. Paris-Diderot/Paris)
Examinateur	Georges DEBREGEAS, DR (UPMC/Paris)
Examinateur	Nicolas MICHALSKI, CR (Pasteur/Paris)
Examinatrice	Vanessa RIBES, CR (Univ. Paris-Diderot/Paris)
Directrice de thèse	Claire WYART, CR (UPMC/Paris)
Encadrant	Pierre-Luc BARDET, CMU (UPMC/Paris)

ACKNOWLEDGMENTS

Allons bon, nous y voilà! La concrétisation de 4 années d'investissement, de moments de doutes sur fonds d'opiniâtreté, de sueurs cérébrales dans l'accomplissement (n'ayons pas peur des grands mots), mais surtout, il faut le dire, de rencontres et d'amitiés qui ont jalonné ce parcours et sont venues lui donner cette teinte tellement plus chaleureuse. J'espère rendre ici justice à tous ceux qui m'ont accompagnée et soutenue lors de cette aventure aussi bien scientifique qu'humaine – et peut-être, finalement, bien plus humaine que scientifique, si on y regarde de plus près.

First, I wish to express my sincerest gratitude to the members of my committee who accepted, even though it probably took a chunk away from their summer time, to read this manuscript. Special thanks to Nadine and Katie who (truly) had to read it and write a report for the doctoral school. Nadine, I am very glad we managed to make it on time and am ready to discuss evolution of sensory cells. Katie, thank you for crossing the ocean for my defense; it was my pleasure to make it happen and to share with you about hair cells. Thank you Nicolas for your patience and being so understanding but, more importantly, for your – always positive and useful - feedbacks at different times during the past year. Thank you Georges, Juliette and Vanessa to kindly agree to join the committee and evaluate this work. I should not forget Céline Revenu and Corinne Houart, who were part of my thesis advisory committee and provided insightful criticism all along my PhD and, thus, contributed to its achievement.

C'est ici, je pense, qu'il me faut remercier les principaux moteurs de cette thèse, qui l'ont rendue possible et l'ont modelée, orientée jusqu'à ce qu'elle prenne le chemin qui nous amène tous ici aujourd'hui. Claire, tout d'abord. Merci d'avoir considéré ma demande, il y a déjà 5 ans de cela ; je me souviens encore de ta réponse rapide et positive, suivie de plusieurs semaines sans réussir à se parler de vive voix. A pattern here, maybe ? J'ai appris depuis ton dévouement pour ton équipe, et cette énergie débordante qui t'es propre et que tu lui dédies. Travailler à tes côté et au sein de ton équipe est riche d'enseignements et d'inspiration même si, il faut le dire, pas de tout repos. Pierre-Luc, maintenant. Ce fût finalement le timing parfait : c'est grâce à ton arrivée dans l'équipe

que j'y ai aussi trouvé une place (ne parlons pas du timing de cette thèse qui a l'ingéniosité de s'inscrire juste entre tes deux enfants ^^). Ici, je me souviens comment nous avons découvert, ensemble, les us et coutumes scientifiques locales (ce qui a indéniablement contribué à mon intégration), de nos entretiens (plus ou moins) philosophiques (dont j'ai souvent battu en retraite), de ton écoute et de ton calme olympien qui m'ont souvent permis de me remettre sur les rails. Et je ne peux, bien sûr, pas oublier de mentionner tous ces débats et questions très 'Pierre-Luc' : le fameux 'But, what is a cell type, really ?' ou encore 'What is a sensory cell ?' au début de l'écriture de la thèse qui, je pense, resteront gravés. Je suis fière d'avoir été ta première étudiante en thèse et d'avoir mené ce projet avec toi. Merci.

Cette aventure n'aurait pas été celle qu'elle a été sans l'ensemble de la team Wyart. To the first generation: of course I miss you guys and it was difficult to see you all leave. I find myself very lucky to keep in touch and see some of you sometimes. Kévin, keep the spirit, I hope to see you in Survivor one day! Kris, I can't wait for next GoT season but, in the mean time, I just enjoy very much every special lunch together whenever you are around. Jenna, welcome to the RNAseq world, you're going to love it! Urs, I am still taking care of the plants you left me and, also, I think it was good for our friendship you didn't witness me go through the entire 2P experiment – it was quite a mess. Lydia, do not change a thing! Maybe you can show me Costco sometime? Andy, you and I are the last ones left here: thank you for being such an awesome FACS buddy (please, publish the RNAseq!) and going on adventures in Paris with me (even if it's just for food). To the new generation, thank you all for making this past year so pleasant, even though it was the last of my PhD. Yasmine, merci pour ton soutien et ta gentillesse à toutes épreuves (et promis, je n'essaie pas de t'acheter à coups de cakes au citron et de fraises séchées !). Olivier, mais qui va te remplacer ? Tu désertes le coin des ex-normaliens handballeurs ! Tes idées sorties de nulle part (comme ce FAFS, le FACS pour poisson) et ta disponibilité peu importe le moment où mon besoin de pause / de parler se présentait vont assurément me manquer ! Adna, you're always such a positive person, you almost made me think that the 2P was not this horrible beast hidden in its cold dark cave (but really, it is). Martin, thank you for keeping the good – entirely home-made - food coming (and you know how much food is important to me). MingYue, we really need to talk some Chinese before I leave (and after I re-listen to my classes). Feng, nos projets ne se recoupent pas beaucoup mais ton aide est toujours précieuse, notamment quand il s'agit de disséquer du poisson

zèbre adulte ou d'*in situ*. Hugo, merci d'avoir coordonné avec brio cet effort avec l'atelier pour nous fournir en matériel pour le set-up de comportement (et aussi, merci de supporter tous mes soupirs au travers du panneau entre nos deux bureaux ^^). Adeline, grâce à toi, j'apprends sans cesse à clarifier la présentation de mes résultats mais aussi le langage marseillais (j'espère pouvoir le ressortir !). Julian, je sais que les manips de 'puff' étaient pénibles mais, quand même, on a écouté de la bonne musique, non ? Fanny, tu caches bien ton jeu (de rugbywoman) ! Je ne sais comment te remercier d'avoir accepté de m'aider sur le génotypage – complètement démesuré – de mes mutants en début d'année ! Et enfin, Yezza, ton arrivée au labo a apporté un nouveau souffle de communauté ; merci de toutes tes attentions et de ce délicieux thé à la menthe mais, surtout, merci de ta patience dans la gestion de l'équipe.

Ces quatre années n'auraient pas été les mêmes sans le soutien extérieur, bien sûr. Un grand merci à tous les amis cachanais, en particulier Alice, Flo, Cath, Guigui, Cam et Margotte. Que de soirées et d'anecdotes ! Nos chemins se sont peut-être séparés mais nous avons construit là un petit noyau qui, je le crois, est assez solide et tiendra dans le temps. Un merci tout particulier à Maëlle : j'ai hâte de rencontrer la sangsue ! Et, enfin, un grand merci à Elise qui doit savoir combien nos dîners du mardi soir, faits de bric et de broc, ainsi que nos conversations jusque tard dans la nuit, me manquent. Merci aux vieux de la vieille, aussi (oui, oui, plus vieux que les cachanais). Pauline, ma vie n'aurait jamais été aussi cultivée sans toi (je crains ne pas t'avoir rendu la pareille avec la culture scientifique malheureusement) et, quand même, 'on se connait depuis plus de la moitié de nos vies maintenant', ce qui est peu dire. Merci aussi à Marie-Claire – ses questions existentielles - et Gwen – longue vie aux licornes !, les deux rescapées du lycée et de la prépa.

Je finirai ici par remercier ma famille chaudement. Je ne vous exprime que rarement mon affection mais je ne serai pas ici sans vous aujourd'hui. Vous ne m'avez jamais laissé croire que je devais me limiter ni que quoi que ce soit m'était impossible. Tout le long, et encore plus loin, je sais que vous êtes là pour moi. Merci. C'est mon regret de ne pas l'avoir plus exprimé aux personnes qui m'ont quittée trop tôt.

‘C’était pour éviter de douter que nous avions renoncé à penser’

Au plaisir de Dieu, Jean D’Ormesson

Sensory systems use specialized receptor cells, many of which detect sensory cues through specialized apical membrane protrusions, such as microvilli. The final shape of the microvilliated apical extension requires specific molecular machinery and determines many of the properties of sensory transduction. The establishment of this structure remains however elusive. What molecular factors orchestrate the initiation and elongation of actin filaments in microvilliated sensory cells (MSCs)? Can we find key elements of morphogenesis common to MSCs? What is the precise role of microvilli structure in sensory function?

I investigated two sensory cell types harboring microvilli: spinal cerebrospinal fluid-contacting neurons (CSF-cNs) and neuromast hair cells (nHCs). The primary goal was to unravel the molecular mechanisms underlying morphogenesis of MSCs by focusing on CSF-cNs. I was able to describe critical steps leading to the development of CSF-cN apical extension. My participation to the transcriptome analysis of CSF-cNs revealed candidate molecular factors associated with each of these steps. I demonstrated the importance of the interaction between Espin and Myo3b to ensure the proper lengthening of CSF-cN apical extension. In this system, I established a direct link between morphology and function by showing that shorter apical extensions lead to reduced sensory response. Altogether, my work shed light on the formation of CSF-cN sensory organelle and its functional role. In parallel, the establishment of the nHC transcriptome dataset revealed similar morphogenetic factors with CSF-cNs, supporting the idea that all MSCs share conserved features for their differentiation.

La détection des stimuli sensoriels est assurée par des cellules réceptrices spécialisées, souvent grâce à des protrusions membranaires apicales telles que les microvillosités. La forme finale des extensions apicales microvilliées conditionne de nombreuses propriétés de la transduction sensorielle mais leur formation reste méconnue. Quels sont les facteurs moléculaires responsables de l'initiation et de l'élongation des filaments d'actine chez les cellules sensorielles microvilliées (CSMs) ? Peut-on décrire des éléments clés de la morphogenèse en commun ? Quel est le rôle structural des microvillosités dans la fonction sensorielle ?

J'ai étudié deux types sensoriels microvilliés : les neurones contactant le liquide cérébrospinal (NcLCS) et les cellules sensorielles des neuromastes (CSn). Mon projet visait à investiguer les mécanismes moléculaires sous-jacents à la morphogenèse des CSMs par l'étude des NcLCS. J'ai décrit les étapes critiques menant à la formation de l'extension apicale des NcLCS auxquelles j'ai pu associer des candidats potentiels grâce à l'analyse transcriptomique de ces cellules. J'ai démontré le rôle critique de l'interaction entre Espin et Myo3b dans l'élongation de l'extension apicale des NcLCS et j'ai établi un lien direct entre structure et fonction en montrant que le raccourcissement de l'extension apicale aboutissait à la réduction de la réponse sensorielle. Mon travail a permis d'apporter des éléments de réponse quant à la formation de l'organe sensoriel des NcLCS. L'analyse transcriptomique des CSn a par ailleurs révélé des facteurs de morphogenèse communs avec les NcLCS, suggérant que toutes les CSMs partagent des propriétés de différenciation conservées.

TABLE OF CONTENTS

LIST OF FIGURES

LIST OF TABLES

ABBREVIATIONS

ABP: actin-binding protein

AJ: adherens junction

AJC: apical junctional complex

BAIAP2 : brain-specific angiogenesis inhibitor 1-associated protein 2

CNS: central nervous system

CSF: cerebrospinal fluid

CSF-cN: CSF-contacting neuron

ERM: ezrin, radixin, moesin

FACS: fluorescent activated cell sorting

GPCR: G protein-coupled receptor

iHC: inner hair cell (of the inner ear)

nHC: neuromast hair cell

I-BAR: inverse Bin-amphipysin-Rvs167

IRSp53: insulin receptor tyrosine kinase substrate of 53 kDa

MSC: microvilliated sensory cell

vORN: vomeronasal olfactory receptor neuron

PCP: planar cell polarity

TJ: tight junction

bTJ: bicellular tight junction

tTJ: tricellular tight junction

TRC: taste receptor cell

VNO: vomeronasal organ

WASP: Wiskott-Aldrich Syndrom protein

WH2: WASP-homology 2

ZO: Zonula Occludens

CHAPTER 1: MORPHOLOGY AND FUNCTION OF MICROVILLIATED SENSORY CELLS

To ensure their survival and reproduction, living organisms constantly probe and sense their environment to gather information. From ancient times to present days, sensation has always been a source of fascination for philosophers, artists and scientists. In a first attempt of classification, the Greek philosopher Aristotle defined five senses (*De Anima* book): vision, audition, olfaction, taste and touch. Neurobiologists have since then extended and refined this classification by including a variety of modalities detecting internal parameters that are as critical for survival and bodily function. Together with the classic five senses, balance forms the 'exteroceptive senses' and provides information about the outside world. Their counterpart, the so-called 'interoceptive senses', provide information from within the body and commonly regroup somatic (proprioception, pain, temperature) and visceral sensations (Kandel *et al.*, 2013). Each modality relies on highly specialized sensory cells, sometimes located in dedicated sense organs, expressing receptors specific to the type of stimulus (Table 1). Sensory cells act as transducers capable of transforming the information into electrical signals that can then be interpreted by the central nervous system (CNS). In the light of this definition based on cellular specialization, a growing number of cells have been described as sensory and the list is probably still not exhaustive. Notably, a novel interoceptive modality has emerged, carried by spinal neurons contacting the cerebrospinal fluid (cerebrospinal fluid-contacting neurons or CSF-cNs) (Kolmer, 1921; Agduhr, 1922; Vigh and Vigh-Teichmann, 1973; Dale *et al.*, 1987). Recent studies provided evidence for these cells detecting chemical cues from the CSF (Orts-Del'Immagine *et al.*, 2012; Jalalvand *et al.*, 2016) and mechanical stimuli associated with spinal bending and CSF flow (Böhm *et al.*, 2016; Jalalvand *et al.*, 2016; Sternberg *et al.*, 2018) (see also Chapter 2, I.A).

Table 1 illustrates the fascinating diversity of sensory cells that is expressed at various levels – structural, molecular and sensory - making it difficult to assign functional groups. Each sensory system is dedicated to a specific set of tasks and employs specialized receptor cells, many of which detect chemical or mechanical stimuli through apical membrane protrusions, such as microvilli and/or cilia. When present, the shape of a specialized sensory compartment or organelle is admittedly instrumental to the sensory function and requires specific molecular machinery. Therefore, one way to classify sensory cells is to focus on their morphological appendices used to collect information (Table 1). Although scientists often relate to morphology to assume cell function and commonly associate apical extensions with sensory function, their structure and formation remain elusive. During my PhD, I investigated two sensory cell types harboring microvilli: CSF-cNs, interoceptive cells, and hair cells of the neuromasts (nHCs), specific exteroceptive cells developed by bony and cartilaginous fish. While tuned to distinct stimuli, CSF-cNs and nHCs share obvious morphological features with the elaboration of a microvilliated apical extension. I therefore asked whether we can

find common key molecular factors, underlying morphology of CSF-cNs and nHCs and I investigated the role of the microvilliated apical extension for the sensory function.

Cell type / *Organ*	Type	Stimulus	Modality	Sensory organelle	Organism
Rods, Cones / *Retina*	exteroceptive	light (photons)	vision	cilia	human / mouse / zebrafish
Hair cells					
- *Cochlea*	exteroceptive	sound (wave pressure)	audition	stereocilia (microvilli)	human / mouse / zebrafish
- *Vestibule*		gravity	balance		human / mouse / zebrafish
- *Semi-circular canals*		motion	balance		human / mouse
- *Neuromast*		water motion	distant touch		zebrafish
Taste receptor cells / *Taste buds*	exteroceptive	tastants	gustation	microvilli	human / mouse / zebrafish
Solitary chemosensory cells / *scattered*	exteroceptive	tastants / bacterial products	defense	microvilli	human / mouse / zebrafish
Olfactory receptor neurons (ORNs)					
- main ORNs / *Olfactory epithelium*	exteroceptive	odorants	olfaction	cilia	human / mouse / zebrafish*
- vomeronasal ORNs / *Vomeronasal organ*		pheromones		microvilli	human / mouse / zebrafish*
- crypt neurons / *Olfactory epithelium*		kin odorants		cilia & microvilli	zebrafish
- Kappe neurons / *Olfactory epithelium*		?		microvilli	zebrafish
Touch receptor cells / *Skin*					
- Merkel cells	exteroceptive	skin deformation	touch	microvilli	human / mouse / zebrafish
- Meissner's corpuscules				--	human / mouse
- Pacinian corpuscules				--	human / mouse
- Ruffini endings				--	human / mouse
- Rohon-beard neurons				--	zebrafish
Nociceptors / *scattered*	interoceptive	chemicals after damage	pain	--	human / mouse / zebrafish
Thermoreceptors / *Skin & Hypothalamus*	interoceptive	temperature		--	human / mouse / zebrafish
Proprioceptors / *Muscle spindles & Golgi tendons*	interoceptive	muscle tone	body posture	--	human / mouse
CSF-contacting neurons / *Ependyme*	interoceptive	CSF compounds, motion	locomotion	microvilli	human / mouse / zebrafish
Visceral receptors / *scattered*	interoceptive	diverse (osmolarity, pH, ...)	somatic	--	human / mouse / zebrafish

Table 1. Classification of sensory cell types
* In zebrafish, vomeronasal and main ORNs are found together in the olfactory epithelium.
In red: cells reviewed in this first chapter
Underlined: cells studied during the PhD in chapters 2 and 3

Searching the literature about microvilliated sensory cells (MSCs), I found many studies covering each cell type individually. Morphogenesis and sensory function of hair cells in the inner ear have been thoroughly investigated for example. Few reviews also offer a comparative study between two sensory cell types, but are restricted to specific questions such as sensory transduction. A general comparative review highlighting similarities and differences between MSCs is missing. In this first chapter, I will attempt to fill this gap, focusing on four conserved microvilliated cell types in Vertebrates: inner hair cells of the inner ear (iHCs), vomeronasal olfactory receptor neurons (vORNs), taste receptor cells (TRCs) and spinal CSF-cNs (Table 1). This is a non-exhaustive list, which, however, should provide a good illustration of the different existing MSCs since they often are highly related to one of these four cell types.

I. MICROVILLIATED SENSORY CELLS DETECT A VARIETY OF SENSORY CUES

A. Chemo- and mechano-sensory modalities in microvilliated sensory cells

Sensation starts with the reception by sensory cells of pieces of information about the external world or from within the body. The information, or stimulus, gathered by sensory cells can take various forms and needs to be processed into an interpretable

signal for the CNS. As a consequence, many attributes of sensation are defined by the type of stimulus considered.

Sound and iHCs. Sound is a purely mechanical phenomenon: it is a pressure wave that travels through space, allowing sensing at distance. In humans, the range of detection goes from 20 kHz (1.7 cm) to 20 Hz (17 m) assuming that sound is traveling through air at a sonic speed of 340 m/s. The amount of energy carried by acoustic units depends greatly on the vibrational frequency. For example, at 10 kHz, an acoustic wave has $3x10^{-6}$ cal/mol (Torre *et al.*, 1995; Yoshioka and Sakakibara, 2013). In addition to frequency, two other features of the acoustic stimulus are of importance: the amplitude, perceived as loudness, and phase, giving access to spatial information (Levine, 2006). One of the specificity of hearing lies in the fact that the quantal phonic energy is much lower than thermal noise, which implies that noise constitutes the main limitation to sound detection rather than quantization of the stimulus.

Pheromones and vORNs. Odorants are volatile chemicals that provide broad information about the external environment, notably predators, conspecifics and preys. Odorants usually need to be solubilized to reach the olfactory organs where lie ORNs. The binding energy of an odorant molecule is roughly estimated to be $3.9x10^{5}$ kcal/mol, much higher than thermal noise (Yoshioka and Sakakibara, 2013). Only a subset of ORNs is microvilliated (Miragall, Breipohl and Bhatnagar, 1979) and is specifically tuned to pheromones, a particular type of olfactory cues (Stowers and Kuo, 2015). Pheromones are specialized odors, of tremendous diversity, capable of inducing robust pre-set behaviors in conspecifics without prior experience. Pheromones play important roles in mating and social interactions (Karlson and Lüscher, 1959; Ferrero *et al.*, 2013; Haga-Yamanaka *et al.*, 2014; Kaur *et al.*, 2014). In rodents, the pheromone-tuned ORNs are mainly located in the vomeronasal organ (VNO) (Halpern, 1987), connected to the nasal cavity; in fish, the vomeronasal ORNs (vORNs) are located together with the 'classic' ORNs in the olfactory pit (Hansen and Zeiske, 1998; Hashiguchi and Nishida, 2006). In this work, we will only focus on vORNs since classic ORNs are not microvilliated but ciliated.

Tastants and TRCs. Gustatory stimuli, or tastants, are water-soluble chemical cues that mainly provide organisms with nutritional information about their environment. As the two main chemosensory exteroceptive systems, gustation and olfaction share common features. As in olfaction tuned to pheromones, taste has direct effects on specific behaviors such as hunting, feeding or autonomic responses. Furthermore, these senses enable the detection of a wide diversity of chemical cues, which makes the description of general basic principles of the stimulus more difficult. A certain agreement has however emerged about the existence of at least five primary taste sub-modalities: sweet, umami, sour, salty and bitter (Chaudhari and Roper, 2010; Roper and Chaudhari, 2017). Sweet, low concentration of Na^{+} and umami are attractants since they are

associated with respectively high caloric, salt and proteic content, all critical in terms of nutritional aspects. On the other hand, sour, bitter and high concentration of Na^+ are more commonly aversive stimuli because associated to poisonous or spoiled food. It is commonly thought that all tastes can be produced by a combination of these sub-modalities (Henning, 1916). Across gustative modalities, there is a strong distinction between the purely chemical sweet/umami/bitter tastes and the mineral salt/sour tastes, based on small ion detection whose underlying mechanisms are complex and not yet understood (see I.B) (Liman, Zhang and Montell, 2014).

The mixed case of CSF-cNs. Since their initial description almost a century ago (Kolmer, 1921; Agduhr, 1922), the morphology and position of CSF-cNs suggested that these cells may be sensory by probing CSF content (Agduhr, 1922; Vigh and Vigh-Teichmann, 1973) and/or being part of a novel mechanosensory organ in the spinal cord (Kolmer, 1921). The idea that CSF-cNs are chemically- and mechanically-tuned was recently supported by *in vitro* and *in vivo* studies. CSF-cNs were first shown to be sensitive to pH and osmolarity changes in the CSF (Huang *et al.*, 2006; Orts-Del'Immagine *et al.*, 2012; Böhm, 2016; Jalalvand *et al.*, 2016). More recently, CSF-cNs have been shown to respond to mechanical stimuli associated with tail bending movements in the zebrafish spinal cord (Böhm *et al.*, 2016) and CSF flow in lamprey (Jalalvand *et al.*, 2016) and zebrafish (Sternberg *et al.*, 2018). Overall, the work of the last decade indicates that CSF-cNs are polymodal interoceptive sensory neurons with evidence for both chemo- and mechano-sensory functions (Djenoune and Wyart, 2017) whose relevance for locomotion, spinal cord development and physiology is under investigation (Wyart *et al.*, 2009; Fidelin *et al.*, 2015; Böhm *et al.*, 2016; Hubbard *et al.*, 2016).

MSCs carry a diversity of sensory modalities classified into two main groups: chemo-sensory and mechano-sensory. One can assume that chemosensory MSCs will share common features compared to mechanosensory MSCs. For example, TRCs and vORNs, both carrying chemosensory modalities, can detect quantal amounts of energy because the binding of a chemical cue is energetically greater than thermal noise, in contrast to mechanosensory iHCs. CSF-cNs do not seem to fall in any of these two categories, and rather lie in between, showing both chemo- and mechano-properties, hence relating to TRCs/vORNs and iHCs altogether (Fig.1).

As other sensory cells types, MSCs act as transducers: they transform the information stimulus into a readable signal for the CNS. The transduction of a specific kind of information is enabled by the expression of specialized receptors that are capable of collecting the stimuli.

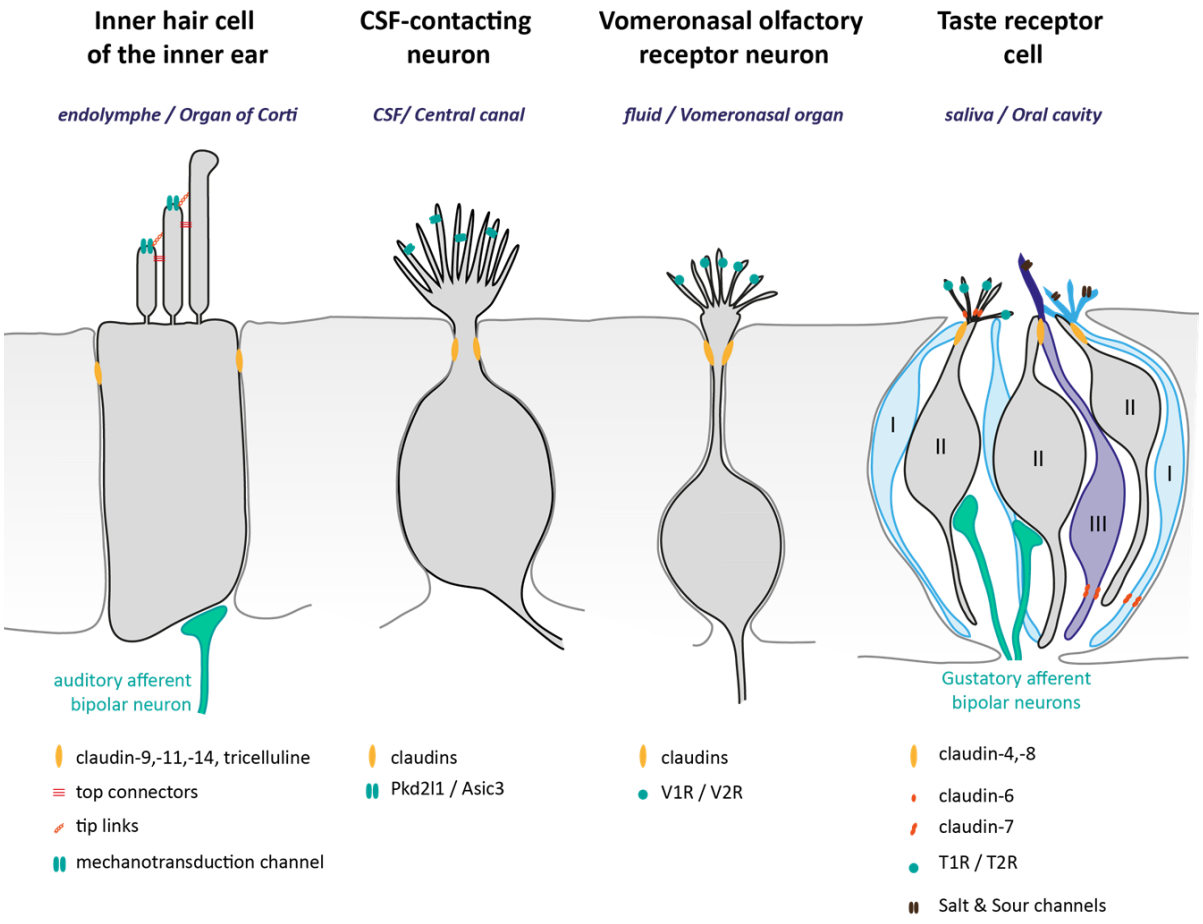

		Type	
mechanoreceptor	**mixed**	**chemoreceptor**	**chemoreceptor**
		Nature	
non neuronal	neuronal	neuronal	non neuronal
		Activation	
direct (ion channel)	unknown	indirect (GPCR)	indirect (GPCR)
		Actin-bundling factors	
espin fascin fimbrin/plastin	unknown	espin villin	espin villin fimbrin/plastin
		Microvilliated apical extension	
staircase pattern 50 – 450 microvilli l = 1.5–5.5 µm up to 900 filaments/bundle (chick, Tilney, Tilney and Derosier, 1992)	**no obvious organization** several microvilli l = 4 µm w = 114 nm (Xenopus, Dale *et al.*, 1987)	**no obvious organization** numerous microvilli l = 2 µm w = 40-100 nm (thin) (rat, Höfer et al, 2000)	**no obvious organization** Type I: l = 1-2 µm, w = 0.5-2 µm Type II: l = 1 µm, w = 0.25 µm Type III: blunt-ended thick tip (rabbit, Murray, 1986; necture Cummings, Delay and Roper, 1987)
		Projections	
brainstem	spinal motor circuits	hypothalamus	thalamus
		Physiological response & behavior	
communication	locomotion	aggression, parental behavior, reproduction, …	feeding, hunting, …

Figure 1. Morphological and functional properties of four microvilliated sensory cells
(adapted from different sources)
In the 'Microvilliated apical extension' section, l = length, and w = width.

B. Sensory transduction and generation of a receptor potential

Receptors and channels, expressed by sensory cells, determine the sensory specificity of the cell towards one type of stimulus or another. During sensory transduction, sensory cells use the information carried by stimuli to generate an electrical response, the means of communication of the CNS. The generation of an electrical signal involves the activation of a so-called transduction channel allowing flow of ion currents responsible for the membrane depolarization. Two molecular mechanisms for transduction are classically distinguished: direct and indirect activation of the transduction channel (Torre *et al.*, 1995). In the former, the transduction channel is *directly* activated and gated by the stimulus while, in the latter, the stimulus is initially detected by a receptor, commonly a G protein-coupled receptor (GCPR), which induces a cytoplasmic cascade with second messengers eventually leading to the activation of the transduction channel.

Direct activation – the case of the iHCs. As implied by its name, during direct activation, the stimulus directly induces the gating of ion channels, called transduction channels, responsible for the electrical signal. Exemplified by iHCs, direct activation implies the opening of mechanotransduction channels triggered by microvilli movements on a nanoscale generated by the acoustic waves. This modality allows fast gating, on a time scale of the microsecond, which is suited for the detection of auditory stimuli at high frequencies and to discriminate sound sources (Torre *et al.*, 1995; Frings, 2009). The molecular nature of the factors responsible for mechanotransduction in iHCs has long been sought in the field. Genetic studies of hereditary deafness in human patients (Michalski and Petit, 2015), and mutagenesis screens, like in zebrafish (Haffter *et al.*, 1997; Nicolson *et al.*, 1998), helped the identification of a panel of different factors involved in the mechanotransduction machinery of iHCs (Michalski and Petit, 2015; Zhao and Müller, 2015; Nicolson, 2017). Most of these factors are ultrastructural components, participating to the gating of the transduction channel, which we will discuss in the next section (see II.B). Four different proteins have been linked to the transduction channel so far: TMC1, TMC2 (Pan *et al.*, 2013), LHFPL5 (Xiong *et al.*, 2012) and TMIE (Zhao *et al.*, 2014) (Fig.2). For each of these proteins, loss of function results in affected signal transduction, which suggests an important role in mechanotransduction. Current evidence also suggests that the channel complex may contain additional, yet to be identified, components. Further studies are required to identify the pore-forming subunits of the mechanotransducer channel.

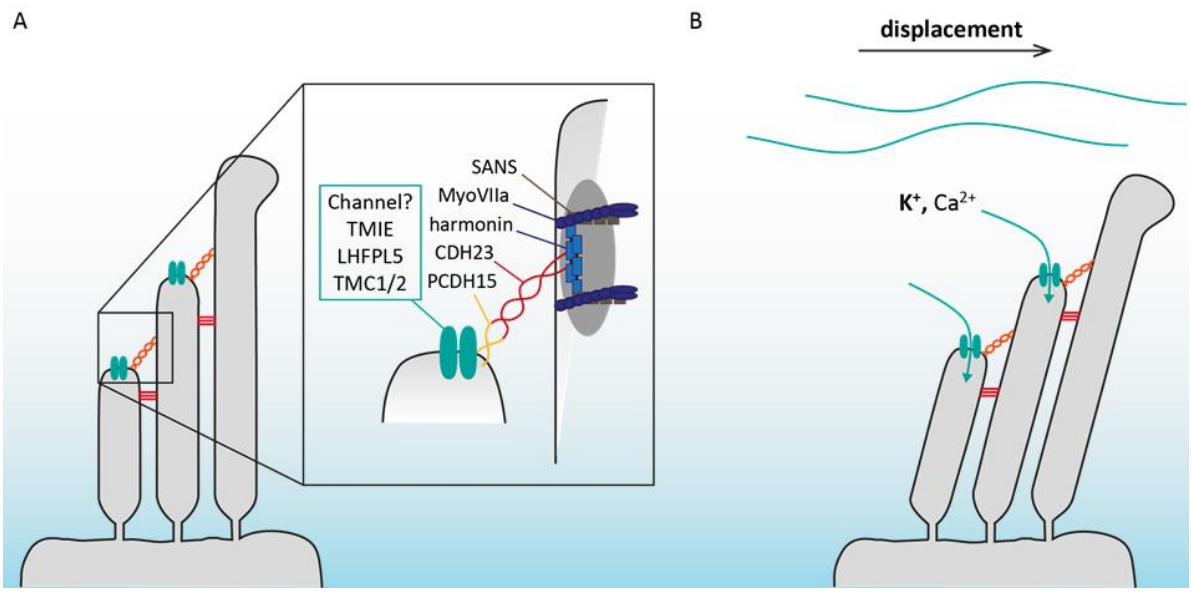

Figure 2. Elements of mechanotransduction in hair cells
(adapted from (Michalski and Petit, 2015; Zhao and Müller, 2015))
A, Current model of the tip-link complex involved in mechanotransduction. The tip link is constituted of homodimers of CDH23 and PCD15 and is anchored to the neighbour stereocilium membrane through the ternary complex formed by harmonin, Myosin-VIIa (MyoVIIa) and SANS. Although the molecular nature of the mechanotransduction channel remains elusive, TMC1 and TMC2 are strong candidates. The channel is thought to interact with the PCDH15 homodimer, hence the basal end of the tip link, through LHFPL5 and TMIE.
B, Illustration of the mechanotransduction induced in hair cells. Due to vibrations generated by incoming sound waves along the basilar membrane, shearing movement occurs between the basilar membrane and the tectorial membrane and stereocilia are displaced. Tension applies to tip links which opens mechanotransduction channels. This sequence of events results in the entry of K^+ from the K^+-rich endolymph surrounding stereocilia.

Indirect activation – chemical senses. In contrast to iHCs, vORNs and TRCs (in the case of umami, bitter and sweet) detect cues through membrane receptors, GPCRs (Mombaerts, 2004; Frings, 2009), which are associated with intracellular cascades of second messengers and subsequent activation of a transduction channel. The generation of second messengers constitutes an additional step, which inherently makes the transduction slower but leaves room for amplification and modulation of the signal and allows adaptation and desensitization to take place. In the case of the olfactory receptors specifically tuned to pheromones, two families were identified: V1R (Dulac and Axel, 1995; Pfister and Rodriguez, 2005) and V2R (Herrada and Dulac, 1997; Matsunami and Buck, 1997; Ryba and Tirindelli, 1997). Members of these two families bind ligands with high specificity and sensitivity (Leinders-Zufall *et al.*, 2000), and use the same amplification cascade going through phospholipase C to release second messengers - mainly IP_3, Ca^{2+} and diacylglycerol - to activate TRPC2, the transduction channel (Buck, 2000) (Fig.1). Similarly, two families of taste receptors were identified: T2Rs and T1Rs, which are expressed in distinct groups of TRCs (Chandrashekar *et al.*, 2006; Chaudhari and Roper, 2010; Matsumoto, Ohmoto and Abe, 2013). T2Rs were demonstrated to be involved in the detection of the aversive bitter tastants

(Chandrashekar *et al.*, 2000) while heterodimers of the T1R family were shown to be responsible for tasting sweet via T1R2/T1R3 (Nelson *et al.*, 2001; Zhao *et al.*, 2003) and umami via T1R1/T1R3 (Li *et al.*, 2002; Nelson *et al.*, 2002; Zhao *et al.*, 2003). Taste receptors share a common transduction pathway via PLCβ2 activation, IP_3 synthesis and Ca^{2+} release from intracellular stores, resulting in the gating of the transduction channel TRPM5 (Zhang *et al.*, 2003) (Fig.1,5). Note that transduction pathways induced by vORN activation share more similarities with taste transduction than with the canonical olfactory pathway from ORNs in the main olfactory epithelium. In fact, V1Rs and V2Rs are distantly related to respectively bitter (Dulac and Axel, 1995) and sweet taste receptors (Herrada and Dulac, 1997; Matsunami and Buck, 1997). Because chemosensory systems face a diversity of chemical compounds, they require a great repertoire of receptors to discriminate between molecules. In the case of taste, the current understanding describes the encoding as loosely conforming to a labeled line system. Taste sub-modalities are mainly detected by TRC populations, 'specialists', linked to specific behaviors (Liman, Zhang and Montell, 2014) but many TRCs are 'generalists' and can respond to stimuli of various kinds and intensities (Gilbertson *et al.*, 2001). The retrieval of the information still remains unclear but likely relies on pattern discrimination across activated cells (Carleton, Accolla and Simon, 2010). The encoding of pheromone identity is not clearly understood since, except for a few exceptions, the exact nature of these stimuli remains largely uncharacterized. However, the great similarity at both the molecular and the cellular levels between taste transduction and transduction of pheromone signals suggests that these two systems might have evolved from a common precursor (Dulac, 2000; Liman, Zhang and Montell, 2014). One might then think that this similarity also applies to the encoding.

Quid of salt/sour taste modalities? Sour and salty are referred to as 'mineral' tastes, distinct from the three other classic taste submodalities, because they are rely on the detection of small ions (protons, small acids, sodium, lithium and potassium). Na^+ and H^+ are capable of interacting with a variety of membrane proteins. Especially, H^+ can virtually modify all proteins that are sensitive to pH changes. Because of the nature of the stimulus, so simple and omnipresent, it has been difficult to identify candidate receptors. Sour taste is evoked by acidic pH and organic acids, such as acetic acid, that penetrate the cell membrane. Salty taste is elicited by Na^+ concentrations ranging from 10 mM to 500 mM.

Over the years, a number of candidates for sour receptors or components of sour signaling have been proposed, including ASICs, HCNs, K^+ channels and, most recently, PKD2L1 and PKD1L3 (Roper, 2007). However, presently there is no evidence that any of these proteins mediate sour taste and knockouts of mouse PKD2L1 or PKD1L3 only slightly attenuate nerve responses to acid stimulation (Horio *et al.*, 2011). Nonetheless, PKD2L1-expressing cells respond to and are required for sensory response to acids (Huang *et al.*, 2006; Chang, Waters and Liman, 2010; Oka *et al.*, 2013). The response of

PKD2L1-expressing cells is mediated by an unusual proton-selective ion channel (Chang, Waters and Liman, 2010; Bushman, Ye and Liman, 2015). Proton selectivity allows the cells to respond to acids without interference from Na^+, which may vary independently in concentration. The molecular identity of the proton channel remains unknown. Several lines of evidence have converged to propose the amiloride-sensitive Na^+ channel ENaC as a candidate for sodium detection (Lin *et al.*, 1999). In general, the precise mechanisms underlying these two tastes remain difficult to define. What seems clear is that both sour and salt modalities involve the direct activation of ion channels as opposed to the other 'classic' taste sub-modalities detected indirectly through GPCRs. In addition, it was shown that, while sweet, bitter and umami tastes are processed by Type II cells, commonly referred to as the actual taste receptor cells (TRCs) in taste buds, salt and sour may be detected by respectively Type I (Vandenbeuch, Clapp and Kinnamon, 2008) and Type III (Tomchik *et al.*, 2007) cells (Fig.5).

And CSF-cNs? The CSF-cN case is complex. The emerging consensus is that CSF-cNs respond to 1/ pH changes via ASICs in mouse and lamprey (Orts-Del'Immagine *et al.*, 2012; Jalalvand *et al.*, 2016) and 2/ mechanical stimuli associated to tail bending in zebrafish (Böhm *et al.*, 2016) or CSF flow in zebrafish and lamprey (Jalalvand *et al.*, 2016; Sternberg *et al.*, 2018) via PKD2L1. CSF-cNs also respond to osmolarity changes but the nature of the channel varies depending on the study: in mouse, PKD2L1 was involved (Orts-Del'Immagine *et al.*, 2012), and ASIC3 in lamprey (Jalalvand *et al.*, 2016). It is thus interesting that ASICs and PKD2L1 were also shown to be involved in known CSF-cN sensory functions that involve what seems to be the direct activation of ion channels in a similar fashion to salt and sour in TRCs. Whether these channels constitute the transduction channels or whether these channels support the activation of an intracellular cascade leading to the activation of another transduction channel is not clear. More likely, the situation in Type I and III cells, and CSF-cNs is a mixed case between the classic mechano-sensation in iHCs, with the direct activation of ion channels, and chemo-sensation in vORNs and TRCs, with the presence of transduction pathway within the cell.

At rest, cells are charged negatively; sensory transduction results in membrane depolarization by generating a 'receptor potential', whose amplitude and duration vary as a function of the intensity and time course of the stimulation. In order to convey information all the way to the brain, the local depolarizations/hyperpolarizations induced by the receptor potential are turned into action potentials with a frequency proportional to the amplitude of the signal. The generation of action potentials can happen either in the sensory cell itself, as it is the case for vORNs and CSF-cNs, or through the release of neurotransmitters onto afferent nerve fibers, as for iHCs and TRCs. Changes in pattern of activity encode intensity and temporal properties of the stimulus.

C. Access of sensory cues to sensory receptors

The detection of stimuli requires the stimuli to reach the MSCs, located at the liquid interface in sensory organs, and that express specific sensory receptors.

Living organisms are surrounded by a huge amount of environmental cues. In that sense, they are constantly subjected to stimuli in a passive manner. They can also adopt investigating behaviors to actively probe their environment in order to, for example, look for preys or conspecifics to mate. In its most simple forms, investigation involves pointing the sensory organ towards the source of the stimulus to optimize its detection. In the case of pheromones, the difficult access of vORNs in the VNO of terrestrial vertebrates requires specific behaviors to facilitate the delivery directly into the organ: nose rubbing, licking or facial grimacing such as flehmen, to only cite a few.

In addition to specific behaviors, stimuli need to be 'channeled' in order to reach MSCs. External chemical cues are dissolved in fluids before they can be detected by sensory cells. In rodents, pheromones are pumped through a water-filled duct and carried by nasal mucus to vORNs in the VNO; tastants are solubilized in saliva before detection by TRCs in the oral cavity. In some aquatic animals, original mechanisms have also been demonstrated to help the collection of already solubilized cues. A recent study in zebrafish showed that the beating of motile cilia in the olfactory pit helped the capture and exchange of odors at the olfactory epithelium (Reiten *et al.*, 2017). In the case of CSF-cNs, interoceptive receptor cells, the chemical cues are readily available in the CSF, a complex fluid that carries a variety of substances coming from within the body. One could imagine that cilia beating might play a similar role as in the olfactory pit to direct CSF flow and its content towards the sensory CSF-cNs (Fame *et al.*, 2016; Grimes *et al.*, 2016; Sternberg *et al.*, 2018).

An exquisite example of stimulus channeling is illustrated by the audition system. Hearing starts with the capture of sound by the external ear. Sound is then transferred to the inner ear through the middle ear as vibrations along three tiny ossicles: the malleus, the incus and the stapes, the tiniest bones in the body. The vibrations transmitted by the ossicles encode the frequency and intensity of sound and are propagated throughout liquid in the inner ear. Once in the inner ear, acoustic stimuli of various frequencies and intensities induce maximal motion at a specific location on the basilar membrane according to quasi logarithmic mapping (Fig.3). The basilar membrane behaves as a frequency analyzer that distributes stimuli to specific iHCs along its length according to a tonotopic map (Hudspeth, 1989; Kandel *et al.*, 2013).

The sole expression of specific receptors by MSCs is not sufficient for the proper detection of stimuli. The ear nicely illustrates the importance of a very precise and sophisticated organization of the sensory organ to collect the acoustic stimuli, which

also participates to the encoding of the stimulus in this particular case. Not all sensory organs show the same degree of organization as the ear; however, all MSCs are integrated within a functional sensory tissue and display a cellular organization relevant for the proper collection of stimuli.

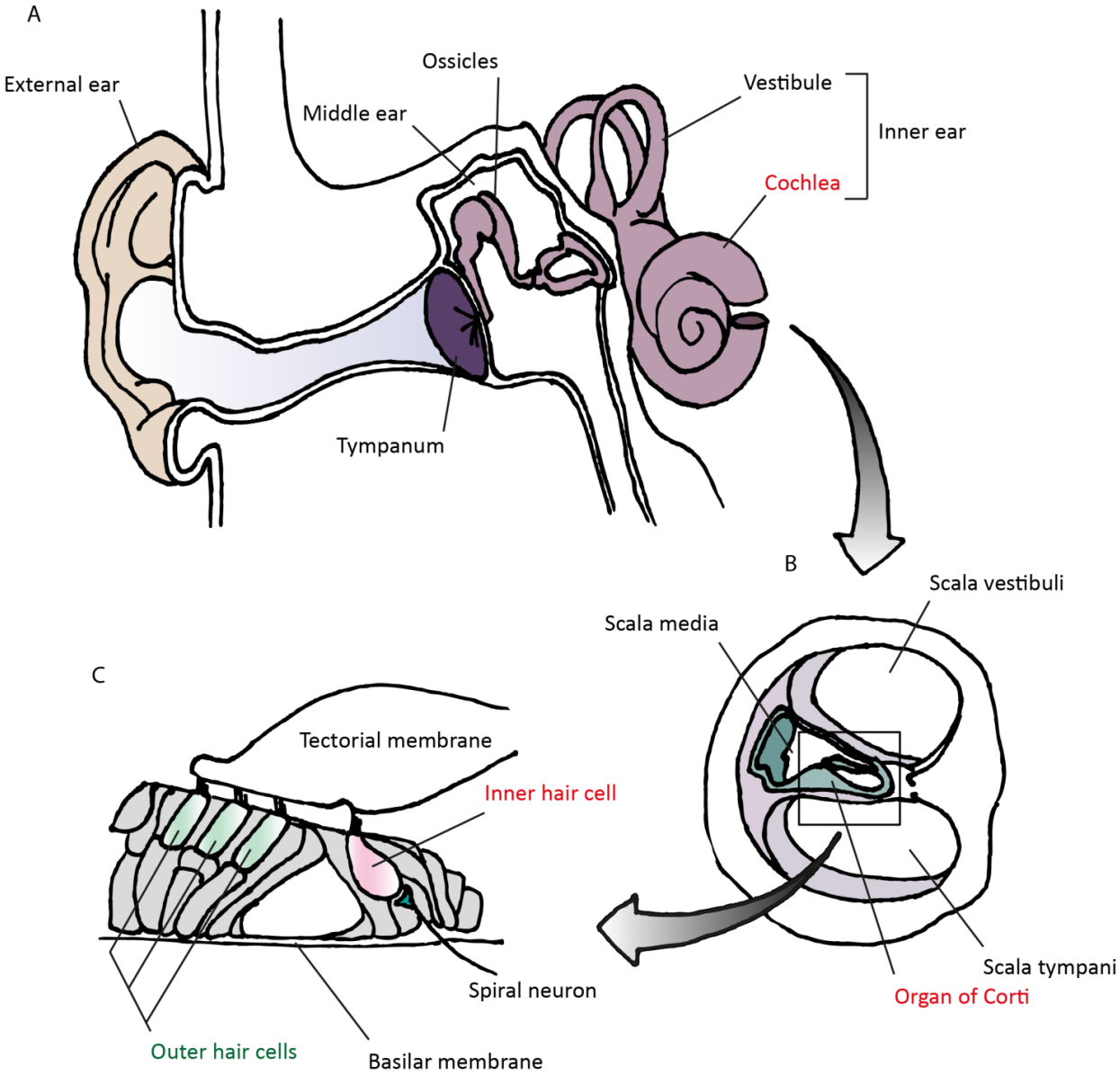

Figure 3. The sophisticated organization of the ear (adapted from different sources)
A, Incoming sound waves are channeled through the external ear to reach the tympanum attached to the ossicles of the middle ear. Airborne vibrations are transmitted through the ossicles to the inner ear where they are transformed into electrical signals by specialized sensory receptor cells, the hair cells.
B, Transversal section of the cochlea, the fluid-filled hearing end-organ. The cochlea is a continuous duct divided into three compartments where lies the sensory organ responsible for hearing, the Organ of Corti.
C, The Organ of Corti lies on the basilar membrane that conducts vibrations throughout the entire cochlea: the membrane resonates at a particular location in the cochlea depending on the vibration frequency. The Organ of Corti contains two types of receptor sensory cells: outer and inner hair cells. Hair cells extend stereocilia at their apical surface; the shearing movement between the basilar membrane and the tectorial membrane induced by incoming vibrations results in the deflection of the hair cells' bundles. Inner and outer hair cells are innervated by afferent fibers (not shown for outer hair cells), spiral sensory neurons, that transmit the signals to the CNS.

II. TISSUE AND CELL ORGANIZATION OF MICROVILLIATED SENSORY CELLS

A. Tissue integration of microvilliated sensory cells

MSCs are transducers within specialized tissues. Exteroceptive TRCs, vORNs and iHCs lie within sensory epithelia in direct or indirect contact with the external world. Interoceptive neurons contacting the CSF, CSF-cNs, lie within an epithelium-derived tissue in the spinal cord. Signals carrying information are filtered, channeled and delivered to sensory epithelial tissues where MSCs perform the conversion into electrical signals. Within the sensory tissue, only a subset of cells is sensory. The surrounding cells, although not directly sensory, often take part in sensory processing. The organization and integration of MSCs with neighboring non-sensory cells form a coherent sensory tissue.

Cell-cell adhesion. Sensory epithelia are constituted of multiple cell types, typically sensory and non-sensory supporting cells, arranged in evolutionary conserved patterns. In the inner ear, iHCs and supporting cells are organized according to a checkerboard-like or mosaic pattern, with the alternation of iHCs and supporting cells. The vomeronasal epithelium is pseudostratified with supporting cells in the most superficial layer while vORNs form the layers below (Halpern, 1987; Keverne, 1999). TRCs are found together with Type I (glial-like) and Type III (pre-synaptic) cells in onion-shaped taste buds embedded into the gustatory epithelium (Roper and Chaudhari, 2017) (Fig.1). It is interesting to note here that HCs of the lateral line of bony and cartilaginous fish are integrated with supporting cells and mantle cells in 'buds' of similar shape referred to as neuromasts (Ghysen and Dambly-Chaudière, 2004). Finally, CSF-cNs are typically found intermingled with ependymal and radial glia cells along the walls of the central canal, in the neurogenic niche of the spinal cord (Djenoune *et al.*, 2014).

The establishment of cellular patterns and cohesive tissue requires cell-cell adhesion and differential tension at the level of these junctions (Lecuit, 2005; Steinberg, 2007; Heisenberg and Bellaïche, 2013). The major molecular factors responsible for cell-cell adhesion are constituents of the Adherens Junctions (AJs): cadherins and nectins (Meng and Takeichi, 2009). Cadherins are essential Ca^{2+}-dependent adhesion molecules, indirectly associated with the actin cytoskeleton through catenins (Harris and Tepass, 2010). Cadherins are capable of bridging cells together through homophilic interactions, enabling the segregation of cells expressing the same proteins (Takeichi, 1988) (Fig.4B). Nectins are immunoglobin-like molecules capable of forming interactions of different strengths depending on the members involved. Cadherins and nectins are associated together during the formation of cell-cell adhesions (Meng and Takeichi, 2009). Recent data suggest that the combination of homophilic interactions between cadherins (Chacon-Heszele *et al.*, 2012) and heterophilic interactions of different nectins (Togashi *et al.*, 2011) enables the checkerboard-like patterning of iHCs. Cell-cell adhesion might

play a similar role in modulating cellular patterning of MSCs other than iHCs with non-sensory cells in sensory tissues.

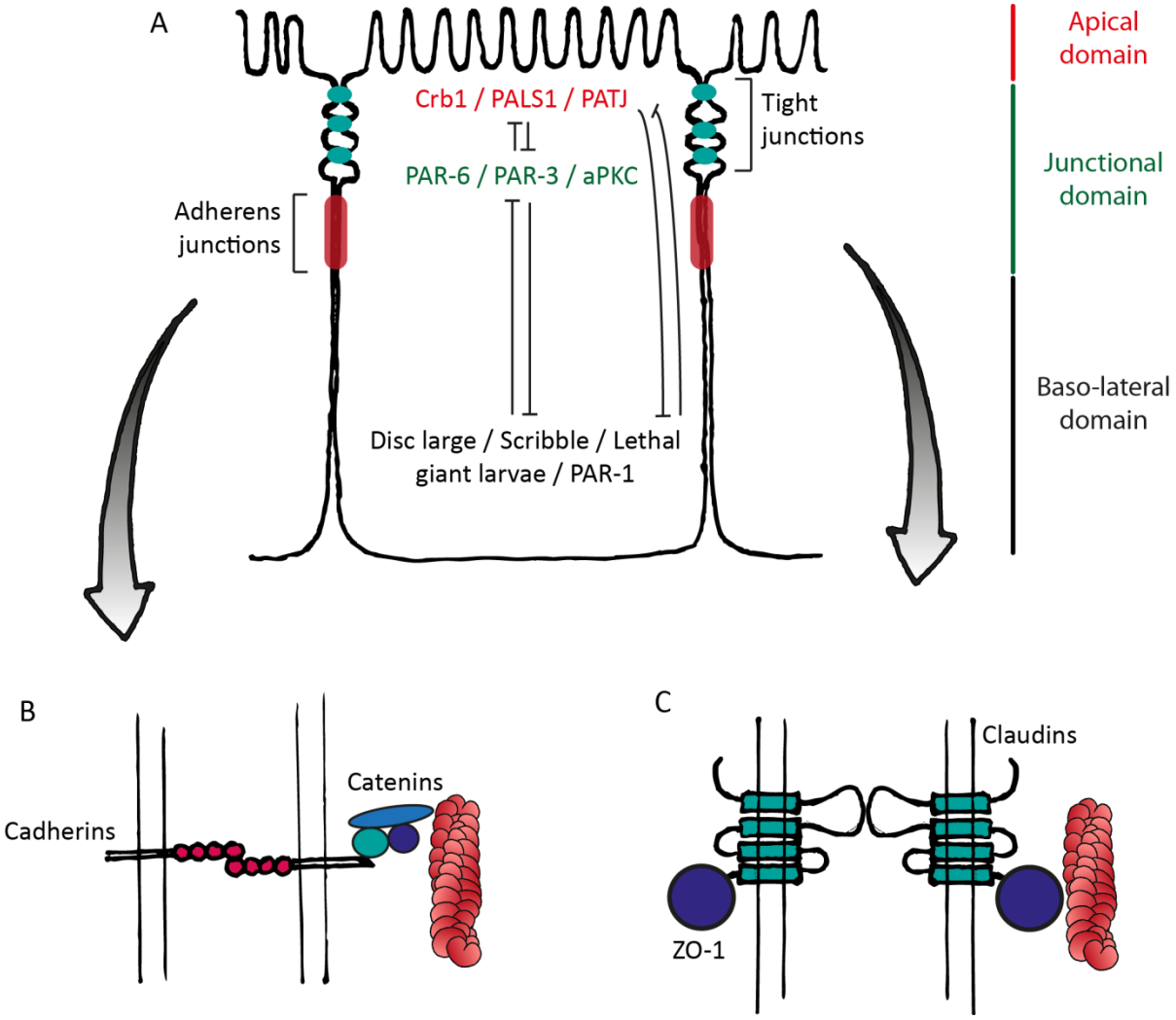

Figure 4. Apico-basal polarity and apical junctional complexes in epithelial cells
A, Mutually exclusive complexes control the establishment of cell apico-basal polarity and functionally different domains (adapted from (St Johnston and Sanson, 2011))
B, Adherens junctions are responsible for cell-cell adhesion and cohesion of the tissue. They rely on homophilic interactions between cadherins. Cadherins physically interact with cortical actin filaments through the catenin complex formed by p120-catenin (green) - associated with cadherin, β-catenin (dark blue) – scaffold protein, and α-catenin (light blue) – attached to F-actin (adapted from (Ratheesh and Yap, 2012))
C, Tight junctions are responsible for the selective permeability of the tissue. They mainly rely on claudins, membrane proteins forming paracellular barriers and pores. Claudins are indirectly associated to the actin cytoskeleton through members of the ZO family such as ZO-1 (dark blue) (adapted from (Günzel and Yu, 2013))

Tight junctions in MSC tissues. In epithelial tissues, AJs are accompanied by tight junctions (TJs) at the apical side of the cell to form the apical junctional complex (AJC). Epithelia constitute a selective permeable barrier, controlling the transport of specific molecules. While the major role of AJs is to maintain the tight association between cells,

hence the cohesion of the tissue, TJs ensure and control tissue paracellular permeability. TJs are described as rows or strands of membrane contacts, whose number and organization depend on the tissue type. Factors constituting TJs are mainly transmembrane and scaffolding proteins (Van Itallie and Anderson, 2014). Major constituents and determinants of TJ permeability are members of the Claudin family. Claudins are strand-forming proteins whose organization and location to the AJC into circumferential barriers depend on interactions with the scaffolding proteins of the Zonula Occludens (ZO) family (Fig.4C) (Fanning and Anderson, 2009; Günzel and Yu, 2013). ZO-1, -2 or -3 seemingly act as nucleators of claudin fibrils at the membrane (Van Itallie and Anderson, 2014). ZO-1 and ZO-2 are capable of directly interacting with cadherins and catenins, which could constitute a positional signal to relocate ZO members to early cell-cell contacts in order to recruit specific factors leading to TJ assembly (Yonemura *et al.*, 1995; Fanning and Anderson, 2009). Consequently, the assembly of TJs is subsequent to the initial establishment of AJs with the recruitment of specific factors to form the paracellular barrier. Interestingly, recent evidence showed that loss of ZO proteins results in delayed and/or defective AJs, suggesting a direct role in regulating AJ assembly (Fanning and Anderson, 2009).

TJ major constituents, claudins are present in all known epithelial tissues but in combinations of different isoforms that determine selective permeability of the tissue (Günzel and Yu, 2013). In the cochlea, the epithelial sheet formed by iHCs and supporting cells together constitutes a barrier separating two compartments filled with fluids of different ionic compositions, the endo- and the peri-lymph. This compartmentalization is accomplished by atypical TJs between iHCs and supporting cells: bicellular (bTJs) – between two cells - and tricellular (tTJs) – at the point where three cells contact one another. The differential ion composition of the endolymph versus the perilymph results in a strong gradient of K^+ (high in the endolymph and low in the perilymph) that contributes to the endocochlear potential (Hudspeth, 1989; Hibino and Kurachi, 2006). Several claudins were shown to be critical for the assembly and maintenance of TJs at the interface of iHCs and supporting cells, and between supporting cells: claudin-9 (Nakano *et al.*, 2009), claudin-11 (Gow *et al.*, 2004; Kitajiri *et al.*, 2004) and claudin-14 (Wilcox *et al.*, 2001) (Fig.1). Mutations in these proteins are associated with defects in the ion barrier functions and hearing loss in humans and/or mice (Wilcox *et al.*, 2001; Gow *et al.*, 2004; Kitajiri *et al.*, 2004). In the same vein, mutations in tricellulin, a protein concentrated at and maintaining bTJs and tTJs, segregate with non-syndromic deafness in humans (Riazuddin *et al.*, 2006).

Similarly, TJs in taste buds involve a unique subset of claudins: claudin-4, -6, -7 and -8 (Michlig, Damak and Le Coutre, 2007; Günzel and Yu, 2013). Claudin-4 and -8 are found to form a ring surrounding the pore at the level of TJs. These proteins maintain a cationic barrier between the taste pore and the basolateral region of the taste bud. In a similar fashion than in the auditory epithelium, this process might contribute to the sensory transduction in MSCs. Claudin-6 and -7 are expressed outside of TJs suggesting different

functions than tissue permeability. Claudin-6 is specifically expressed by TRCs just above the pore, in the microvilli where its role remains unexplored (Michlig, Damak and Le Coutre, 2007). Claudin-7 is found at the basolateral membrane of Type I and Type III cells in the taste buds supposedly contributing to cell-cell adhesion (Michlig, Damak and Le Coutre, 2007) (Fig.1).

The situation for TJs involved in sensory epithelia where CSF-cNs and vORNs are nested remains elusive. Evidence for TJs comes from early ultrastructural studies performed using electron microscopy (Lamotte, 1987) and freeze-etching (Miragall, Breipohl and Bhatnagar, 1979). CSF-cNs and surrounding ependymal cells line up the central canal and establish the barrier enclosing CSF where TJs are definitely involved. TJs were described around the central canal in mammals (Lamotte, 1987), but specific TJ components have not been identified. Similarly, the molecular architecture and function of TJs described at the interface of vORNs and supporting cells in the vomeronasal organ (Miragall, Breipohl and Bhatnagar, 1979) have not been investigated.

Coordinated planar cell polarity of iHCs within the auditory epithelium. In addition to specific properties of cohesion and permeability, the auditory epithelium displays an extra level of organization with the coordinated orientation of iHC microvilliated apical extensions within the tissue. In iHCs, the apical extension is constituted of rigid microvilli derivatives, historically referred to as stereocilia, that are strictly organized in a stereotyped staircase pattern (Fig.1). Stereocilia staircases are uniformly oriented within the tissue, aligned along the direction of fluid movement, an essential feature to maximize the coordinated activation of iHCs upon deflection of the hair bundle (Fig.2). Such organization at the tissue level involves planar cell polarity (PCP) and conserved core PCP proteins, first described in invertebrates. Six core PCP genes were described in *Drosophila*, all with their mammalian counterparts listed below (Ezan and Montcouquiol, 2013; Lu and Sipe, 2016): CELSR1, PKL1 & 2 and VANGL1 & 2, forming the proximal complex, and FZD1, 2, 3 & 6 and DVL2 & 3, forming the distal complex with CELSR1. Each core protein depends on the activity of the five others, which results in the asymmetrical accumulation between the neural and the abneural sides of iHCs. The proximal core PCP complex, at the abneural side, eventually stimulates the formation of stereocilia with the correct staircase orientation. Apical extensions are uniformly oriented across the sensory epithelium even though iHCs are interspaced by supporting cells. Thus, the organization of iHC apical extensions involves a long range signaling, transmitted across the tissue, and interactions between neighboring iHCs and supporting cells. PCP proteins are mainly located at the intercellular junctions and show an asymmetrical distribution between cell sides (Ezan and Montcouquiol, 2013). In the Drosophila wing, Frizzled was shown to be responsible for this non-autonomous PCP signaling, enabling the establishment of a PCP gradient through the tissue. In the mammalian cochlea, VANGL2 was proposed as a candidate but the mechanisms underlying this phenomenon remain unclear (Ezan and Montcouquiol, 2013). Mutations in core PCP genes result in

abnormally oriented apical extension in iHCs and hearing defects (Michalski and Petit, 2015).

The particular case of non-neuronal MSCs - iHCs and TRCs. More complex tissue organization are found with non-neuronal MSCs. TRCs and iHCs are capable of generating a graded receptor potential but require the presence of afferent fibers and/or accessory cells in order to transmit the electrical signal to the CNS. In the case of TRCs, the current working hypothesis involves the integration of the three cell types present in the taste bud in a paracrine transmission model (Roper and Chaudhari, 2017) (Fig.5).

Upon activation, TRCs release ATP that depolarizes afferent fibers but also Type III pre-synaptic cells in a paracrine manner. The activation of Type III cells by ATP induces the release of 5-HT and GABA (Huang *et al.*, 2007), which provide negative feedback onto Type II cells/TRCs during taste excitation by inhibiting ATP release (Dvoryanchikov *et al.*, 2011). 5-HT produced by Type III cells also directly activates the afferent gustatory nerve fibers through 5-HT_3 receptors (Larson *et al.*, 2015). In gustation, afferent fibers come from bipolar gustatory ganglion neurons that are either 'specialist' neurons receiving synapses from TRCs responding to only one taste modality and 'generalist' neurons receiving inputs from many TRCs and/or Type III cells (Roper and Chaudhari, 2017). Gustatory ganglion neurons transmit signals to the nucleus of the solitary tract in the hindbrain. Similarly, iHCs are innervated by bipolar neurons, mostly spiral ganglion neurons forming specialized synapses on inner iHCs: the ribbon synapses (Safieddine, El-Amraoui and Petit, 2012). Ribbon synapses are characterized by a presynaptic electron-dense structure, to which synaptic vesicles containing the neurotransmitter Glutamate are tethered. Ribbon synapses are not exclusive to iHCs in the inner ear but are also found in other HCs of the vestibular or lateral line, as well as in photoreceptors and pineal gland sensory cells (Safieddine, El-Amraoui and Petit, 2012). Upon activation, iHCs generate a receptor potential graded according to the intensity of the stimulus. In turn, the receptor potential tunes Glutamate release probability at the ribbon synapse. This feature is key for audition as it sets a rate code for action potential frequency in auditory neurons as a function of stimulus intensity (Glowatzki, Grant and Fuchs, 2008; Safieddine, El-Amraoui and Petit, 2012).

The modulation by accessory cells of the synaptic transmission from a MSC to a bipolar neuron adds another layer of regulation of the signal transmission to the CNS. MSCs develop and differentiate to be fully integrated within a sensory epithelium, intermingled with non-sensory cells, supporting cells. The non-sensory cells can play important roles in the sensory function as they participate to the establishment of a functional sensory epithelium through cell-cell interactions, and the regulation of the homeostasis of various ions and molecules. Supporting cell functions have been the

most thoroughly studied in the inner ear (Wan, Corfas and Stone, 2013) but might play similar roles in tissues where TRCs, vORNs and CSF-cNs reside.

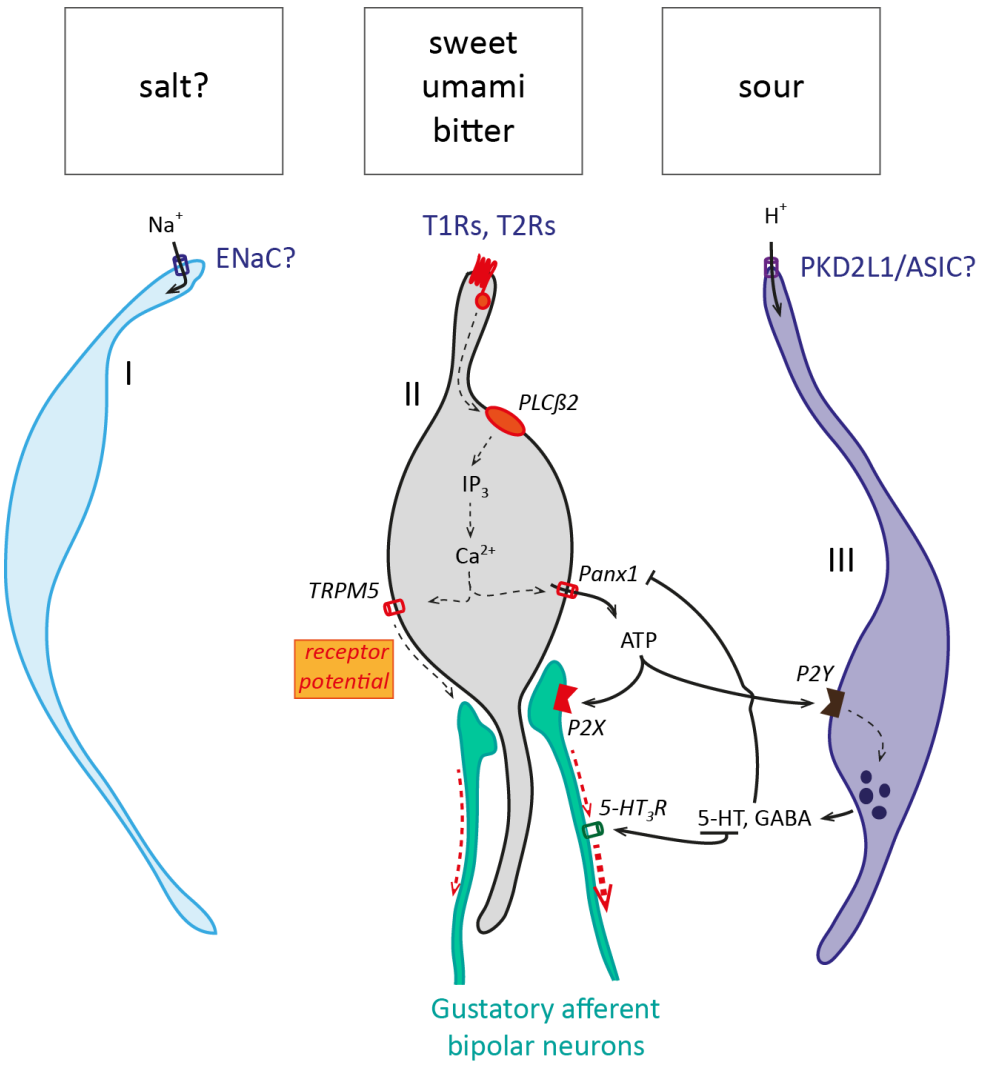

Figure 5. The paracrine model of cell-cell signaling in taste buds (adapted from (Chaudhari and Roper, 2010))

Taste receptor cells, or Type II cells, detect sweet, bitter and umami through heterodimeric GPCRs (T1Rs and T2Rs), generate graded receptor potential and release ATP. Both ATP and graded receptor potential are detected by and activate afferent fibers.

Presynaptic cells, or Type III cells, respond to sour taste stimuli and, in a paracrine manner, to ATP released by Type II cells. Type III cells provide negative feedback onto Type II cells by secreting GABA and 5-HT. 5-HT has multiple targets within the taste bud; in addition to inhibit Type II cells, it directly excites afferent fibers.

Glial-like cells, or Type I cells, are proposed to detect salt and help buffering neurotransmitters within the taste bud.

B. The specialized cellular organization of microvilliated sensory cells

MSCs are highly polarized and structured cells that develop a microvilliated apical extension into the extracellular space, where they can detect sensory cues. The ability of epithelial cells, and in particular MSCs, to develop an apico-basal polarity is an important pre-requisite to the tissue organization.

Apico-basal polarity in MSCs. Like other epithelial cells, MSCs establish and maintain two cellular domains – apical and baso-lateral, through a network of polarity factors. Polarity factors mutually exclude each other, resulting in their polarized distribution and in the positioning of the junctional domain at the interface between the apical and baso-lateral ones. Crumbs recruit PALS1 and PATJ to form the apical complex and specify apical identity. The apical complex directly interacts with the PAR-6/PAR-3/aPKC complex determining the junctional domain where AJs and TJs take place. Beneath, the baso-lateral domain is marked by the presence of discs large homologue, lethal giant larvae, scribble, and PAR-1 which, together, limit the extension of both the apical and junctional complexes. The factors strictly basal are not clearly defined yet but might involve integrins and FAK (Rodriguez-Boulan and Macara, 2014; Campanale, Sun and Montell, 2017) (Fig.4A). Among all the factors involved, aPKC and PAR-1 are thought to play a pivotal role in polarity signaling by directly altering the localization of several polarity factors through phosphorylation. CDC42, a small rho GTPase, was also shown to be a key regulator (Margolis and Borg, 2005; Campanale, Sun and Montell, 2017).
Polarization is a key element in the MSC morphogenesis. It enables the cell a degree of spatial organization with different domains bearing various functions. The apical domain of MSCs is in direct contact with the environment; it is specialized to carry the sensory function through the formation of the microvilliated apical extension. The microvilliated apical extension is essential to increase cell surface and constitutes the particular site of segregation of a multitude of membrane proteins relevant for the sensory transduction. The junctional domain is the site of cell-cell contact through the establishment of cell-cell adhesion, mostly AJs but also TJs. Key polarity proteins of the apico-basal polarity program play an important role in the assembly and maintenance of both AJs and TJs (Rodriguez-Boulan and Macara, 2014). In addition, throughout establishment, maintenance and remodeling, AJs and TJs are tightly coupled to the actin cytoskeleton through cadherin-catenin (Harris and Tepass, 2010) and claudin-ZO (Fanning *et al.*, 1998; Fanning and Anderson, 2009) interactions respectively. The interplay between junctions and actin promotes the maturation of junctions and the shaping of F-actin underneath. Altogether, junctions and actin are responsible for force transmission and strengthening within the tissue. In MSCs, epithelium-derived cells, this interplay results in the shaping of F-actin into its unique circumferential belt configuration (Yonemura *et al.*, 1995; Harris and Tepass, 2010). This process is supported by the recruitment of diverse actin regulators, such as nucleators like the Arp2/3 complex or actin polymerization factors,

by cadherin-catenin (Harris and Tepass, 2010) and claudin-ZO (Fanning and Anderson, 2009) complexes. Thus, through junctions, the establishment of apico-basal polarity in MSC is essential for both the integration and orientation within the sensory tissue, and the recruitment of actin cytoskeleton machinery to the apical side where the microvilliated apical extension will arise.

The great example of the sophisticated organization of the iHC apical extension. The formation of the microvilliated apical extension itself has been more extensively studied in iHCs of the inner ear. The morphological organization of iHCs, especially the planar polarization of the so-called hair bundle, was shown to be as critical to hearing as the sophisticated organization at the level of the auditory organ and tissue. In addition to orientation within the auditory epithelium and their apico-basal polarity, iHCs display polarization along their orthogonal axis. The so-called cell-autonomous PCP is responsible for the shaping of the apical extension in a staircase fashion with stereocilia (microvilli derivatives) organized in rows of increasing height. Two signaling mechanisms have been demonstrated to be of importance to establish the hair bundle organization: the kinocilium and the cell-intrinsic PCP (Lu and Sipe, 2016).

Early during iHC differentiation, a primary cilium referred to as kinocilium, emerges at the center of the apical surface and migrates towards the cell's abneural edge. The position of the kinocilium defines the vertex of the apical extension: once the kinocilium in place, stereocilia grow differentially around it, forming the typical staircase pattern. The kinocilium is crucial for the establishment of the typical hair bundle shape and orientation. Mutations in genes causing kinocilium defects lead to misshapen bundles found in Bardet-Biedl (Ross *et al.*, 2005), Meckel-Gruber (Cui *et al.*, 2011) and Alström (Jagger *et al.*, 2011) syndromes. Specific deletions of ciliary genes expressed in the inner ear involved in the intraflagellar transport, such as *Ift88*, *Kif3a* or *Ift20*, also result in abnormal development of the iHC apical extension (Jones *et al.*, 2008; Sipe and Lu, 2011; May-Simera *et al.*, 2015).

The cell-intrinsic PCP machinery involves RAC-PAK, CDC42-aPKC (Grimsley-Myers *et al.*, 2009; Kirjavainen *et al.*, 2015) and LGN/Gαi/dynein (Ezan *et al.*, 2013; Sipe *et al.*, 2013) signaling. Many of the factors involved in these pathways show polarized distributions at the apical surface (Ezan *et al.*, 2013), discriminating between the neural and ab-neural sides where the kinocilium migrates to. Perturbations of these factors result in aberrant positioning of the kinocilium and misshapen stereocilia indicating a role orientation of the basal body. These cell-autonomous mechanisms were shown to be robust and independent on the tissue polarity cues described in the section above.

Mechanosensory transduction in iHCs not only relies on the staircase organization of the hair bundle but also on its stiffness achieved by bridging stereocilia via different types of links. At the mature state, top connectors – near the tip, tip links – oblique links at the tip, and putatively lateral links – along the bundles, ensure the cohesion between stereocilia (Pickles, Comis and Osborne, 1984; Michalski and Petit, 2015). The discovery

of tip links, interconnecting each stereocilium to its taller neighbour, was a key finding in the understanding of the mechano-transduction in iHCs (Pickles, Comis and Osborne, 1984). Tip links gate the mechanotransduction channel: upon mechanical stimulation, the displacement of stereocilia change tension in tip links, which in turn modulates the probability of the channel opening (Assad, Shepherd and Corey, 1991) (Fig.2). The staircase organization of stereocilia is essential for the directionality of the signaling: deflections in the direction of the tallest stereocilia increase channel opening probability while deflections toward the shortest stereocilia reduce it. The combination of genetic studies of hereditary deafness in human patients with the use of mouse models allowed the identification of the molecular components of the tip links (Petit and Richardson, 2009). In particular, the study of the Usher Syndrome Type I, responsible for deaf-blindness, revealed several genes: *cadherin-23*, *protocadherin-15*, *harmonin*, *sans*, *myosin-VIIa* and *cib2*. The associated proteins were later demonstrated to be either components of the tip links or to participate to their anchoring to the actin cytoskeleton (Boëda *et al.*, 2002; Ahmed *et al.*, 2006; Michalski *et al.*, 2009; Caberlotto *et al.*, 2011). Dimers of CDH23 and PCDH15 form the tip link (Söllner *et al.*, 2000; Kazmierczak *et al.*, 2007) while harmonin, MYO7A (myosin-VIIa) and sans form the anchoring complex (Fig.2) (Adato *et al.*, 2005; Michalski and Petit, 2015; Zhao and Müller, 2015). Any alteration of this fine structural organization results in hearing defects, demonstrating the critical role of these factors for mechanotransduction.

In contrast to iHCs, the importance of the apical extension structural organization has not been thoroughly studied in other MSCs and fostered my interest. Can we find similar factors involved in the organization of MSCs? If so, do they conserve similar functions?

C. The actin cytoskeleton, a key organizer in microvilliated sensory cell morphogenesis

Molecular mechanisms underlying specialized organization at the tissue and cellular levels are tightly coupled to the cell cytoskeleton. In particular, actin filaments play a pivotal role in shaping cells and provide a driving force during internal rearrangements or between cells in a tissue. Such features of the actin cytoskeleton are controlled by a multitude of accessory proteins, the actin-binding proteins (ABPs). In this section, I will briefly present the basic principles of the actin system (see (Revenu *et al.*, 2004; Chhabra and Higgs, 2007; Kessels *et al.*, 2011; Lodish *et al.*, 2013; Alberts *et al.*, 2014; Schwayer *et al.*, 2016)).

Overview of the functions of the actin cytoskeleton. Actin filaments can be found scattered throughout the cell, organized in tight bundles, or localized in a loose network in the cortex, just beneath the plasma membrane. Actin filaments are capable of supporting cell shape, providing cell stiffness and building projections of various stability, such as short-lived filopodia and more stable microvilli. The actin cytoskeleton

participates to the establishment of cell polarity by enabling the discrimination between the apical and basolateral sides through differently organized filaments. It is involved in the formation and maintenance of cell-cell contacts, mainly AJs and TJs, allowing the establishment of a driving force and the transmission of polarity signaling between cells within a tissue (see II.A and II.B). Actin also allows the attachment of cells to subtract through interactions of integrins with the extracellular matrix.

Main properties of the actin cytoskeleton. A common feature to all cytoskeletal systems is their fast dynamics and ability to form polymerized structures referred to as filaments. Actin filaments, also called microfilaments or F-actin (F for filamentous), are helical polymers with a diameter of 8 nm built from small and compact subunits, actin monomers or G-actin (G for globular). Actin subunits self-associate through head-to-head protein non-covalent interactions, allowing rapid assembly and disassembly to adapt to different structures and conditions. Because actin monomers are asymmetrical, their association into filaments results in a polarized structure with a barbed and a pointed end (Fig.6). The two ends of an actin filament behave differently. Namely, association and dissociation of actin monomers occur at both ends but at different rates: much slower at the pointed end than at the barbed end. As a result, during elongation, actin filaments virtually grow in one direction, the direction of the barbed end where polymerization is ten times faster. Such polarity gives the cell means to use actin filaments as a source of mechanical force with a specific direction. At the steady state, when free G-actin concentration reaches a critical point, assembly/disassembly rates at both ends of the filament balance each other, which results in treadmilling, meaning a net flow of actin subunits through the filament (Revenu *et al.*, 2004). The precise balance between actin polymerization and depolymerization enables the dynamic steady state of cell shape and structures. Cells can leave the steady state and modulate actin structures to adjust to their environment by controlling G-actin availability: below the critical concentration, actin filaments will decrease and, inversely, they will grow in response to higher G-actin concentration (Revenu *et al.*, 2004).

Nucleation of actin, the rate-limiting step of the formation of actin filaments. G-actin monomers can assemble spontaneously but this initial step is energetically unfavorable because of the high instability of actin subunits. To efficiently promote the elongation of filaments, at least 3 actin subunits must first be aggregated into a nucleus, stabilized by multiple interactions, from which addition of more subunits can spontaneously take place. This process is called nucleation and it is the rate-limiting step in the formation of actin filaments. To overcome the kinetic barrier of nucleation, cells use actin-nucleating factors. Actin nucleators possess several actin-binding domains, which enables them to bring several actin subunits together to form the nucleus. To date, three different types of actin nucleators have been described: the Arp2/3 complex, formins and WASP-homology 2 (WH2) domain-containing nucleators (Fig.6) (Chhabra and Higgs, 2007;

Kessels *et al.*, 2011). The Arp2/3 complex is constituted of two actin-related proteins, Arp2 and Arp3, and five other proteins. The complex mimics the barbed end of actin filaments and thus serves as a template for monomer addition. Because of its low basal activity, the complex requires to be activated by nucleation-promoting factors, mainly from the Wiskott-Aldrich Syndrome protein (WASP) family (Chhabra and Higgs, 2007; Kessels *et al.*, 2011). Formins constitute a large diverse group of factors characterized by the presence of formin homology 2 domains. Formins dimerize to form a donut-shaped structure driving actin nucleation and surrounding the barbed end of growing filaments to protect it from capping proteins (see below) (Chhabra and Higgs, 2007; Kessels *et al.*, 2011). Finally, WH2 domain-containing factors, such as Spire or Cordon-bleu, use their WH2 domains to bind actin monomers and assemble actin nuclei *de novo* to support subsequent elongation (Kessels *et al.*, 2011). The final structural organization of the actin network greatly depends on the type of nucleator involved. For example, Arp2/3 complexes give rise to 70°-branched actin filaments found in lamellipodia while formins generate long linear filaments found in AJs and filopodia (Chhabra and Higgs, 2007).

Elongation of filaments and its control. Numerous ABPs can modulate the elongation of actin filaments (Fig.6) (Revenu *et al.*, 2004; Lodish *et al.*, 2013; Alberts *et al.*, 2014). The filament assembly first depends on the availability of monomers in the cell. G-actin can be virtually stored by factors such as thymosin that form a complex with monomers, which prevents association with F-actin. On the contrary, G-actin can be recruited by different monomer-binding proteins, such as profiling, capable of enhancing polymerization at the barbed end of filaments. Then, a large panel of ABPs can bind F-actin to modulate the behavior of filaments themselves. Capping proteins, such as CapZ or tropomodulin, reduce the exchanges of G-actin by directly binding the barbed or the pointed end. Because the polymerization/depolymerization primarily occur at filament ends, even very low amounts of capping proteins can dramatically modify the dynamics and structuration of actin cytoskeleton. Severing proteins, such as gelsolins and cofilins, increase the number of available filament ends for polymerization/depolymerization by breaking filaments into smaller ones. Altogether, ABPs modulate actin dynamics by regulating the treadmilling rate of F-actin. ABPs themselves are subject to regulation, through post-translational modifications or interactions with various cofactors (Revenu *et al.*, 2004).

The loose binding of actin monomers within a filament is critical for rapid assembly/disassembly, which provides needed flexibility to actin-based structures. However, actin filaments are still capable of providing mechanical strength and generating of force in the cell. This is achieved by the supra-organization of microfilaments into higher-order networks depending on 1) the actin-nucleating factor and 2) different factors capable of binding filaments to each other (Chhabra and Higgs, 2007). Notably, higher-order actin networks support the development of membrane

protrusions by differentiated or migrating cells. In the case of MSCs, the actin cytoskeleton underlies the formation and maintenance of the sensory microvilliated apical extension through a very specific supra-organization: parallel unbranched filaments forming a bundle, the parallel actin bundle.

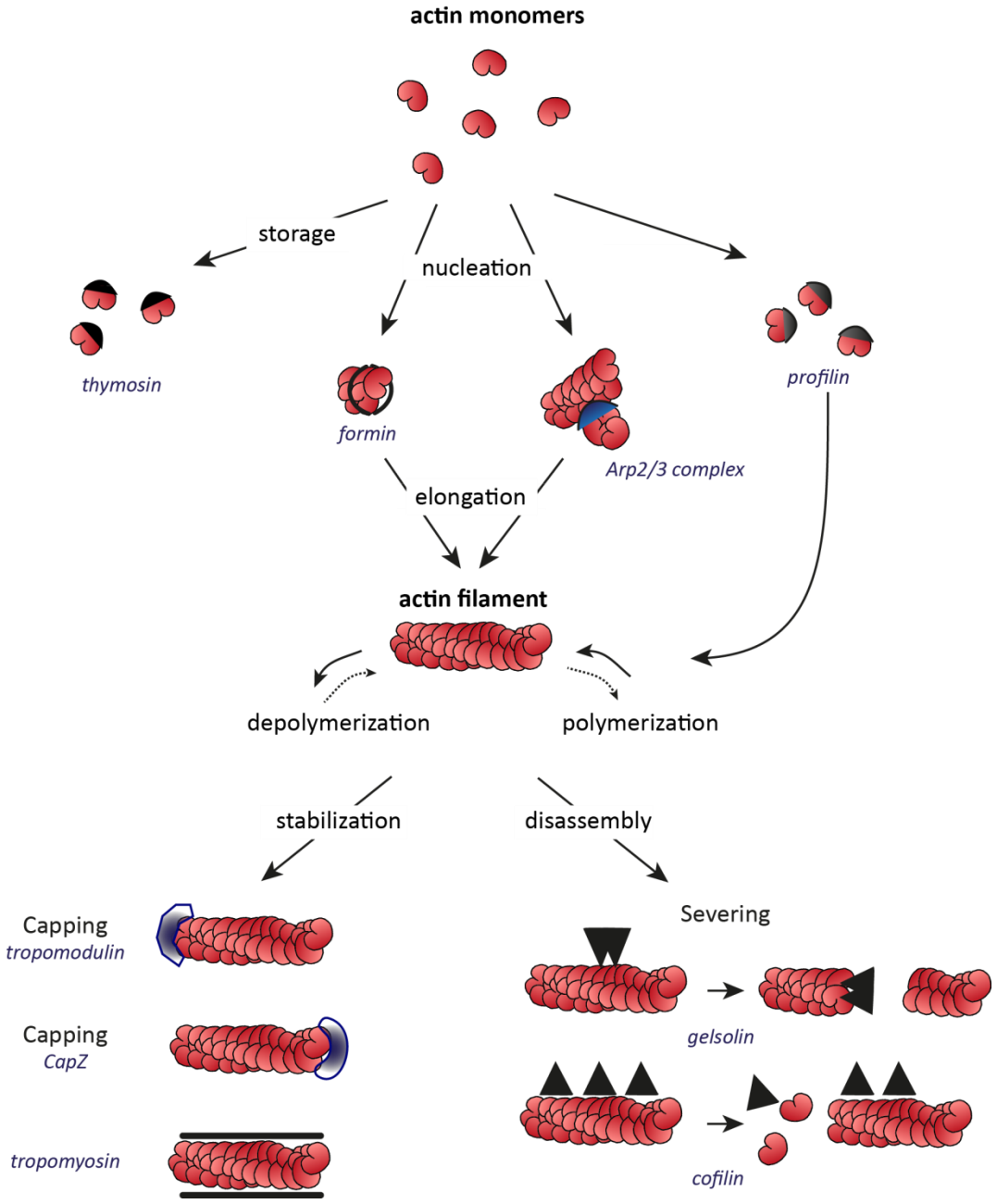

Figure 6. Actin cytoskeleton and its actin-binding proteins (adapted from (Alberts *et al.*, 2014))
Actin is present in two forms: actin subunits, also called actin monomers or G-actin, and actin filaments, also called F-actin. To polymerize into a filament, several actin subunits need to assemble through a process called nucleation. The assembly of a nucleus is modulated by several actin nucleators such as formins and the Arp2/3 complex. Once formed, the actin filament reaches a steady state where actin subunits undergo a net flux through the polymer that maintains a constant length: this process is called treadmilling. Several actin-binding proteins regulate nucleation, polymerization and depolymerization. Examples of each type are depicted here.

III. THE PARALLEL ACTIN BUNDLE, THE CORE COMPONENT OF THE SENSORY ORGANELLE

A. The making of the parallel actin bundle

MSC microvilli are thin membrane protrusions supported by one bundle of unbranched actin filaments, the parallel actin bundle (Fig.7). Each bundle is constituted of straight, tightly packed filaments with their barbed ends located at the tip (DeRosier and Tilney, 2000; Revenu *et al.*, 2004). Comparisons across many microvilliated cell types suggest a common cell factory responsible for the generation of short bundle modules at a specific location to generate microvilli (DeRosier and Tilney, 2000). The bundle-making factory fulfills two roles: the initiation step with the nucleation of G-actin and the lengthening of the generated filaments (Fig.7).

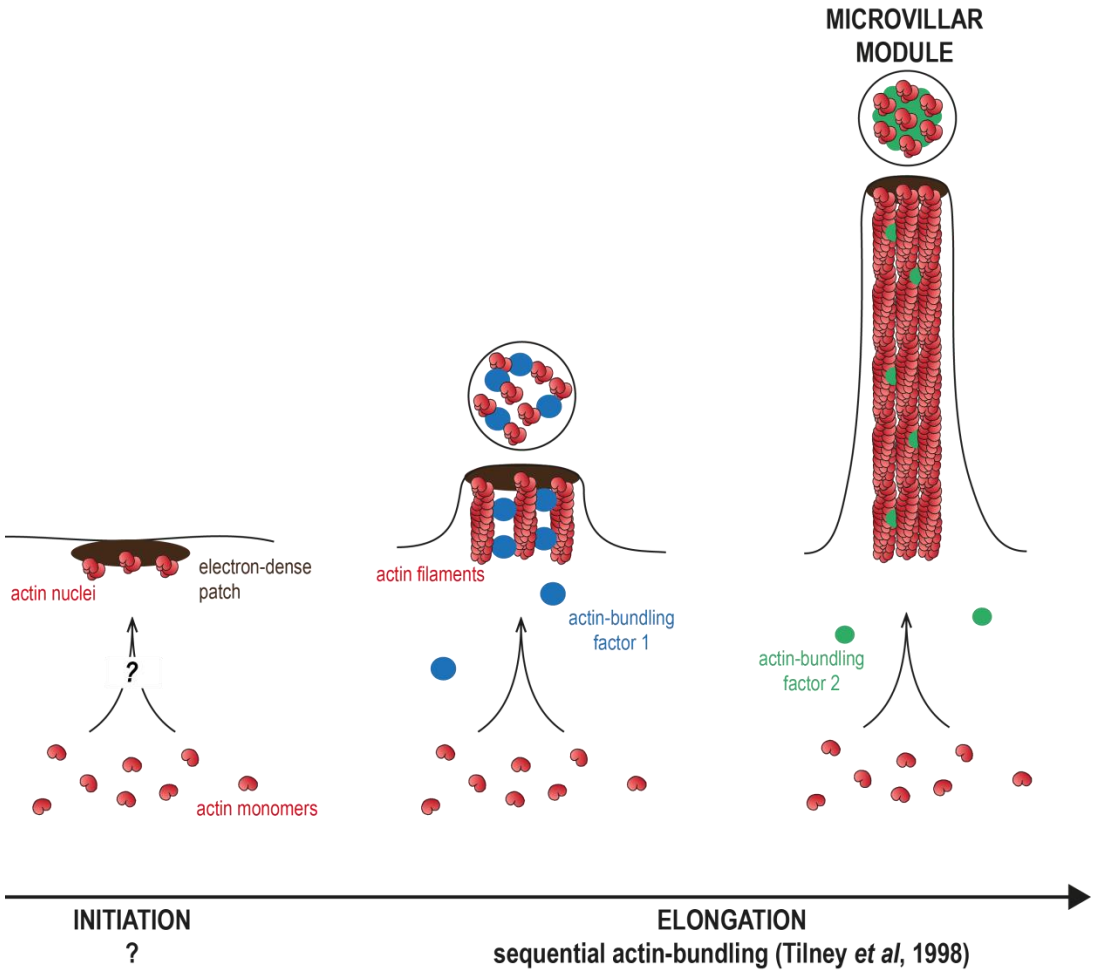

Figure 7. Formation and structure of parallel actin bundle modules to establish microvilli
(adapted from (DeRosier and Tilney, 2000))
Microvilli are thin membrane protrusions supported by actin cytoskeleton organized in parallel actin bundles.
The formation of parallel actin bundles takes place in two steps: (1) the initiation of actin protrusions at specific membrane sites by actin nucleation factors and (2) the elongation and cross-linking of these actin filaments through the sequential activity of at least two different actin-bundling factors.

Current understanding of the mechanisms underlying the formation of parallel actin bundles mainly comes from studies on the brush border of the gut epithelial cells and iHC stereocilia.

Nucleation of the actin filaments forming the parallel actin bundle. The molecular mechanisms underlying actin nucleation initiating the formation of actin bundles are still unclear. Several lines of evidence can be derived from the study of filopodia, another type of thin protrusions constituted by one parallel actin bundle (Revenu *et al.*, 2004). Despite their differences, the molecular mechanisms underlying filopodia and microvilli assembly share many similarities. The nucleation of parallel actin bundle-based microvilli seems to occurs near the plasma membrane at an electron-dense region (DeRosier and Tilney, 2000). Interestingly, a study using correlative time lapse-electron microscopy to examine filopodia initiation showed that filopodial parallel actin bundles similarly emerged from marginal dense patches (Steketee, Balazovich and Tosney, 2001). In addition, the authors showed that filopodia initiation critically relied on focal electron-dense phases that corresponded to adhesion sites containing a donut-shaped focal ring from which radiated filopodial actin filaments (Steketee, Balazovich and Tosney, 2001). Focal rings could be observed in numerous filopodial structures, which suggests a prevalent role in their initiation that could be extended to microvilli (Steketee, Balazovich and Tosney, 2001). The detection of these small actin-based focal rings is challenging and therefore sometimes missed.
A major promotor of filopodia formation at the cell periphery is CDC42 (Nobes and Hall, 1995), this small rho GTPase we already mentioned (see II.B,C), through its interaction with the insulin receptor tyrosine kinase substrate of 53 kDa (IRSp53) (Krugmann *et al.*, 2001). IRSp53, also known as brain-specific angiogenesis inhibitor 1-associated protein 2 (BAIAP2), has a dual role in membrane dynamics and actin cytoskeleton. Its several protein-protein modules enable IRSp53 to bind and organize actin cytoskeleton and its inverse bin-amphipysin-rvs167 (I-BAR) domain to sense and generate negative membrane curvature (Scita *et al.*, 2008; Zhao, Pykäläinen and Lappalainen, 2011). IRSp53 thus serves as an integrative node involved in the generation of a variety of membrane protrusions. In addition to IRSp53, downstream effectors of CDC42 include the Arp2/3 complex involved in actin filament nucleation (Fig.6 and II.C). The Arp2/3 complex thus comes as a good candidate actin nucleator in filopodia except that it is known to promote branched actin networks, not parallel filaments, and that it is not present in mature filopodia (Svitkina *et al.*, 2003). However, a very detailed kinetic-structural analysis of filopodia initiation suggested that the role of the Arp2/3 complex in promoting filopodia formation consists in the creation of a branched actin array whose actin filaments subsequently assemble into bundles (Svitkina *et al.*, 2003). A key determinant in this convergent elongation model is the binding of cross-linking factors and molecules preventing the capping of barbed ends to respectively enable the tight packing into a bundle and further elongation of the filaments to form filopodia (Svitkina

et al., 2003). Alternatively, when filopodia initiate *de novo*, in the absence of Arp2/3 complex-mediated branched actin networks, parallel actin filaments can be nucleated at the plasma membrane directly by formins (Faix and Rottner, 2006). In both models, IRSp53 would play a key role in recruiting specific factors to protruding membranes along with ABPs and actin cytoskeleton to enable the initiation and elongation of parallel actin bundles (Ahmed, Goh and Bu, 2010). In iHCs, the Arp2/3 complex is the only actin nucleator detected (Barr-Gillespie, 2015). One could then imagine a similar contribution of the nucleation function of the Arp2/3 complex and others in the initiation of actin bundles constituting the apical extension of iHCs and, more generally, of MSCs.

Packing actin filaments to form the parallel actin bundle. After nucleation of G-actin at the electron-dense patch of apical membrane, actin filaments polymerize and form short bundles (Fig.7). The regulation of the length of bundle modules was proposed to be determined by a two-component mechanism involving the concentration of available components and the coupling of this concentration to the number of nucleation sites (Tilney, Tilney and Derosier, 1992; DeRosier and Tilney, 2000). According to this model, because the concentration of bundle components is proportional to the number of nucleation sites at a specific time during development, actin modules formed simultaneously will be of a constant average length. We already mentioned the different kinds of ABPs involved in elongation and its regulation (Fig.6). An additional class of ABPs is needed to enable the packing of filaments into bundles: actin-bundling factors. Actin-bundling factors contain at least several actin-binding modules to support the cross-linking of actin filaments together, along with other protein-protein interaction motifs and regulatory domains responsible for the regulation of their actin-bundling function (Bartles, 2000). MSCs, and all cells developing parallel actin bundle-based protrusions, express at least two different actin-bundling factors; TRCs express villin, fimbrin and espin, vORNs villin and espin, iHCs fimbrin, villin and espin (Fig.1) (Bartles, 2000; DeRosier and Tilney, 2000; Sekerková *et al.*, 2006).

Why the need for several actin-bundling factors of, a priori, redundant function? Early studies on the formation of Drosophila neurosensory bristles, long curved protrusions containing multiple parallel actin bundles, showed that cells assemble parallel actin bundles through the sequential activity of Forked and Fascin: actin filaments are first loosely packed together by Forked, then maximally cross-linked by Fascin (Tilney *et al.*, 1998). The sequential model extends to all known parallel actin bundles and provides sensible explanation for the need of two or more cross-linking factors. According to this model, actin filaments are first packed into a loose bundle through the activity of an early actin-bundling factor – generally a large protein with relatively distant actin-binding sites - facilitating the entry of a second actin-bundling factor – generally smaller with close tandem actin-binding sites - capable of packing bundles into a tighter hexagonal structure (Fig.7). In line with Tilney's idea, the bundling-based organization of actin filaments depends on the concentration of the actin-bundling factor expressed by

the cell. The distinct actin-binding activities and regulation properties of the different actin-bundling factors combined to their level of expression allows the proper development of the parallel actin bundle according to a specific sequence of events. Notably, the second actin-bundling factor should theoretically show a somewhat weak actin-binding activity in order to enable cross-links to come and go until maximal three-dimensional packing is achieved. There was, before my PhD work, no study investigating the expression of actin-bundling factors in CSF-cNs.

Attachment of the actin filaments to the tip and lateral membranes. A critical feature of microvilli is the lateral attachment of actin filaments to the membrane in order to ensure resistance of the structure and mechanical tension. Factors capable of binding both actin cytoskeleton and membrane components, often lipids such as phosphatidyl-inositol 4,5-biphosphate, form ultrastructural links. In microvilli, unconventional myosins and ezrin/radixin/moesin, also referred to as the ERM proteins, are the main factors responsible for the tethering of the parallel actin bundle actin core to the membrane (Sauvanet *et al.*, 2015). Myosins simultaneously bind lipids of the plasma membrane and F-actin through, respectively, their C-terminal domain and motor head domain. Similarly, ERM proteins contain an N-terminal FERM domain to bind lipids of the membrane and a C-terminal ERM-association domain to bind F-actin (Sauvanet *et al.*, 2015). ERM proteins show clear tissue expression specificity as well as polarized activity within the cells where they are found dormant in the cytosplasm and active at the apical surface and/or microvilli. ERM proteins are first recruited, through their FERM domain, to apical membranes, where they are activated by phosphorylation, which unmasks their C-terminal ERM-association domain domain to facilitate actin anchoring (Sauvanet *et al.*, 2015).

iHC stereocilia contain various unconventional myosins present at different location along the parallel actin bundle: Myosin-III, Myosin-VII, Myosin-XV at the tip, and Myosin-VI at the base (Rzadzinska *et al.*, 2004; Michalski and Petit, 2015). All four myosins interact with several other factors to form distinct molecular complexes capable of tethering actin filaments to the membrane and support the stiffness of the hair bundle. Because of their motor domain, myosins are also involved in trafficking along actin filaments, which enables the complexes to transport proteins or 'cargos' along the stereocilia. The Myosin-III complex promotes stereocilia growth by addressing the actin-bundling factor Espin-1 (see III.B) to the tip of the bundles. The Myosin-VII and Myosin-XV complexes transport ABPs to the tip as well, such as the actin-capping twinfilin-2 or gelsolin (Fig.6), which regulate actin assembly/disassembly rates. As a consequence, the myosin-based complexes appear to play a critical role in the regulation of stereocilia lengthening. Finally, because of the backward-stepping motor activity of myosin-VI, the associated complex involving the ERM radixin protein remains located at the base of the stereocilia, seemingly helping to stabilize the structure (Michalski and Petit, 2015). Radixin is the only ERM protein detected in iHC stereocilia.

The large body of work devoted to iHC stereocilia development highlighted the dual role of unconventional myosins that not only ensure proper structural resistance but also greatly participate to the regulation of the parallel actin bundle lengthening through their motor function. Cargo trafficking within the actin-based protrusions is instrumental to address specific ABPs responsible for the parallel actin bundle proper development. In iHCs, any mutation or loss of function of unconventional myosins results in stereocilia length defects and hearing impairments (Michalski and Petit, 2015).
Although not yet investigated in other MSCs, the expression of specific unconventional myosins and members of the ERM family is likely required to support the assembly and elongation of microvilliated apical extensions. In particular, unconventional myosins play an important part in the entry of the second actin-bundling factor at a specific time, to the proper location and at the right concentration in the sequential model of parallel actin bundle assembly.

Higher-order structure: the stereocilia. Short modules generated by the bundling cell factory can get secondarily assembled into larger and/or more complex bundles according to a specific organization as it is the case for the iHC stereocilia (DeRosier and Tilney, 2000). During iHC differentiation, stereocilia first appear as short microvilli at the apical surface due to the actin-bundling activity of fimbrin. The transformation into stiff mature stereocilia involves the tighter packing of the parallel actin bundle together with newly added filaments to eventually form a paracrystalline array and a second step of elongation to achieve the staircase pattern (Tilney, Tilney and Derosier, 1992). This transformation is achieved through the collaborative functions of unconventional myosins and the actin-bundling factor Espin. Myosin-XV and Myosin-III isoforms are critical for this transformation. Myosin-XV complex promotes the elongation of the original bundle modules by addressing several ABPs to the stereocilia tips (Rzadzinska *et al.*, 2004; McGrath, Roy and Perrin, 2017). Myosin-IIIA and B transport their cargo Espin to the tips as well and enable actin elongation and cross-linking involved in further lengthening and widening (see below) (Ebrahim *et al.*, 2016; McGrath, Roy and Perrin, 2017). More recent data *in vitro* and in zebrafish iHCs has suggested that Fascin2, another actin-bundling factor, could be involved as well: the tight packing of numerous actin filaments to eventually form the thick bundle of stereocilia requires the coordination of Fascin2 and Espin (Chou *et al.*, 2011). To conclude, the formation of stereocilia involves a fine orchestration of actin-bundling factors allowed by their precise regulation and addressing. Fimbrin is recruited first to produce the loose bundle modules later assembled and elongated to form the higher order structure of the stereocilium by Espin and Fascin2.

One key step towards the transformation of bundle modules into stereocilia is the prominent tapering of actin filaments at the junction with the apical cell surface (Fig.1,2). The taper comes as a result of distinct behaviors between core filaments and surrounding ones: only the most central actin filaments project into the iHC cell body

while other filaments terminate at the taper. This structural property is essential to hearing function as it allows bending to occur at the level of the taper while preventing it at higher position (Fig.2). There is, to date, no description of the mechanism underlying the tapering of stereocilia during the development of the iHC apical extension although Fascin2 was proposed as a candidate to facilitate actin depolymerization specifically in the taper region (Chou *et al.*, 2011).

It is important here to remember that actin filaments remain highly dynamic structures even when constituting stable protrusions such as microvilli. As reviewed above (see II.C), the stable state of the actin-bundle-based protrusions is the result of the treadmilling of actin through filaments (Rzadzinska *et al.*, 2004). Different parallel actin bundles show different treadmilling rates with values 10 to 100 times lower in stereocilia than microvilli, mostly due to the stabilization of stereocilia by numerous actin cross-linking proteins (McGrath, Roy and Perrin, 2017). The dynamic steady-state of actin filaments in the parallel actin bundles is assisted by the force produced by myosins between the paracrystalline actin core and membranes.

B. Espin, an actin-bundling factor common to all microvilliated sensory cells

As nicely illustrated by the staircase pattern of iHC stereocilia, the length of the parallel actin bundle is precisely regulated. The regulation of parallel actin bundle lengthening is, in part, achieved by the type and concentration of the actin-bundling factors expressed by the cell. In the previous section, we mentioned that MSCs express a combination of actin-bundling factors in order to orchestrate the development of their microvilliated apical extension (Fig.1). This feature, in accordance with the sequential model of formation of the parallel actin bundle, is shared by all cells extending protrusions based on actin bundles, including filopodia. One striking characteristic that seems to distinguish the making of filopodia from microvilli is the presence of Espin proteins in microvilliated cells. Bartles and his group have provided a great body of work demonstrating the expression at high levels of Espins by all MSCs and their relevance for their sensory function.

Espins and their activities. Espins are the most recently identified members of the actin-bundling factor group from which they differ significantly because of their capacity to interact with numerous partners. The first Espin isoform was described two decades ago to localize at the thin layer of parallel actin bundles of the junctional plaque formed by Sertoli cells in rat testis (Bartles, Wierda and Zheng, 1996). Espins get their name from this peculiar location: espin = ectoplasmic specialization –in. More isoforms were later discovered in the brush border microvilli (Bartles *et al.*, 1998), iHC stereocilia (Zheng *et al.*, 2000; Li *et al.*, 2004) and Purkinje cell dendritic spines (Sekerková *et al.*, 2003). The analysis of the complete sequence of the *espin* gene derived from mouse genomic DNA

showed that the four different isoforms arise from a single gene through different transcription start sites (Chen *et al.*, 1999). Eventually, thorough investigations demonstrated that Espin is in all known MSCs (Sekerková *et al.*, 2004). This result obtained in rat and mouse tissues is confirmed by my own observations in zebrafish: all MSCs present at three days post-fertilization (dpf) are labeled for Espin immunostaining, namely: ORNs, CSF-cNs and iHCs of the inner ear and the lateral line (Fig.8). Espin is also detected from 5 dpf in taste buds (*data not shown*).

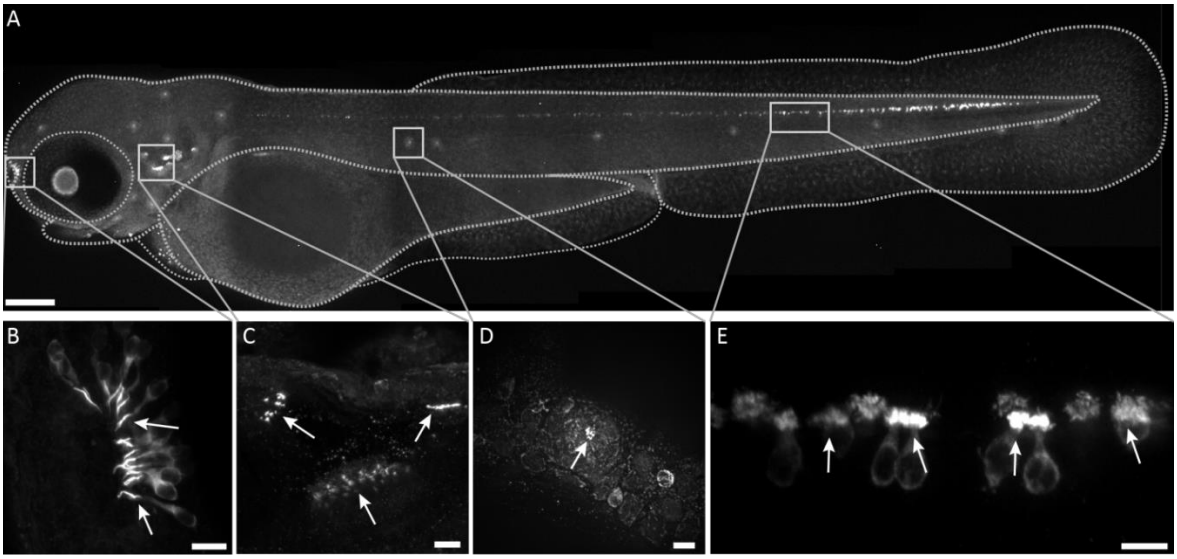

Figure 8. Espin is expressed in all microvilliated sensory cell types present at 3 days post-fertilization in zebrafish (unpublished data)
A, Immunohistochemistry using the rabbit polyclonal antibody against all Espin isoforms (Bartles, Wierda and Zheng, 1996) was performed on whole-mount zebrafish 3 days post-fertilization larvae. Scale bar, 100 µm.
Espin is enriched at the apical extension of olfactory receptor neurons in the olfactory pit (**B**), hair cells in the inner ear (**C**), hair cells of neuromasts (**D**) and CSF-cNs (**E**). Arrows point towards few apical extensions in each example. Scale bars, 10 µm.

Espins were characterized to contain a variety of domains for protein-protein interactions from their very first description. All Espin isoforms contain a 116-amino acid C-terminal conserved actin-bundling module showing 39% identity with a peptide in the Drosophila Forked protein responsible for the formation of parallel actin bundles in bristles (Bartles, Wierda and Zheng, 1996; Bartles *et al.*, 1998; Chen *et al.*, 1999). The actin-bundling module includes at least two F-actin-binding sites and is necessary and sufficient for the Espin-mediated actin-bundling and parallel actin bundle elongation activities *in vitro* and *in vivo* (Bartles, Wierda and Zheng, 1996; Bartles *et al.*, 1998; Loomis *et al.*, 2003). All known Espin isoforms also display a WH2 G-actin-binding domain right upstream of the actin-bundling module, a domain capable of locally increasing G-actin concentration and, thus, enhancing Espin activities (Sekerková *et al.*, 2004; Loomis *et al.*, 2006). The different isoforms then differ in their N-terminal part (Fig.9) (Sekerková *et al.*, 2006). All three isoforms 2, 3 and 4 exhibit a shorter N-terminal region than the longest isoform 1 and, thus, fewer domains. The N-terminal domains are

involved in protein-protein interactions and explain the capacity of Espins to interact with numerous factors. The presence of these domains greatly influences the Espin-mediated bundling activity as suggested by the formation of fewer but thicker parallel actin bundles by the long isoforms (1, 2A and 3B) as opposed to more but thinner microvilli by small Espin (isoform 4) (Loomis *et al.*, 2003). The N-terminal region can include ankyrin-like repeats, an additional F-actin-binding site, a binding site for phosphatidyl-inositol 4,5-biphosphate and one or two proline-rich regions (Fig.9). The ankyrin repeat module is only present in isoform 1 and can bind to the tail homology domain I of Myosin-III paralogs A and B (Salles *et al.*, 2009; Liu *et al.*, 2016). The proline-rich regions enable Espins to bind actin organizers, especially profilin (see II.C) (Bartles, Wierda and Zheng, 1996; Bartles *et al.*, 1998; Chen *et al.*, 1999), and to enhance the recruitment of actin monomers by the WH2 domain. When both proline-rich regions are present, they also allow interactions with SH3-containing factors such as IRSp53 (see III.A) (Sekerková *et al.*, 2003).

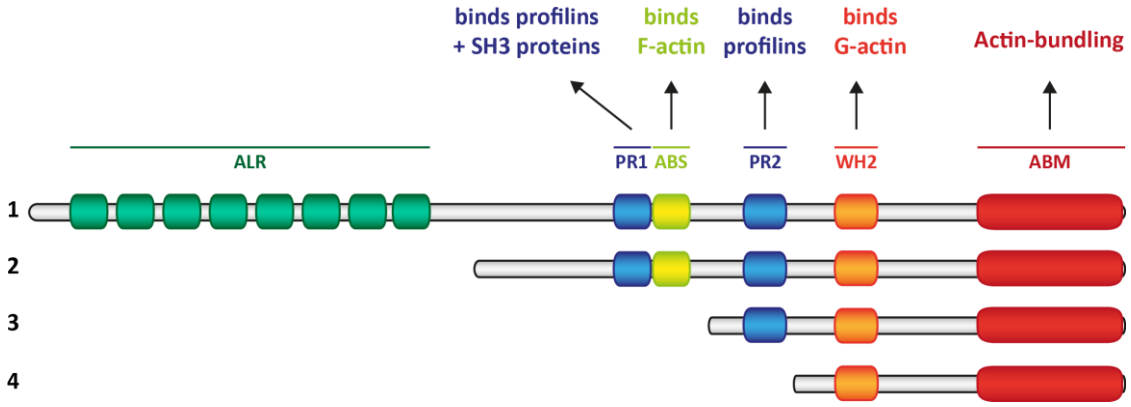

Figure 9. Espin isoforms and their relative functional domains (adapted from (Sekerková *et al.*, 2006))
Stick-figure diagrams representative of the four Espin isoforms. The four isoforms share a conserved actin-bundling module (ABM) and a conserved WH2 domain responsible for the potent Ca^{2+}-resistant bundling activity and parallel actin bundle elongation of Espins. The length of their N-terminal part varies according to different transcription start sites and includes several other functional modules. The proline-rich peptides (PR1, PR2) enable Espins to bind profilins and the presence of the N-terminal PR1 especially enables them to bind SH3-containing proteins such as IRSp53. The longest isoforms 1 and 2 include an additional F-actin-binding site (ABS). And the isoform 1 displays a region with 10 ankyrin-like repeats (ALR), a module capable of binding the tail-homology domain I of myosin-III paralogs A and B.
Isoforms of the type 3 are especially found in microvilliated sensory cells (Sekerková *et al.*, 2004).

Like other actin-bundling factors, the actin-bundling activity of Espins depends on their concentration (Loomis *et al.*, 2003). This characteristic is very nicely illustrated by the positive correlation between the gradual increase in stereocilia length along the basilar membrane in the cochlear spiral and Espin levels in iHCs (Loomis *et al.*, 2003).

Espins in stereocilia. The third Espin isoform to be identified was found in iHC stereocilia (Zheng *et al.*, 2000). This isoform, referred to as the isoform 3, is of intermediate length between the isoform 1 in Sertoli cell's ectoplasmic specialization and the isoform 4 in the brush border microvilli (Fig.9). Its N-terminal region starts upstream of the first

proline-rich peptide, missing the ankyrin-like repeats. The identification of Espin expression in stereociliated iHCs motivated the investigation of related candidate deafness genes mapping to the *espin* gene. A spontaneous recessive autosomal mutation, called *jerker* mutation (Grüneberg, Burnett and Snell, 1941) was found to be related to a frameshift mutation in the conserved actin-bundling module, leading to truncated Espin proteins for all isoforms (Zheng *et al.*, 2000). As a result, *jerker* homozygote mice showed no or strongly reduced level of Espin protein in testis, kidney and HCs. iHCs in mice bearing the *jerker* mutation at the homozygous state first develop normally but quickly degenerate at the onset of hearing function (Grüneberg, Burnett and Snell, 1941). The degeneration of iHCs follows the one of stereocilia that first appear as abnormally short, and then loosen and shrink before the cell itself disappears. A more detailed structural analysis of the developmental effects of the loss of Espins in iHCs showed that the *jerker* mutation was associated with, in general, much thinner and much shorter stereocilia (Sekerková, Richter and Bartles, 2011). The *jerker* phenotype is characterized by complete deafness, head-jerking movements and circling movement reflecting defects in iHCs in the cochlea and the vestibular system respectively. This correlation between the loss of Espin function and stereocilia defects resulting in the *jerker* phenotype strongly suggested that Espin actin-bundling activity is critical for the formation and maintenance of stereocilia. The causative role of Espins in non-syndromic hearing loss was also supported by the identification of mutations in the *espin* gene associated with human cases of deafness (Donaudy *et al.*, 2006).

Further investigation later showed that, actually, other Espin isoforms are expressed in iHCs in the inner ear and that their spatio-temporal expression is precisely regulated during development (Sekerková *et al.*, 2006). In adulthood, mature iHCs mainly express the isoform 1 along with lower levels of isoforms 3 and 4 at their stereocilia (Sekerková *et al.*, 2004). At the embryonic stage, however, the isoforms 2 and 3 are predominant and it is only at late embryonic stages that levels of isoform 2 decrease concomitantly with the increase in isoforms 3 and the apparition of isoform 1. Then, the postnatal phase of stereocilia maturation is associated with a dramatic increase in isoform 1 and the apparition of isoform 4, a finding consistent with the proposed role of Espins in stereocilia elongation (Loomis *et al.*, 2003; Sekerková *et al.*, 2006). As opposed to isoforms 3 and 4 present all along the parallel actin bundle, isoform 1 is specifically located at the tip of stereocilia according to a tip-to-base gradient following the one of Myosin-IIIA. The tip localization of Espin-1 results of its transport by the unconventional Myosin-IIIA through the interaction between the Espin ankyrin-like domain and the myosin tail homology domain I (Salles *et al.*, 2009; Liu *et al.*, 2016). Interestingly, Espin-1 also interacts with Myosin-IIIB, for which it serves as a 'crutch'. The presence of numerous actin-binding sites in Espin-1, especially at the actin-bundling module, compensates for the missing actin-binding domain of Myosin-IIIB and helps its migration to stereocilia tips (Merritt *et al.*, 2012). Both Myosin-IIIA and B then enhance Espin WH2-

mediated elongation activity at the barbed end of actin filaments to promote parallel actin bundle lengthening and actin-bundling activity (Liu *et al.*, 2016).
These observations demonstrate that the formation of the microvilliated apical extension of MSCs, here the hair bundle of iHCs, can involve a particularly complex spatiotemporal pattern of expression of the different Espin isoforms, which can be orchestrated by protein-protein interactions. It furthermore highlights the fine control of parallel actin bundle width and length by the synergistic activities of Espins with other ABPs such as unconventional myosins. Altogether, these results bring more evidence to support the critical role of Espins in the formation and maintenance of iHC stereocilia and suggest that distinct Espin isoforms can fulfill different functions.

So, why Espins? The expression of Espins can be considered as a landmark of MSCs where they are found especially enriched at the level of the microvilliated apical extension (Sekerková *et al.*, 2004). Compared to other microvilliated cells, the presence of Espins in MSCs is associated with longer microvilli in average, constituting the sensory apical extension displaying various size and organization and where sensory transduction takes place as opposed to shorter microvilli as in the brush border of the gut. What advantage does the presence of Espins confer to MSCs? Altogether, the detailed studies about Espins' functions highlighted a number of biological activities that distinguish them from other actin-bundling factors (Sekerková *et al.*, 2006). First, Espins show 10 to 100-fold higher affinity to bind G-actin and more efficient actin-bundling activity (Chen *et al.*, 1999). The great potency of Espins to promote the formation of large parallel actin bundles is related to the unique combination of multiple F-actin binding sites and the WH2 domain which, together, ensure the availability of actin monomers at the right location, and further elongation and cross-linking of actin filaments (Loomis *et al.*, 2006). In addition, a singularity of Espins among other actin-bundling factors lies in the fact that their actin-bundling activity is not inhibited by Ca^{2+} (Bartles *et al.*, 1998; Chen *et al.*, 1999). The resistance of Espins to Ca^{2+} is instrumental to the maintenance of the parallel actin bundle-based structures in MSCs while experiencing big calcium transients during sensory transduction. One can also argue that the same logic applies to Purkinje Cells that express isoforms 3 of Espin since they are actually subject to some of the largest transients in the brain. Beyond providing Ca^{2+}-resistant cross-links, transfection studies in cultured epithelial cells showed that Espins dramatically increase the steady-state length of parallel actin bundles. Espins enhance actin assembly at the barbed end of the filaments in a concentration-dependent fashion (Loomis *et al.*, 2003; Rzadzinska *et al.*, 2004), another unique feature compared to other actin-bundling factors.

Espins thus appear as essential actin-bundling factors to support and orchestrate the formation of the parallel actin bundle-based sensory microvilli. The special link between Espins and MSCs, exemplified by iHCs, can be partly explained by the unique features of

Espin isoforms that make them suited actin-bundling factors to build sensory apical extensions. Although many of the best characterized properties of Espins stem from their actin-bundling module, it is likely that there is still much to be learned. Especially, additional features associated to the N-terminal domains remain to be investigated to better understand how Espin activities are regulated in both temporal and spatial manners, at the subcellular level or between different cell types.

C. Diversity in unity

All MSCs detect chemical or mechanical stimuli through parallel actin bundle-based membrane protrusions: microvilli or, in the case of iHCs, derivatives of microvilli, stereocilia. It is commonly admitted that the microvilliated apical extension is instrumental to the MSC sensory function. Because MSCs carry out a diversity of sensory modalities, they must develop sensory apical extensions that are suited to detect stimuli and enable sensory transduction under the environmental constraints the cell is subject to (Table1, Fig1 and I.A). However, thorough structural investigations have been missing for MSCs other than iHCs.

In chick HCs, the grounding work of Tilney and collaborators described that stereocilia could contain up to 900 actin filaments and vary in length between 1.5 and 5.5 µm (Tilney, Tilney and Derosier, 1992). This study also showed that the number of stereocilia per iHC depended on the cell position along the basilar membrane in the cochlea: iHCs at the proximal end could form up to 450 stereocilia, ten times more than iHCs at the distal end. These numbers can of course vary depending on the species (Fig.1).
The presence, and succinct description, of microvilli in other MSCs was documented by structural studies of sensory organs using electronic microscopy.
The different cell types in taste buds possess distinct microvilliated apical extensions: in rabbit, the predominant Type I cells, first referred to as ‘dark cells’ because of their electron-dense cytoplasm, display a tuft of long thin microvilli of various length (1-2 µm) and width (0.5-2 µm), while Type II cells or TRCs, formerly referred to as ‘light cells’, extend uniform short microvilli (1 µm long and 0.25 µm wide) (Murray and Murray, 1967; Cummings, Delay and Roper, 1987). In *Necturus maculosus*, Type III cells, a minor population described later, appear to end bluntly in a single thick apical microvillus within the taste bud’s pore (Fig.1) (Cummings, Delay and Roper, 1987).
In rat, vORNs were described to extend a knob of short (2 µm) and thin (40 – 100 nm) microvilli at the end of a long dendritic process (Fig.1) (Ciges *et al.*, 1977; Höfer, Shin and Drenckhahn, 2000).
The unusual morphology of CSF-cNs projecting an apical extension in the lumen of the central canal raised questions on their sensory functions (Kolmer, 1921; Agduhr, 1922). Few ultrastructural studies have provided information about their ultrastructure. In Xenopus, spinal CSF-cNs are notably distinguished from surrounding ependymal cells by the extension of short (4 µm) and thin (0.114 µm) microvilli among which a cilium

emerges (Dale *et al.*, 1987). This morphology has been described in spinal CSF-cNs of many vertebrate species (Vigh and Vigh-Teichmann, 1973; Vigh *et al.*, 1983) although the presence of a cilium is a source of debate. CSF-cN morphology recalls the one of vORNs, bearing a microvilliated apical extension and projecting a basal axon into the CNS.

It is increasingly evident that the sensory apical extension of MSCs owes many of its properties to the parallel actin bundle's characteristics which reflect the spatiotemporal pattern of activity of a combination of actin-bundling factors. As a consequence, it is no surprise that microvilliated apical extensions vary in size, shape, organization, in order to support the distinct sensory functions carried by MSCs. The formation of the parallel actin bundle follows a sequential model where the different actin-bundling activities are orchestrated to enable the thickening and lengthening of the bundle. Consequently, mutations or loss of function of one of the actin-bundling factors result in different structural phenotypes. There are three major actin-bundling factor classes described in MSCs: Fimbrin, Villin and Espin (Fig.1). The previous section highlighted the great functions of Espins in the formation of the sophisticated hair bundle of iHCs, functions that could be similarly relevant to other MSCs. The existence of multiple Espin isoforms and their cooperation with other actin-bundling factors in the process of parallel actin bundling might, in part, explain how MSCs can develop a diversity of apical extensions. In an attempt to explain the different shapes of apical extension formed by MSCs, we could assume a model where Fimbrin and Villin would be involved in the formation of the short bundle modules, in a generic fashion, while Espins and their interaction with other ABPs would refine the organization of actin filaments to eventually produce a parallel actin bundle of the proper length and width, with a given stability.

The microvilliated apical extensions of MSCs other than iHCs do not display the same obvious high-order organization showed by the hair bundle but, rather, 'simpler' parallel actin bundle-based protrusions. One might assume that, as opposed to the formation of stereocilia characterized by a second phase of extensive elongation and bundling, the sensory organelle of TRCs, vORNs and CSF-cNs is constituted of microvilli directly generated by the actin-bundling cell factory (see III.A) without extensive subsequent structuring. Evidence to support this hypothesis is however difficult to provide with the current understanding of the ultrastructure of these apical extensions, their development and the molecular factors they involve.

OPEN QUESTIONS

Microvilliated sensory cells are sensory cells that detect chemical or mechanical stimuli through their microvilliated sensory organelle, an apical extension constituted of thin actin-based protrusions. The core component of microvilli is the parallel actin bundle, a group of actin filaments tightly packed into a hexagonal structure. The final length, width and shape of the parallel actin bundle are probably important to determine the sensory properties of the apical extension. As a consequence, the establishment of this structure must be precisely regulated and orchestrated. Our current understanding involves two critical steps in the making of parallel actin bundles in microvilli: the initiation of short bundle modules and their subsequent packing into a functional structure. This bundle factory relies on the dynamics of the actin cytoskeleton and its numerous organizers, the actin-binding proteins. The organization of actin filaments into bundles is enabled by specific proteins, actin-bundling factors. The expression of Espins, a family of actin-bundling factors, notably constitutes a landmark of microvilli in MSCs.

Most of what we know in vertebrates comes from thorough investigations of the hair bundle in hair cells. As opposed to other MSCs, hair cells display a microvilliated apical extension with an obvious stereotyped organization with rows of stereocilia of increasing height, which explains the great interest this particular cell type aroused. A large body of work unraveled a list of molecular factors involved in the morphogenesis of the hair bundle, supported by the description of mutations responsible for deafness in human patients and/or animal models (Michalski and Petit, 2015).

Still, many questions remain. One of the concerns is how actin filaments are nucleated at the initiation step. There is, up-to-now, no good candidate molecular mechanism to explain early steps of microvilli formation at the apical side to give rise to the future apical extensions. In order to occur at the right subcellular location, the initiation step has to be somehow interconnected to cell polarity which is, in turn, interconnected to the establishment of apical junctional complexes. How polarity factors and cell-cell contacts interplay with the emergence of the actin protrusions forming the apical extension remains unexplored. Although numerous actin-binding factors, especially Espins and their partners, have been involved in the formation of stereocilia, their specific role and sequence of intervention in other MSC types remains to be clarified and integrated. Finally, the precise role of microvilli structure in sensory function have been generalized in different types of MSCs but not investigated.

During my PhD, I investigated in vivo *the molecular mechanisms underlying the elaboration of the MSC microvilliated apical extension, focusing on CSF-cNs in the zebrafish spinal cord.*

References

Adato, A. *et al.* (2005) 'Interactions in the network of Usher syndrome type 1 proteins', *Human Molecular Genetics*, 14(3), pp. 347–356. doi: 10.1093/hmg/ddi031.

Agduhr, E. (1922) 'Über ein zentrales Sinnesorgan (?) bei den Vertebraten.', *Zeitschrift für Anatomie und Entwicklungsgeschichte*, 66, pp. 223–360. doi: 10.1007/BF02593586.

Ahmed, S., Goh, W. I. and Bu, W. (2010) 'I-BAR domains, IRSp53 and filopodium formation', *Seminars in Cell and Developmental Biology*. Elsevier Ltd, 21(4), pp. 350–356. doi: 10.1016/j.semcdb.2009.11.008.

Ahmed, Z. M. *et al.* (2006) 'The Tip-Link Antigen, a Protein Associated with the Transduction Complex of Sensory Hair Cells, Is Protocadherin-15', *Journal of Neuroscience*, 26(26), pp. 7022–7034. doi: 10.1523/JNEUROSCI.1163-06.2006.

Alberts, B. *et al.* (2014) *Molecular Biology of the Cell (6th edition)*.

Assad, J. A., Shepherd, G. M. G. and Corey, D. P. (1991) 'Tip-link integrity and mechanical transduction in vertebrate hair cells', *Neuron*, 7(6), pp. 985–994. doi: 10.1016/0896-6273(91)90343-X.

Barr-Gillespie, P.-G. (2015) 'Assembly of hair bundles, an amazing problem for cell biology', *Molecular Biology of the Cell*, 26(15), pp. 2727–2732. doi: 10.1091/mbc.E14-04-0940.

Bartles, J. R. *et al.* (1998) 'Small Espin: A third Actin-bundling Protein and Potential Forked Protein Ortholog in Brush Border Microvilli', *Journal of Cell Biology*, 143(1), pp. 107–119. doi: 10.1083/jcb.143.1.107.

Bartles, J. R. (2000) 'Parallel actin bundles and their multiple actin-bundling proteins', *Current Opinion in Cell Biology*, 12, pp. 72–78. doi: 10.1016/S0955-0674(99)00059-9.

Bartles, J. R., Wierda, A. and Zheng, L. (1996) 'Identification and characterization of espin, an actin-binding protein localized to the F-actin-rich junctional plaques of Sertoli cell ectoplasmic specializations', *Journal of cell science*, 109, pp. 1229–1239.

Boëda, B. *et al.* (2002) 'Myosin VIIa, harmonin and cadherin 23, three Usher I gene products that cooperate to shape the sensory hair cell bundle', *EMBO Journal*, 21(24), pp. 6689–6699. doi: 10.1093/emboj/cdf689.

Böhm, U. L. *et al.* (2016) 'CSF-contacting neurons regulate locomotion by relaying mechanical stimuli to spinal circuits', *Nature Communications*, 7:10866, pp. 1–8. doi: 10.1038/ncomms10866.

Böhm, U. L. (2016) *Physiological inputs to cerebrospinal fluid-contacting neurons*.

Buck, L. B. (2000) 'The Molecular Architecture Odor and Pheromone Sensing in Mammals', *Cell*, 100, pp. 611–618. doi: 10.1016/S0092-8674(00)80698-4.

Bushman, J. D., Ye, W. and Liman, E. R. (2015) 'A proton current associated with sour taste: Distribution and functional properties', *FASEB Journal*, 29(7), pp. 3014–3026. doi: 10.1096/fj.14-265694.

Caberlotto, E. *et al.* (2011) 'Usher type 1G protein sans is a critical component of the tip-link complex, a structure controlling actin polymerization in stereocilia', *Proceedings of the National Academy of Sciences*, 108(14), pp. 5825–5830. doi: 10.1073/pnas.1017114108.

Campanale, J. P., Sun, T. Y. and Montell, D. J. (2017) 'Development and dynamics of cell polarity at a glance', *Journal of Cell Science*, 130(7), pp. 1201–1207. doi: 10.1242/jcs.188599.

Carleton, A., Accolla, R. and Simon, S. A. (2010) 'Coding in the mammalian gustatory system', *Trends in Neurosciences*. Elsevier Ltd, 33(7), pp. 326–334. doi: 10.1016/j.tins.2010.04.002.

Chacon-Heszele, M. F. *et al.* (2012) 'Regulation of cochlear convergent extension by the vertebrate planar cell polarity pathway is dependent on p120-catenin', *Development*, 139(5), pp. 968–978. doi: 10.1242/dev.065326.

Chandrashekar, J. *et al.* (2000) 'T2Rs Function as Bitter Taste Receptors', *Cell*, 100, pp. 703–711. doi: 10.1016/S0092-8674(00)80706-0.

Chandrashekar, J. *et al.* (2006) 'The receptors and cells for mammalian taste', *Nature*, 444(7117), pp. 288–294. doi: 10.1038/nature05401.

Chang, R. B., Waters, H. and Liman, E. R. (2010) 'A proton current drives action potentials in genetically identified sour taste cells', *Proceedings of the National Academy of Sciences*, 107(51), pp. 22320–22325. doi: 10.1073/pnas.1013664107.

Chaudhari, N. and Roper, S. D. (2010) 'The cell biology of taste', *Journal of Cell Biology*, 190(3), pp. 285–296. doi: 10.1083/jcb.201003144.

Chen, B. *et al.* (1999) 'Espin contains an additional actin-binding site in its N terminus and is a major actin-bundling protein of the Sertoli cell-spermatid ectoplasmic specialization junctional plaque', *Molecular biology of the cell*, 10(12), pp. 4327–39. doi: 10.1091/mbc.10.12.4327.

Chhabra, E. S. and Higgs, H. N. (2007) 'The many faces of actin: matching assembly factors with cellular structures', *Nature Cell Biology*, 9(10), pp. 1110–1121. doi: 10.1038/ncb1007-1110.

Chou, S.-W. *et al.* (2011) 'Fascin 2b is a component of stereocilia that lengthens actin-based protrusions', *PLoS ONE*, 6(4). doi: 10.1371/journal.pone.0014807.

Ciges, M. *et al.* (1977) 'Ultrastructure of the organ of Jacobson and comparative study with olfactory mucosa', *Acta Otolaryngol*, 83, pp. 47–58.

Cui, C. *et al.* (2011) 'Disruption of Mks1 localization to the mother centriole causes cilia defects and developmental malformations in Meckel-Gruber syndrome', *Disease Models & Mechanisms*, 4(1), pp. 43–56. doi: 10.1242/dmm.006262.

Cummings, T. A., Delay, R. J. and Roper, S. D. (1987) 'Ultrastructure of apical specializations of taste cells in the mudpuppy Necturus maculosus', *Journal of Comparative Neurology*, 261, pp. 604–615. doi: 10.1002/cne.902770208.

Dale, N. *et al.* (1987) 'The morphology and distribution of "Kolmer-Agduhr cells", a class of cerebrospinal-fluid-contacting neurons revealed in the frog embryo spinal cord by GABA immunocytochemistry', *Proc. R. Soc. Lond.*, B232, pp. 193–203.

DeRosier, D. J. and Tilney, L. G. (2000) 'F-Actin Bundles Are Derivatives of Microvilli: What Does This Tell Us about How Bundles Might Form?', *Journal of Cell Biology*, 148(1), pp. 1–6. doi: 10.1083/jcb.148.1.1.

Djenoune, L. *et al.* (2014) 'Investigation of spinal cerebrospinal fluid-contacting neurons expressing PKD2L1: evidence for a conserved system from fish to primates', *Frontiers in Neuroanatomy*, 8(26). doi: 10.3389/fnana.2014.00026.

Djenoune, L. and Wyart, C. (2017) 'Light on a sensory interface linking the cerebrospinal fluid to motor circuits in vertebrates', *Journal of Neurogenetics*. Informa UK Limited, trading as Taylor & Francis Group, 31(3), pp. 113–127. doi: 10.1080/01677063.2017.1359833.

Donaudy, F. *et al.* (2006) 'Espin gene (ESPN) mutations associated with autosomal dominant hearing loss cause defects in microvillar elongation or organisation', *Journal of Medical Genetics*, 43, pp. 157–161. doi: 10.1136/jmg.2005.032086.

Dulac, C. (2000) 'Sensory coding of pheromone signals in mammals', *Current Opinion in Neurobiology*, 10(4), pp. 511–518. doi: 10.1016/S0959-4388(00)00121-5.

Dulac, C. and Axel, R. (1995) 'A novel family of genes encoding putative pheromone receptors in mammals', *Cell*, 83(2), pp. 195–206. doi: 0092-8674(95)90161-2 [pii].

Dvoryanchikov, G. *et al.* (2011) 'GABA, Its Receptors, and GABAergic Inhibition in Mouse Taste Buds', *Journal of Neuroscience*, 31(15), pp. 5782–5791. doi: 10.1523/JNEUROSCI.5559-10.2011.

Ebrahim, S. *et al.* (2016) 'Stereocilia-staircase spacing is influenced by myosin III motors and their cargos espin-1 and espin-like', *Nature Communications*, 7:10833. doi: 10.1038/ncomms10833.

Ezan, J. *et al.* (2013) 'Primary cilium migration depends on G-protein signalling control of subapical cytoskeleton', *Nature Cell Biology*. Nature Publishing Group, 15(9), pp. 1107–1115. doi: 10.1038/ncb2819.

Ezan, J. and Montcouquiol, M. (2013) 'Revisiting planar cell polarity in the inner ear', *Seminars in Cell and Developmental Biology*. Elsevier Ltd, 24(5), pp. 499–506. doi: 10.1016/j.semcdb.2013.03.012.

Faix, J. and Rottner, K. (2006) 'The making of filopodia', *Current Opinion in Cell Biology*, 18, pp. 18–25. doi: 10.1016/j.ceb.2005.11.002.

Fame, R. M. *et al.* (2016) 'Directional cerebrospinal fluid movement between brain ventricles in larval zebrafish', *Fluids and Barriers of the CNS*. BioMed Central, 13(11). doi: 10.1186/s12987-016-0036-z.

Fanning, A. S. *et al.* (1998) 'The Tight Junction Protein ZO-1 Establishes a Link between the Transmembrane Protein Occludin and the Actin Cytoskeleton', *The journal of biological chemistry*, 273(45), pp. 29745–29753. doi: 10.1074/jbc.273.45.29745.

Fanning, A. S. and Anderson, J. M. (2009) 'Zonula Occludens-1 and -2 are cytosolic scaffolds that Regulate the Assembly of Cellular Junctions', *Ann N Y Acad Sci*, pp. 113–120. doi: 10.1111/j.1749-6632.2009.04440.x.Zonula.

Ferrero, D. M. *et al.* (2013) 'A juvenile mouse pheromone inhibits sexual behaviour through the vomeronasal system', *Nature*. Nature Publishing Group, 502(7471), pp. 368–371. doi: 10.1038/nature12579.

Fidelin, K. *et al.* (2015) 'State-Dependent Modulation of Locomotion by GABAergic Spinal Sensory Neurons', *Current Biology*. Elsevier, 25(23), pp. 3035–3047. doi: 10.1016/j.cub.2015.09.070.

Frings, S. (2009) 'Primary processes in sensory cells: Current advances', *Journal of Comparative Physiology A*, 195(1), pp. 1–19. doi: 10.1007/s00359-008-0389-0.

Ghysen, A. and Dambly-Chaudière, C. (2004) 'Development of the zebrafish lateral line', *Current Opinion in Neurobiology*, 14(1), pp. 67–73. doi: 10.1016/j.conb.2004.01.012.

Gilbertson, T. A. *et al.* (2001) 'Distribution of gustatory sensitivities in rat taste cells: whole-cell responses to apical chemical stimulation.', *The Journal of neuroscience*, 21(13), pp. 4931–4941. doi: 21/13/4931 [pii].

Glowatzki, E., Grant, L. and Fuchs, P. (2008) 'Hair cell afferent synapses', *Current Opinion in Neurobiology*, 18(4), pp. 389–395. doi: 10.1016/j.conb.2008.09.006.

Gow, A. *et al.* (2004) 'Deafness in Claudin 11-Null Mice Reveals the Critical Contribution of Basal Cell Tight Junctions to Stria Vascularis Function', *Journal of Neuroscience*, 24(32), pp. 7051–7062. doi: 10.1523/JNEUROSCI.1640-04.2004.

Grimes, D. T. *et al.* (2016) 'Zebrafish models of idiopathic scoliosis link cerebrospinal fluid flow defects to spine curvature', *Science*, 352(6291), pp. 1341–1344. doi: 10.1126/science.aaf6419.

Grimsley-Myers, C. M. *et al.* (2009) 'The Small GTPase Rac1 Regulates Auditory Hair Cell Morphogenesis', *Journal of Neuroscience*, 29(50), pp. 15859–15869. doi: 10.1523/JNEUROSCI.3998-09.2009.

Grüneberg, H., Burnett, J. B. and Snell, G. D. (1941) 'The Origin of Jerker, a New Gene Mutation of the House Mouse, and Linkage Studies Made with It', *Proceedings of the National Academy of Sciences of the*

United States of America, 27(12), pp. 562–565. Available at: http://www.pubmedcentral.nih.gov/articlerender.fcgi?artid=1078382&tool=pmcentrez&rendertype=abstract.

Günzel, D. orothe. and Yu, A. S. L. (2013) *Claudins and the Modulation of Tight Junction Permeability*, *Physiological Reviews*. doi: 10.1152/physrev.00019.2012.

Haffter, P. *et al.* (1997) 'The identification of genes with unique and essential functions in the development of the zebrafish, Danio rerio', *Development*, 123, pp. 1–36.

Haga-Yamanaka, S. *et al.* (2014) 'Integrated action of pheromone signals in promoting courtship behavior in male mice', *eLife*, 2014(3), pp. 1–19. doi: 10.7554/eLife.03025.001.

Halpern, M. (1987) 'The Organization and Function of the Vomeronasal System', *Annual Review of Neuroscience*, 10(1), pp. 325–362. doi: 10.1146/annurev.ne.10.030187.001545.

Hansen, A. and Zeiske, E. (1998) 'The peripheral olfactory organ of the zebrafish, Danio rerio: An ultrastructural study', *Chemical Senses*, 23(1), pp. 39–48. doi: 10.1093/chemse/23.1.39.

Harris, T. J. . C. and Tepass, U. (2010) 'Adherens junctions: From molecules to morphogenesis', *Nature Reviews Molecular Cell Biology*. Nature Publishing Group, 11(7), pp. 502–514. doi: 10.1038/nrm2927.

Hashiguchi, Y. and Nishida, M. (2006) 'Evolution and origin of vomeronasal-type odorant receptor gene repertoire in fishes', *BMC Evolutionary Biology*, 6, pp. 1–13. doi: 10.1186/1471-2148-6-76.

Heisenberg, C.-P. and Bellaïche, Y. (2013) 'Forces in tissue morphogenesis and patterning', *Cell*, 153(5), pp. 948–962. doi: 10.1016/j.cell.2013.05.008.

Henning, H. (1916) 'Der Geruch', *Zeitschrift für Psychologie*.

Herrada, G. and Dulac, C. (1997) 'A novel family of putative pheromone receptors in mammals with a topographically organized and sexually dimorphic distribution', *Cell*, 90(4), pp. 763–773. doi: 10.1016/S0092-8674(00)80536-X.

Hibino, H. and Kurachi, Y. (2006) 'Molecular and Physiological Bases of the K+ Circulation in the Mammalian Inner Ear', *Physiology*, 21(5), pp. 336–345. doi: 10.1152/physiol.00023.2006.

Höfer, D., Shin, D.-W. and Drenckhahn, D. (2000) 'Identification of cytoskeletal markers for the different microvilli and cell types of the rat vomeronasal sensory epithelium', *Journal of Neurocytology*, 29(3), pp. 147–156. doi: 10.1023/A:1026548020851.

Horio, N. *et al.* (2011) 'Sour taste responses in mice lacking PKD channels', *PLoS ONE*, 6(5), pp. 1–10. doi: 10.1371/journal.pone.0020007.

Huang, A. L. *et al.* (2006) 'The cells and logic for mammalian sour taste detection', *Nature*, 442(7105), pp. 934–938. doi: 10.1038/nature05084.

Huang, Y.-J. *et al.* (2007) 'The role of pannexin 1 hemichannels in ATP release and cell-cell communication in mouse taste buds', *Proceedings of the National Academy of Sciences*, 104(15), pp. 6436–6441. doi: 10.1073/pnas.0611280104.

Hubbard, J. M. *et al.* (2016) 'Intraspinal Sensory Neurons Provide Powerful Inhibition to Motor Circuits Ensuring Postural Control during Locomotion', *Current Biology*, 26(21), pp. 2841–2853. doi: 10.1016/j.cub.2016.08.026.

Hudspeth, A. J. (1989) 'How the ear's works work', *Nature*, 341, pp. 397–404. doi: 10.1038/341397a0.

Van Itallie, C. M. and Anderson, J. M. (2014) 'Architecture of tight junctions and principles of molecular composition', *Seminars in Cell and Developmental Biology*. Elsevier Ltd, 36, pp. 157–165. doi: 10.1016/j.semcdb.2014.08.011.

Jagger, D. *et al.* (2011) 'Alström Syndrome protein ALMS1 localizes to basal bodies of cochlear hair cells and regulates cilium-dependent planar cell polarity', *Human Molecular Genetics*, 20(3), pp. 466–481. doi: 10.1093/hmg/ddq493.

Jalalvand, E. *et al.* (2016) 'Ciliated neurons lining the central canal sense both fluid movement and pH through ASIC3', *Nature Communications*. doi: 10.1038/ncomms10002.

Jones, C. *et al.* (2008) 'Ciliary proteins link basal body polarization to planar cell polarity regulation', *Nature Genetics*, 40(1), pp. 69–77. doi: 10.1038/ng.2007.54.

Kandel, E. R. *et al.* (2013) *Principles of Neural Science (5th edition)*.

Karlson, P. and Lüscher, M. (1959) '"Pheromones": a new term for a class of biologically active substances', *Nature*, 183(4653), pp. 55–56. doi: 10.1038/183055a0.

Kaur, A. W. *et al.* (2014) 'Murine pheromone proteins constitute a context-dependent combinatorial code governing multiple social behaviors', *Cell*. Elsevier Inc., 157(3), pp. 676–688. doi: 10.1016/j.cell.2014.02.025.

Kazmierczak, P. *et al.* (2007) 'Cadherin 23 and protocadherin 15 interact to form tip-link filaments in sensory hair cells', *Nature*, 449(7158), pp. 87–91. doi: 10.1038/nature06091.

Kessels, M. M. *et al.* (2011) 'Controlling actin cytoskeletal organization and dynamics during neuronal morphogenesis', *European Journal of Cell Biology*. Elsevier GmbH., 90, pp. 926–933. doi: 10.1016/j.ejcb.2010.08.011.

Keverne, E. B. (1999) 'The vomeronasal organ', *Science*, 286.

Kirjavainen, A. *et al.* (2015) 'The Rho GTPase Cdc42 regulates hair cell planar polarity and cellular patterning in the developing cochlea', *Biology Open*, 4(4), pp. 516–526. doi: 10.1242/bio.20149753.

Kitajiri, S. *et al.* (2004) 'Compartmentalization established by claudin-11-based tight junctions in stria vascularis is required for hearing through generation of endocochlear potential', *Journal of Cell Science*, 117(21), pp. 5087–5096. doi: 10.1242/jcs.01393.

Kolmer, W. (1921) 'Das ,,Sagittalorgan" der Wirbeltiere', *Anatomy and Embryology*, (3), pp. 652–717. doi: 10.1007/BF02593657.

Krugmann, S. *et al.* (2001) 'Cdc42 induces filopodia by promoting the formation of an IRSp53:Mena complex', *Current Biology*, 11(21), pp. 1645–1655. doi: 10.1016/S0960-9822(01)00506-1.

Lamotte, C. C. (1987) 'Vasoactive intestinal polypeptide cerebrospinal fluid-contacting neurons of the monkey and cat spinal central canal', *Journal of Comparative Neurology*, 258(4), pp. 527–541. doi: 10.1002/cne.902580405.

Larson, E. D. *et al.* (2015) 'The Role of 5-HT3 Receptors in Signaling from Taste Buds to Nerves', *Journal of Neuroscience*, 35(48), pp. 15984–15995. doi: 10.1523/JNEUROSCI.1868-15.2015.

Lecuit, T. (2005) 'Adhesion remodeling underlying tissue morphogenesis', *Trends in Cell Biology*, 15(1), pp. 34–42. doi: 10.1016/j.tcb.2004.11.007.

Leinders-Zufall, T. *et al.* (2000) 'Ultrasensitive pheromone detection by mammalian vomeronasal neurons', *Nature*, 405, pp. 792–796. doi: 10.1038/35015572.

Levine, M. W. (2006) *Fundamentals of Sensation and Perception (3rd edition)*.

Li, H. *et al.* (2004) 'Correlation of Expression of the Actin Filament-Bundling Protein Espin with Stereociliary Bundle Formation in the Developing Inner Ear', *Journal of Comparative Neurology*, 468(1), pp. 125–134. doi: 10.1002/cne.10944.

Li, X. *et al.* (2002) 'Human receptors for sweet and umami taste', *Proceedings of the National Academy of Sciences*, 99(7), pp. 4692–4696. doi: 10.1073/pnas.072090199.

Liman, E. R., Zhang, Y. V. and Montell, C. (2014) 'Peripheral coding of taste', *Neuron*, 81(5), pp. 984–1000. doi: 10.1016/j.neuron.2014.02.022.

Lin, W. *et al.* (1999) 'Epithelial Na+ channel subunits in rat taste cells: localization and regulation by aldosterone', *The Journal of comparative neurology*, 405, pp. 406–420. doi: Doi 10.1002/(Sici)1096-9861(19990315)405:3<406::Aid-Cne10>3.0.Co;2-F.

Liu, H. *et al.* (2016) 'Myosin III-mediated cross-linking and stimulation of actin bundling activity of Espin', *eLife*, (January).

Lodish, H. *et al.* (2013) *Molecular Biology of the Cell (7th edition)*.

Loomis, P. A. *et al.* (2003) 'Espin cross-links cause the elongation of microvillus-type parallel actin bundles in vivo', *Journal of Cell Biology*, 163(5), pp. 1045–1055. doi: 10.1083/jcb.200309093.

Loomis, P. A. *et al.* (2006) 'Targeted wild-type and jerker espins reveal a novel , WH2-domain-dependent way to make actin bundles in cells', *Journal of cell science*, 119(8), pp. 1655–1665. doi: 10.1242/jcs.02869.

Lu, X. and Sipe, C. W. (2016) 'Developmental regulation of planar cell polarity and hair bundle morphogenesis in auditory hair cells: lessons from human and mouse genetics', *Wiley Interdiscip Rev Dev Biol.*, 5(1), pp. 85–101. doi: 10.1126/science.1249098.Sleep.

Margolis, B. and Borg, J.-P. (2005) 'Apicobasal polarity complexes', *Journal of Cell Science*, 118(22), pp. 5157–5159. doi: 10.1242/jcs.02597.

Matsumoto, I., Ohmoto, M. and Abe, K. (2013) 'Functional diversification of taste cells in vertebrates', *Seminars in Cell and Developmental Biology*. Elsevier Ltd, 24(3), pp. 210–214. doi: 10.1016/j.semcdb.2012.10.004.

Matsunami, H. and Buck, L. B. (1997) 'A multigene family encoding a diverse array of putative pheromone receptors in mammals', *Cell*, 90(4), pp. 775–784. doi: 10.1016/S0092-8674(00)80537-1.

May-Simera, H. L. *et al.* (2015) 'Ciliary proteins Bbs8 and Ift20 promote planar cell polarity in the cochlea', *Development*, 142(3), pp. 555–566. doi: 10.1242/dev.113696.

McGrath, J., Roy, P. and Perrin, B. J. (2017) 'Stereocilia morphogenesis and maintenance through regulation of actin stability', *Seminars in Cell and Developmental Biology*. Elsevier Ltd, 65, pp. 88–95. doi: 10.1016/j.semcdb.2016.08.017.

Meng, W. and Takeichi, M. (2009) 'Adherens junction: molecular architecture and regulation', *Cold Spring Harbor perspectives in biology*. doi: 10.1101/cshperspect.a002899.

Merritt, R. C. *et al.* (2012) 'Myosin IIIB uses an actin-binding motif in its espin-1 cargo to reach the tips of actin protrusions', *Current Biology*, 22(4), pp. 320–325. doi: 10.1109/TMI.2012.2196707.Separate.

Michalski, N. *et al.* (2009) 'Harmonin-b, an actin-binding scaffold protein, is involved in the adaptation of mechanoelectrical transduction by sensory hair cells', *Pflugers Archiv European Journal of Physiology*, 459(1), pp. 115–130. doi: 10.1007/s00424-009-0711-x.

Michalski, N. and Petit, C. (2015) 'Genetics of auditory mechano-electrical transduction', *Pflugers Archiv - European Journal of Physiology*, 467, pp. 49–72. doi: 10.1007/s00424-014-1552-9.

Michlig, S., Damak, S. and Le Coutre, J. (2007) 'Claudin-based permeability barriers in taste buds', *J Comp Neurol*, 502(2), pp. 1003–1011. doi: 10.1002/cne.

Miragall, F., Breipohl, W. and Bhatnagar, K. P. (1979) 'Ultrastructural investigation on the cell membranes of the vomeronasal organ in the rat: A freeze-etching study', *Cell and Tissue Research*, 200(3), pp. 397–

408. doi: 10.1007/BF00234851.

Mombaerts, P. (2004) 'Genes and ligands for odorant, vomeronasal and taste receptors', *Nature Reviews Neuroscience*, 5(4), pp. 263–278. doi: 10.1038/nrn1365.

Murray, R. G. (1986) 'The mammalian taste bud type III cell: A critical analysis', *Journal of Ultrastructure Research and Molecular Structure Research*, 95(1–3), pp. 175–188. doi: 10.1016/0889-1605(86)90039-X.

Murray, R. G. and Murray, A. (1967) 'Fine Structure of Taste Buds of Rabbit Foliate Papillae', *J Ultrastructure Research*, 19, pp. 327–353.

Nakano, Y. *et al.* (2009) 'A claudin-9-based ion permeability barrier is essential for hearing', *PLoS Genetics*, 5(8). doi: 10.1371/journal.pgen.1000610.

Nelson, G. *et al.* (2001) 'Mammalian Sweet Taste Receptors', *Cell*, 106, pp. 381–390. doi: 10.1016/S0092-8674(01)00451-2.

Nelson, G. *et al.* (2002) 'An amino-acid taste receptor', *Nature*, 416(6877), pp. 199–202. doi: 10.1038/nature726.

Nicolson, T. *et al.* (1998) 'Genetic analysis of vertebrate sensory hair cell mechanosensation: The zebrafish circler mutants', *Neuron*, 20(2), pp. 271–283. doi: 10.1016/S0896-6273(00)80455-9.

Nicolson, T. (2017) 'The genetics of hair-cell function in zebrafish', *Journal of Neurogenetics*, 31(3), pp. 102–112. doi: 10.1080/01677063.2017.1342246.

Nobes, C. D. and Hall, A. (1995) 'Rho, Rac, and Cdc42 GTPases regulate the assembly of multimolecular focal complexes associated with actin stress fibers, lamellipodia, and filopodia', *Cell*, 81(1), pp. 53–62. doi: 10.1016/0092-8674(95)90370-4.

Oka, Y. *et al.* (2013) 'High salt recruits aversive taste pathways', *Nature*. Nature Publishing Group, 494(7438), pp. 472–475. doi: 10.1038/nature11905.

Orts-Del'Immagine, A. *et al.* (2012) 'Properties of subependymal cerebrospinal fluid contacting neurones in the dorsal vagal complex of the mouse brainstem', *Journal of Physiology*, 590(16), pp. 3719–3741. doi: 10.1113/jphysiol.2012.227959.

Pan, B. *et al.* (2013) 'TMC1 and TMC2 are components of the mechanotransduction channel in hair cells of the mammalian inner ear', *Neuron*, 79(3), pp. 504–515. doi: 10.1016/j.neuron.2013.06.019.

Petit, C. and Richardson, G. P. (2009) 'Linking genes underlying deafness to hair-bundle development and function', *Nature Neuroscience*, 12(6), pp. 703–710. doi: 10.1038/nn.2330.

Pfister, P. and Rodriguez, I. (2005) 'Olfactory expression of a single and highly variable V1r pheromone receptor-like gene in fish species.', *Proceedings of the National Academy of Sciences of the United States of America*, 102(15), pp. 5489–5494. doi: 10.1073/pnas.0402581102.

Pickles, J. O., Comis, S. D. and Osborne, M. P. (1984) 'Cross-links between stereocilia in the guinea pig organ of Corti, and their possible relation to sensory transduction', *Hearing Research*, 15(2), pp. 103–112. doi: 10.1016/0378-5955(84)90041-8.

Ratheesh, A. and Yap, A. S. (2012) 'A bigger picture: classical cadherins and the dynamic actin cytoskeleton', *Nature Reviews Molecular Cell Biology*. Nature Publishing Group, 13(10), pp. 673–679. doi: 10.1038/nrm3431.

Reiten, I. *et al.* (2017) 'Motile-Cilia-Mediated Flow Improves Sensitivity and Temporal Resolution of Olfactory Computations', *Current Biology*. Elsevier Ltd., 27(2), pp. 166–174. doi: 10.1016/j.cub.2016.11.036.

Revenu, C. *et al.* (2004) 'The co-workers of actin filaments: from cell structures to signals', *Nature Reviews*

Molecular Cell Biology, 5(8), pp. 635–646. doi: 10.1038/nrm1437.

Riazuddin, S. *et al.* (2006) 'Tricellulin Is a Tight-Junction Protein Necessary for Hearing', *The American Journal of Human Genetics*, 79(6), pp. 1040–1051. doi: 10.1086/510022.

Rodriguez-Boulan, E. and Macara, I. G. (2014) 'Organization and execution of the epithelial polarity programme', *Nature Reviews Molecular Cell Biology*, 15(4), pp. 225–242. doi: 10.1038/nrm3775.

Roper, S. D. (2007) 'Signal transduction and information processing in mammalian taste buds', *Pflugers Archiv*, 454(5), pp. 759–776. doi: 10.1007/s00424-007-0247-x.Signal.

Roper, S. D. and Chaudhari, N. (2017) 'Taste buds: Cells, signals and synapses', *Nature Reviews Neuroscience*. Nature Publishing Group, 18(8), pp. 485–497. doi: 10.1038/nrn.2017.68.

Ross, A. J. *et al.* (2005) 'Disruption of Bardet-Biedl syndrome ciliary proteins perturbs planar cell polarity in vertebrates', *Nature Genetics*, 37(10), pp. 1135–1140. doi: 10.1038/ng1644.

Ryba, N. J. P. and Tirindelli, R. (1997) 'A new multigene family of putative pheromone receptors', *Neuron*, 19(2), pp. 371–379. doi: 10.1016/S0896-6273(00)80946-0.

Rzadzinska, A. K. *et al.* (2004) 'An actin molecular treadmill and myosins maintain stereocilia functional architecture and self-renewal', *Journal of Cell Biology*, 164(6), pp. 887–897. doi: 10.1083/jcb.200310055.

Safieddine, S., El-Amraoui, A. and Petit, C. (2012) 'The Auditory Hair Cell Ribbon Synapse: From Assembly to Function', *Annual Review of Neuroscience*, 35(1), pp. 509–528. doi: 10.1146/annurev-neuro-061010-113705.

Salles, F. T. *et al.* (2009) 'Myosin IIIa boosts elongation of stereocilia by transporting espin 1 to the plus ends of actin filaments', *Nature Cell Biology*, 11(4), pp. 443–450. doi: 10.1038/ncb1851.

Sauvanet, C. *et al.* (2015) 'Structure, Regulation, and Functional Diversity of Microvilli on the Apical Domain of Epithelial Cells', *Annual Review of Cell and Developmental Biology*, 31(1), pp. 593–621. doi: 10.1146/annurev-cellbio-100814-125234.

Schwayer, C. *et al.* (2016) 'Actin Rings of Power', *Developmental Cell*, 37(6), pp. 493–506. doi: 10.1016/j.devcel.2016.05.024.

Scita, G. *et al.* (2008) 'IRSp53: crossing the road of membrane and actin dynamics in the formation of membrane protrusions', *Trends in Cell Biology*, 18(2), pp. 52–60. doi: 10.1016/j.tcb.2007.12.002.

Sekerková, G. *et al.* (2003) 'Novel Espin Actin-bundling Proteins Are Localized to Purkinje Cell Dendritic Spines and Bind the SH3 Adapter Protein Insulin Receptor Substrate p53', *The Journal of Neuroscience*, 23(4), pp. 1310–1319. doi: 23/4/1310 [pii].

Sekerková, G. *et al.* (2004) 'Espins Are Multifunctional Actin Cytoskeletal Regulatory Proteins in the Microvilli of Chemosensory and Mechanosensory Cells', *Journal of Neuroscience*, 24(23), pp. 5445–5456. doi: 10.1523/JNEUROSCI.1279-04.2004.

Sekerková, G. *et al.* (2006) 'Espins and the actin cytoskeleton of hair cell stereocilia and sensory cell microvilli', *Cellular and Molecular Life Sciences*, 63(19–20), pp. 2329–2341. doi: 10.1007/s00018-006-6148-x.

Sekerková, G., Richter, C.-P. and Bartles, J. R. (2011) 'Roles of the Espin Actin-Bundling Proteins in the Morphogenesis and Stabilization of Hair Cell Stereocilia Revealed in CBA/CaJ Congenic Jerker Mice', *PLoS Genetics*, 7(3). doi: 10.1371/journal.pgen.1002032.

Sipe, C. W. *et al.* (2013) 'Lis1 mediates planar polarity of auditory hair cells through regulation of microtubule organization', *Development (Cambridge, England)*, 140(8), pp. 1785–95. doi: 10.1242/dev.089763.

Sipe, C. W. and Lu, X. (2011) 'Kif3a regulates planar polarization of auditory hair cells through both ciliary and non-ciliary mechanisms', *Development*, 138(16), pp. 3441–3449. doi: 10.1242/dev.065961.

Söllner, C. *et al.* (2000) 'Mutations in cadherin 23 affect tip links in zebrafish sensory hair cells', *Nature*, 428, pp. 955–959.

St Johnston, D. and Sanson, B. (2011) 'Epithelial polarity and morphogenesis', *Current Opinion in Cell Biology*, 23(5), pp. 540–546. doi: 10.1016/j.ceb.2011.07.005.

Steinberg, M. S. (2007) 'Differential adhesion in morphogenesis: a modern view', *Current Opinion in Genetics and Development*, 17(4), pp. 281–286. doi: 10.1016/j.gde.2007.05.002.

Steketee, M., Balazovich, K. and Tosney, K. W. (2001) 'Filopodial initiation and a novel filament-organizing center, the focal ring.', *Molecular biology of the cell*, 12(8), pp. 2378–95. doi: 10.1091/mbc.12.8.2378.

Sternberg, J. R. *et al.* (2018) 'Pkd2l1 is required for mechanoception in cerebrospinal fluid-contacting neurons and maintenance of spine curvature', *Nature Communications*, pp. 1–10. doi: 10.1038/s41467-018-06225-x.

Stowers, L. and Kuo, T.-H. (2015) 'Mammalian pheromones: emerging properties and mechanisms of detection', *Current Opinion in Neurobiology*. Elsevier Ltd, 34, pp. 103–109. doi: 10.1016/j.conb.2015.02.005.

Svitkina, T. M. *et al.* (2003) 'Mechanism of filopodia initiation by reorganization of a dendritic network', *Journal of Cell Biology*, 160(3), pp. 409–421. doi: 10.1083/jcb.200210174.

Takeichi, M. (1988) 'The cadherins: cell-cell adhesion molecules controlling animal morphogenesis', *Development*, 102(4), pp. 639–655.

Tilney, L. G. *et al.* (1998) 'Why Are Two Different Cross-linkers Necessary for Actin Bundle Formation In Vivo and What Does Each Cross-link Contribute?', *Journal of Cell Biology*, 143(1), pp. 121–133. doi: 10.1083/jcb.143.1.121.

Tilney, L. G., Tilney, M. S. and Derosier, D. J. (1992) 'Actin filaments, stereocilia, and hair cells: how cells count and measure', *Annu. Rev. Cell Biol.*, 8, pp. 257–274.

Togashi, H. *et al.* (2011) 'Nectins Establish a Checkerboard-Like cellular pattern in the auditory epithelium', *Science*, 333, pp. 1144–1147. doi: 10.1126/science.1208467.

Tomchik, S. M. *et al.* (2007) 'Breadth of Tuning and Taste Coding in Mammalian Taste Buds', *Journal of Neuroscience*, 27(40), pp. 10840–10848. doi: 10.1523/JNEUROSCI.1863-07.2007.

Torre, V. *et al.* (1995) 'Transduction and adaptation in sensory receptor cells', *The Journal of Neuroscience*, 15(12), pp. 7757–7768. doi: www.jneurosci.org/content/jneuro/15/12/7757.full.pdf.

Vandenbeuch, A., Clapp, T. R. and Kinnamon, S. C. (2008) 'Amiloride-sensitive channels in type I fungiform taste cells in mouse', *BMC Neuroscience*, 9(1). doi: 10.1186/1471-2202-9-1.

Vigh, B. *et al.* (1983) 'Cerebrospinal fluid-contacting neurons of the central canal and terminal ventricle in various vertebrates', *Cell and Tissue Research*, 231(3), pp. 615–621. doi: 10.1007/BF00218119.

Vigh, B. and Vigh-Teichmann, I. (1973) 'Comparative Ultrastructure of the Cerebrospinal fluid-contacting neurons', *International Review of Cytology*, 35, pp. 189–251.

Wan, G., Corfas, G. and Stone, J. S. (2013) 'Inner ear supporting cells: Rethinking the silent majority', *Seminars in Cell and Developmental Biology*. Elsevier Ltd, 24(5), pp. 448–459. doi: 10.1016/j.semcdb.2013.03.009.

Wilcox, E. R. *et al.* (2001) 'Mutations in the gene encoding tight junction claudin-14 cause autosomal recessive deafness DFNB29', *Cell*, 104(1), pp. 165–172. doi: 10.1016/S0092-8674(01)00200-8.

Wyart, C. *et al.* (2009) 'Optogenetic dissection of a behavioural module in the vertebrate spinal cord', *Nature*. Nature Publishing Group, 461(7262), pp. 407–410. doi: 10.1038/nature08323.

Xiong, W. *et al.* (2012) 'TMHS is an integral component of the mechanotransduction machinery of cochlear hair cells', *Cell*, 151(6), pp. 1283–1295. doi: 10.1016/j.cell.2012.10.041.

Yonemura, S. *et al.* (1995) 'Cell-to-cell adherens junction formation and actin filament organization: similarities and differences between non-polarized fibroblasts and polarized epithelial cells.', *Journal of cell science*, 108, pp. 127–142.

Yoshioka, T. and Sakakibara, M. (2013) 'Physical aspects of sensory transduction on seeing, hearing and smelling', *Biophysics*, 9, pp. 183–191. doi: 10.2142/biophysics.9.183.

Zhang, Y. *et al.* (2003) 'Coding of sweet, bitter, and umami tastes: Different receptor cells sharing similar signaling pathways', *Cell*, 112(3), pp. 293–301. doi: 10.1016/S0092-8674(03)00071-0.

Zhao, B. *et al.* (2014) 'TMIE is an essential component of the mechanotransduction machinery of cochlear hair cells', *Neuron*, 84(5), pp. 954–967. doi: 10.1016/j.neuron.2014.10.041.

Zhao, B. and Müller, U. (2015) 'The elusive mechanotransduction machinery of hair cells', *Current Opinion in Neurobiology*, 34, pp. 172–179. doi: 10.1016/j.conb.2015.08.006.

Zhao, G. Q. *et al.* (2003) 'The receptors for mammalian sweet and umami taste', *Cell*, 115(3), pp. 255–266. doi: 10.1016/S0092-8674(03)00844-4.

Zhao, H., Pykäläinen, A. and Lappalainen, P. (2011) 'I-BAR domain proteins: linking actin and plasma membrane dynamics', *Current Opinion in Cell Biology*, 23, pp. 14–21. doi: 10.1016/j.ceb.2010.10.005.

Zheng, L. *et al.* (2000) 'The Deaf Jerker Mouse Has a Mutation in the Gene Encoding the Espin Actin-Bundling Proteins of Hair Cell Stereocilia and Fails to Accumulate Espins', *Cell*, 102(3), pp. 377–385. doi: 10.1016/S0092-8674(00)00042-8.

CHAPTER 2: TRANSCRIPTOME ANALYSIS OF MICROVILLIATED SENSORY CELLS

I. TRANSCRIPTOME ANALYSIS OF CSF-CNS: UNRAVELING CSF-CN-SPECIFIC GENES

A. Spinal CSF-cNs are interoceptive sensory neurons

The cerebrospinal fluid (CSF) is a complex fluid primarily secreted by the choroid plexuses into the brain ventricles; from there it flows down the central canal in the spinal cord. The study of CSF content has been challenging for several reasons. Because of its location in small cavities deep within the nervous tissue and, in non-human vertebrates, its small volume, the CSF is not easily sampled. Over the years, a large body of work has contributed to emphasize its complexity, describing a constantly changing composition, influenced by circadian rhythms, of numerous peptides and proteins, hormones, growth factors and inflammatory markers to only cite a few (Lehtinen *et al.*, 2011). Anatomists originally proposed that the main function of the CSF was to provide hydromechanical protection to the central nervous system (CNS), due to the fact it surrounds the entire nervous system, and to facilitate the disposal of waste. This idea was extended in the light of accumulating evidence for a role for CSF in homeostasis and development of the CNS (Gato *et al.*, 2005). Notably, it was shown that CSF content could modulate larger physiological functions such as sleep and feeding (Pappenheimer, Miller and Goodrich, 1967; Heinrich Martin, Ricardo Seoane and Baile, 1973). Thus, CSF composition probably reflects the physiological state of the organism, especially of the CNS (Djenoune and Wyart, 2017).

CSF-cNs are at the interface between the CSF and the CNS. CSF circulates in the ventricular system, which is delimited by a layer of ependymal and subependymal cells. Intermingled between these cells lies a peculiar population of neurons, the CSF-contacting neurons (CSF-cNs). Altogether, ependymal cells, subependymal cells and CSF-cNs form the interface between the CNS and the CSF. CSF-cNs are unique neurons breaking the ependymal barrier and sending an apical projection directly into the CSF. Not surprisingly, CSF-cNs aroused interest from early on: Kolmer and Agduhr first described them almost a century ago and showed that CSF-cNs are conserved across over 200 vertebrate species (Kolmer, 1921; Agduhr, 1922).

The spinal CSF-cN morphology is reminiscent of sensory cells. A comparative study of CSF-cN ultrastructure by Vigh and Vigh-Teichmann revealed that the morphology of CSF-cNs differs depending on species and CNS region (Vigh and Vigh-Teichmann, 1973; Vigh *et al.*, 1983) and led to the description of common characteristics. CSF-cNs are bipolar neurons projecting a basal axon within the CNS and an apical extension into the CSF. In the spinal cord, the apical extension is characterized by the presence of microvilli and, in some species, a kinocilium (Vigh and Vigh-Teichmann, 1973). The structure of the CSF-cN apical extension aroused interest early on because it is reminiscent of the hair bundle

development by hair cells although without the regular staircase organization. The CSF-cN microvilli and kinocilium can be compared to the stereocilia and kinocilium constituting the hair cell mechanosensory organelle.

Spinal CSF-cNs are interoceptive sensory neurons. The favorable location of spinal CSF-cNs at the interface between the CSF and the CNS and their peculiar sensory-like morphology enabling contact with CSF prompted scientists to think of CSF-cNs as a novel sensory system. Kolmer proposed a mechanosensory function resembling that of hair cells (Kolmer, 1921) while Agduhr suggested that CSF-cNs could carry chemosensory functions related to the CSF content and participate in homeostatic regulations (Agduhr, 1922). The lack of genetic tools to target CSF-cNs and their location deep in brain and spinal cord tissues considerably hampered the study of these cells. The fortuitous discovery of a marker of CSF-cNs in mouse, the transient potential receptor channel PKD2L1 (Huang *et al.*, 2006), greatly facilitated their study. The description of PKD2L1 in CSF-cNs (Huang *et al.*, 2006; Djenoune *et al.*, 2014; Orts-Del'Immagine *et al.*, 2014) further supported the hypothesis that these cells are sensory since PKD2L1 was originally identified for its possible involvement in sour taste (Huang *et al.*, 2006) (see Chapter 1, I.B) and belongs to the family of transient receptor potential channels known to be involved in various sensory modalities (Damann, Voets and Nilius, 2008). Since then, a great effort has been made to tackle the question of the physiological role(s) of CSF-cNs. Several studies provided evidence for the sensitivity of CSF-cNs to pH changes supported by ASIC channels in mouse (Orts-Del'Immagine *et al.*, 2012) and lamprey (Jalalvand *et al.*, 2016). Unpublished data from the lab show that this property is conserved in zebrafish with Asic-like responses to CSF acidification from spinal CSF-cNs (Böhm, 2016). Furthermore, CSF-cNs were demonstrated to respond to mechanical cues associated with osmolarity changes (Orts-Del'Immagine *et al.*, 2012), CSF flow and tail bending in a Pkd2l1-dependent fashion in zebrafish (Böhm *et al.*, 2016; Sternberg *et al.*, 2018) or possibly through Asic3 in the lamprey (Jalalvand *et al.*, 2016). Together, these results obtained in different system models converge to demonstrate that CSF-cNs carry both chemo- and mechano-sensory functions. *In vivo* implications are that CSF-cNs might be capable of sensing changes in the CSF content, at least pH and osmolarity, and there is now clear indications that they are tuned to CSF flow in the zebrafish spinal cord during early development (Sternberg *et al.*, 2018). Thus, spinal CSF-cNs can be considered as an additional interoceptive class of sensory cells.

Evidence for two functionally distinct spinal CSF-cN subtypes. As previously stated, spinal CSF-cNs display a peculiar morphology of bipolar sensory neurons, which makes them stand out of the ependymal cell layer. Another feature that distinguishes them from surrounding cells is the presence of various granules and vesicles located within the apical extension or in the subapical region, suggesting a neurosecretory function (Djenoune and Wyart, 2017; Djenoune *et al.*, 2017). CSF-cNs were also originally

identified as GABAergic neurons, definitely expressing both GABA and proteins implicated in GABA synthesis and vesicular loading (Djenoune and Wyart, 2017). Although not restricted to CSF-cNs in the spinal cord, GABA can be used as a marker of CSF-cNs along with PKD2L1 as previously mentioned (Huang *et al.*, 2006; Djenoune *et al.*, 2014).

Apart from these landmarks of the spinal CSF-cN group, there is growing evidence that CSF-cNs do not constitute a homogenous population. Spinal CSF-cNs exhibit distinct patterns of expression restricted to only subsets of cells for glutamate, glycine, dopamine, serotonin and neuropeptides (Djenoune and Wyart, 2017). This idea is further supported by the fact that CSF-cNs arise from two distinct progenitor domains in mouse (Petracca *et al.*, 2016) and zebrafish (Park, Shin and Appel, 2004). Recent studies in our lab provided molecular evidence to distinguish two subtypes of CSF-cNs within the zebrafish spinal cord (Djenoune *et al.*, 2017). Through the establishment of a quantitative analysis of the morphological features of CSF-cNs, my work showed that these subtypes displayed different shapes of apical extensions (Djenoune *et al.*, 2017) (Annex). These results were reinforced by the demonstration that these subtypes are also functionally distinct and exhibit different sensory-mediated activities (Böhm *et al.*, 2016; Hubbard *et al.*, 2016; Sternberg *et al.*, 2018).

Many questions remain about spinal CSF-cNs. Although described almost a century ago, CSF-cNs have remained a mysterious population. The discovery of PKD2L1 ten years ago as a specific marker of spinal CSF-cNs provided the community with a tool to genetically target these cells. Since then, the understanding of CSF-cN functions has dramatically leaped forward and a great effort was made acquiring evidence indicating that CSF-cNs represent a conserved interoceptive sensory system in tune with the CSF. However, many questions remain unanswered. First, considering the complexity of the changing CSF content (thought to be the source of sensory cues) and the heterogeneity of the CSF-cN population itself, it is most likely that we have only scratched the surface of the functional potential of these cells. If CSF-cNs are indeed sensing the CSF, they must exhibit a panel of channels and receptors in order to detect the diversity of sensory cues propagated by this fluid. Analysis of gene expression in CSF-cNs can thereby help to achieve a more comprehensive view of the sensory profile of the cells and to further distinguish functional CSF-cN subgroups. Second, the physiological relevance of the CSF-cN interface with the CSF still remains poorly understood. In zebrafish, CSF-cNs have been involved in tuning locomotion through projections onto elements of spinal circuits (Fidelin *et al.*, 2015; Hubbard *et al.*, 2016; Djenoune *et al.*, 2017). The full extent of the CSF-cN connectome still needs to be described. In the same vein, the hypothesis that CSF-cNs carry secretory functions needs to be confirmed and further investigated. Last but not least, the ultrastructural organization and the molecular determinants underlying the formation of the CSF-cN apical extension are unknown. Thus, the precise role of the apical extension in CSF-cN sensory function has not been demonstrated.

Much effort in the lab has been dedicated to tackle these different questions in the zebrafish spinal cord. A first wave of results has already yielded insightful data about the sensory functions of CSF-cNs (Böhm *et al.*, 2016; Sternberg *et al.*, 2018) and their role in modulating locomotion (Fidelin *et al.*, 2015; Hubbard *et al.*, 2016). My own project aimed at unraveling the molecular mechanisms underlying the CSF-cN morphogenesis. Prior to this study, only a handful of CSF-cN specific genes had been identified. To further pursue the investigation of CSF-cNs, we sought to analyze their transcriptome profile.

B. A FACS-based approach to perform the transcriptome analysis of CSF-cNs

To unravel the gene expression profile of CSF-cNs, we performed the analysis of their transcriptome by RNA sequencing. *This study was done in collaboration with Dr Andrew Prendergast in the lab.*

A FACS-based approach. We isolated spinal CSF-cNs from 3-dpf old larvae through fluorescent activated cell sorting (FACS). The FACS-based approach has already proven to be useful to efficiently extract RNA from specific zebrafish cell types in other studies (Covassin *et al.*, 2006; Cerda, Hargrave and Lewis, 2009; Stuckenholz *et al.*, 2009; Gallardo *et al.*, 2010; Gallardo and Behra, 2013).

(1) The first step of the procedure consisted in preparing our 3-dpf larvae. We used the double transgenic *Tg(pkd2l1:Gal;UAS:GFP)* line that expressed strong fluorescence in spinal CSF-cNs but also ectopic GFP in the hindbrain and the heart (Fig.10A). To avoid non-CSF-cN GFP-positive cells, we systematically beheaded larvae after anesthesia by sectioning them with a scalpel at the intersection between the hindbrain and the trunk (Fig.10A, dashed line). Up to 200 larvae were processed at the time and all tail tissues were kept on ice. Few non-fluorescent siblings were processed in parallel to constitute our 'control' population for FACS.

(2) CSF-cNs are located deep in the spinal cord tissue. To avoid cellular stress and possible gene expression changes due to prolonged time of tissue processing, we favored mechanical dissociation over enzyme digestion. We followed the rapid (~10-15 min) protocol established by Manoli & Driever (Manoli and Driever, 2012) to dissociate tail tissues from control and GFP-positive sibling larvae. During dissociation, cells were quickly filtered through a 30-µm mesh and resuspended into the cell dissociation sorting buffer.

(3) Single-cell suspensions were rapidly processed by FACS. The control suspensions obtained from the dissociation of non-fluorescent larvae were used to demarcate the gates to sort GFP-negative (GFP- or 'dark') versus GFP-positive (GFP+ or 'green') cell populations (Fig.10B, left panel). GFP- and GFP+ populations from cell suspension of fluorescent larvae tails (Fig.10B) were then directly collected into lysis buffer to minimize further cellular stress and loss of material. Sorting typically yielded between 3000 and 15000 GFP+ cells from an initial pool of ~150-200 3-dpf larvae and take about 45 min.

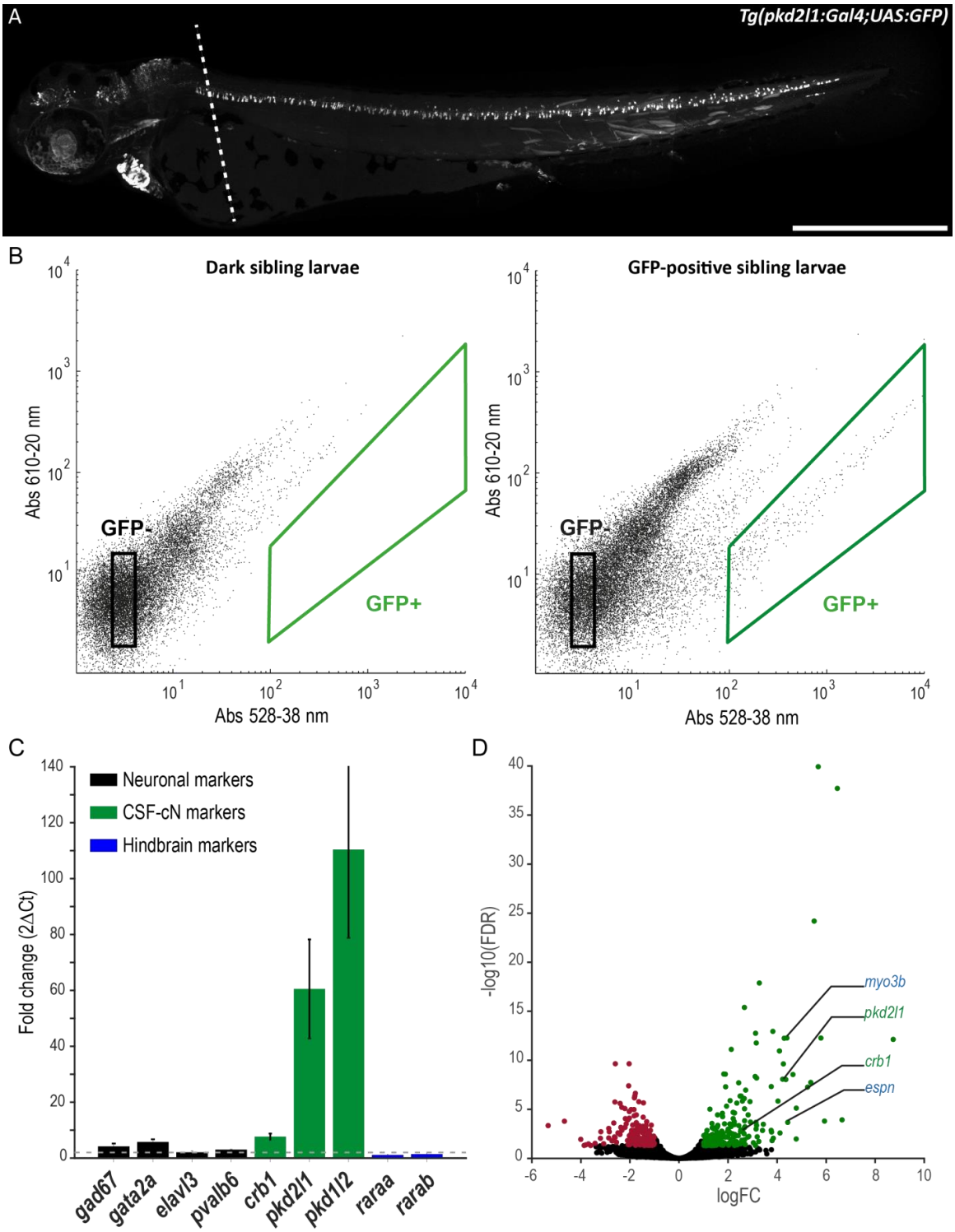

Figure 10. FACS-based approach to perform the transcriptome analysis of CSF-cNs

A, 3 days post fertilization *Tg(pkd2l1:Gal;UAS:GFP)* larva fixed and immunostained against GFP. Prior to mechanical dissociation and sorting, larvae were beheaded following the plane indicated by the dashed line. Scale bar, 500 µm.

B, Illustrative FACS plots showing the characteristic autofluorescent 'tail' where most cells follow a 1:1 green:red scatter. Dark sibling larvae were used as a negative control to draw the gates (left panel). In the GFP-positive samples, a small fraction of green-shifted cells (between 0.3 and 0.5%) fall into the GFP+ gate (right panel).

C, Total RNA was extracted from GFP- ("dark") and GFP+ ("green") fractions. Enrichment in the green

fraction in CSF-cNs was tested by qPCR and comparing gene expression between the green and the dark populations. Previously known CSF-cN markers - *crb1*, *pkd2l1* and *pkd1l2* - show strong enrichment in the 'green' pool in contrast to hindbrain markers - *raraa* and *rarab* - underexpressed. GABA – *gad67* and *gata2* - and neuronal – *elavl3* and *pvalb6* - markers are slightly enriched in the green sample, reflecting the GABAergic neuronal nature of CSF-cNs but also the presence of other non-CSF-cN GABAergic neurons in the spinal cord. In our analysis, we considered as up-regulated all genes showing a 2-fold enrichment (dotted line) compared to the reference population.
D, Volcano plot of all 5 RNAseq replicates aligned to Zv10 genome annotations. *pkd2l1* and *crb1*, two already known CSF-cN markers (green), as well as two new markers, *espin* and *myo3b* (blue), further studied in the next chapter, are indicated among the pool of genes found as upregulated in the green population.

(4) After FACS, total RNA was quickly extracted from both the dark and the green population. RNA quality and concentration were assessed using a nanodrop and/or a bioanalyzer allowing the visualization of ribosomal RNA bands. RNA samples were stored at -80°C before further use.

Because our RNA samples were typically low in concentration, they were either devoted to qPCR or RNA sequencing but we could not systematically test our samples by qPCR prior to RNA sequencing. The first two replicates were used to confirm the enrichment of the green population in CSF-cNs by comparing gene expression levels with the dark population by qPCR (Fig.10C). We tested the expression of 20 genes falling into three categories: CSF-cN known markers (positive control), hindbrain markers (negative control) and others, for example neuronal markers or candidates of interest (Fig.10C and *data not shown*). Neuronal markers, *elavl3* and *pvalb6*, were not found to be particularly enriched in the GFP+ population, probably because of the fact that the majority of cells in the GFP- population are neurons. However, the small increase in the relative amount of *gad67* and *gata2a* reflect the GABAergic nature of CSF-cNs. Contrary to other neuronal markers, GABAergic ones are enriched due to the presence of a small proportion of non-CSF-cN GABAergic neurons in the GFP- fraction. In contrast, CSF-cN markers were strongly enriched while hindbrain ones were down-regulated in the green population, which indicated that our approach was efficient at specifically sorting CSF-cNs.
Up to five biological replicates (a replicate being a pair constituted of the green population and its reference dark population) were used to perform RNA sequencing with a depth of ~60 million reads per sample. Reads were mapped to Zv10 genome annotation by the bioanalysis facility of the ICM and a mean fold change of 2 was used as a cut-off to consider a gene up-regulated in either one of the populations. Altogether, this strategy provided us with a rich dataset of ~200 genes enriched in CSF-cNs compared to other cells in the trunk (Fig.10D).

Validation of the transcriptome dataset. Because this study was the first one to provide gene expression profiling of spinal CSF-cNs, we could not compare our dataset to already described ones. After verification, we confirmed the presence in our list of all the known CSF-cN markers already described. In order to further validate our strategy and to verify

the expression of novel genes detected in our CSF-cN transcriptome dataset, we performed whole-mount fluorescent *in situ* hybridization (FISH). Within the framework of my project, I focused on testing the expression of genes related to the CSF-cN apical extension structure, namely actin-binding factors encoding genes *baiap2a*, *baiap2l1b*, *myo3b* and *espin* as well as cilia-related *dcdc2b*, *foxj1a*, *foxj1b*, *katnal2*, *kif19* and *tppp3*. At 24 hpf, all genes were reliably detected in CSF-cNs but *foxj1a*, *foxj1b*, and *katnal2* appeared to be more broadly expressed in the ventral spinal cord (Fig.11). Also performed at 3 dpf, the stage when the RNA sequencing was performed, FISH results clearly indicated the expression of *myo3b* and *espin* specifically in CSF-cNs (see Chapter 3) but were not as conclusive for the other genes, a result hard to interpret due to the difficulty for probes to penetrate larvae tissues (*data not shown*). Together with others from the lab, my results demonstrated that 33 out of 42 of the top hits in our dataset were expressed in CSF-cNs, yielding a ~ 80% degree of success for our approach.

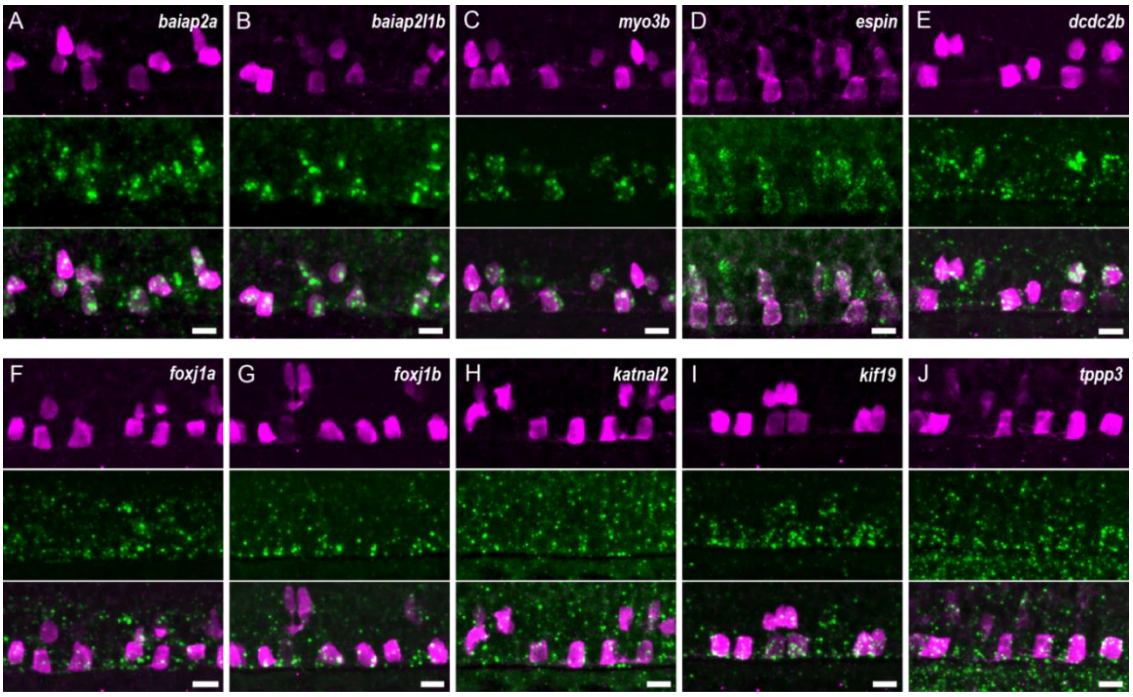

Figure 11. Validation of the CSF-cN transcriptome dataset by fluorescent *in situ* hybridization
Fluorescent *in situ* hybridization was performed at 24 hpf in *Tg(pkd2l1:TagRFP)* (or *Tg(pkd2l1:GCaMP5G)* in the case of *espin*) embryos followed by immunostaining against RFP (or GFP) to detect CSF-cNs in the spinal cord. Scale bars, 10 µm.
Various actin organizers - *baiap2a* (**A**), *baiap2l1b* (**B**), *myo3b* (**C**), *espin* (**D**) – as well as cilia-related genes – *dcdc2b* (**E**), *foxj1a* (**F**), *foxj1b* (**G**), *katnal2* (**H**), *kif19* (**I**), *tppp3* (**J**) – are found enriched at 24 hpf reflecting the importance of both actin and microtubule cytoskeletons for CSF-cNs.

C. Extension of the polymodality of CSF-cNs

By performing FISH at different stages, we demonstrated that our FACS/RNAseq strategy was efficient at detecting genes expressed by spinal CSF-cNs in zebrafish. Among the top

hits of this list, we find the strong markers of CSF-cNs such as *urp1*, *urp2*, *pkd2l1* or *sst1* (Djenoune *et al.*, 2017). Our CSF-cN transcriptome dataset proved to be informative and yielded a list of ~200 genes whose expression is enriched in CSF-cNs. Notably, numerous genes expressed by CSF-cNs are associated with neurotransmission, an observation consistent with the neuronal nature of the cells. The rest of the genes found in CSF-cNs can be roughly grouped into four categories according to the broad functions they are associated with (Fig.12A).

A

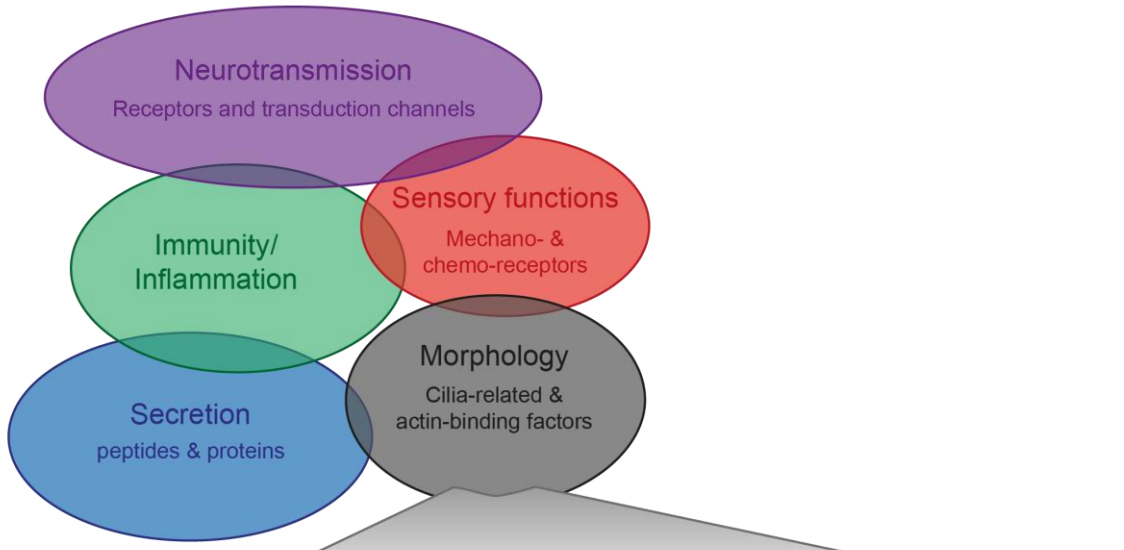

B

Gene name	Ensembl ID (GRCz10)	Fold enrich.	Pvalue	Mouse Homolog
espn	ENSDARG00000076414	5,93	6,09E-07	ESPN
myo3b	ENSDARG00000006892	5,79	2,64E-16	MYO3B
rhpn2	ENSDARG00000014577	3,16	7,69E-12	RPHN2
baiap2a	ENSDARG00000062799	1,86	1,33E-06	BAIAP2
clstn2	ENSDARG00000060637	1,77	8,03E-08	CLSTN2
scinlb	ENSDARG00000058348	1,54	3,71E-06	not reported
cdh8	ENSDARG00000037478	1,41	6,97E-05	CDH8
pcdh15b	ENSDARG00000008127	2,31	2,07E-03	PCDH15
baiap2l1b	ENSDARG00000031119	2,14	1,27E-02	BAIAP2L1

Figure 12. The polymodality of CSF-cNs further revealed by their transcriptome analysis
A, Main functions carried by the up-regulated transcripts found in our dataset that revealed novel CSF-cN genes involved in immunity, secretion, chemo- and mechano-sensory functions and morphogenesis.
B, Up-regulated actin-binding proteins in CSF-cNs found in our transcriptome analysis.

The most predominant category in terms of number of candidates and degree of enrichment after 'Neurotransmission' is the 'Neurosecretion' group. Our dataset revealed the expression by CSF-cNs of several proteins and peptides either secreted or involved in secretion. This observation reinforces the neurosecretory function hypothesis based on the description of large numbers of granules and vesicles at the apical region of the cells (Djenoune *et al.*, 2017). According to our transcriptome results, neurosecretion by CSF-cNs would be involved in various biological processes among which immune-related functions. The 'Immunity/inflammation' group is the second most represented with the expression of several genes taking part in pathogen detection, inflammatory response, immune cell migration and activation. In a third

group are the 'Sensory' genes responsible for detection (channels and receptors) of mechano- and chemo-sensory cues and the transduction of the signal. Interestingly, among the chemoreceptors detected, some could be associated with the detection of pathogens. Finally, a great number of genes are related to actin and microtubule cytoskeleton modulation suggesting a role in cellular morphogenesis of CSF-cNs, including of the apical extension constituted of actin-based protrusions and a primary cilium.

The study of the CSF-cN gene expression profile opens several lines of investigation for CSF-cNs. Our dataset revealed the expression of several receptors, thus extending the sensory potential of the cells. It consolidated the hypothesis that CSF-cN are neurosecretory cells, initially based on ultrastructural observations, and provided us with a list of candidate secreted proteins and peptides to investigate. Whether CSF-cNs are capable to secrete these factors directly into the CSF to establish a long-range communication with other cell types remains unclear. The analysis of the gene expression profile also provided strong indication that CSF-cNs might collaborate with the immune system by modulating the behavior of immune cells, detecting pathogens through specialized receptors and modulating inflammation. Finally, the transcriptome analysis of CSF-cNs described the expression of several genes of interest in the context of my study, notably a short list of actin-binding proteins (Fig.12B).

The FACS-based approach and the subsequent RNA sequencing provided me with molecular factors to investigate for their role in the formation of the CSF-cN microvilliated apical extension (see Chapter 3) and, more generally, set the foundations for several projects in the lab.

In the context of the biological question I addressed during my PhD - tackling the molecular mechanisms underlying the formation of sensory microvilli -, it was important to compare my results about CSF-cNs to another microvilliated sensory system. The transcriptome analysis of zebrafish nHCs has proven to be challenging. I sought to adapt the FACS/RNAseq protocol previously applied to CSF-cNs to establish the gene expression profile of nHCs and compare the morphogenetic factors expressed by the two cell types.

II. TRANSCRIPTOME ANALYSIS OF NHCS: REFINING OUR UNDERSTANDING OF NHC-SPECIFIC GENE EXPRESSION

A. Zebrafish nHCs are homologous to mammalian hair cells

Neuromast hair cells (nHCs) represent a great field of study: the simplicity and accessibility of this system facilitates the analysis of a number of fundamental processes of interest that take place during its development (Ghysen and Dambly-Chaudière,

2004). nHCs are closely related to iHCs that we extensively described in Chapter 1. Thus, nHCs also represent a relevant system to study mechanotransduction in HCs and better understand the mechanisms underlying deafness, a major public health issue. Here, I will briefly review the main characteristics of the nHC system in zebrafish that distinguish them from iHCs.

The lateral line system in fish. Aquatic animals necessarily experience hydrodynamic stimuli when maneuvering in water. Most aquatic animals have developed a dedicated sensory system to exploit the wealth of information carried by water movements and/or pressure fluctuations and adjust behavior accordingly. In cartilaginous and bony fish (and amphibians), this sensory system is called the lateral line and is involved in a variety of behaviors (Coombs and Montgomery, 1999). The lateral line comprises a set of superficial discrete sensory organs called neuromasts arranged in lines on the body surface according to a species-specific pattern. The lateral line is typically divided into two branches: the anterior lateral line on the head and the posterior lateral line on the trunk. Each neuromast is constituted of a cluster of 15-20 hair cells, homologous to iHCs in the inner ear, surrounded by support cells, themselves surrounded by mantle cells (Hernández *et al.*, 2007). Each neuromast is also innervated by at least two sensory afferent neurons and efferent fibers. Afferent neurons are bipolar neurons located in cranial ganglia: between the ear and the eye for the anterior lateral line and posterior to the ear for the posterior lateral line (Ghysen and Dambly-Chaudière, 2004). All afferent neurons form characteristic ribbon synapses with nHCs (Nicolson, 2015) and project to the hindbrain. Similarly, each neuromast is innervated by at least two sets of efferent neurons contributing to the modulation of the nHC responses: one cholinergic set from the hindbrain and one dopaminergic set from the forebrain (Bricaud *et al.*, 2001). Most of what we know about the lateral line system comes from studies of the posterior branch.

Development of the lateral line in zebrafish. The principles of the posterior lateral line development involved fundamental biological processes including collective cell migration, tissue patterning and morphogenesis. The development of the lateral line system has long fascinated embryologists because of its unusual aspect of neuromast deposition by a migrating primordium according to a predefined pattern. In zebrafish, the primordium for the first line of the posterior lateral line begins its migration at 22 hpf and ends its course at 48 hpf (Metcalfe, Kimmel and Schabtach, 1985). The deposition of a neuromast involves the detachment from the still moving primordium's trail of a group of ~20 cells that slow down and finally stop migrating to form proneuromasts.

The deposition of cells from the trailing edge of the primordium is the result of complex signaling and cell behavior. The migratory potential is heterogeneous within the primordium and determines different categories of cells, namely migrating cells versus

cells being deposited. Cell migratory behavior is coordinated within the primordium by an intrinsic mechanism. In the case of the posterior lateral line, it is controlled by the interaction between the ligand SDF1, expressed along the preexisting pathway of migration, and the chemokine receptor CXCR4 (David *et al.*, 2002). Cells at the leading edge express CXCR4 and respond to the guidance cue SDF1 while cells at the trailing edge lose this ability (Ghysen and Dambly-Chaudière, 2007). The establishment of restricted domains of expression for CXCR4 is critical for the establishment of a virtual local gradient of SDF1 signal. This gradient is achieved by the expression of another chemokine receptor in trailing cells, CXCR7 capable of sinking SDF1 away from CXCR4 (Dambly-Chaudière, Cubedo and Ghysen, 2007).

Future proneuromast cells appear to organize themselves according to a rosette-like pattern that prefigures the shape of the future neuromast. The formation of epithelial rosettes is driven by FGF signaling restricted to the trailing zone of the primordium through mutual inhibition with Wnt, itself restricted to the leading edge (Lecaudey *et al.*, 2008; Nechiporuk and Raible, 2008). A few hours after deposition, proneuromasts start differentiating still under the regulation of FGF. At the center of the proneuromast, nHC precursors are characterized by the up-regulation of *atoh1a* and *deltaD* while surrounding cells express *notch3*. The expression of the DeltaD ligand by central cells on one side, and the Notch receptor by surrounding cells on the other side allows the lateral inhibition of *atoh1a* by central HC precursors in surrounding cells, resulting in their specification as support cells (Thomas *et al.*, 2015).

Singularities of mechanosensory functions in neuromasts. Mechanotransduction in nHCs follows the same principles than in iHCs (see Chapter 1). The mechanotransduction channel is thought to exhibit the same molecular organization than in iHCs (see Chapter 1, I.B and II.B). Notably, a recent study demonstrated the critical role of Tmc2b for mechanotransduction in nHCs of the posterior lateral line (Chou *et al.*, 2017), similar to its orthologous counterparts TMC1 and TMC2 in mammals (Pan *et al.*, 2013). At the structural level, the nHC apical extension exhibits the same stereotyped staircase pattern with the singularity of retaining the kinocilium after differentiation and a larger number of stereocilia.

nHCs share the same basic functional principles with iHCs: they are depolarized when the bundle is deflected towards the kinocilium and hyperpolarized when it moves in the opposite direction. The establishment of morphological polarity in nHCs involves planar cell polarity (PCP) as it is the case in the inner ear (see Chapter 1, II.A). In the inner ear, PCP is critical for the uniform orientation of iHC bundles throughout the tissue. In neuromasts, PCP results in the orientation of all nHC bundles along the same axis but with a roughly equal number of nHCs of opposite polarity. This arrangement is achieved through the generation of pairs of cells along an axis of mirror symmetry initially determined by the PCP axis: two sister cells from the same pair will adopt opposite orientation. The coordination of nHC orientation within a neuromast was shown to

depend on Van-Gogh like 2 signaling, a canonical PCP protein (Lopez-Schier and Hudspeth, 2006; Mirkovic, Pylawka and Hudspeth, 2012). As a result, each neuromast can equally respond to stimuli of opposite direction along the perpendicular axis to the PCP axis. nHCs dedicated to one direction or the other are innervated by distinct afferent neurons (Faucherre *et al.*, 2009). It was shown that neuromasts from the posterior lateral line responded to stimuli oriented along the antero-posterior axis while those located around the eye best responded to stimuli in the axis tangential to the eye perimeter (Chou *et al.*, 2017). Altogether, neuromasts covering the fish set a Cartesian coordinate system for the detection of hydrodynamic stimuli.

Another landmark of zebrafish HCs is that they retain their kinocilium after differentiation as opposed to iHCs in mammals and birds. The exact role of the kinocilium in mature HCs remains elusive. A recent study, based on the analysis of the *ift88* cilia mutant, cast some light on its possible roles. The authors demonstrated that the loss of the kinocilium does not result in PCP defects, in contrast to what was shown in mouse iHCs (Jones *et al.*, 2008), indicating that it is not involved in the morphogenesis of the hair bundle (see Chapter 1, II.B) (Kindt, Finch and Nicolson, 2012). Rather, they showed that the kinocilium is required for early mechanosensitivity exhibited by immature nHCs prior to the functional switch when the hair bundle comes to maturity and tip links appear (Kindt, Finch and Nicolson, 2012).

Differences that distinguish mechanosensory function and structural organization of nHCs in the lateral line system from iHCs in the inner ear are thus adaptations tuned to the detection from early on of a multi-facetted stimulus, water flow and vibrations coming from different directions.

Regeneration properties of hair cells in zebrafish. HCs in general are susceptible to chemical exposure and mechanical insults and this is particularly true for nHCs that are directly exposed to the outside world. In contrast to their mammalian counterpart, HCs in zebrafish have the ability to regenerate after damage and to restore nHC number and neuromast polarity. Regeneration of HCs rapidly occurs after injury, within 72 hours. Within 24 hours, neighbor support cells divide and give rise to two daughter precursors of HCs through asymmetric division (Lopez-Schier and Hudspeth, 2006). Precursors are characterized by the down-regulation of *notch3* resulting in the consolidation of *atoh1a* signal, a molecular determinant of nHCs. The regeneration system of nHCs in zebrafish was qualified “inexhaustible” by Pinto-Texeira and colleagues in (Pinto-Teixeira *et al.*, 2015) where they showed that regeneration efficiency was unaffected by age and recurrent damage.

Regeneration capacity is lost in mammals and HCs that have undergone trauma or toxicity degenerate in a fashion thought to be irreversible. HC loss necessarily results in deafness and represents a major public health concern. Thus, regeneration of zebrafish HCs has constituted a great field of investigation.

Remaining questions about nHCs. The zebrafish lateral line system has emerged as a model to study fundamental biological processes such as collective cell migration, tissue patterning or cell fate in regeneration process. The wealth of information provided by nHCs in zebrafish opens numerous questions.

First, regarding the development of the lateral line and the establishment of functional neuromasts: although different migration behaviors within the primordium are clearly controlled by SDF1/CXCR4 signaling, the molecular pathways underlying this complex mechanism remain elusive. For example, the nature of the source of SDF1, described as a stripe defining the migration pathway of the primordium, remains unclear. It is also not clear whether SDF1 acts as a diffusible reagent or as a bound molecule. It is all the more important to answer this question because the SDF1-CXCR4 interaction is involved in other cell migration-dependent mechanisms such as the formation of metastases in cancer, or homing of lymphocytes (Müller *et al.*, 2001). Unlike other chemokines, SDF1 does not establish a gradient to guide the primordium; instead, it is the asymmetrical activity of the CXCR4 receptor within the primordium that is responsible for the directional migration. The establishment of this intrinsic gradient is not fully understood and requires further investigation. The establishment of PCP also carries its load of open questions and the original signal determining the PCP axis is unknown.

Second, regarding the regeneration process in nHCs: the molecular mechanisms underlying cell fate and differentiation taking place in cells becoming hair cell precursors after damage are essentially not understood. During the regeneration process, support cells supply the neuromast with hair cell precursors through asymmetrical divisions (Lopez-Schier and Hudspeth, 2006; Mirkovic, Pylawka and Hudspeth, 2012). The identity and location of the stem cell population giving rise to hair cell precursors are not known. In the same vein, the molecular trigger and pathways underlying the activation of hair cell differentiation into latent precursor cells require further investigation. The study of changes in gene expression associated with regeneration will help to identify signaling pathways involved in this process (Jiang *et al.*, 2014). Support cells constitute a heterogeneous population seemingly organized in domains exhibiting various levels of Notch signaling (Pinto-Teixeira *et al.*, 2015), which is thought to determine the geometric order of hair cell regeneration. The study of the spatiotemporal control of the Notch receptor within neuromasts will provide insightful information.

The unique features of nHCs have aroused great interest from the community and established the zebrafish lateral line as a model system to elucidate fundamental mechanisms involved in development and regeneration (Dambly-Chaudière *et al.*, 2003). Its simplicity and accessibility in zebrafish make the lateral line a good alternative system to investigate mechanotransduction and morphogenesis in HCs with the assumption that principles are transposable between nHCs and iHCs. However, only a few studies have examined the principles of mechanotransduction in nHCs and even fewer have investigated the molecular determinants of hair bundle formation and organization.

B. Adapting the FACS-based approach to nHCs

The study of the transcriptome profile of nHCs in zebrafish has been challenging due to their relative scarcity and the difficulty to isolate them. Several hair cell transcriptome analysis have been carried out in comparative studies aiming at answering specific questions regarding gene expression changes occurring in mutant animals, during regeneration or after exposure to drugs (McDermott Jr., Baucom and Hudspeth, 2007; Jiang *et al.*, 2014). Few studies have investigated the gene expression profile of zebrafish HCs under physiological conditions (Gallardo and Behra, 2013; Erickson and Nicolson, 2015; Matern *et al.*, 2018). The isolation techniques either involve tissue dissociation using FAC sorting (Gallardo and Behra, 2013) or RNA pulldown (Erickson and Nicolson, 2015; Matern *et al.*, 2018). To perform the transcriptome analysis of nHCs specifically in zebrafish, we adapted the previous FACS-based protocol that proved to be efficient for CSF-cNs. *This study was done in collaboration with Julian Roussel in the lab.*

The specific labeling of nHCs by the vital dye YO-PRO-1. Published transcriptome profiling of zebrafish HCs often do not distinguish between ear and neuromast HCs, mostly due to the fact that there is, up to now, no known molecular marker to discriminate between them. To overcome the problem of isolating nHCs specifically via the use of transgenic lines, we turned to vital dye staining proven to be reliably labelling nHCs only (Santos *et al.*, 2006). We used YO-PRO-1, a monomeric cyanine dye discovered 15 years ago to selectively label nHC nuclei for at least 48 hours (Macdonald, Raible and Rubel, 2002). The selectivity of these staining techniques relies on the fact that monomeric cyanine dyes are cell-non-permeant but can enter active nHCs through their large cationic channels. By bath applying 3-dpf old AB larvae with YO-PRO-1 (4 µM, 30 min), we obtained strong and specific labeling of nHCs from the posterior and anterior lateral line (Fig.13A1). When we tested the specificity of our staining, we found that YO-PRO-1 stains only nHC nuclei in our transgenic line expressing LifeAct under the control of the *myob6* promoter (Fig.13A2). We typically used ~50-100 YO-PRO-labeled AB 3-dpf old larvae to sort nHCs and perform their transcriptome analysis.

The FACS/RNAseq approach. Once nHCs labeled with YO-PRO-1 in 3-dpf wild-type larvae, we followed the same strategy as previously described (in I.B) Briefly, cells from YO-PRO-treated larvae were mechanically dissociated to obtain single cell suspension and sort YO-PRO-negative (‘dark’) versus YO-PRO-positive (‘green’) populations (Fig.13B, right panel). The gates to discriminate between the two populations were demarcated using a control cell suspension obtained from non-treated sibling larvae (Fig.13B, left panel). Sorting typically yielded between 3000 and 15000 GFP+ cells for ~50-100 3-dpf larvae and take about 30 min. Total RNA extraction from both ‘green’ and ‘dark’ cell populations for this approach resulted in higher RNA concentrations than for the CSF-cN FACS approach.

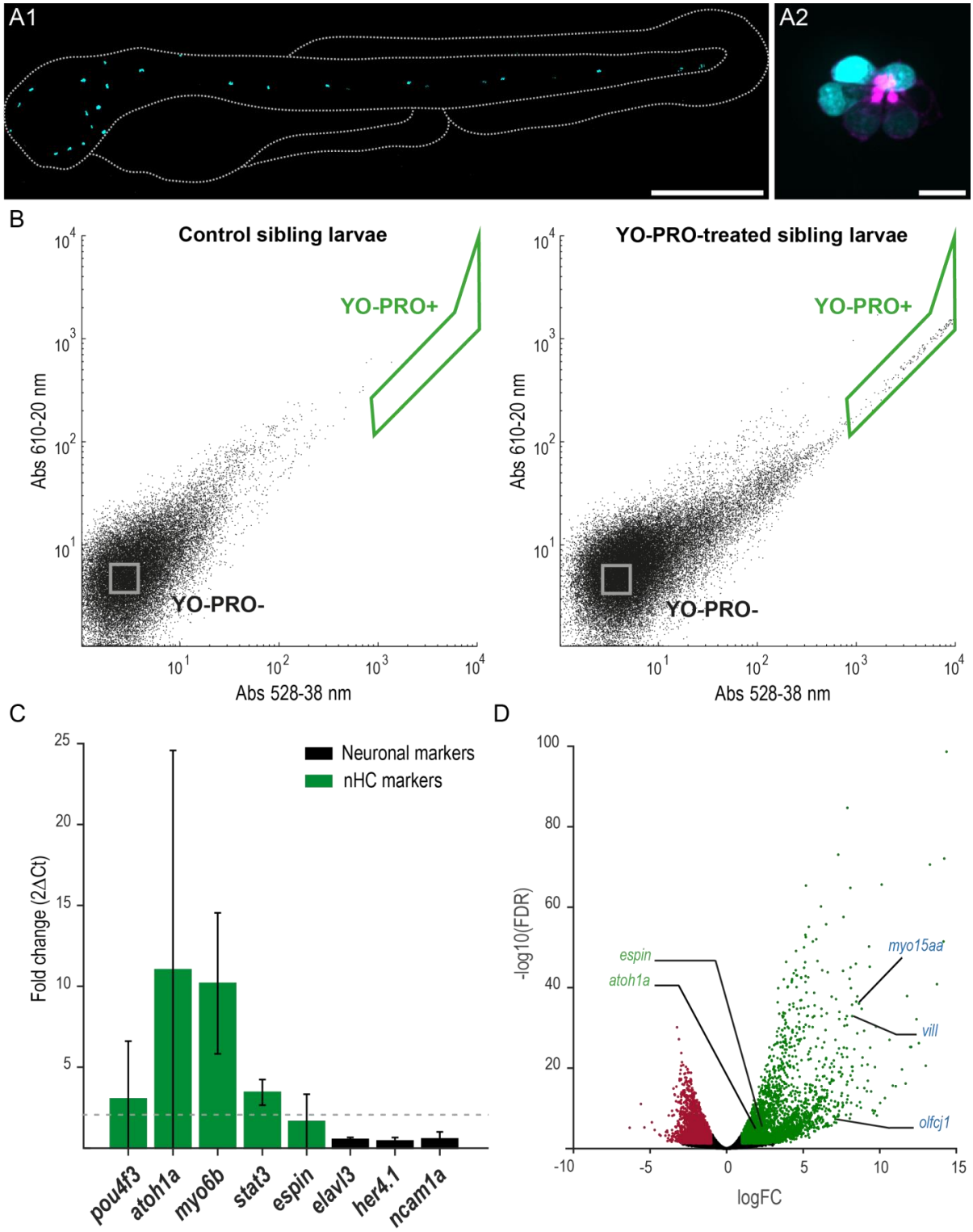

Figure 13. FACS/RNAseq approach adapted to the transcriptome analysis of nHCs

A, Illustrative images of the specific YO-PRO-1 labelling in nHCs at 3 dpf. **A1**, YO-PRO-1 staining (4 µm, 30 min) in a 3-dpf old AB larva is specific to nHCs of both anterior and posterior branches of the lateral line. Dotted lines outline the fish body. Scale bar, 500 µm. **A2**, Illustrative image of the YO-PRO-1 staining performed in *Tg(myo6b:LifeAct-TagRFP;cryaa:C)* 3-dpf larvae (this line was generated in the context of my PhD project). F-actin is marked in HCs by LifeAct-TagRFP (magenta) under the control of the *myo6b* promoter. YO-PRO-1 (cyan) only labels HC nuclei and not surrounding cells in the neuromast. Scale bar, 10 µm.

B, Illustrative FACS plots showing the characteristic autofluorescent 'tail' where most cells follow a 1:1 green:red scatter. Unstained sibling larvae were used as a negative control to draw the gates (left panel).

In the YO-PRO-positive samples, a small fraction of green-shifted cells (between 0.2 and 0.4%) fall into the YO-PRO+ gate (right panel).
C, Total RNA was extracted from YO-PRO- ("dark") and YO-PRO+ ("green") fractions. Enrichment in the green fraction in nHCs was tested by qPCR and comparing gene expression between the green and the dark populations. Known nHC markers – *pou4f3, atoh1a, myo6b, stat3* and *espin* - show enrichment in the 'green' pool as opposed to neuronal markers – *elavl3*, *her4.1* and *ncam1a*.
D, Volcano plot of all 6 RNAseq replicates aligned to Zv10 genome annotations. *atoh1a* and *espin,* two already known nHC markers (green), as well as three new markers, *myo15aa, vill* and *olfcj1* (blue). *myo15aa* and *vill* encore an unconventional myosin and an actin-bundling factor respectively known to be involved in the stereocilia formation and maintenance in iHCs (Chapter1, IIIA). o*lfcj1*, encoding an olfactory receptor, is one of the many unexpected hits of the transcriptome dataset that suggest that nHCs could carry other sensory modalities.

Prior to sequencing, the enrichment in nHCs of our sorted 'green' population was confirmed by qPCR, testing a set of nHC-specific markers (positive control) and neuronal genes (negative control) (Fig.13C and *data not shown*). Four nHC markers out of five were found to be enriched in the green population, *atoh1a*, *myo6b*, *stat3* and *pou4f3*, while neuronal markers were down-regulated. *espin* fell under the enrichment cutoff, which probably reflects low expression levels in nHCs (Fig.8).
Again, up to five biological replicates were used to perform the transcriptome analysis of nHCs with a depth of 44 million reads per sample.

This strategy provided us with an extraordinarily rich dataset of ~2500 enriched genes in YO-PRO-stained cells with a cut-off of a mean fold change of 2 (Fig.13D). We verified that our list contained the previously known nHC markers, such as *atoh1a*, *espin*, *pou4f3*, *myo6b*, and others (Fig.13D and *data not shown*). Our transcriptome approach was successful at detecting many of the landmark genes of HCs and specific to nHCs involved in mechanotransduction, structure and regeneration (Fig.14). Surprisingly, our results indicated the expression of by nHCs of numerous novel genes involved in chemosensation and neuromodulation through the expression of serotoninergic receptors and channels (Fig.14). Validation of this dataset by classical whole mount FISH and using the novel RNAscope® technology, and functional analysis of best candidate genes are currently on-going. Preliminary data strongly suggest that, indeed, nHCs respond to serotonin (*data not shown*). The source of serotonin potentially detected by nHCs and the biological relevance of this signaling remain open questions. The validation of our hits for chemosensation is still unclear and requires further investigation.

If validated, our nHC transcriptome analysis will supply the zebrafish community with a useful dataset to explore novel genes and functions, and unravel the molecular mechanisms underlying fundamental biological processes of interest. More generally, after confirmation, some of these results could be extended to all HCs, including HCs of the inner ear in mammals and birds.3

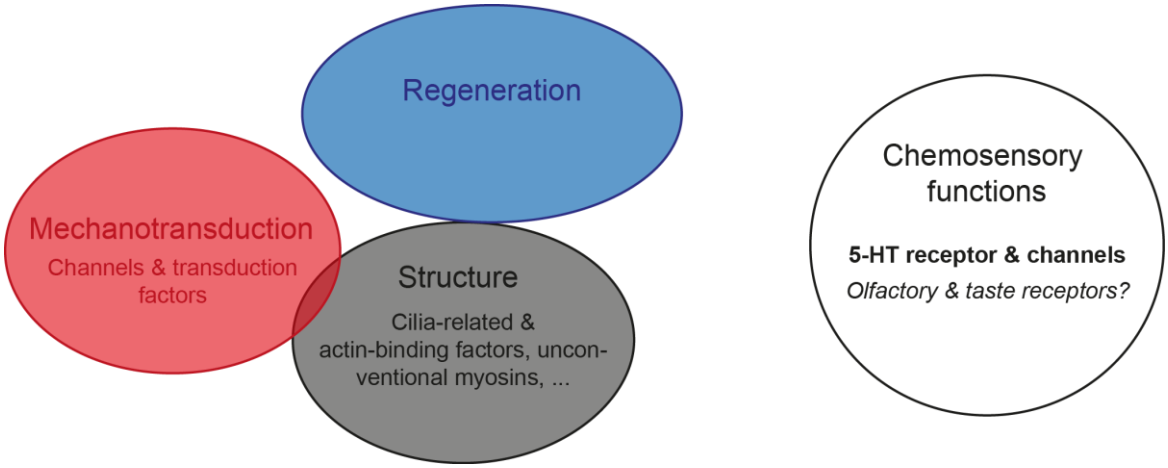

Figure 14. The transcriptome analysis of nHCs detects typical nHC groups of genes and suggests novel functions
Our FACS/RNAseq approach produced a rich dataset of genes enriched in nHCs and efficiently detected many of the known markers typically expressed by nHCs for mechanotransduction, structure, and regeneration. In addition, our transcriptome analysis detected numerous genes involved in chemosensory functions with numerous serotoninergic receptor and channel components as well as many receptors usually associated with olfactory and taste sensory cells.
Preliminary data seem to confirm the ability of nHCs to respond to serotonin. The validation of expression and function of chemosensory receptors requires further investigation.
The validation of the transcriptome dataset by *in situ* hybridization techniques is currently on-going.

C. Comparison of the morphogenetic factors found in CSF-cNs and nHCs

My PhD project aimed at investigating the molecular mechanisms underlying the formation by microvilliated sensory cells (MSCs) of their apical extension, focusing on CSF-cNs. The transcriptome analysis of CSF-cNs provided me with a short list of candidate genes to investigate (see I.C). In the light the results of functional experiments I have carried out (see Chapter 3), I started building a comprehensive model of the elaboration of sensory microvilli in CSF-cNs (see Chapter 4, Fig21). The description of the morphogenetic gene expression profile of nHCs should help to determine whether the basic principles of this model can be extended to other MSCs such as HCs. More generally speaking, the comparison between the CSF-cN and nHC expression profiles should highlight the similarities and differences in the molecular pathways underlying morphogenesis in the two cell types, thus providing molecular basis of the making of specialized sensory microvilliated apical extensions.

The study of CSF-cN morphogenesis led to the description of four main groups of factors involved in 1/ cell polarization (Crb1), 2/ initiation and protrusion of actin filaments (Baiap2a, Baiap2l1b), 3/ elongation and tight packing of actin filaments by actin-bundling factors (Espin) with the support of 4/ unconventional myosins (Myo3b) (see Chapter 3, Chapter 4, Fig.21). I compared enriched genes for each category between CSF-cNs and nHCs with the addition of the Usher syndrome type I proteins critical for the structural cohesion of stereocilia in HCs (see Chapter 1, II.B) (Table 2).

I found that, overall, CSF-cNs and nHCs express equivalent factors, namely paralogs, for each group, suggesting that both cell types rely on similar molecular mechanisms to form their apical extension. The expression of different sets of paralogs, could underlie some of the structural differences observed in the mature apical extensions: rigid microvilli derivatives organized in a stereotypical staircase fashion for nHCs and a tuft of microvilli without obvious organization for CSF-cNs (Fig.1). The comparison highlighted the expression of numerous unconventional myosins in nHCs in contrast to just one in CSF-cNs, these myosins being involved in the sub-structural organization and/or maintenance of stereocilia. Interestingly, the analysis of the Usher syndrome type I factors revealed that CSF-cNs express *pcdh15b*, a component of the tip links connecting stereocilia to one another and gating the mechanotransduction channel in iHCs (see chapter 1, II.B). This observation suggests that CSF-cNs might form links between their microvilli, which could play a role in the cohesion of the apical extension subject to CSF flow and/or in their mechanosensory function (Böhm *et al.*, 2016).

CSF-cNs			nHCs		
Gene name	Fold enrich.	Pvalue	Gene name	Fold enrich.	Pvalue
Cell polarity					
crb1	2,51	1,3E-05	crb3a	4,89	4,5E-08
			crb3b	4,83	1,3E-09
Initiation & protrusion of actin filaments					
baiap2l1b	2,14	1,3E-02	baiap2l2b	5,18	1,1E-09
baiap2a	1,86	1,3E-06	baiap2l1b	4,14	7,6E-23
			baiap2a	2,68	4,9E-04
Actin-bundling of actin filaments					
espn	5,93	6,1E-07	vill	8,20	5,4E-36
			espnla	4,77	3,4E-07
			espnlb	3,74	5,1E-07
			espn	2,35	2,1E-06
Unconventional myosins					
myo3b	5,79	2,6E-16	myo15aa	8,64	3,0E-39
			myo5c	5,06	2,3E-09
			myo15ab	4,85	6,1E-06
			myo1cb	3,98	2,0E-43
			myo6a	3,66	6,6E-28
			myo6b	3,64	6,9E-07
			myo15b	2,61	6,7E-04
			myo3b	1,35	8,7E-02
Usher syndrome type I factors					
pcdh15b	2,31	2,1E-03	myo7aa	3,92	8,4E-05
			pcdh15a	1,39	3,9E-02
			cdh23	1,70	8,2E-02

Table 2. Comparison of the morphogenetic factors expressed by CSF-cNs versus nHCs

The existence of different isoforms could not be evaluated with the depth of our RNA sequencings but can not be neglected. In rodent, Espin exist in different isoforms associated with specific functions in addition to their main actin-bundling one (Sekerková *et al.*, 2006). The existence of different Espin isoforms in fish has not been investigated but it is possible that different splicing variants exist as well. Consequently, distinct isoforms could support the formation of parallel actin bundles in CSF-cNs and nHCs.

MATERIAL & METHODS

Fluorescence activated cell sorting (FACS) and qPCR validation

- ***CSF-cNs*:** Roughly 150 3-dpf zebrafish larvae obtained from *Tg(pkd2l1:Gal4;UAS:GFP)* double transgenic line were manually dechorionated prior to decapitation at the intersection of the hindbrain with the spinal cord (Fig.10A). The remaining trunk tissue was immediately de-yolked in deyolking buffer (55 mM NaCl, 1.8 mM KCl, 1.25 mM $NaHCO_3$)and mechanically dissociated in FACSmax cell dissociation buffer (AMS Biotechnology, Abingdon, UK; T200100) following the protocol described by Manoli & Driever (Manoli and Driever, 2012). The resulting cell suspension was kept on ice until sorting on a BD Biosciences FACS Jazz sorter (Imagoseine FACS platform, Jacques Monod Institute, Paris, France) to isolate CSF-cNs. Sorting consisted in isolating distinct cell population according to fluorescence, typically GFP-positive cells (corresponding to CSF-cNs) versus non GFP-positive cells (mixture of non-fluorescent cells) referred to as 'green' and 'dark' populations respectively (Fig.9B). Sorting usually yielded 0.3% of 'green' cells for a total amount of 3000 to 15000 cells/run. Cells were sorted directly into lysis buffer (corresponding to Lysis Solution from the RNA isolation kit) and total RNA was quickly extracted using the RNAqueous-Micro total RNA isolation kit (ThermoFisher, AM1931) for both qPCR validation and RNAseq library preparation. To verify the enrichment of our 'green' population in CSF-cNs, we verified the expression of several marker genes by qPCR. Several sorting runs were diverted to this analysis: total RNA was converted into cDNA using the SuperScript VILO cDNA synthesis kit (Thermofisher, 11754050). qPCR was performed comparing the relative expression of a panel of diagnostic transcripts including known CSF-cN-specific genes (positive controls), hindbrain-specific ones (negative control) and neuronal markers between 'green' and 'dark' cDNA pools (Fig.10C).
- ***nHCs:*** The same strategy was applied to obtain RNA from nHCs. The sorting was carried out on cell suspensions dissociated from roughly 80 wild-type 3-dpf zebrafish larvae stained with Yo-Pro-1 (Invitrogen, Y3603) for 30 min at 4 µM (Fig.13A1). The sorting yielded in average 0.15% of 'green' cells for a total amount of 3000-15000 cells/run. The enrichment of sorting cells in nHCs was validated by qPCR using a panel of marker genes for nHCs (positive control) and neurons (negative control) (Fig.13C).

Library preparation and RNA sequencing

Library preparation and RNA sequencing were performed by the on-site sequencing facility from total RNA samples. The initial total amount of RNA per sample determined the choice of the kits used for the following steps.

- ***CFS-cNs*:** CSF-cN RNA samples typically yielded low amounts of RNA. Double-stranded cDNA was generated using the SMART-Seq v4 Ultra Low Input RNA Kit (Clontech/Takara, 634888) adapted to amounts as low as 10 pg of RNA. cDNA was subsequently fragmented and tagged with sequencing adapters using the Nextera DNA

Library Preparation Kit (Illumina). Replicates from 6 different sorting runs were used, each constituted of two RNA samples from 'green' cells and 'dark cells'.

- ***nHCs:*** Sorted cells from nHCs typically yielded higher RNA amounts and thus allowed us to use the standard process of library preparation with the KAPA mRNA HyperPrep Kit (Roche) capturing polyadenylated RNAs to produce fragmented and tagged cDNA. Replicates from 5 different sorting runs were used, each constituted of two RNA samples from 'green' cells and 'dark cells'.

After library preparation, standard Illumina sequencing was performed using High Output Flowcell Cartridge from the NextSeq 500/550 Output v2 kit (75 cycles, up to 400 million reads, Illumina).

Fluorescent *in situ* hybridation in CSF-cNs

3-dpf cDNA was generated from wild-type larvae using the RNeasy Mini Kit (QIAGEN, 74104) for total RNA extraction followed by reverse transcription using SuperScript IV (ThermoFisher, 18090010) to generate cDNA. DNA fragments corresponding to 10 candidate genes found as upregulated in the transcriptome dataset were amplified by PCR, gel-extracted using the QIAquick Gel extraction kit (QIAGEN, Germany) and cloned into the pCRII-Blunt-TOPO vector (Life Technologies, Carlsbad, CA, USA). Clones and orientation were verified by sequencing. Products were then generated by a second high-fidelity PCR using Phu polymerase (Phusion High-Fidelity DNA polymerase, New England Biolabs). Antisense digoxigenin-incorporating probes were transcribed from these clones using the T7 RNA polymerase with the RNA labeling kit (Sigma-Aldrich). All probes were purified using the mini Quick Spin RNA columns (Roche, Basel, Switzerland) and hydrolyzed to ~300 bp as previously described (Thisse and Thisse, 2008). Whole-mount fluorescent *in situ* hybridization was performed on 24-hpf embryos (Fig.11) and 72-hpf larvae (*data not shown*) of the transgenic line *Tg(pkd2l1:TagRFP)* prior to fluorescent immunohistochemistry to reveal GFP or RFP respectively to specifically label CSF-cNs. All samples were prepared by fixation in 4% PFA in PBS overnight at +4°C. At 72 hpf, larvae were additionally treated with Proteinase K in PBST for 20 minutes at 100 µg/mL to ensure the penetration of the probes. Probes were usually diluted to 1/200 for hybridization overnight at +70°C. To reveal the expression of candidate genes, primary anti-digoxigenin-POD coupled antibodies (Sigma-Aldrich) were added to 1/300. Staining was realized using FITC (1/200) tyramide-fluorophore solution for 30 min. Imaging was performed on an Olympus FV1000 confocal microscope equipped with a x20 water immersion objective.

The completion of fluorescent *in situ* hybridization demonstrated the convincing expression of 7 candidates out of 10 at 24 hpf. Other validations by *in situ* hybridization were carried out in the lab, leading to a total count of 33 confirmed hits out of 42 tested (*data not shown*).

References

Agduhr, E. (1922) 'Über ein zentrales Sinnesorgan (?) bei den Vertebraten.', *Zeitschrift für Anatomie und Entwicklungsgeschichte*, 66, pp. 223–360. doi: 10.1007/BF02593586.

Böhm, U. L. *et al.* (2016) 'CSF-contacting neurons regulate locomotion by relaying mechanical stimuli to spinal circuits', *Nature Communications*, 7:10866, pp. 1–8. doi: 10.1038/ncomms10866.

Böhm, U. L. (2016) *Physiological inputs to cerebrospinal fluid-contacting neurons*.

Bricaud, O. *et al.* (2001) 'Early efferent innervation of the zebrafish lateral line', *Journal of Comparative Neurology*, 434(3), pp. 253–261. doi: 10.1002/cne.1175.

Cerda, G. A., Hargrave, M. and Lewis, K. E. (2009) 'RNA profiling of FAC-sorted neurons from the developing zebrafish spinal cord', *Developmental Dynamics*, 238(1), pp. 150–161. doi: 10.1002/dvdy.21818.

Chou, S.-W. *et al.* (2017) 'A molecular basis for water motion detection by the mechanosensory lateral line of zebrafish', *Nature Communications*. Springer US, 8(1), p. 2234. doi: 10.1038/s41467-017-01604-2.

Coombs, S. and Montgomery, J. C. (1999) 'The Enigmatic Lateral Line System', in Fay, R. R. and Popper, A. N. (eds) *Comparative Hearing: Fish and Amphibians*. New York, NY: Springer New York, pp. 319–362. doi: 10.1007/978-1-4612-0533-3_8.

Covassin, L. *et al.* (2006) 'Global analysis of hematopoietic and vascular endothelial gene expression by tissue specific microarray profiling in zebrafish', *Developmental Biology*, 299(2), pp. 551–562. doi: 10.1109/TMI.2012.2196707.Separate.

Damann, N., Voets, T. and Nilius, B. (2008) 'TRPs in Our Senses', *Current Biology*, 18(18), pp. 880–889. doi: 10.1016/j.cub.2008.07.063.

Dambly-Chaudière, C. *et al.* (2003) 'The lateral line of zebrafish: A model system for the analysis of morphogenesis and neural development in vertebrates', *Biology of the Cell*, 95(9), pp. 579–587. doi: 10.1016/j.biolcel.2003.10.005.

Dambly-Chaudière, C., Cubedo, N. and Ghysen, A. (2007) 'Control of cell migration in the development of the posterior lateral line: antagonistic interactions between the chemokine receptors CXCR4 and CXCR7/RDC1', *BMC Developmental Biology*, 7(23). doi: 10.1186/1471-213X-7-23.

David, N. B. *et al.* (2002) 'Molecular basis of cell migration in the fish lateral line: role of the chemokine receptor CXCR4 and of its ligand, SDF1.', *Proceedings of the National Academy of Sciences*, 99(25), pp. 16297–16302. doi: 10.1073/pnas.252339399.

Djenoune, L. *et al.* (2014) 'Investigation of spinal cerebrospinal fluid-contacting neurons expressing PKD2L1: evidence for a conserved system from fish to primates', *Frontiers in Neuroanatomy*, 8(26). doi: 10.3389/fnana.2014.00026.

Djenoune, L. *et al.* (2017) 'The dual developmental origin of spinal cerebrospinal fluid-contacting neurons gives rise to distinct functional subtypes', *Scientific Reports*. Springer US, 7(719). doi: 10.1038/s41598-017-00350-1.

Djenoune, L. and Wyart, C. (2017) 'Light on a sensory interface linking the cerebrospinal fluid to motor circuits in vertebrates', *Journal of Neurogenetics*. Informa UK Limited, trading as Taylor & Francis Group, 31(3), pp. 113–127. doi: 10.1080/01677063.2017.1359833.

Erickson, T. and Nicolson, T. (2015) 'Identification of sensory hair-cell transcripts by thiouracil-tagging in zebrafish', *BMC Genomics*. BMC Genomics, 16(842). doi: 10.1186/s12864-015-2072-5.

Faucherre, A. *et al.* (2009) 'Afferent neurons of the zebrafish lateral line are strict selectors of hair-cell

orientation', *PLoS ONE*, 4(2). doi: 10.1371/journal.pone.0004477.

Fidelin, K. *et al.* (2015) 'State-Dependent Modulation of Locomotion by GABAergic Spinal Sensory Neurons', *Current Biology*. Elsevier, 25(23), pp. 3035–3047. doi: 10.1016/j.cub.2015.09.070.

Gallardo, V. E. *et al.* (2010) 'Molecular dissection of the migrating posterior lateral line primordium during early development in zebrafish', *BMC Developmental Biology*. BioMed Central Ltd, 10(120). doi: 10.1186/1471-213X-10-120.

Gallardo, V. E. and Behra, M. (2013) 'Fluorescent activated cell sorting (FACS) combined with gene expression microarrays for transcription enrichment profiling of zebrafish lateral line cells', *Methods*. Elsevier Inc., 62(3), pp. 226–231. doi: 10.1016/j.ymeth.2013.06.005.

Gato, Á. *et al.* (2005) 'Embryonic cerebrospinal fluid regulates neuroepithelial survival, proliferation, and neurogenesis in chick embryos', *Anatomical Record - Part A*, 284A(1), pp. 475–484. doi: 10.1002/ar.a.20185.

Ghysen, A. and Dambly-Chaudière, C. (2004) 'Development of the zebrafish lateral line', *Current Opinion in Neurobiology*, 14(1), pp. 67–73. doi: 10.1016/j.conb.2004.01.012.

Ghysen, A. and Dambly-Chaudière, C. (2007) 'The lateral line microcosmos', *Genes and Development*, 21(17), pp. 2118–2130. doi: 10.1101/gad.1568407.

Heinrich Martin, F., Ricardo Seoane, J. and Baile, C. A. (1973) 'Feeding in satiated sheep elicited by intraventricular injections of CSF from fasted sheep', *Life Sciences*, 13(2), pp. 177–184. doi: 10.1016/0024-3205(73)90193-8.

Hernández, P. P. *et al.* (2007) 'Regeneration in zebrafish lateral line neuromasts: expression of the neural progenitor cell marker sox2 and proliferation-dependent and-independent mechanisms of hair cell renewal.', *Developmental neurobiology*, 67(5), pp. 637–654. doi: 10.1002/dneu.

Huang, A. L. *et al.* (2006) 'The cells and logic for mammalian sour taste detection', *Nature*, 442(7105), pp. 934–938. doi: 10.1038/nature05084.

Hubbard, J. M. *et al.* (2016) 'Intraspinal Sensory Neurons Provide Powerful Inhibition to Motor Circuits Ensuring Postural Control during Locomotion', *Current Biology*, 26(21), pp. 2841–2853. doi: 10.1016/j.cub.2016.08.026.

Jalalvand, E. *et al.* (2016) 'Ciliated neurons lining the central canal sense both fluid movement and pH through ASIC3', *Nature Communications*. doi: 10.1038/ncomms10002.

Jiang, L. *et al.* (2014) 'Gene-expression analysis of hair cell regeneration in the zebrafish lateral line', *Proceedings of the National Academy of Sciences*, 111(14), pp. E1383–E1392. doi: 10.1073/pnas.1402898111.

Jones, C. *et al.* (2008) 'Ciliary proteins link basal body polarization to planar cell polarity regulation', *Nature Genetics*, 40(1), pp. 69–77. doi: 10.1038/ng.2007.54.

Kindt, K. S., Finch, G. and Nicolson, T. (2012) 'Kinocilia Mediate Mechanosensitivity in Developing Zebrafish Hair Cells', *Developmental Cell*, 23(2), pp. 329–341. doi: 10.1016/j.devcel.2012.05.022.

Kolmer, W. (1921) 'Das ,,Sagittalorgan" der Wirbeltiere', *Anatomy and Embryology*, (3), pp. 652–717. doi: 10.1007/BF02593657.

Lecaudey, V. *et al.* (2008) 'Dynamic Fgf signaling couples morphogenesis and migration in the zebrafish lateral line primordium', *Development*, 135(16), pp. 2695–2705. doi: 10.1242/dev.025981.

Lehtinen, M. K. *et al.* (2011) 'The Cerebrospinal Fluid Provides a Proliferative Niche for Neural Progenitor Cells', *Neuron*. Elsevier Inc., 69(5), pp. 893–905. doi: 10.1016/j.neuron.2011.01.023.

Lopez-Schier, H. and Hudspeth, A. J. (2006) 'A two-step mechanism underlies the planar polarization of regenerating sensory hair cells', *Proceedings of the National Academy of Sciences*, 103(49), pp. 18615–18620. doi: 10.1073/pnas.0608536103.

Macdonald, G., Raible, D. W. and Rubel, E. W. (2002) 'Zebrafish neuromast hair cell nuclei are labeled in vivo by uptake of monomeric cyanine dyes', *Microsc. Microanal.*, 8.

Manoli, M. and Driever, W. (2012) 'Fluorescence-activated cell sorting (FACS) of fluorescently tagged cells from zebrafish larvae for RNA isolation', *Cold Spring Harbor Protocols*, 7(8), pp. 879–886. doi: 10.1101/pdb.prot069633.

Matern, M. S. *et al.* (2018) 'Transcriptomic Profiling of Zebrafish Hair Cells Using RiboTag', *Frontiers in Cell and Developmental Biology*, 6(47). doi: 10.3389/fcell.2018.00047.

McDermott Jr., B. M., Baucom, J. M. and Hudspeth, A. J. (2007) 'Analysis and functional evaluation of the hair-cell transcriptorne', *Proceedings of the National Academy of Sciences*, 104(28), pp. 11820–11825. doi: 10.1073/pnas.0704476104.

Metcalfe, W. K., Kimmel, C. B. and Schabtach, E. (1985) 'Anatomy of the posterior lateral line system in young larvae of the zebrafish', *Journal of Comparative Neurology*, 233(3), pp. 377–389. doi: 10.1002/cne.902330307.

Mirkovic, I., Pylawka, S. and Hudspeth, A. J. (2012) 'Rearrangements between differentiating hair cells coordinate planar polarity and the establishment of mirror symmetry in lateral-line neuromasts.', *Biology open*, 1(5), pp. 498–505. doi: 10.1242/bio.2012570.

Müller, A. *et al.* (2001) 'Involvement of chemokine receptors in breast cancer metastasis.', *Nature*, 410(6824), pp. 50–56. doi: 10.1038/35065016.

Nechiporuk, A. and Raible, D. W. (2008) 'FGF-Dependent Mechanosensory organ patterning in zebrafish', *Science*, 320.

Nicolson, T. (2015) 'Ribbon synapses in zebrafish hair cells', *Hearing Research*, 330, pp. 170–177. doi: 10.1016/j.heares.2015.04.003.

Orts-Del'Immagine, A. *et al.* (2012) 'Properties of subependymal cerebrospinal fluid contacting neurones in the dorsal vagal complex of the mouse brainstem', *Journal of Physiology*, 590(16), pp. 3719–3741. doi: 10.1113/jphysiol.2012.227959.

Orts-Del'Immagine, A. *et al.* (2014) 'Morphology, Distribution and Phenotype of Polycystin Kidney Disease 2-like 1-Positive Cerebrospinal Fluid Contacting Neurons in The Brainstem of Adult Mice', *PLoS ONE*, 9(2). doi: 10.1371/journal.pone.0087748.

Pan, B. *et al.* (2013) 'TMC1 and TMC2 are components of the mechanotransduction channel in hair cells of the mammalian inner ear', *Neuron*, 79(3), pp. 504–515. doi: 10.1016/j.neuron.2013.06.019.

Pappenheimer, J. R., Miller, T. B. and Goodrich, C. A. (1967) 'Sleep-promoting effects of cerebrospinal fluid from sleep-deprived goats.', *Proceedings of the National Academy of Sciences of the United States of America*, 58(2), pp. 513–517. doi: 10.1073/pnas.58.2.513.

Park, H.-C., Shin, J. and Appel, B. (2004) 'Spatial and temporal regulation of ventral spinal cord precursor specification by Hedgehog signaling', *Development*, 131(23), pp. 5959–5969. doi: 10.1242/dev.01456.

Petracca, Y. L. *et al.* (2016) 'The late and dual origin of cerebrospinal fluid-contacting neurons in the mouse spinal cord', *Development*, 143, pp. 880–891. doi: 10.1242/dev.129254.

Pinto-Teixeira, F. *et al.* (2015) 'Inexhaustible hair-cell regeneration in young and aged zebrafish', *Biology Open*, 4(7), pp. 903–909. doi: 10.1242/bio.012112.

Santos, F. *et al.* (2006) 'Lateral line hair cell maturation is a determinant of aminoglycoside susceptibility in

zebrafish (Danio rerio)', *Hearing Research*, 213, pp. 25–33. doi: 10.1016/j.heares.2005.12.009.

Sekerková, G. *et al.* (2006) 'Espins and the actin cytoskeleton of hair cell stereocilia and sensory cell microvilli', *Cellular and Molecular Life Sciences*, 63(19–20), pp. 2329–2341. doi: 10.1007/s00018-006-6148-x.

Sternberg, J. R. *et al.* (2018) 'Pkd2l1 is required for mechanoception in cerebrospinal fluid-contacting neurons and maintenance of spine curvature', *Nature Communications*, pp. 1–10. doi: 10.1038/s41467-018-06225-x.

Stuckenholz, C. *et al.* (2009) 'FACS-Assisted Microarray Profiling Implicates Novel Genes and Pathways in Zebrafish Gastrointestinal Tract Development', *Gastroenterology*, 137(4), pp. 1321–1332. doi: 10.1053/j.gastro.2009.06.050.

Thisse, C. and Thisse, B. (2008) 'High-resolution in situ hybridization to whole-mount zebrafish embryos', *Nature Protocols*, 3(1), pp. 59–69. doi: 10.1038/nprot.2007.514.

Thomas, E. D. *et al.* (2015) 'There and Back Again: Development and Regeneration of the Zebrafish Lateral Line System', *Wiley Interdiscip Rev Dev Biol.*, 4(1), pp. 1–16. doi: 10.1111/j.1743-6109.2008.01122.x.Endothelial.

Vigh, B. *et al.* (1983) 'Cerebrospinal fluid-contacting neurons of the central canal and terminal ventricle in various vertebrates', *Cell and Tissue Research*, 231(3), pp. 615–621. doi: 10.1007/BF00218119.

Vigh, B. and Vigh-Teichmann, I. (1973) 'Comparative Ultrastructure of the Cerebrospinal fluid-contacting neurons', *International Review of Cytology*, 35, pp. 189–251.

CHAPTER 3: MOLECULAR DETERMINANTS OF MORPHOGENESIS AND SENSORY FUNCTION OF SPINAL CSF-cNs

Abstract

Multiple types of microvilliated sensory cells exhibit an apical extension thought to be instrumental in the detection of sensory cues. The investigation of the mechanisms underlying morphogenesis of sensory apparatus is critical to understand the biology of sensation. Most of what we currently know comes from the study of the hair bundle of the inner ear sensory cells (Barr-Gillespie, 2015). But morphogenesis and function of other microvilliated apical extensions remain poorly understood. We focused on spinal sensory neurons (CSF-cNs) in contact with the cerebrospinal fluid through the projection of a microvilliated apical process in the central canal (Kolmer, 1921; Agduhr, 1922; Vigh and Vigh-Teichmann, 1973). CSF-cNs respond to pH and osmolarity changes as well as mechanical stimuli associated with changes of flow and tail bending (Orts-Del'Immagine *et al.*, 2012; Böhm *et al.*, 2016; Jalalvand *et al.*, 2016; Sternberg *et al.*, 2018). *In vivo* time-lapse imaging in zebrafish embryo revealed that CSF-cNs are atypical neurons that do not lose their apical attachment and form a ring of actin at the apical junctional complex that they retain during differentiation. We show that the actin-based protrusions constituting the microvilliated apical extension arise and elongate from this ring of actin and we identify candidate molecular factors underlying every step of CSF-cN morphogenesis. We demonstrate that Myo3b and Espin orchestrate the lengthening of CSF-cN apical extension and, using calcium imaging in *espin* mutants, that the size of the apical extension modulates the amplitude of CSF-cN sensory response to bending of spinal cord. Based on our results, we propose that the apical ring of actin could be a common site of initiation of actin protrusions in microvilliated sensory cells. Furthermore, our work provides a set of actors underlying actin-protrusion elongation shared by different sensory cell types and highlights the critical role of the apical extension shape in sensory detection.

Spinal sensory neurons require the actin-bundling factor Espin for apical extension morphogenesis and mechanosensory response

Laura Desban[1], Andrew Prendergast[1], Julian Roussel[1], Claire Wyart[1,*], Pierre-Luc Bardet[1,*]

1 Institut du Cerveau et de la Moelle epiniere (ICM), Inserm U 1127, CNRS UMR 7225, Sorbonne Universite, 75013 Paris, France

* Co-corresponding authors.

Short title : Spinal sensory neurons morphogenesis and mechanosensation

Introduction

Cells assume a variety of shapes known to be instrumental in their specific functions. Morphologies of neurons are among the most complex and diverse: they extend protrusions, build dendritic arborizations and project axons in an intricate and stereotypical manner (Kessels *et al.*, 2011). Sensory neurons in particular display a high degree of specialization allowing them to detect sensory cues, transduce the information into electrical signals, and propagate action potentials to the central nervous system. Much effort has been invested in the identification of molecular determinants underlying sensory detection and transduction, mostly in hair cells, non-neuronal sensory cells, to decipher the pathways and morphological features of audition (Hudspeth, 1989; Zhao and Müller, 2015). In contrast, mechanisms responsible for the morphological differentiation of sensory neurons and the role of their morphology in sensory functions remain elusive. Here, we tackle these questions by studying spinal cerebrospinal fluid-contacting neurons (CSF-cNs), a class of evolutionarily conserved sensory neurons (Djenoune and Wyart, 2017). We investigated the molecular mechanisms underlying the morphogenesis of CSF-cN apical extension and its role in the sensory-mediated activity.

Spinal CSF-cNs are located along the central canal, into which they extend an apical extension constituted of one motile cilium surrounded by actin-based protrusions, in direct contact with the CSF (Vigh and Vigh-Teichmann, 1973; Dale *et al.*, 1987; Djenoune *et al.*, 2014; Orts-Del'Immagine *et al.*, 2014). Over the past decade, much effort was dedicated to investigate the hypothesis of Kolmer and Agduhr (Kolmer, 1921; Agduhr, 1922) that CSF-cNs are sensory and detect cues through their apical extension reminiscent of the hair bundle in hair cells. Diverse sensory cues can be detected by CSF-cNs including changes in pH and osmolarity (Orts-Del'Immagine *et al.*, 2012; Jalalvand *et al.*, 2016), and

mechanical stimuli associated with CSF flow (Jalalvand *et al.*, 2016; Sternberg *et al.*, 2018) or spine curvature (Böhm *et al.*, 2016). CSF-cNs express the transient potential receptor channel PKD2L1, also referred to as TRPP3 (Huang *et al.*, 2006; Orts-Del'Immagine *et al.*, 2012; Djenoune *et al.*, 2014). While CSF-cN response to pH changes seems to be carried by ASICs rather than by PKD2L1 (Orts-Del'Immagine *et al.*, 2012; Jalalvand *et al.*, 2016), multiple lines of evidence indicate that PKD2L1 is necessary for responses to mechanosensory inputs such as changes of osmolarity, CSF flow and tail bending (Orts-Del'Immagine *et al.*, 2012; Böhm *et al.*, 2016; Sternberg *et al.*, in revision). The PKD2L1 channel is abundantly enriched at the CSF-cN apical extension (Sternberg *et al.*, 2018), as is the mechanotransduction channel in hair cells (Zhao and Müller, 2015). This localization suggests that the CSF-cN apical extension might play a similarly important role in sensory functions than the hair bundle in hair cells. During embryogenesis, spinal CSF-cNs are born from two ventral progenitor domains in mouse and zebrafish (Park, Shin and Appel, 2004; Yang, Rastegar and Strähle, 2010; Petracca *et al.*, 2016). This dual origin is associated with two functionally and morphologically distinct subpopulations organized in two ventral and dorso-lateral rows (Böhm *et al.*, 2016; Hubbard *et al.*, 2016; Djenoune *et al.*, 2017; Sternberg *et al.*, 2018). We previously showed that ventral and dorso-lateral CSF-cNs exhibit differently shaped apical extensions (Djenoune *et al.*, 2017). When considered with the localization of PKD2L1 in the microvilli (Sternberg *et al.*, 2018), this observation suggests that this morphological distinction might underlie the distinct sensory functions described in the two CSF-cN subtypes. How CSF-cNs form their apical extensions and how their shapes contribute to sensory functions remain unknown.

The CSF-cN neural progenitors are epithelial cells displaying an apico-basal polarity with their apical side facing the CSF. At this side, CSF-cN precursors form apical junctional complexes (AJCs), including adherens junctions and tight junctions, closely associated with actin filaments organized in a circumferential belt (Schwayer *et al.*, 2016). Together, AJCs and actin cytoskeleton control the cohesiveness and permeability of the developing tissue (Paridaen and Huttner, 2014; Singh and Solecki, 2015). The apical localization and maintenance of AJCs rely on the activity of a family of transmembrane proteins, the Crumbs family (Zou *et al.*, 2013). Neural progenitors give birth to differentiating neurons through self-renewing asymmetric divisions (Alexandre *et al.*, 2010). It was recently shown that the daughter cell fated to become a neuron loses its apical domain and adhesiveness (Das and Storey, 2014), a process thought to be key for its subsequent differentiation into a neuron (Paridaen and Huttner, 2014; Singh and Solecki, 2015). During their differentiation, many neurons then exhibit actin-based protrusions in a polarized fashion, which indicates that they re-establish an apico-basal polarity. It is unknown whether CSF-cNs also differentiate through a process of apical domain loss and polarity re-establishment or not.

In the case of sensory neurons, specialized protrusions called microvilli car arise at their apical side to constitute the sensory organelle. Our current understanding of the formation of actin-based protrusions comes from studies of filopodia, short –lived thin actin-based processes, and involves two critical steps: initiation and elongation (Revenu *et al.*, 2004; Faix and Rottner, 2006). The initiation of filopodia is characterized by the recruitment of actin nucleators and organizers to the apical membrane specifically. IRSp53 family members, including Baiap and Baiap-like proteins, are key elements of this step since they are capable of inducing membrane curvature and recruiting actin nucleators essential for the initiation of protrusions (Ahmed, Goh and Bu, 2010). So far, it is not known whether this model translates to long-lived actin protrusions found in sensory cells (Barr-Gillespie 2015).

After their initiation, protrusions lengthen and, in the case of microvilli, stabilize. The elongation of sensory microvilli has thoroughly been studied in hair cells of the inner ear which form rigid microvilli derivatives referred to as stereocilia (Nayak *et al.*, 2007; Barr-Gillespie, 2015). Through the isolation of mutations responsible for deafness in humans and animal models, multiple genes have been linked to the morphogenesis of the sophisticated hair cell's sensory organelle (Michalski and Petit, 2015). Among these genes, *espin* and *myo3b* encode proteins that have been shown to interact to ensure the proper lengthening of stereocilia (Merritt *et al.*, 2012; Ebrahim *et al.*, 2016). Their loss of function leads to stereocilia defects and, eventually, degeneration followed by hair cell death (Sekerková, Richter and Bartles, 2011; Michalski and Petit, 2015). It remains to be demonstrated that this elongation mechanism translates to other microvilliated sensory cells.

Here, we monitored CSF-cN differentiation by long-term time-lapse imaging of F-actin and report three critical steps in their morphogenesis: i) the presence of a ring of actin at the level of the AJCs, ii) the initiation and iii) the elongation of actin protrusions from the actin ring. We show that in contrast to other newborn neurons, CSF-cNs do not withdraw from the ependymal surface to migrate and differentiate. Instead, they appear to retain their apical cell polarity throughout differentiation, an original element of their morphogenesis. We describe new molecular factors known to be involved in cell polarity and/or morphogenesis, which are specifically enriched in CSF-cNs in the spinal cord. We identified polarity factors (*crb1*) and several actin cytoskeleton interactors – *baiap2a*, *baiap2l1b*, *myo3b* and *espin*. Our observations suggest a model in which these factors cooperate to regulate each step of the formation of the CSF-cN apical extension. Using a dominant-negative form of Myo3b, we demonstrate that this protein is required to address the actin-bundling factor Espin to the apical extension and enable microvilli elongation. The analysis of newly generated *espin* mutant indicates that Espin actin-bundling activity is necessary for the correct elongation of CSF-cN apical extension. Finally, functional analysis

demonstrated that shorter apical extensions were associated to reduced mechanosensory responses in CSF-cNs lacking Espin. Altogether, these results provide insightful elements to build a mechanistic model of the formation of the apical extension by CSF-cNs and how its structure conditions the CSF-cN sensory functions.

Results

Critical steps to form a specialized apical extension

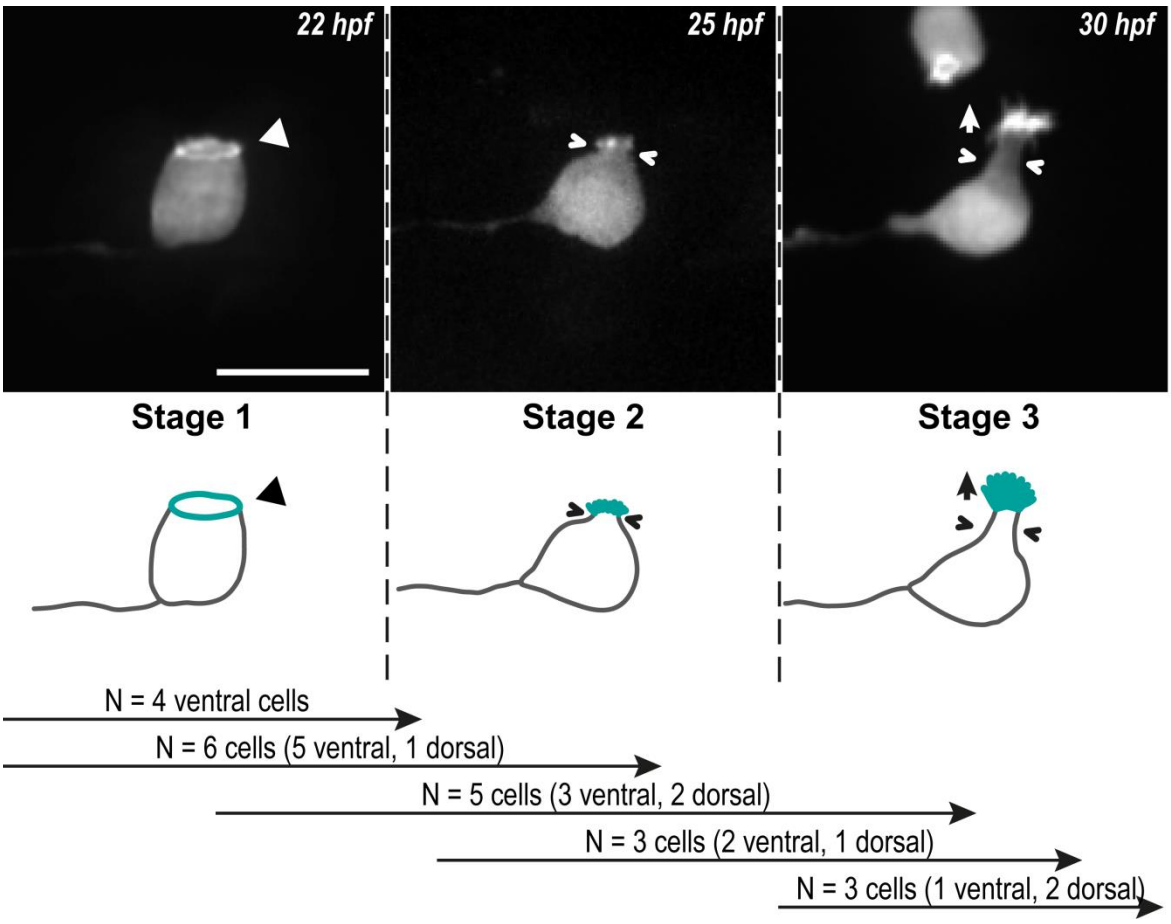

Fig 1. CSF-cNs go through three critical steps to form their apical extension.
Illustrative z-projections from time-lapse acquisitions (top panels, lateral view with rostral to the left) and schematics (bottom panels) showing the three stages CSF-cNs go through during the formation of their apical extension. CSF-cN soma become round and short actin protrusions (Stage 2) arise from the ring of actin (Stage 1, arrowhead) concomitantly with a subapical constriction (Stage 2 and 3, chevrons). Gradually, actin-based protrusions lengthen to form the apical extension (Stage 3, arrow) characteristic of differentiated CSF-cNs. Data collected over 13 time-lapse sessions for 15 ventral and 6 dorso-lateral cells. The number of cells imaged transitioning from one stage to the next is indicated in the bottom legend. Scale bar, 10 µm.

To investigate the formation of the actin-based apical extension, we used the mosaic expression of LifeAct, a marker of F-actin (Riedl *et al.*, 2008), under the control of the *pkd2l1* promoter (Fidelin *et al.*, 2015). We performed long-term time-lapse imaging on single CSF-cNs in live zebrafish from 20-22 hours post-

fertilization (hpf) (S1 movie). Using this promoter, CSF-cNs first appear as cuboidal, with a growing axon and a ring of actin at the apical side (Fig 1, Stage 1). Then, while CSF-cN soma become round, short protrusions progressively arise from the actin ring (Fig 1, Stage 2). Finally, CSF-cNs acquire the typical pear-like shape with elongating actin-based protrusions (Fig 1, Stage 3). The same sequence of events was observed in several cells from the two populations (ventral and dorsal, Fig 1) and confirmed on fixed tissues after immunostaining at different time points during development in double trangenic animal expressing LifeAct under the control of the *pkd2l1* promoter at 24, 48 and 72 hpf (Fig 2, and data *not shown*).

Our results indicate that the actin cytoskeleton goes through dynamic and extensive remodeling, suggesting that it actively participates in CSF-cN morphogenesis. F-actin is first organized at the apical side of the cells to form a ring. Later on, protrusions seem to be initiated at this level and elongate to shape the apical extension.

The ring of actin co-localizes with CSF-cN apical junctional complexes

The location and shape of the ring of actin are reminiscent of the circumferential structure formed by actin and adherens and tight junctions at the apical junctional complexes (AJCs) in epithelial cells (Schwayer *et al.*, 2016). These complexes are usually lost in newborn neurons to allow their withdrawal from the ventricular zone in order to migrate and differentiate (Das and Storey, 2014; Paridaen and Huttner, 2014). To confirm the presence of AJCs in CSF-cNs and the co-localization with the ring of actin, we chose three different markers representative of various complexes: apical domain of polarization, Crumbs 1 (Crb1) (Zou *et al.*, 2013), adherens junctions, Cadherin 2 (Cdh2) (Revenu *et al.*, 2014), and tight junctions, ZO-1 (Fanning *et al.*, 1998). We performed multiple staining with a transgenic line (cdh2 (Revenu *et al.*, 2014)) and antibodies to check the subcellular location of these proteins in CSF-cNs in relation to F-actin at 24 and 72 hpf. At 24 hpf, we observed CSF-cNs (marked specifically by LifeAct) displaying the typical rings of actin at their apical side (Fig 2A-C, arrowheads). The three markers Cdh2 (Fig 2A), ZO-1 (Fig 2B) and Crb1 (Fig 2C) were detected in CSF-cNs at the apical side, at the vicinity of the ring of actin. These results confirm that F-actin is enriched at the level of the AJCs in CSF-cNs at 24 hpf.

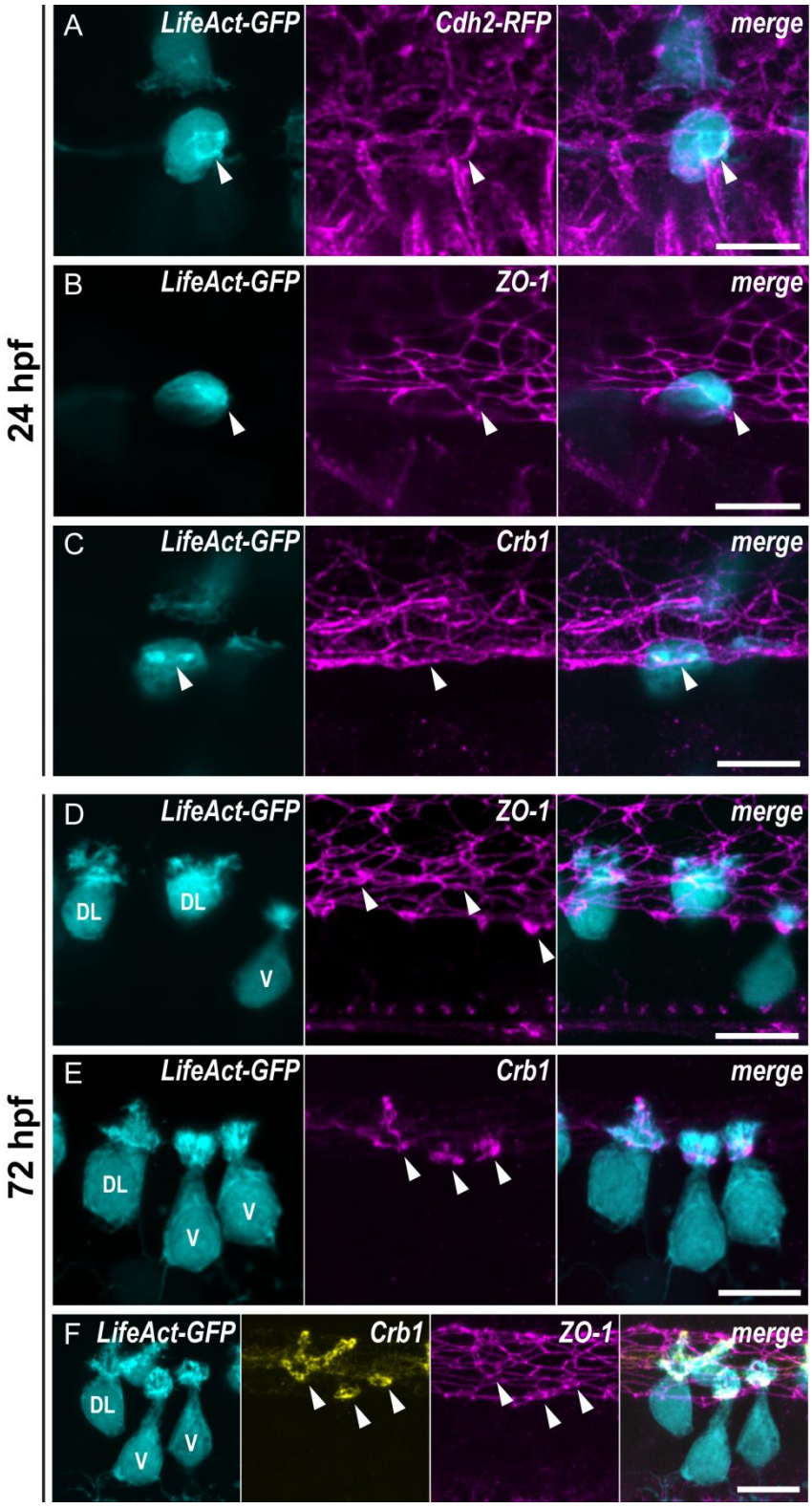

Fig 2. The ring of actin co-localizes with the CSF-cN apical junctional complexes.
(A-C) Illustrative z-projections from lateral views of the spinal cord in 24-hpf embryos showing the co-localization of the ring of actin (LifeAct, arrowheads) with different markers of the apical junction complexes: Cdh2 for adherens junctions (**A**), ZO-1 for tight junctions (**B**) and Crb1 for the apical domain (**C**). (**A)** Double immunostaining for GFP and RFP in triple transgenic *Tg(pkd2l1:Gal4;UAS:LifeAct-GFP;cryaa:V;cdh2:cdh2-RFP)* embryos. (**B**,**C)** Double immunostaining for GFP and ZO-1 (**B**), or Crb1 (**C**) in *Tg(pkd2l1:Gal4;UAS:LifeAct-GFP;cryaa:V)*

embryos. (**D-F)** Illustrative z-projections from lateral views of 72-hpf *Tg(pkd2l1:Gal4;UAS:LifeAct-GFP;cryaa:V)* larvae immunostained for GFP and: ZO-1 (**D**), or Crb1 (**E**), or ZO-1 and Crb1 (**F**). The markers ZO-1 and Crb1 are retained at the apical junctional complexes (arrowheads) in both ventral (V) and dorso-lateral (DL) CSF-cNs after differentiation. In dorso-lateral cells, Crb1 expands to the apical extension. Scale bars, 10 µm.

In the spinal cord of 72-hpf larvae, in contrast to ZO-1 expressed in all cells lining the central canal (Fig 2D,F, arrowheads), the expression of Crb1 (Fig 2E,F, arrowheads) was specific to CSF-cNs and showed distinct patterns between ventral (V) and dorso-lateral (DL) cells (Fig 2F). Crb1 was retained in ventral cells, forming a ring, as seen in 24-hpf embryos, while the protein expanded in the entire apical extension of dorso-lateral cells (Fig 2E,F). The specificity of Crb1 expression at 72 hpf in CSF-cNs and the differences observed between ventral and dorso-lateral cells suggest that Crb1 might play a special role in the maturation of the apical extension.
Altogether, these results show that a ring of actin is formed early on in CSF-cNs at the level of the AJCs and that both persist after the apical extension is formed. This observation highlights a peculiarity of CSF-cNs compared to other neurons since they retain their apical polarity during their differentiation. The initiation and elongation of the actin protrusions from the ring of actin formed at the AJC suggest that it participates in the formation of the CSF-cN apical extension.

CSF-cNs specifically express multiple factors involved in the initiation and the lengthening of actin protrusions

We hypothesized that, once formed, AJC-located actin ring serves as a platform to recruit specific actin modifying proteins and monomers of actin to enable the initiation and the elaboration of the apical extension. We searched in the literature for actin organizers involved in the formation of actin protrusions. We investigated the expression of these factors in CSF-cNs by performing fluorescent *in situ* hybridization (FISH) combined with immunohistochemistry (IHC) for fluorescent proteins under the control of the *pkd2l1* promoter. In 24-hpf embryos, we found at least four factors specifically enriched in both ventral and dorso-lateral CSF-cNs (Fig 3, and data *not shown*) in the spinal cord: *baiap2a* (Fig 3A1), *baiap2l1b* (Fig 3A2), *myo3b* (Fig 3A3) and *espin* (Fig 3A4). The same analysis was carried out in 72-hpf larvae: while *baiap2a* (Fig 3B1) and *baiap2l1b* (Fig 3B2) RNA was not clearly detected in CSF-cNs, both *myo3b* (Fig 3B3) and *espin* (Fig 3B4) still showed strong and specific expression. The expression and subcellular location of Espin protein was also confirmed by immunohistochemistry with a specific polyclonal antibody (Fig 5A) (Bartles, Wierda and Zheng, 1996). These observations provided candidate molecular factors potentially involved in the critical steps of the elaboration of the mature CSF-cN apical extension. The specific expression of Myo3b and Espin, along with their known role in actin

bundle lengthening (Sekerková *et al.*, 2004, 2006; Merritt *et al.*, 2012), indicate that these two factors might contribute to the elongation of CSF-cN apical extension.

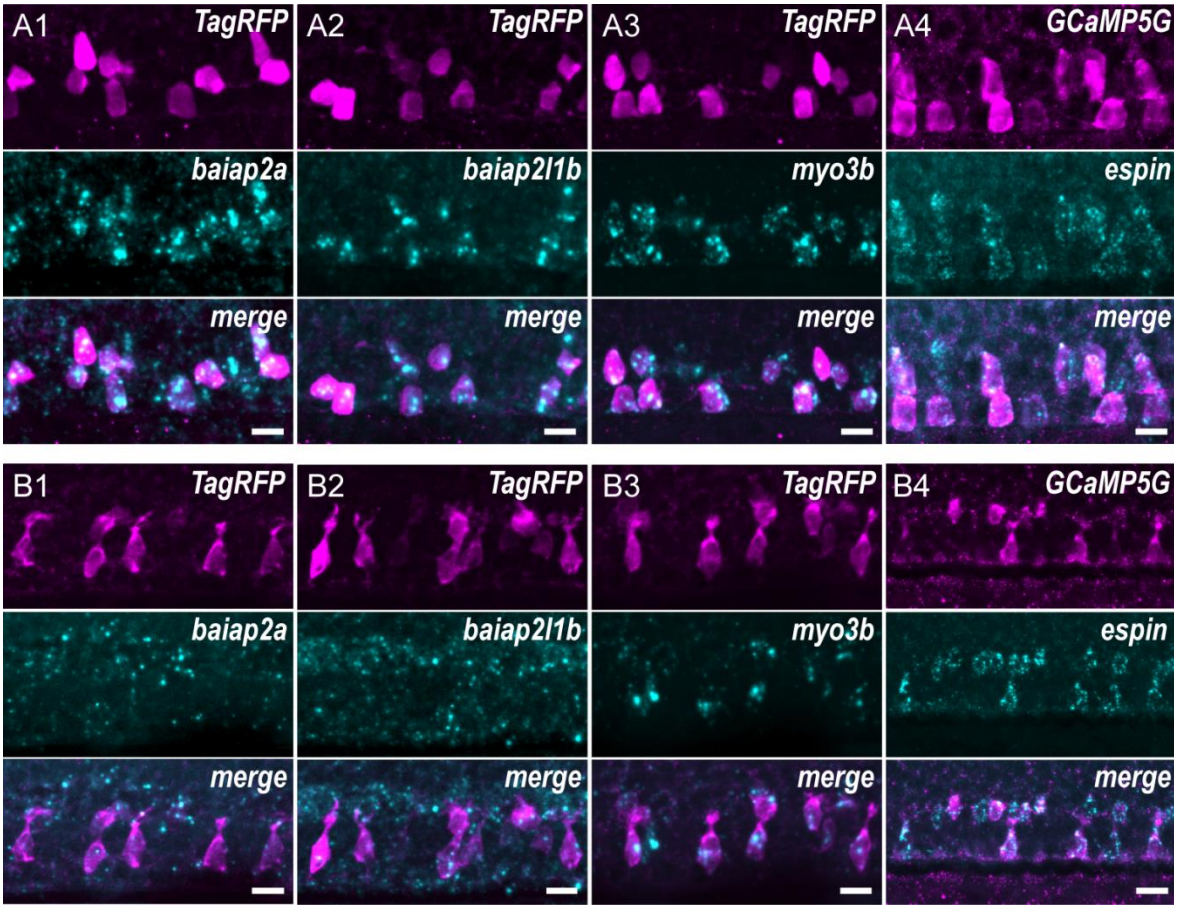

Fig 3. CSF-cNs express a set of morphogenetic factors previously found in hair cells. Expression of candidate factors known to be involved in the formation of actin protrusions – *baiap2a*, *baiap2l1b*, *myo3b* and *espin* – assessed by fluorescent *in situ* hybridization (FISH) at 24 hpf (**A1-4**) and 72 hpf (**B1-4**). Expression in CSF-cNs was validated by combining FISH to immunohistochemistry (IHC) for RFP or GFP in *Tg(pkd2l1:TagRFP)* (**A1-3**, **B1-3**) or *Tg(pkd2l1:GCaMP5G)* (**A4**, **B4**) transgenic embryos respectively. In 24-hpf animals, *baipa2a* (**A1**), *baiap2l1b* (**A2**), *myo3b* (**A3**) and *espin* (**A4**) were enriched in CSF-cNs. In 72-hpf larvae, expression of *baiap2a* (**B1**) and *baiap2l1b* (**B2**) was not clearly detected while *myo3b* (**B3**) and *espin* (**B4**) remained enriched in CSF-cNs. Scale bars, 10 µm.

Myo3b is necessary for Espin localization at the CSF-cN apical extension and correct microvilli lengthening

Myo3b was shown to interact with Espin (Merritt *et al.*, 2012) and to influence stereocilia lengthening in hair cells (Ebrahim *et al.*, 2016). Because *myo3b* and *espin* are strongly enriched in spinal CSF-cNs from 24 to 72 hpf (Fig 2A3,A4,B3,B4), we checked whether Myo3b and Espin could similarly interact to enable the proper elongation of CSF-cN actin protrusions. We first induced Myo3b loss of function by expressing a dominant-negative form of the protein lacking the motor domain, referred to as Myo3b-DN, specifically in CSF-cNs.

Mosaic expression of this form enabled us to compare cells with reduced Myo3b function and control cells within the same animal (Fig 4A). At 72 hpf, the expression of Myo3b-DN in CSF-cNs resulted in strongly reduced Espin apical staining and smaller apical extensions (Fig 4A). We quantified this size effect by comparing the area covered by apical extensions of ventral CSF-cNs expressing Myo3b-DN or not. We found that cells lacking Myo3b function exhibit smaller apical extensions (reduction of 25% on average, Fig 4B).
These results suggest, consistently with what has been previously described in hair cells, that Myo3b in CSF-cNs is required for the proper addressing of Espin to the actin-based protrusions and is critical for the correct lengthening of the apical extension.

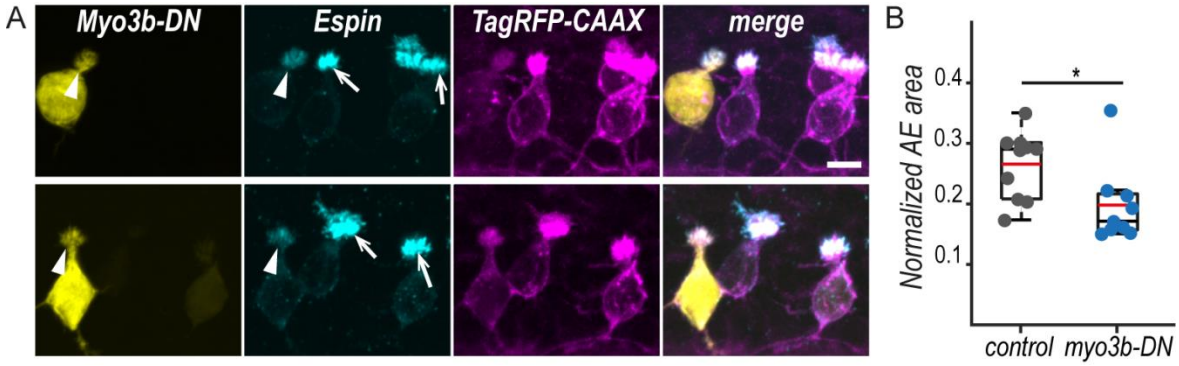

Fig 4. Myo3b is required for Espin addressing to the apical extension and microvilli lengthening.
(A) Illustrative confocal z-projections of spinal cord in *Tg(pkd2l1:Gal4;UAS:TagRFP-CAAX;cmlc2:GFP)* 72-hpf larvae showing mosaic expression of the dominant-negative form of Myo3b (Myo3b-DN) under the control of the *pkd2l1* promoter. Multiple immunostaining reveals Espin (cyan) in TagRFP-CAAX-labelled CSF-cNs (magenta) expressing Myo3b-DN (yellow, arrowheads), or not (arrow). When CSF-cNs express Myo3b-DN, Espin staining was severely reduced (observed in 9 cells out of 9) and the apical extension appeared smaller. Scale bar, 5 µm. (**B)** Quantification of the apical extension area in ventral cells expressing Myo3b-DN normalized to the cell body area compared to non-expressing neighboring cells (control) in 72-hpf larvae. Cells expressing Myo3b-DN form a significantly smaller apical extension (N = 9 versus 11 in 5 different fish, 25% of reduction on average) (two sample Kolmogorov-Smirnov test, * means that $p < 0.05$).

The actin-bundling factor Espin promotes the elongation of the CSF-cN apical extension

In hair cells, Espin is dependent on Myo3b to reach the tip of stereocilia and ensure stereocilia lengthening through its actin-bundling activity (Merritt *et al.*, 2012; Ebrahim *et al.*, 2016). To investigate whether the shortening of microvilli we described with Myo3b-DN is coincident with Espin loss at the CSF-cN apical extension, we generated a mutant allele of *espin* using the CRISPR/Cas9-mediated genome editing. In zebrafish, there is a single *espin* paralog, whose predicted products share a high sequence identity for the main domains and modules described in the rat Espin protein. The *espin* gene is located on chromosome 8 and displays 13 exons (S2 Fig, panel A). Because several Espin

isoforms have been described in rodents (Bartles, Wierda and Zheng, 1996; Bartles *et al.*, 1998; Sekerková *et al.*, 2003), we designed our gRNA against the sequence in exon 11 encoding for the very first amino-acids of the conserved actin-bundling module (ABM) (S2 Fig, panel B). This ABM domain is essential for the protein actin-bundling function and present in all described isoforms (Bartles, Wierda and Zheng, 1996; Bartles *et al.*, 1998; Loomis *et al.*, 2003). We generated a mutant espin^{icm26} allele with a 5-bp deletion in exon 11, disturbing the sequence of the ABM from the first amino-acid (S2 Fig, panels B and D). We checked the immunoreactivity of Espin in wild-type or mutant sibling fish at different stages (Fig 5A, and data *not shown*) using a polyclonal rabbit antibody against Espin isoforms (S2 Fig, panel D) (Bartles, Wierda and Zheng, 1996). Consistent with our FISH results (Fig 3B4), Espin labelling in 72-hpf wild-type larvae showed a strong and specific enrichment at the level of the apical extension of all CSF-cNs (Fig 5A, top panel) that was lost in *espin*$^{icm26/icm26}$ mutant siblings (Fig 5A, bottom panel) confirming that the induced mutation results in the complete loss of Espin protein in these cells.

We observed that CSF-cNs in *espin*$^{icm26/icm26}$ larvae display smaller apical extensions than in control siblings (Fig 5A-C). To analyze the impact of Espin loss on the elaboration of the CSF-cN apical extension, we quantified CSF-cN morphological features using a previously published method (Fig 5B) (Djenoune *et al.*, 2017). We assessed the area covered by the apical extension formed by CSF-cNs in 72-hpf mutant compared to control siblings (Fig 5C). We found that both ventral and dorso-lateral CSF-cNs formed significantly smaller apical extensions in *espin*$^{icm26/icm26}$ larvae compared to *espin*$^{+/+}$ siblings (~20% reduction in ventral cells and ~22% in dorso-lateral cells, Fig 5C).

One of our concerns was that this effect might be due to a developmental delay in mutant animals. In order to test this hypothesis, we performed the same analysis at a later stage. We found a similar significant reduction in size of the CSF-cN apical extension at 6 days post-fertilization (dfp) (~20% reduction in ventral cells and ~26% in dorso-lateral cells, Fig 5D). Altogether, our results suggest that Espin is necessary for the proper lengthening of these extensions after they have been initiated.

The size of the CSF-cN apical extension tunes the response to mechanical stimulus

CSF-cN respond to mechanical stimulus stimuli associated with CSF flow at 24 (Sternberg *et al.*, 2018) and tail bending in 4-5-dpf larvae (Böhm *et al.*, 2016). To investigate the functional consequence of the loss of Espin, we tested CSF-cN mechanosensory function using an assay previously described (Böhm *et al.*, 2016). In paralyzed wild-type larvae, deformation of the tail with a glass probe induced large intracellular calcium transients in ipsilateral dorso-lateral cells (Fig 5E, S3 Movie). In *espin*$^{icm26/icm26}$ larvae, CSF-cN calcium transients were smaller

in response to tail bending (Fig 5E', S3 Movie). We quantified this effect by comparing the amplitude of the calcium transients and found that *espin*$^{icm26/icm26}$ CSF-cNs showed significantly reduced response to the mechanical stimulation (~60% of reduction, Fig 5F).

These observations demonstrate that the shape of the apical extension is essential for tuning the amplitude of CSF-cN mechanosensory response.

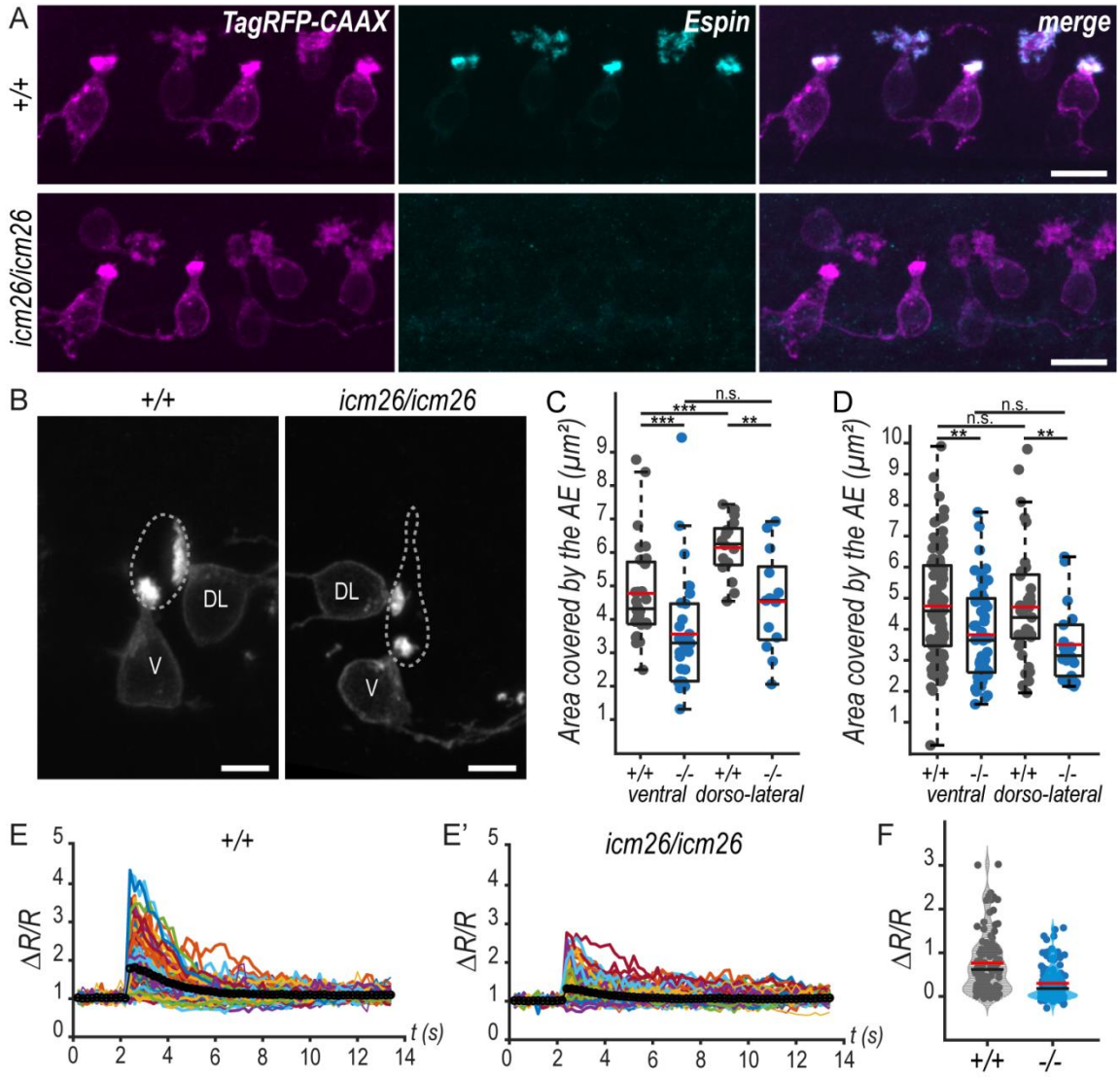

Fig 5. In absence of Espin, CSF-cNs form smaller apical extensions and show reduced response to passive tail bending.

(**A**) Immunohistochemistry for Espin showing the loss of Espin immunoreactivity in *espin*$^{icm26/icm26}$ 72-hpf *Tg(pkd2l1:Gal4;UAS:TagRFP-CAAX;cmlc2:eGFP)* larvae compared to wild-type siblings. In wild-type larvae, Espin is enriched at the CSF-cN apical extension. Scale bar, 10 µm. (**B**) High resolution z-projections from transversal sections showing ventral (V) and dorso-lateral (DL) TagRFP-CAAX-positive CSF-cNs at 72 hpf illustrating the smaller apical extension in *espin*$^{icm26/icm26}$ (right panel) compared to control *espin*$^{+/+}$ siblings (left panel). The central canal is outlined (dotted lines) according to ZO-1 staining (not shown). Scale bars, 5 µm. (**C**) Quantification of the area covered by the CSF-cN apical extension at 72 hpf in ventral and dorso-lateral cells in *espin*$^{icm26/icm26}$ mutant larvae (blue) versus wild-type siblings (dark grey) (n = 30 and 28 ventral cells and n = 13 and 17 dorso-lateral cells in N = 2 mutant and 3 wild-type larvae respectively). In both CSF-cN subtypes, the apical extension in cells missing Espin were smaller (two-sample Kolmogorov-Smirnov test, *** means $p < 0.001$, ** means $p < 0.01$). (**D**) The same

quantification at 6 dpf similarly shows a reduction of the apical extension's area in wild-type (N = 8 larvae, n = 89 ventral cells and 37 dorso-lateral cells) versus mutant *espin*$^{icm26/icm26}$ siblings (N = 4 fish, n = 51 ventral cells and 18 dorso-lateral cells) (two-sample Kolmogorov-Smirnov test, ** means $p < 0.01$). (**E**,**E'**) Calcium transients in response to passive tail bending (Böhm *et al.*, 2016) in ipsilateral dorso-lateral CSF-cNs in response to passive tail bending (Böhm *et al.*, 2016) in control wild-type siblings (**E**, N = 6 fish, n = 111 cells) versus *espin*$^{icm26/icm26}$ mutant (**E'**, N = 7 fish, n = 123 cells) larvae. (**F**) The amplitude of CSF-cN calcium transients shown in **E** is reduced in *espin*$^{icm26/icm26}$ mutant (mean = 0.30616) compared to wild-type siblings (mean = 0.7642) (Kolmogorov-Smirnov test, $p = 1.11.10^{-9}$)

Discussion

CSF-cN retain their apical junction and the accompanying actin ring

To investigate how CSF-cNs develop their apical extension, we undertook a descriptive approach based on long-term time-lapse imaging to monitor F-actin in single cells. We show that early during their differentiation, CSF-cNs display an apical ring of actin beneath the AJCs that they retain throughout further differentiation. It is generally thought that newborn-cells fated to become neurons withdraw their apical domain - including the primary cilium - while they differentiate (Das and Storey, 2014; Paridaen and Huttner, 2014). Although we cannot exclude an early delamination event before the expression of the *pkd2l1* promoter, our results strongly suggest that CSF-cNs are not subject to apical abscission or retraction, but rather differentiate while retaining their apical cell polarity and AJCs. This is consistent with previous findings that differentiated CSF-cNs still possess a cilium at their apical extension (Vigh and Vigh-Teichmann, 1973; Dale *et al.*, 1987; Böhm *et al.*, 2016). The loss of apical domain has been proposed to allow neuronal differentiation by preventing Shh cilium-dependent signaling (Das and Storey, 2014). Zebrafish spinal CSF-cNs remain in contact with the source of Shh ligand, the CSF, throughout differentiation but attenuate their responsiveness to Shh through a decrease in Notch signaling (Huang *et al.*, 2012). Whether this constant exposure to the CSF allows the reception of other signals than Shh important for their differentiation remains to be determined.

Actin protrusions originate from the actin ring

Our time-lapse movies suggest that the ring of actin is precisely the site of emergence of actin protrusions to form the apical extension. This actin ring could therefore represent a site for the recruitment of the machinery necessary for protrusions initiation, including the IRSp53 family proteins that we found specifically expressed in CSF-cNs. This idea is further supported by the observation of actin rings at the apical side of the mechanosensory hair cells of the zebrafish lateral line prior to the sensory microvilli differentiation (Kindt et al. 2015). The initiation of the apical extension directly from the AJCs would ensure the correct positioning of the sensory apparatus, and its development directly into the extracellular compartment in contact with the medium it senses from. The establishment of a strong apico-basal polarity and the specific organization of

AJCs and F-actin in circumferential belts are landmarks of microvilliated cell types (Apodaca, 2018). Thus, our hypothesis of an involvement of the F-actin circumferential belt in the arising of protrusions offers new avenue to solve the long-standing problem of apical microvilli initiation in different cell types, like intestinal brush border epithelial cells or sensory cells (Barr-Gillespsie 2015, Crawley et al. 2014).

Special role of Crb1 in CSF-cNs

Our results suggest that polarization factors are involved in the establishment of the apical domain and AJCs, hence the ring of actin, and are critical for the formation of the apical extension. One of these factors, Crb1, particularly drew our attention. First, Crb1 is retained and becomes specifically expressed by spinal CSF-cNs at 72 hpf, while being downregulated in the other cells lining the central canal. Second, Crb1 shows distinct patterns of expression in ventral CSF-cNs, where it forms a ring of actin at the vicinity of the AJCs; conversely, in dorso-lateral cells, it covers the entire apical domain and protrusions. Since the two CSF-cN subtypes were shown to form different shapes of apical extension (Djenoune *et al.*, 2017), we can speculate that Crb1 differential localization contributes to the final shaping of the apical extension. Finally, Crumbs proteins have been demonstrated to regulate morphogenesis of sensory protrusions in zebrafish photoreceptors (Zou, Wang and Wei, 2012) and wing hairs in drosophila (Salis *et al.*, 2017). The precise mechanisms of actin protrusion regulation by Crumbs protein in drosophila are far from being understood (Apocada, 2017). Our work suggests that this role is conserved in vertebrates, and calls for further studies on the role of Crb1 and other polarization factors and/or Crb1 interactors for the morphogenesis of sensory apical extension.

I-BAR containing factors as initiators of the actin protrusions in CSF-cNs

We show that CSF-cNs specifically express in a transient fashion at least two I-BAR factors at 24 hpf, *baiap2a* and *baiap2l1b*. I-BAR domain proteins are capable of binding both actin cytoskeleton and membrane lipids, which enables them to simultaneously sense and induce membrane curvature (Scita *et al.*, 2008; Zhao, Pykäläinen and Lappalainen, 2011). We know from the literature that I-BAR family members are capable of generating negative membrane curvature and modulating actin dynamics to induce the formation of filopodia (Ahmed, Goh and Bu, 2010). However, the role of these factors in the establishment of more stable microvilli in sensory cell types has never been investigated. Unfortunately, current loss of function approaches are challenging in zebrafish due to high redundancy or IRSp53 factors and we failed to see an effect with a dominant-negative form (data *not shown*). To our knowledge, this study is the first evidence for their possible involvement in the initiation of the actin protrusions forming a sensory apical extension.

The actin-bundling protein Espin and its interactors are key players in the formation of the CSF-cN actin protrusions

We also show that CSF-cNs express *myo3b* and *espin* during their differentiation. Myo3b is a class III unconventional myosin, while Espin is an actin-bundling factor. Actin-bundling factors are able to cross-link actin filaments together and form higher-magnitude actin structures, such as microvilli (Bartles, 2000; DeRosier and Tilney, 2000; Barr-Gillespie, 2015). In particular, Espin is commonly found in mechano- and chemo-sensory microvillliated cells where this factor is a critical actin organizer in the development and maintenance of the sensory apparatus (Sekerková *et al.*, 2004, 2006). Previous work in inner ear hair cells demonstrated that Espin and Myo3b are inter-dependent to be transported to the tip of stereocilia, where Espin ensures the lengthening of actin filaments (Merritt *et al.*, 2012; Ebrahim *et al.*, 2016). Our results indicate that CSF-cNs similarly use Myo3b and Espin for the lengthening of actin protrusions forming the apical extension.

Our work further shows that suppressing one actin-bundling factor, Espin, shortens but does not suppress the actin-based CSF-cN apical extension. It has been shown that the development of bundles of actin filaments involves a combination of at least two different factors, usually in a sequential manner (Revenu *et al.*, 2004). The activity of several actin cross-linkers is required to subsequently initiate loose bundling, then tight packing of the bundles into an organized functional structure (Tilney *et al.*, 1998). Thus, our work suggests that other actin bundling factors, yet to be identified, are necessary during earlier phases of of microvilli initiation and elongation of the CSF-cN apical extension.

It is interesting to note here that Baiap factors contain an SH3 domain, which was shown to strongly interact with the proline-rich regions in the longest isoform of Espin (S2 Fig, panel D) (Sekerková *et al.*, 2003). Our results indicate that members of the Baiap family and Espin/Myo3b could potentially act together in CSF-cNs to coordinate the initiation and the elongation of actin protrusions.

The length of microvilli tunes mechanosensory function in CSF-cNs

The functional relevance of Espin has been largely documented in hair cells of the inner ear where Espin loss is associated with incorrect lengthening of stereocilia, which leads to degenerescence of hair cells and deafness (Zheng et al., 2000; Donaudy et al., 2006; Sekerková, Richter and Bartles, 2011). In this study, we show that the loss of Espin in CSF-cNs does not induce degeneration of these sensory cells but impacts the length of microvilli within the apical extension, a result consistent with the current understanding of Espin actin-bundling functions (Loomis et al., 2003).

The reduction of microvilli length without CSF-cN degeneration provided a unique opportunity to investigate the contribution of microvilli to the process of mechanotransduction. We show that the reduction of microvillar length is associated with a reduction in amplitude of CSF-cN sensory response to passive

bending of the spinal cord indicating that the CSF-cN apical extension acts as a sensory antenna where mechanotransduction occurs. This observation is consistent with previous work in the lab demonstrating that CSF-cN-mediated detection of spinal bending (Böhm, Prendergast et al., 2016), CSF flow and pressure applied against the membrane (Sternberg *et al.*, 2018) requires the Pkd2l1 channel (Böhm *et al.*, 2016; Sternberg *et al.*, 2018), which is confined to the apical extension (Sternberg *et al.*, 2018).

The fact that the length of microvilli tunes the amplitude of CSF-cN sensory response suggests that the mechanism underlying mechanotransduction in CSF-cNs is constrained by microvilli length. One possible explanation for such effect could be that the length of microvilli determines the number of Pkd2l1 channels located at the membrane, which sets the amplitude of CSF-cN response to spinal cord bending. Longer microvilli may furthermore enable CSF-cNs to sample changes of CSF flow associated with spinal bending over larger volumes in the central canal, and thereby amplify the mechanosensory response. The investigation of dynamic mechanisms underlying CSF-cN mechanotransduction in relation to the shape of microvilli will be the subject of future studies.

In hair cells of the inner ear, a large body of work has demonstrated the critical role of the staircase organization and patterned elongation of stereocilia for hearing (Barr-Gillespie, 2015). Our results in CSF-cNs, where microvilli show no obvious organization, suggest that the lengthening of actin protrusions nonetheless finely modulates sensory function. Further physiological investigation in other microvillated cells such as olfactory receptor neurons or solitary chemosensory cells will reveal whether our observation may be generalized.

Acknowledgements

We thank Céline Revenu for the Tg(cdh2:cdh2-TagRFO, crybb1:eCFP)Zf518Tg line, James R. Bartles, Christine Petit, Xiangyun Wei for rabbit polyclonal antibodies against Espin, Myo3b and Crb1 respectively, Jean-Paul Concordet for Cas9 protein, Katie Kindt for sharing her movie showing rings of actin during neuromast hair cell development and feedbacks on the manuscript. We thank the ICM Quant imaging facility for extensive instrument use. We thank Sophie Nunes-Figueiredo, Natalia Maties, Bogdan Buzurin, Monica Dicu, Antoine Arneau for fish care, Yasmine Cantaut-Belarif for useful tips to perform IHC, Lydia Djenoune for guidance in carrying out FISH, Urs Böhm for training for the passive tail bending assay and calcium imaging analysis, and all the members of the Wyart lab (https://wyartlab.org/) for critical feedbacks on the project. This work was supported by ERC Starting Grant 'Optoloco' (grant no. 311673), Human Frontier Science Program (HFSP) Research Grant (grant no. RGP063), the New York Stem Cell Foundation (NYSCF) (grant no. NYSCF-R-NI39). The research leading to these results has received funding from the program 'Investissements d'avenir' ANR-11-INBS-0011 – NeurATRIS: Translational Research Infrastructure for Biotherapies in Neurosciences. This work has received doctoral fellowship

from the Ministry of Higher Education and Research and funding from the Medical Research Foundation (grant no. FDT20170437143) for LD.

Contributions

LD, CW and PLB designed experiments. LD performed all experiments. JR cloned Myo3b-DN using the p3'-T2A-GFP construct generated by AP. AP provided essential guidance in the design and cloning of crRNA and FISH probes. LD analyzed all data, with the help of PLB for the morphology assessment in the Myo3b-DN experiment. LD wrote Matlab scripts for the analysis of CSF-cN morphology in the *espin*^{icm26} mutant. LD and CW adapted the Matlab scripts for calcium imaging in *espin*^{icm26}. CW and PLB supervised research. LD, CW and PLB wrote the manuscript with feedbacks from all authors.

Material & Methods

Animal care. Animal handling and protocols were carried out with the validation of the Institut du Cerveau et de la Moelle épinière in agreement with the French National Ethics Committee (Comité National de Réflexion Ethique sur l'Expérimentation Animale, Ce5/2011/056) and European Communities Council Directive (2010/63/EU). As experimentation on zebrafish larvae prior to 5 days old does not require approval of a protocol by the ethics committee, our project received the approval from the local ICM health and ethics committee. Zebrafish adults and embryos/larvae were reared and maintained in a 14/10 hour light cycle. Embryos and larvae were raised at 28.5°C until the start of experiments conducted at room temperature. When performed below 48 hpf, staging was assessed by counting somites (30 at 24 hpf) according to (Kimmel *et al.*, 1995).

Generation of transgenic lines. Transgenic lines used in this study are listed in the Table 1. Transgenic lines generated using the Tol2 system are already described in (Djenoune *et al.*, 2017).

Generation of mutant lines and genotyping. We used the CRISPR/Cas9-mediated genome editing system to generate our *espin* mutant lines. The crRNA was designed using the online CRISPOR program (crispor.tefor.net/, Tefor®) (Haeussler *et al.*, 2016) and selected to target the sequence CCAGAACAAGACCAGCGTGG in exon 11 containing the BstXI restriction site (S2 Fig, panels A,B). crRNA and universal 67mer tracrRNA were ordered from Integrated DNA Technologies®. crRNA and tracRNA were annealed in Duplex buffer and complexed with the Cas9 protein (provided by Jean-Paul Concordet lab) prior to injections into one-cell stage wild-type eggs. The efficacy of the crRNA was assessed directly after injection at 2 dpf by performing genotyping on usually 8 pools of 5 injected embryos. The genotyping workflow consisted in 1) isolating genomic DNA by lysing embryos in proteinase K solution (10 mM Tris pH 8, 2 mM EDTA, 0.2% Triton X-100, 200 µg/mL proteinase K), 2) performing PCR to amplify the target region (FastStart mix, Roche®) using the forward primer 5'-CAAAACCCAACGACACCC-3' and reverse primer 5'-ACTTCAACTCATGTTTGGCA-3', and 3) digesting the PCR product BstXI restriction enzyme. When efficient editing was observed, siblings of the genotyped embryos were raised to sexual maturity. This F0 generation was screened to find actual transmitters of mutations by crossing them to AB wild type fish and genotyping the offspring at 2 dpf. When mutations were transmitted, siblings of the genotyped offspring were raised to F1 and adults were genotyped: a piece of fin tissue was sectioned under anesthesia (fin-clipping) using 0.02% MS-222 (Sigma-Aldrich) and the PCR product was sequenced (GATC technology) using either the forward or the reverse primer described above to determine the type of mutation. For our study, we selected a 5-bp deletion in

exon 11 resulting in truncated Espin proteins lacking the conserved ABM and we named the resulting mutated allele *espin^{icm26}* (S2 Fig, panels B-D).

Time-lapse imaging. To monitor the formation of the CSF-cN apical extension, we performed live imaging of single CSF-cNs labelled with LifeAct-GFP, a marker of F-actin (Riedl *et al.*, 2008), during early development. To obtain mosaic labelling, we injected ~1ng of the DNA construct *UAS:LifeAct-GFP;cryaa:V* (Djenoune *et al.*, 2017) with Tol2 transposase RNA (~3.5ng) into *Tg(pkd2l1:Gal4)* (Fidelin *et al.*, 2015) or *Tg(1020:Gal4)* (Scott *et al.*, 2007) eggs at the one-cell stage. Imaging was initiated as soon as LifeAct-GFP-positive cells were detected in the spinal cord, usually between 20 and 22 hpf. LifeAct-positive embryos were first anaesthetized in 0.02% MS-222 (Sigma-Aldrich), then mounted laterally in 1.5% low-melting agarose in 50 mm glass bottom dishes (MatTek #P50G-1.5-14-F, USA). Since the imaging took place at early development of the fish, we made sure to set areas to image, containing at least one positive cell for LifeAct, large enough to not lose the cell over time because of developmental growth. Z-stacks spanning the entire cell depth were taken every 5 minutes during several consecutive 1 hour-long sessions using Slidebook software. Imaging was performed using Zeiss x40 or x63 water-immersion objectives on a custom spinning disk microscope (Intelligent Imaging Innovation, Denver, CO, USA) with a 488 nm laser.

Fluorescent immunohistochemistry (IHC) and imaging. We followed a similar protocol in fluorescent-positive embryos and larvae after screening. First, samples were fixed in 4% PFA at +4°C for 4h, then washed in PBS Tween 0.01%, blocked for 2-5h at room temperature in 1% DMSO, 10% NGS, 0.5% Triton X-100 PBS 1X and incubated with primary antibodies: mouse IgG1 anti-ZO-1 (1/200, Invitrogen #339100), chicken anti-GFP (1/500, Abcam #ab13970), mouse IgG1 anti-RFP (1/500, Thermo Fisher #ma5615257) or rabbit anti-RFP (1/500, Life Technologies #R10367), rabbit anti-Crb1 (1/500, kind gift from Xiangyun Wei lab), rabbit anti-Espin (50ng/µL, kind gift from James R Bartles lab), rabbit anti-Myo3b (1/500, kind gift from Christine Petit lab) in 1% DMSO, 1% NGS, 0.5% Triton X-100 PBS 1X at +4°C overnight. After washing three times for at least 10 min in PBS 0.1X Tween 0.01% (PBST), samples were incubated with the secondary antibody (usually diluted to 1/500) and DAPI (1/4000) in the dark, overnight, at +4°C. The next day, embryos or larvae were washed again in PBST for at least three times 30 min and proper staining was assessed by checking the pattern of fluorescence of DAPI control staining before proceeding to mounting. Samples were mounted using a mounting medium (Vectashield® Antifade Mounting) and imaged using an Olympus FV1000 confocal microscope equipped with a x63 oil immersion objective using the 405, 473, 543 or 567, and 633 nm laser lines.

Fluorescent *in situ* hybridization (FISH) and imaging. All the probes were generated by amplifying coding fragments from zebrafish 72-hpf larvae total cDNA. The resulting PCR product was extracted from gel using the QIAquick Gel extraction kit (QIAGEN, Germany) and cloned into the pCRII-Blunt-TOPO vector (Life Technologies, Carlsbad, CA, USA). Clones and orientation were verified by sequencing. For *espin*, the selected plasmid was linearized using NotI and the resulting product was purified and measured for DNA concentration. For *myo3b*, *baipa2a* and *baiap2l1b*, the product was generated by a second high-fidelity PCR using T7 forward primer, the corresponding reverse primer (see Table 3) and Phu polymerase (Phusion® High-Fidelity DNA polymerase, New England BioLabs). The transcription was performed using the Digoxigenin-labeled antisense probes were synthesized using the T7 RNA polymerase with the RNA labeling kit (Sigma-Aldrich). All probes were then purified using the mini Quick Spin RNA columns (Roche, Basel, Switzerland). In the case of myo3b, baipa2a and baiap2l1b, probes went through an additional step of hydrolysis by adding 40 mM of $NaHCO_3$ and 60 mM Na_2CO_3 for 10 min at 60°C. The reaction was stopped and precipitated by adding 4 volumes of H2O, 0.33 volumes of 3 M NaOA, 0.025 volumes of glacial acetic acid and 11 volumes of cold ethanol. The primers and restriction enzymes used for every probe are listed in Table 3. Whole-mount fluorescent ISH was performed on 24-hpf embryos and 72-hpf larvae of the transgenic line *Tg(pkd2l1:GCaMP5G)* or *Tg(pkd2l1:TagRFP)* prior to fluorescent immunohistochemistry to reveal GFP or RFP respectively to specifically label CSF-cNs. For FISH, Samples were prepared by fixation in 4% PFA in PBS overnight at +4°C. At 72 hpf, larvae were treated with Proteinase K in PBST for 20 minutes at 100 µg/mL to ensure the penetration of the probes. Probes were diluted to 1/200 for hybridization overnight at +70°C. To reveal the expression of candidate genes, primary anti-digoxigenin-POD coupled antibodies (Sigma-Aldrich) were added to 1/300. Staining was realized using either TAMRA (1/100) in *Tg(pkd2l1:GCaMP5G)* samples or FITC (1/200) in *Tg(pkd12l1:TagRFP)* tyramide-fluorophore solution for 30 min. Imaging was performed on an Olympus FV1000 confocal microscope equipped with a x20 water immersion objective.

Morphological analysis of cells lacking Myo3b. To interfere with Myo3b activity, we built a truncated version of the protein devoid of the motor domain, reasoning that it would act as dominant-negative form by titrating the interactors of the functional Myo3b (Merritt *et al.*, 2012). The part of the cDNA encoding the 235 C-terminal amino-acids was amplified by PCR (Phusion® High-Fidelity DNA polymerase, New England BioLabs) from zebrafish 72-hpf larvae total cDNA, using primers containing attB site for Gateway cloning (fw: GGGGACAAGTTTGTACAAAAAAGCAGGCTGAATTCACCATGAATCTGATGTTGCGGGAAGTGATCG, rev: GGGGACCACTTTGTACAAGAAAGCTGGGTCTCCGGATCCTCTGGAAGAGATAGTGGGCGG). The stop codon was removed and a GSG sequence was added to allow efficient co-expression of T2A-eGFP (Wang *et al.*, 2015). The PCR

product was then recombined into the pDONR221 and assembled into the final expression vector in a three-fragment gateway reaction (ThermoFisher Scientific) using p5E-10XUAS, pME-Myo3b-DN-GSG, p3E-T2A-eGFP and pDest-cryaa:Venus. p3E-T2A-EGFP was subcloned from pME-HA-UPRT-T2A-EGFP (gift of Teresa Nicolson, (Erickson and Nicolson, 2015)) using *att*-site tagged primers
(F: GGGGACAGCTTTCTTGTACAAAGTGGGGGTTAACGGCAGTGGAGAGGG,
R: GGGGACAACTTTGTATAATAAAGTTGGTTACTTGTACAGCTCGTCCATG).
The resulting fragment was inserted into pDONR p2rp3 in a BP recombination reaction (Thermo Fisher). The resulting plasmid was injected into one-cell eggs carrying a combination of *Tg(UAS:TagRFP-CAAX;cmlc2:eGFP)icm22* and *Tg(pkd2l1:Gal4)icm10*. Confocal images of laterally mounted spinal cords were acquired and we performed a Z-projection of individual ventral CSF-cNs either expressing Myo3b-DN (GFP & RFP positive) or control (RFP only positive). The area of the apical extension and the cell body was assessed by drawing a polygon around the structure and measuring the area covered using Fiji.ct/ (Schindelin *et al.*, 2012).

Detailed analysis of the CSF-cN apical extension morphology. High-resolution images of the CSF-cN apical extension on spinal cord microtome sections were acquired following the procedure presented in our previous work (Djenoune *et al.*, 2017). We used the stable *Tg(UAS:TagRFP-CAAX;cmlc2:eGFP)icm22* and *Tg(UAS:LifeAct-GFP, cryaa:V)icm28* transgenic lines crossed to *Tg(pkd2l1:Gal4)icm10* to access the CSF-cN apical extension morphology. To assess the area covered by the CSF-cN apical extension in espin$^{+/+}$ wild-type and espin$^{icm26/icm26}$ mutant siblings, we drew polygons outlining the apical extension on z-projections using the polygon tool in Fiji.sc/ (Schindelin *et al.*, 2012) and used the 'area' measurement.

Functional analysis of the mutants. To assess the sensory function of the CSF-cNs in mutant versus wild-type siblings, we performed the same passive tail bending assay as described in (Böhm *et al.*, 2016). *Tg(pkd2l1:GCaMP5G;pkd2l1:TagRFP)espin$^{icm26/+}$* adult fish were. Embryos were screened for GCaMP5G and TagRFP fluorescence at 72 hpf after light anesthesia in 0.02% MS-222 (Sigma-Aldrich). Double positive 5-dpf larvae were embedded in 1.5% low melting point agarose and paralyzed by injecting 0.5 nL of α-Bungarotoxin (0.5mM, Tocris #11032-79-4) in the musculature above the swimming bladder. Half of the tail was freed unilaterally to give access to the glass probe. Calcium imaging was performed using a two-photon microscope (Intelligent Imaging Innovations) using a x20 water objective. Both GCaMP and RFP signals were recorded simultaneously at 5 Hz for 770 frames, allowing for 11 probe deflections to bend the tail every 70 frames, starting at 10 frames. A new version of the Matlab script used in (Böhm *et al.*, 2016) was used to perform the analysis. Regions of interest were manually selected in Matlab by drawing the

CSF-cN cell bodies in the region of deflection. In order to correct for artefactual and/or experimental movements, we registered all image time series based on a TagRFP reference frame built as the average over 50 frames in a quiet period after the first stimulation. Background noise, calculated in a region with no signal, was subtracted to every frame. Raw signal was extracted for both GCaMP and TagRFP channels and, to correct for motion artefacts, the ratio ΔR/R was calculated as $(F_{GCaMP}(t)*F_{0\text{-}TagRFP})/(F_{TagRFP}(t)*F_{0\text{-}GCaMP})$ at every time point with F_0 the average fluorescence of the 10 first frames. The calcium transient amplitude was calculated as the difference $(\Delta R/R)_{post}$-$(\Delta R/R)_{pre}$ with $(\Delta R/R)_{post}$ the average of the 3 frames right after stimulation and $(\Delta R/R)_{pre}$ the average of the 10 frames before stimulation.

Statistics. All statistics were ran on Matlab. To accommodate for the non-normal distribution of the data, we used the two-sample Kolmogorov-Smirnov test for all our hypothesis testing. Values are mean (red line) or median (black line). In figure 4, the bottom and top edges of the box plots indicate the 25th and the 75th percentiles respectively and whiskers extend to the most extreme data points not considered as outliers (outliers are plotted individually).

Allele name	Transgenic	Labelling	Reference
s1020tEt	*Tg(1020:Gal4)*	Motorneurons, CSF-cNs	(Scott *et al.*, 2007)
Zf518Tg	*Tg(cdh2:cdh2-RFP, crybb1:eCFP)*	Cdh2	(Revenu *et al.*, 2014)
icm07	*Tg(pkd2l1:GCaMP5G)*	CSF-cNs	(Böhm *et al.*, 2016)
icm10	*Tg(pkd2l1:Gal4)*	CSF-cNs	(Fidelin *et al.*, 2015)
icm17	*Tg(pkd2l1:TagRFP)*	CSF-cNs	(Böhm *et al.*, 2016)
icm22	*Tg(UAS:TagRFP-CAAX;cmlc2:eGFP)*	Non applicable	(Djenoune *et al.*, 2017)
icm28	*Tg(UAS:LifeAct-GFP;cryaa:V)*	Non applicable	(Djenoune *et al.*, 2017)

Table 1. Transgenic lines used in this study.

Gene	Primers (from 5' to 3')	Product size (bp)	Restriction enzyme	Riboprobe hydrolysis?
espin	fw: **AAGATCTACCGCTTCCTCCACC** rev: **CCAGCTTGGTTTCATCATAGCCT**	825	NotI	no
myo3b	fw: **TGTTTGATAAAGGATTTTGAGACTCGTC** rev: **ATATTATATGTACAGCACATTCCGTAGC**	3155	No (use rev primer)	yes
baiap2a	fw: **GATAACAAACCACGAGCAGCAAAACAC** rev: **AGATAATACATGAGGGATTCACAAAACG**	2265	No (use rev primer)	yes
baipa2l1b	fw: **GAGTTATTGTGGAGTAAATCGACTGAAC** rev: **ACAACCTTAAAACAAGCTGAATAATCCG**	1937	No (use rev primer)	yes

Table 2. Primers and restriction enzymes used to generate the FISH probes in this study.

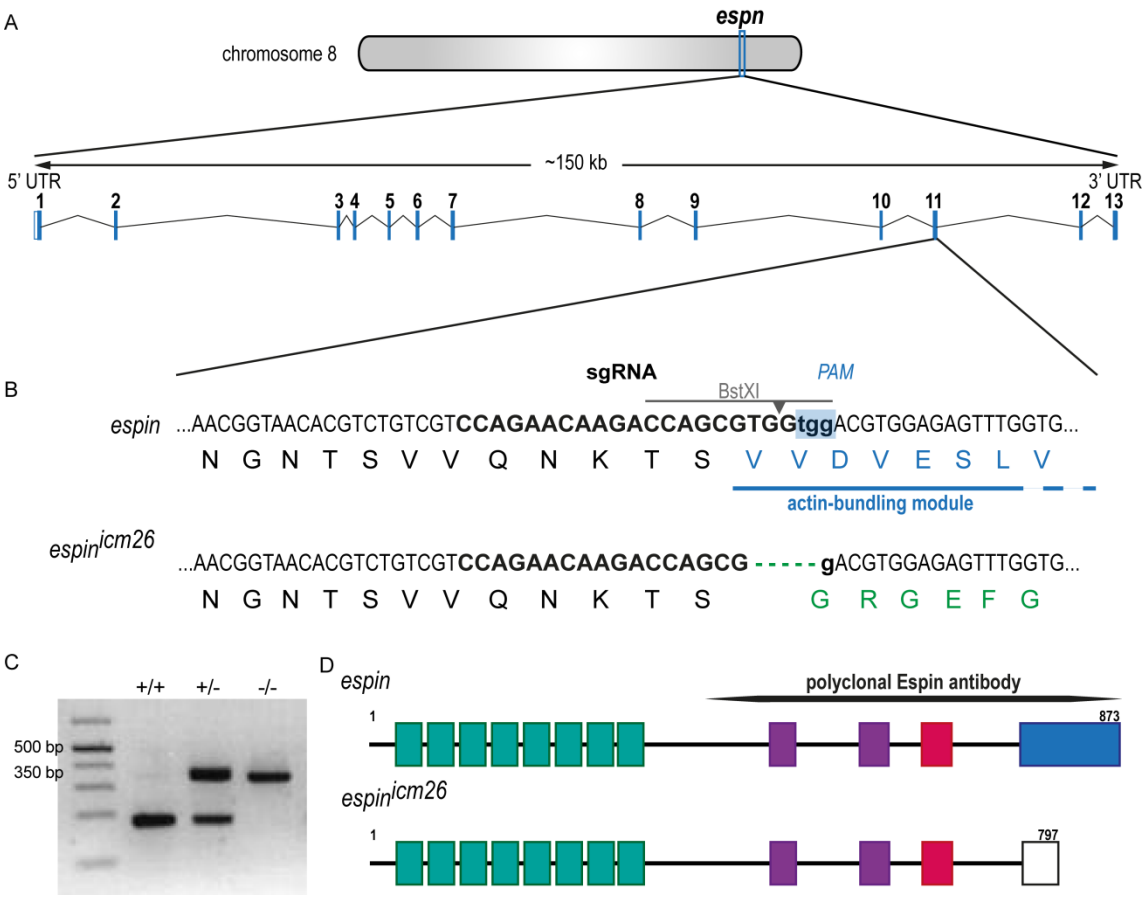

S2 Figure. *Espin* locus organization and generation of the *espin* ^{icm26} mutant.
(A) Location and genomic structure of the unique *espin* locus in zebrafish on chromosome 8. The conserved actin-bundling module is encoded by exons 11 to 13. (**B**) Top, genomic region targeted by the sgRNA in exon 11 (sequence in bold), right upstream of the coding sequence for the actin-bundling module (amino-acid sequence indicated in blue). The target region contains a BstXI digestion site, upstream of the PAM, which is disabled when editing occurs and enables a 2-step genotyping with a PCR followed by BstXI digestion. Bottom, sequence of the espin^{icm26} allele generated showing the 5-bp deletion (green dots) generated by the CRISPR-Cas9 system. In *espin*^{icm26}, the coded amino-acid sequence of the actin-bundling module is disturbed from the first codon (amino-acid sequence in green). (**C**) Illustrative gel revealing the result of the 2-step genotyping for the 3 different genetic conditions: wild-type (+/+), heterozygote (+/-) or mutant (-/-). The PCR product is 350-bp long and is entirely digested into 170- and 180-bp bands by BstXI. In the presence of the icm26 mutation, the loss of the BstXI site on one (+/-) or two (-/-) alleles results in the conservation of the intact 350-bp band. (**D)** Schematics showing the predicted mutant truncated Espin protein obtained with the *espin*^{icm26} 5-bp deletion. The actin-bundling module is entirely disabled (white box). Green boxes: ankyrin-like repeats; violet boxes: proline-rich regions; red box: WH2 domain; blue box: actin-bundling module.

References

Agduhr, E. (1922) 'Über ein zentrales Sinnesorgan (?) bei den Vertebraten.', *Zeitschrift für Anatomie und Entwicklungsgeschichte*, 66, pp. 223–360. doi: 10.1007/BF02593586.

Ahmed, S., Goh, W. I. and Bu, W. (2010) 'I-BAR domains, IRSp53 and filopodium formation', *Seminars in Cell and Developmental Biology*. Elsevier Ltd, 21(4), pp. 350–356. doi: 10.1016/j.semcdb.2009.11.008.

Alexandre, P. *et al.* (2010) 'Neurons derive from the more apical daughter in asymmetric divisions in the zebrafish neural tube', *Nature Neuroscience*. Nature Publishing Group, 13(6), pp. 673–679. doi: 10.1038/nn.2547.

Apodaca, G. (2018) 'Role of Polarity Proteins in the Generation and Organization of Apical Surface Protrusions', *Cold Spring Harbor Perspectives in Biology*. doi: 10.1101/cshperspect.a027813.

Barr-Gillespie, P.-G. (2015) 'Assembly of hair bundles, an amazing problem for cell biology', *Molecular Biology of the Cell*, 26(15), pp. 2727–2732. doi: 10.1091/mbc.E14-04-0940.

Bartles, J. R. *et al.* (1998) 'Small Espin: A third Actin-bundling Protein and Potential Forked Protein Ortholog in Brush Border Microvilli', *Journal of Cell Biology*, 143(1), pp. 107–119. doi: 10.1083/jcb.143.1.107.

Bartles, J. R. (2000) 'Parallel actin bundles and their multiple actin-bundling proteins', *Current Opinion in Cell Biology*, 12, pp. 72–78. doi: 10.1016/S0955-0674(99)00059-9.

Bartles, J. R., Wierda, A. and Zheng, L. (1996) 'Identification and characterization of espin, an actin-binding protein localized to the F-actin-rich junctional plaques of Sertoli cell ectoplasmic specializations', *Journal of cell science*, 109, pp. 1229–1239.

Böhm, U. L. *et al.* (2016) 'CSF-contacting neurons regulate locomotion by relaying mechanical stimuli to spinal circuits', *Nature Communications*, 7:10866, pp. 1–8. doi: 10.1038/ncomms10866.

Dale, N. *et al.* (1987) 'The morphology and distribution of "Kolmer-Agduhr cells", a class of cerebrospinal-fluid-contacting neurons revealed in the frog embryo spinal cord by GABA immunocytochemistry', *Proc. R. Soc. Lond.*, B232, pp. 193–203.

Das, R. M. and Storey, K. G. (2014) 'Apical Abscission Alters Cell Polarity and Dismantles the Primary Cilium During Neurogenesis', *Science*, 343(6167), pp. 200–204. doi: 10.1126/science.1247521.

DeRosier, D. J. and Tilney, L. G. (2000) 'F-Actin Bundles Are Derivatives of Microvilli: What Does This Tell Us about How Bundles Might Form?', *Journal of Cell Biology*, 148(1), pp. 1–6. doi: 10.1083/jcb.148.1.1.

Djenoune, L. *et al.* (2014) 'Investigation of spinal cerebrospinal fluid-contacting neurons expressing PKD2L1: evidence for a conserved system from fish to primates', *Frontiers in Neuroanatomy*, 8(26). doi: 10.3389/fnana.2014.00026.

Djenoune, L. *et al.* (2017) 'The dual developmental origin of spinal cerebrospinal fluid-contacting neurons gives rise to distinct functional subtypes', *Scientific Reports*. Springer US, 7(719). doi: 10.1038/s41598-017-00350-1.

Ebrahim, S. *et al.* (2016) 'Stereocilia-staircase spacing is influenced by myosin III motors and their cargos espin-1 and espin-like', *Nature Communications*, 7:10833. doi: 10.1038/ncomms10833.

Erickson, T. and Nicolson, T. (2015) 'Identification of sensory hair-cell transcripts by thiouracil-tagging in zebrafish', *BMC Genomics*. BMC Genomics, 16(842). doi: 10.1186/s12864-015-2072-5.

Faix, J. and Rottner, K. (2006) 'The making of filopodia', *Current Opinion in Cell Biology*, 18, pp. 18–25. doi: 10.1016/j.ceb.2005.11.002.

Fanning, A. S. *et al.* (1998) 'The Tight Junction Protein ZO-1 Establishes a Link between the Transmembrane Protein Occludin and the Actin Cytoskeleton', *The journal of biological chemistry*, 273(45), pp. 29745–29753. doi: 10.1074/jbc.273.45.29745.

Fidelin, K. *et al.* (2015) 'State-Dependent Modulation of Locomotion by GABAergic Spinal Sensory Neurons', *Current Biology*. Elsevier, 25(23), pp. 3035–3047. doi: 10.1016/j.cub.2015.09.070.

Haeussler, M. *et al.* (2016) 'Evaluation of off-target and on-target scoring algorithms and integration into the guide RNA selection tool CRISPOR', *Genome Biology*. Genome Biology, 17:148. doi: 10.1186/s13059-016-1012-2.

Huang, A. L. *et al.* (2006) 'The cells and logic for mammalian sour taste detection', *Nature*, 442(7105), pp. 934–938. doi: 10.1038/nature05084.

Huang, P. *et al.* (2012) 'Attenuation of Notch and Hedgehog Signaling is Required for Fate Specification in the Spinal Cord', *PLoS Genetics*, 8(6). doi: 10.1371/journal.pgen.1002762.

Hubbard, J. M. *et al.* (2016) 'Intraspinal Sensory Neurons Provide Powerful Inhibition to Motor Circuits Ensuring Postural Control during Locomotion', *Current Biology*, 26(21), pp. 2841–2853. doi: 10.1016/j.cub.2016.08.026.

Hudspeth, A. J. (1989) 'How the ear's works work', *Nature*, 341, pp. 397–404. doi: 10.1038/341397a0.

Jalalvand, E. *et al.* (2016) 'Ciliated neurons lining the central canal sense both fluid movement and pH through ASIC3', *Nature Communications*. doi: 10.1038/ncomms10002.

Kessels, M. M. *et al.* (2011) 'Controlling actin cytoskeletal organization and dynamics during neuronal morphogenesis', *European Journal of Cell Biology*. Elsevier GmbH., 90, pp. 926–933. doi: 10.1016/j.ejcb.2010.08.011.

Kimmel, C. B. *et al.* (1995) 'Stages of Embryonic Development of the Zebrafish', *Developmental dynamics : an official public*, 203, pp. 253–310. doi: 10.1002/aja.1002030302.

Kolmer, W. (1921) 'Das ,,Sagittalorgan" der Wirbeltiere', *Anatomy and Embryology*, (3), pp. 652–717. doi: 10.1007/BF02593657.

Loomis, P. A. *et al.* (2003) 'Espin cross-links cause the elongation of microvillus-type parallel actin bundles in vivo', *Journal of Cell Biology*, 163(5), pp. 1045–1055. doi: 10.1083/jcb.200309093.

Merritt, R. C. *et al.* (2012) 'Myosin IIIB uses an actin-binding motif in its espin-1 cargo to reach the tips of actin protrusions', *Current Biology*, 22(4), pp. 320–325. doi: 10.1109/TMI.2012.2196707.Separate.

Michalski, N. and Petit, C. (2015) 'Genetics of auditory mechano-electrical transduction', *Pflugers Archiv - European Journal of Physiology*, 467, pp. 49–72. doi: 10.1007/s00424-014-1552-9.

Nayak, G. D. *et al.* (2007) 'Development of the hair bundle and mechanotransduction', *International Journal of Developmental Biology*, 51(6–7), pp. 597–608. doi: 10.1387/ijdb.072392gn.

Orts-Del'Immagine, A. *et al.* (2012) 'Properties of subependymal cerebrospinal fluid contacting neurones in the dorsal vagal complex of the mouse brainstem', *Journal of Physiology*, 590(16), pp. 3719–3741. doi: 10.1113/jphysiol.2012.227959.

Orts-Del'Immagine, A. *et al.* (2014) 'Morphology, Distribution and Phenotype of Polycystin Kidney Disease 2-like 1-Positive Cerebrospinal Fluid Contacting Neurons in The Brainstem of Adult Mice', *PLoS ONE*, 9(2). doi: 10.1371/journal.pone.0087748.

Paridaen, J. T. and Huttner, W. B. (2014) 'Neurogenesis during development of the vertebrate central nervous system', *EMBO Reports*, 15, pp. 351–364. doi: 10.1002/embr.201438447.

Park, H.-C., Shin, J. and Appel, B. (2004) 'Spatial and temporal regulation of ventral spinal cord precursor specification by Hedgehog signaling', *Development*, 131(23), pp. 5959–5969. doi: 10.1242/dev.01456.

Petracca, Y. L. *et al.* (2016) 'The late and dual origin of cerebrospinal fluid-contacting neurons in the mouse spinal cord', *Development*, 143, pp. 880–891. doi: 10.1242/dev.129254.

Revenu, C. *et al.* (2004) 'The co-workers of actin filaments: from cell structures to signals', *Nature Reviews Molecular Cell Biology*, 5(8), pp. 635–646. doi: 10.1038/nrm1437.

Revenu, C. *et al.* (2014) 'Quantitative cell polarity imaging defines leader-to-follower transitions during collective migration and the key role of microtubule-dependent adherens junction formation', *Development*, 141(6), pp. 1282–1291. doi: 10.1242/dev.101675.

Riedl, J. *et al.* (2008) 'LifeAct: a versatile marker to visualize F-actin', *Nature Methods*, 5(7). doi: 10.1038/nmeth.1220.Lifeact.

Salis, P. *et al.* (2017) 'Crumbs, Moesin and Yurt regulate junctional stability and dynamics for a proper morphogenesis of the Drosophila pupal wing epithelium', *Scientific Reports*, 7:16778. doi: 10.1038/s41598-017-15272-1.

Schindelin, J. *et al.* (2012) 'Fiji - an Open Source platform for biological image analysis', *Nature Methods*, 9(7), pp. 676–682. doi: 10.1038/nmeth.2019.Fiji.

Schwayer, C. *et al.* (2016) 'Actin Rings of Power', *Developmental Cell*, 37(6), pp. 493–506. doi: 10.1016/j.devcel.2016.05.024.

Scita, G. *et al.* (2008) 'IRSp53: crossing the road of membrane and actin dynamics in the formation of membrane protrusions', *Trends in Cell Biology*, 18(2), pp. 52–60. doi: 10.1016/j.tcb.2007.12.002.

Scott, E. K. *et al.* (2007) 'Targeting neural circuitry in zebrafish using GAL4 enhancer trapping', *Nature Methods*, 4(4), pp. 323–326. doi: 10.1038/nmeth1033.

Sekerková, G. *et al.* (2003) 'Novel Espin Actin-bundling Proteins Are Localized to Purkinje Cell Dendritic Spines and Bind the SH3 Adapter Protein Insulin Receptor Substrate p53', *The Journal of Neuroscience*, 23(4), pp. 1310–1319. doi: 23/4/1310 [pii].

Sekerková, G. *et al.* (2004) 'Espins Are Multifunctional Actin Cytoskeletal Regulatory Proteins in the Microvilli of Chemosensory and Mechanosensory Cells', *Journal of Neuroscience*, 24(23), pp. 5445–5456. doi: 10.1523/JNEUROSCI.1279-04.2004.

Sekerková, G. *et al.* (2006) 'Espins and the actin cytoskeleton of hair cell stereocilia and sensory cell microvilli', *Cellular and Molecular Life Sciences*, 63(19–20), pp. 2329–2341. doi: 10.1007/s00018-006-6148-x.

Sekerková, G., Richter, C.-P. and Bartles, J. R. (2011) 'Roles of the Espin Actin-Bundling Proteins in the Morphogenesis and Stabilization of Hair Cell Stereocilia Revealed in CBA/CaJ Congenic Jerker Mice', *PLoS Genetics*, 7(3). doi: 10.1371/journal.pgen.1002032.

Singh, S. and Solecki, D. J. (2015) 'Polarity transitions during neurogenesis and germinal zone exit in the developing central nervous system', *Frontiers in Cellular Neuroscience*, 9(62). doi: 10.3389/fncel.2015.00062.

Sternberg, J. R. *et al.* (2018) 'Pkd2l1 is required for mechanoception in cerebrospinal fluid-contacting neurons and maintenance of spine curvature', *Nature Communications*, pp. 1–10. doi: 10.1038/s41467-018-06225-x.

Tilney, L. G. *et al.* (1998) 'Why Are Two Different Cross-linkers Necessary for Actin Bundle

Formation In Vivo and What Does Each Cross-link Contribute?', *Journal of Cell Biology*, 143(1), pp. 121–133. doi: 10.1083/jcb.143.1.121.

Vigh, B. and Vigh-Teichmann, I. (1973) 'Comparative Ultrastructure of the Cerebrospinal fluid-contacting neurons', *International Review of Cytology*, 35, pp. 189–251.

Wang, Y. *et al.* (2015) '2A self-cleaving peptide-based multi-gene expression system in the silkworm Bombyx mori', *Scientific Reports*. Nature Publishing Group, 5:16273. doi: 10.1038/srep16273.

Yang, L., Rastegar, S. and Strähle, U. (2010) 'Regulatory interactions specifying Kolmer-Agduhr interneurons.', *Development*, 137(16), pp. 2713–2722. doi: 10.1242/dev.048470.

Zhao, B. and Müller, U. (2015) 'The elusive mechanotransduction machinery of hair cells', *Current Opinion in Neurobiology*, 34, pp. 172–179. doi: 10.1016/j.conb.2015.08.006.

Zhao, H., Pykäläinen, A. and Lappalainen, P. (2011) 'I-BAR domain proteins: linking actin and plasma membrane dynamics', *Current Opinion in Cell Biology*, 23, pp. 14–21. doi: 10.1016/j.ceb.2010.10.005.

Zou, J. *et al.* (2013) 'Spatial-temporal expressions of Crumbs and Nagie oko and their interdependence in zebrafish central nervous system during early development', *International Journal of Developmental Neuroscience*. International Society for Developmental Neuroscience, 31(8), pp. 770–782. doi: 10.1016/j.ijdevneu.2013.09.005.

Zou, J., Wang, X. and Wei, X. (2012) 'Crb Apical Polarity Proteins Maintain Zebrafish Retinal Cone Mosaics via Intercellular Binding of Their Extracellular Domains', *Developmental Cell*. Elsevier Inc., 22(6), pp. 1261–1274. doi: 10.1016/j.devcel.2012.03.007.

CHAPTER 4: DISCUSSION & PERSPECTIVES

The primary goal of my PhD project was to decipher the molecular mechanisms underlying morphogenesis of microvilliated sensory cells focusing on cerebrospinal fluid-contacting neurons (CSF-cNs) in the zebrafish spinal cord. The descriptive approach I undertook enabled the identification of critical steps leading to the development of the apical extension. In parallel, I participated to the transcriptome analysis that revealed the enrichment of several actin organizers in CSF-cNs. Functional analysis allowed me to associate specific factors with morphogenesis steps. My results notably demonstrated the critical role of the actin-bundling factor Espin and its interactor Myo3b in the lengthening of the CSF-cN apical extension. Finally, I showed that shorter CSF-cN apical extensions in the *espin* mutant resulted in reduced responses to mechanical stimuli, thereby linking morphology and sensory function in CSF-cNs.

Altogether, my work shed light on the molecular determinants underlying the formation of a sensory organelle in CSF-cNs. Better understanding of the making of CSF-cN apical extension provided fundamental knowledge that 1/ can supply us with novel tools to manipulate the formation of the apical extension and study its role, and 2/ can be translated to other microvilliated sensory cell (MSC) types. Together with the transcriptome datasets, this work opened the path for numerous new questions. In the following chapter, I will first discuss technical caveats relative to the strategy I used, then I will address considerations about my results and future perspectives.

I. GENOME-WIDE APPROACH AND REVERSE GENETICS IN ZEBRAFISH

A. Using a FACS-based approach to analyze the transcriptome of cells of interest

In order to have unbiased access to genes expressed in our cells of interest, we undertook a FACS-based approach. We sorted specific cell populations according to fluorescent labelling and extracted total RNA to perform bulk RNA sequencing. Several points appear to be critical to obtain RNA sequencing results of good quality.

A specific and intense fluorescent labeling of the cells of interest. One of the most critical criteria in sorting cells is to have specific and bright enough signal to distinguish fluorescent cells that are of interest from background auto-fluorescence and avoid contamination by other cell types.
With our available tools, and after testing many different conditions, we found that the efficient sorting of CSF-cNs could be achieved by using single color labeling under the control of a *pkd2l1* minimal promoter combined to the UAS/Gal4 amplification system. The double transgenic *Tg(pkd2l1:Gal4;UAS:GFP)* 3-dpf larvae showed bright fluorescence thanks to the UAS/Gal4 amplification system, and labeled CSF-cNs. Although *pkd2l1* expression was shown to be specific to spinal CSF-cNs by *in situ* hybridization (Djenoune *et al.*, 2014), the *Tg(pkd2l1:Gal4;UAS:GFP)* double transgenic

line (Fidelin *et al.*, 2015) does not recapitulate the same specificity with leaky expression at 24 hpf in the spinal cord and, over time, apparition of ectopic fluorescence in the hindbrain and the heart due to the amplification system. Gradually from 2 dpf onwards, the expression in the spinal cord becomes specific to CSF-cNs. We overcame these issues by carrying out the sorting at 3 dpf on systematically beheaded larvae (Fig.10). Recently, our lab has generated a novel *Tg(pkd2l1-KI:Gal4)* transgenic line by intron targeting-mediated knock-in using the CRISPR/Cas9 genome editing system (Hwang *et al.*, 2013; Li *et al.*, 2015). Taking advantage of our new *Tg(pkd2l1-KI:Gal4)* knock-in line, we could overcome the technical challenges encountered in the past.

In the case of nHCs, the commonly used transgenic lines to label these cells also label the hair cells in the inner ear and, sometimes, other cell types. We took advantage of their unique location on the cell body and uptake properties to label them using a monomeric cyanine dye, YO-PRO-1 (Santos *et al.*, 2006). Vital nuclear dyes, such as YO-PRO-1, are cell-impermeant but can pass through large non-selective channels and are reliable indicators of nHCs. This strategy had the advantages to be 1/ selective to our cells of interest, 2/ based on the simple and rapid use of dyes easy to bath apply on wild-type larvae without any prior dissection, and 3/ associated with very bright fluorescence concentrated in the nucleus. Although vital dyes such as YO-PRO-1 have been commonly used to selectively label active nHCs over the past decade, we cannot rule out that other cells could uptake the dye, for example unhealthy cells becoming permeant or sensory cells at the surface, something that we need to keep in mind in our validation and analysis of the transcriptome dataset.

The choice of the developmental stage. The transcriptome analysis of CSF-cNs was greatly motivated by the general need to describe new functional markers, especially channels and receptors, allowing the further investigation of CSF-cN biological functions. Regarding my PhD project, my interest was focused on candidate morphogenetic factors enriched in CSF-cNs potentially involved in the formation and maintenance of the apical extension. CSF-cNs start differentiating as early as 18 hpf in the zebrafish spinal cord (Djenoune *et al.*, 2014). To gain access to the largest set of genes of importance for CSF-cN functions, we thus performed the FAC sorting using 3-dpf larvae. At this stage, the RNA sequencing provided us with a rich dataset of ~200 genes upregulated in CSF-cNs. In addition, we showed that some of these factors, such as the actin organizers I focused on during my PhD (see Chapter 3), were expressed as early as 24 hpf in CSF-cNs as observed by fluorescent *in situ* hybridization results (Fig.11). Thus, although earlier and transient factors of differentiation may be found by performing the transcriptomic analysis at 24 hpf, my work proved to be informative about early steps in the cell development. Because our protocol yielded good RNA samples to perform RNA sequencing of CSF-cNs at 3 dpf, we adapted it to nHCs at the same stage when neuromasts of the first wave are already deposited and mature.

The choice of the reference population. A critical aspect of the analysis of the RNA sequencing data is the choice of the reference population as it is the comparison point to assess up- or down-regulation in the cell population of interest. Because FAC sorting in red is more challenging, we only sorted cells according to the green channel and used the 'dark' population as the reference population. The reference population is therefore a mixture of cells types present in the tail. To be found as enriched in the 'green' population, the population of interest, genes have to be expressed at high levels compared the 'dark' population. Specific enrichment is often considered as a proxy for 'important'. However, essential factors for the cell development and/or functions might be shared with other cell types and/or expressed at low levels. The influence of the choice of the reference population is illustrated by *sst1*. In the spinal cord, *sst1* is specific to CSF-cNs, but *in situ* hybridization revealed that it is also found at high levels in the brain (data *not shown*). Sorting cells after dissecting trunks was most likely critical to detect *sst1* as strongly enriched in CSF-cNs.
Despite the shortcomings of our approach, it was still very successful at highlighting specific/enriched factors expressed by CSF-cNs and nHCs. One could however imagine to further study specific features of these cells by comparing them to a homogenous population of sensory cells or, in the case of CSF-cNs, GABAergic neurons by using specific lines for these cell types as reference population.

The depth of RNA sequencing. Finally, the richness of the output dataset greatly depends on the depth of the RNA sequencing which is influenced by the quality of the input RNA. The more healthy and homogenous cell population after sorting, the more RNA of high quality. The more RNA of high quality, the more sequencing depth. More depth leads to more insight into rare events such as non-coding RNAs, microRNAs or long non-coding RNAs for example, which are expressed at very low levels or splicing variants resulting in different protein isoforms. Thus, the choice of the depth of the RNA sequencing is the result of a tradeoff between the ability to obtain samples with good RNA quality at high concentration and the aims of the study regarding quantification and qualification of the molecular targets. Despite following the same protocol, RNA inputs for CSF-cNs were much lower than for nHCs probably due to a more difficult access of CSF-cN cells. To enable RNA sequencing of CSF-cNs, we used a cDNA library preparation kit adapted to very low amounts of RNA. The use of this kit comes however with the main inconvenient of generating much waste for the analysis. For this reason, the CSF-cN sequencing yielded dramatically lower depth than nHCs: a higher total number of reads per sample (66 versus 40 million) led to a smaller dataset (~200 upregulated candidates versus ~2000). The constant improvement of the sequencing kits with the emergence of single cell RNA sequencing should enable a more sensitive transcriptome analysis of CSF-cNs in the near future. It would notably provide insightful information about channels and receptors potentially not detected in our first analysis due to low expression levels.

One last thing to be considered when performing bulk RNA sequencing is the potential for contamination of the population of interest by other cell types. This is true for protocols based on FACS, but also tissue dissection and immunoprecipitation. This issue is primarily addressed ahead with 1/ the choice of labeling and stage after characterization of the available tools, 2/ a comparison of gene expression levels between 'green' and 'dark' populations by qPCR for specific markers of either the cell type of interest or unwanted neighboring cells. Results from qPCR indicate possible contamination with floor plate in the case of CSF-cNs and solitary chemosensory cells in the case of nHCs.

B. Validating and making sense of the RNA sequencing dataset

Validation of the RNA sequencing dataset. Several methods can help assess the validity of transcriptome datasets resulting from RNA sequencing. As a first checkpoint, we made sure that we found the expected markers known to be specific or enriched in the cells of interest to be also up-regulated in our list. When other datasets are available, the obtained gene expression profile can be further compared to already published ones. We were able to verify the detection of most of the known genes expressed in nHCs in out transcriptome dataset. However, our transcriptome analysis of CSF-cNs was, to our knowledge, the first performed on these cells and very little was known about the genes they express. Due to the lack of antibodies for most markers in zebrafish, we turned to fluorescent *in situ* hybridization combined with immunohistochemistry to verify the expression of several candidate genes found as the most up-regulated in our dataset. A lab effort of validation on CSF-cN transcriptome to test the expression of 42 genes revealed ~80% accuracy. The same validation for nHC enriched populations is on-going and should address the concern of the possible contamination by solitary chemosensory cells.

In situ hybridization is a privileged but challenging technique. Due to probe penetration issues, better signal to noise ratio can be obtained in whole-mount zebrafish 24-hpf embryos compared to 3-dpf larvae. In addition, genes expressed at low levels but of interest might fall below detection threshold allowed by classical ISH protocols. To solve this issue, we are currently collaborating with the ICM histology facility to optimize the RNAscope technology (ACDBio) on whole-mount zebrafish embryos and larvae. The RNAscope technique will hopefully provide quantitative and sensitive detection of RNAs expressed at low levels as typically observed for receptors.

What does RNA sequencing data teach us? Once the RNA sequencing analysis validated, candidates can be confidently selected from the list of up-regulated genes. Within the framework of my PhD project, my goal was to describe morphogenetic factors involved in the formation of the MSC apical extension. I selected a short list of candidates for CSF-cNs based on their known role in cell polarity and actin organization in various parallel actin bundle-based structures, such as filopodia or HC stereocilia. This strategy of

selecting candidates according to previous knowledge comes with the advantage of being safer but leaves aside unknown factors that are maybe of critical relevance for the question.

CSF-cNs constitute a mixed population of functionally and morphologically distinct cells, arising from two different progenitor domains (Djenoune *et al.*, 2017). Our available tools did not enable us to distinguish the two CSF-cN subpopulations and we performed bulk RNA sequencing on all CSF-cNs. Interestingly, the transcriptome dataset has helped unraveling specific markers to differentiate the two CSF-cN subpopulations as revealed by *in situ* hybridization. Our results opened the way to further investigate the distinct functions of the two CSF-cN subpopulations and supplied genetic tools to target either one of these subtypes.

One of the main advantages to perform transcriptome analysis resides in providing researchers with rich datasets of genes to investigate. In the study of a particular phenotype, one way to select the most promising candidate(s) is to undertake a screening approach. Rapid reverse genetic screening can be achieved in zebrafish using the CRISPR/Cas9-mediated genome editing technique that was proven to be a powerful tool to target several genes at once (Shah *et al.*, 2015). Recent studies demonstrated that CRISPR could support rapid reverse genetic screening by following a multiplexed, intersectional-pooling strategy where the effects obtained for pools of several mutated genes are intersected (Shah *et al.*, 2015). Often, unexpected molecular determinants can be discovered, bring new questions and fuel new theories. Both our datasets provided us with novel genes to investigate and revealed novel functions of CSF-cNs and nHCs (Fig.12,14). Together, they supported the creation of several projects in the team to explore novel cell functions.

C. Caveats of functional analysis

RNA sequencing participates to the increasing use of reverse genetics: lists of candidate genes found up-regulated in cell populations of interest are investigated for phenotypic effects through loss of functions. Several caveats have recently emerged in the community regarding knock-out/knock-down methods used to explore gene functions.

The debate of transient versus stable loss of function. For nearly 20 years, a widely used approach relied on antisense RNA technologies, especially morpholino antisense oligonucleotides (Nasevicius and Ekker, 2001). The antisense techniques have proven to be successful in many cases over the last two decades and were first adopted enthusiastically. Despite successes, difficulties in interpreting morpholino-mediated knock-down results have to be acknowledged as morpholino were shown to have widespread side effects, mostly related to off-targets (Eisen and Smith, 2008). The emergence of targeted genome editing techniques during the past decade provided the community with a robust mean to efficiently mutate genes of interest and considerably boosted the reverse genetic screening field. The facile use of TALEN and CRISPR/Cas9

systems progressively supplanted transient and less specific antisense strategies. However, comparison studies of phenotypes obtained in morphants and mutants targeting the same gene revealed striking discrepancies (Kok *et al.*, 2015). A majority of the mutants exhibited no or milder phenotype compared to morphants, further suggesting that we still do not fully understand the fundamental mechanisms underlying the observed phenotypes.

The issue of genetic compensation induced by deleterious mutations. Discrepancies between morphant and mutant phenotypes revived the concern about off-target effects of knock-down reagents. Consequently, the use of morpholino antisense oligonucleotides was first seriously reconsidered and dropped in favor of targeted gene disruption technologies. However, recent studies made the community reevaluate the systematic use of genome engineering techniques. They demonstrated that the milder effects observed for genetic mutations could be explained by genetic compensation, which does not occur in transient gene knock-downs (Rossi *et al.*, 2015). Genetic compensation occurred by the up-regulation of one or more related genes, whose functions can compensate for the mutated one. Further investigation showed that paralogs or family members were transcriptionally up-regulated in mutants and played the role of 'adapting genes' (El-Brolosy *et al.*, 2018).
Studies based on reverse genetics need to not underestimate either the lack of specificity associated to antisense strategies or genetic robustness occurring in mutants. These issues can be overcome by running appropriate and sensitive controls and cross-analyzing phenotypic results obtained with different but complementary techniques.

The issue of functional redundancy. Gene duplication provided cells with different paralogs, hence additional means of compensation to face loss of functions. Thus, the depletion of these different paralogs exhibiting overlapping functions might be necessary to effectively observe phenotypes informative about the studied gene's function(s). In zebrafish in particular, an additional gene duplication event subsequent to the divergence of teleost fish from the rest of vertebrates increased the number of paralogs, hence the potential for genetic compensation.

II. MORPHOGENETIC FACTORS OF CSF-CNS

The transcriptome analysis of CSF-cNs revealed a number of genes of interest to investigate the molecular mechanisms underlying the development of the microvilliated apical extension. I focused my investigations on two of the most enriched actin-binding proteins: Espin (3rd most upregulated) and Myo3b (4th most upregulated). In this section, I will first discuss the results on functional analysis of these genes, and then the potential for other candidate genes whose study is on-going.

A. The Espin-Myo3b interaction and the lengthening of microvilli in CSF-cNs

My results demonstrated the specific expression of Espin and Myo3b proteins in CSF-cNs in the spinal cord with a strong enrichment at the microvilliated apical extension. The study of the *espin* mutant highlighted the importance of the actin-bundling activity of Espin to enable the proper lengthening of the microvilli formed by CSF-cNs. The expression of a dominant-negative form of Myo3b showed similar microvilli length defects associated with the loss of Espin at the apical extension. These results extend the demonstrated role of Espin in HC to CSF-cNs and the importance of its interaction with Myo3b as previously described in culture cells and in mouse HC stereocilia (Merritt *et al.*, 2012; Liu *et al.*, 2016).

Which Espin isoforms are expressed in CSF-cNs? In rodents, Espin proteins come in four major isoforms of various lengths depending on different transcriptional start sites (Chen *et al.*, 1999). This is, to our knowledge, the first study of Espin in zebrafish in which the existence of multiple isoforms has not been demonstrated. This could be tested by first trying to distinguish between short and long Espin isoforms by testing their immunoreactivity using specific antibodies described in literature. Western blots of dissected CSF-cN-containing tissues (for example the skinned trunks of zebrafish larvae where the only Espin-positive cells would be CSF-cNs) would enable the clear differentiation between the different isoforms according to their size.
The role of Espin was mainly investigated in HC stereocilia where *espin* mutations lead to hearing defects (Zheng *et al.*, 2000). In rat HC stereocilia, fine kinetic analysis of Espin expression showed that different isoforms were associated with different steps of the formation of the hair bundle (Sekerková *et al.*, 2006). Therefore, it would be interesting to investigate the possibility that different isoforms could also be associated with distinct steps of the development of the CSF-cN microvilliated apical extension. A simple approach would involve analysis of the temporal pattern of expression via western blots of dissected CSF-cN-containing tissues at different developmental stages.

Could Espin loss of function lead to more severe deficits at later stages? In deaf *jerker* mice, the loss of Espin function is associated with stereocilia morphogenesis defects resulting in altered length and width (Sekerková, Richter and Bartles, 2011). Thus, until the early postnatal period, HCs are still capable of developing actin protrusions, probably as a result of the first phase of actin bundling in the sequential model of parallel actin bundle formation (see Chapter 1, III.A). At the onset of hearing at P11 however, stereocilia in *jerker* mice start degenerating, soon followed by HCs (Zheng *et al.*, 2000). A hypothesis to explain the dramatic stereocilia degeneration correlated with the onset of hearing is that the Ca^{2+}-resistant cross-links built by Espin are necessary to stabilize the parallel actin bundles against depolymerization and mechanical insult.
In the absence of Espin, CSF-cNs still form a microvilliated apical extension, but a shorter one. The effects of Espin loss in zebrafish spinal CSF-cNs resemble the phenotype described in HC stereocilia during the early postnatal period in *jerker* mice. During my PhD, I analyzed effects of Espin loss on CSF-cN morphology up to 6 dpf. However, we

cannot exclude that more severe defects may be observed at later stages, when the Ca^{2+}-resistant actin-bundling activity of Espin could be more critical. To test this hypothesis, I have conducted preliminary staining in one-month old juvenile fish to assess Espin expression and CSF-cN morphology. Unfortunately, the fluorescent labeling driven by *pkd2l1* in the transgenic lines I used was mostly extinct at this stage, preventing any conclusive observation. A newly developed Pkd2l1 antibody in the lab (Sternberg *et al.*, 2018) could now enable to observe Espin and Pkd2l1 by immunohistochemistry directly on cross sections from wild-type and *espin* mutant juvenile zebrafish. Alternatively, the detection of *pkd2l1* mRNAs by fluorescent *in situ* hybridization could be combined to Espin immunohistochemistry.

What are the other actin-bundling factors expressed by CSF-cNs? The analysis of the CSF-cN phenotype in the *espin* mutant showed that CSF-cNs are still capable of developing an apical extension in the absence of the Espin actin-bundling activity.
This result suggests, consistently with the sequential model of the formation of parallel actin bundles, that CSF-cNs express at least one other actin-bundling factors responsible for the early step of actin filaments packing. We searched for all the known actin-bundling factors in our transcriptomic dataset and found that *fscn1b* and *pls1* were also expressed in CSF-cNs although not specifically enriched compared to the reference population. Interestingly, Pls1 (Plastin1) is the zebrafish counterpart of Fimbrin and Fscn1b (Fascin1b) an ortholog of Fscn2 in the mouse. Thus one could imagine a similar sequence of events in the CSF-cN microvilli than in the HC stereocilia with: first, the transient expression of Pls1 to enable the loose packing of actin filaments; second, the stable expression of Espin to further pack the bundle more tightly in a Ca^{2+}-resistant fashion, the structure being stabilized by Fscn1b.
Further investigation is needed to describe other actin-bundling factors expressed by CSF-cNs and the role they play in the development of the microvilliated apical extension. Our transcriptomic results suggest that these two factors are not specific to CSF-cNs but are largely expressed in other cells as well. The expression of our two candidates, Pls1 and Fscn1b, should thus first be verified by *in situ* hybridization or, ideally, by immunohistochemistry to localize the proteins in the cell. Because of the relative unspecific expression of these two factors, it is likely that knock-out or antisense technologies will result in complex phenotypes resulting from impaired function in multiple cell types. An adapted strategy would be designed in order to inactivate their function in CSF-cNs specifically.

What is the role of Myo3b? In rodents, Myo3b was shown to interact with Espin and to enhance actin-bundling activity in stereocilia (Salles *et al.*, 2009; Merritt *et al.*, 2012; Liu *et al.*, 2016). The transcriptomic analysis of CSF-cNs revealed that *myo3b* was also strongly up-regulated. As for Espin, immunostaining against Myo3b revealed a pattern of expression specific to CSF-cNs in the spinal cord where it is enriched at the apical extension. Our first approach to temper with Myo3b function consisted in using a

dominant-negative form of the protein in CSF-cNs. We reasoned that the expression of Myo3b truncated of its motor domain would titrate its normal interactors away from the endogenous full-length protein. We found that it resulted in shorter apical extensions associated with reduced or absent Espin staining. These results suggest that Myo3b is also necessary for the proper addressing of Espin to the CSF-cN apical extension where its actin-bundling activity is required.

In order to confirm these results, we generated a stable mutant *myo3b* line using the CRISPR/Cas9 technology. Preliminary data confirm the mis-addressing of Espin to the apical extension but not the microvilli shortening observed both in the *espin* mutant and with the dominant-negative form Myo3b-DN. Further investigation of the mutant will be necessary to validate these results but it is possible that genetic compensation (see I.C) occurs in our mutant. Notably, one could imagine that Myo3a – that is usually not expressed in CSF-cNs (data *not shown*) – could be up-regulated in the *myo3b* mutant and compensate for the loss of Myo3b protein. Performing the immunohistochemistry against Myo3a in wild-type versus mutant sibling embryos/larvae would allow verifying whether the milder phenotype observed in the mutant is the result of this compensation.

B. How do CSF-cNs initiate the formation of actin-based protrusions?

The time-lapse imaging of CSF-cNs revealed the sequence of events leading to the elaboration of the CSF-cN apical extension. The analysis of CSF-cN transcriptome was complementary in providing candidate molecular factors potentially regulating each step. In the previous section, we discussed the role of Espin and Myo3b proteins in the elongation of CSF-cN microvilli. My work was also informative regarding earlier steps in the formation of parallel actin bundle-based protrusions and opened the way to revisit the long-standing question of their initiation. Below, I will discuss what we discovered studying CSF-cNs and the implications for other microvilliated sensory cell types.

Microvilli arise from an apical ring of actin. Our time-lapse imaging analysis revealed that F-actin is organized into an apical ring of actin prior to the arising of actin protrusions. Interestingly, a similar ring structure was observed to take place prior to the formation of stereocilia in nHCs (data *not shown*, courtesy of Prof. Katie Kindt). The initiation of microvilli is a long standing question in the field of MSCs. Our current working hypothesis is that the ring of actin serves as a platform to recruit actin nucleators/organizers and to promote the initiation of parallel actin bundles. This idea is further supported by the fact that similar structures, referred to as focal rings, were described in a large number of cells at the base of filopodia-to-be protrusions and constitute the initiation site of filopodial parallel actin bundles (Steketee, Balazovich and Tosney, 2001).

The role of cell polarity factors in establishing the ring of actin. Analysis of multiple immunostainings demonstrated that the ring of actin colocalizes with several markers of the CSF-cN apical junctional complexes (see Chapter 1, II.A). To explain the presence of the ring of actin at the apical side of the cell, we reasoned that polarity factors, known to be involved in the positioning of the AJCs, could take part in the formation of the ring. One of the polarity factors we found as enriched specifically in CSF-cNs is Crb1. Interestingly, we observed different patterns of expression for Crb1 in the two CSF-cN subpopulations later in differentiation (Fig.2). This feature is unique among all the factors we investigated so far and places Crb1 as a good candidate to explain the morphological differences between the two CSF-cN subtypes (see Chapter 2, I.A and Annex). These observations reinforce the idea that polarity factors play a critical role in the establishment of the CSF-cN apical extension.

To test Crb1 function in CSF-cNs, we designed specific guide RNAs to target the *crb1* gene and generate a stable mutant line using the CRISPR/Cas9 genome editing technology. Heterozygous fish for the selected mutations are now ready to carry out an analysis of CSF-cN morphology in mutant versus wild-type larvae. This analysis should be performed with the concern that functional redundancy might be an issue here. Indeed, there are four paralogs of Crb1 in zebrafish and, although they were not found to be especially up-regulated in CSF-cNs, their expression by the cells might compensate for the loss of Crb1 function. Alternative strategies should thus be considered to gain access to informative phenotypes (see below, Cdc42).

More generally speaking, the formation of the apical extension at the apical side by MSCs seems consistent with their sensory function. MSCs are part of cohesive, impermeable epithelial tissues forming a selective barrier with the extracellular environment. The projection of the apical extension breaks this barrier and enables MSCs to be in direct contact with the environment where they gather information. This singular position occupied by MSCs is nicely illustrated by the example of CSF-cNs. The ependymal tissue constitutes a barrier from the nervous system, a barrier only broken by CSF-cNs extending their microvilliated apical extension directly into the CSF.

Is the initiation of microvilli supported by Baiap factors? Our transcriptome analysis of CSF-cNs yielded useful information about the up-regulated expression of two Baiap factors, Baiap2a and Baiap2l1b. In the literature, Baiap family members (also known as the IRSp53 family) are described as regulators of the formation of filopodia through their dual role in sensing/inducing membrane curvature and organizing actin cytoskeleton (Scita *et al.*, 2008; Zhao, Pykäläinen and Lappalainen, 2011). Our *in situ* hybridization results confirmed the specific expression of Baiap2a and Baiap2l1b by CSF-cNs at least transiently at 24 hpf, coinciding with the onset of microvilli arising. Based on the current understanding of their biological functions and the description of their interaction with long Espin isoforms (Fig.9) (Sekerková *et al.*, 2003), Baiap members thus appear as good candidates to enable the protrusion of microvilli in CSF-cNs. To test this hypothesis, we

generated a transgenic line where the expression of a dominant-negative form of all Baiap members (IRSp53-DN) is controlled by the *pkd2l1* promoter with the UAS/Gal4 system. We will analyze CSF-cN morphology when the cells express IRSp53-DN. Alternatively, we can generate mutants using the CRISPR/Cas9 technology as previously done for other factors with the concern of compensation due to the presence of numerous Baiap paralogs.
To our knowledge, my work constitutes the first description of Baiap factors being expressed in MSCs.

Cdc42, a factor to rule them all. A common feature of polarity factors like Crb1 and membrane sensors like Baiap factors is that they are regulated by Cdc42. Cdc42 is a small Rho GTPase shown to be a key regulator of cell polarization (Margolis and Borg, 2005; Campanale, Sun and Montell, 2017) and a major promoter of filopodia formation through its interaction with IRSp53 (Krugmann *et al.*, 2001). In addition, a downstream effector of Cdc42 is the Arp2/3 complex, an actin nucleator behind branched actin networks. Although Cdc42 did not appear as up-regulated in CSF-cNs, which is explained by its ubiquity and its post-translational regulation, we can predict that Cdc42 orchestrates the initiation of actin-based protrusions by regulating and recruiting various key organizers at the apical side of the cell. Cdc42 would support the coordination of seemingly interconnected events to enable the arising of microvilli: 1/ cell polarization and establishment of the AJCs (with Crb1), 2/ the formation of the ring of actin at these complexes, 3/ the recruitment of actin nucleators (such as the Arp2/3 complex) to F-actin at the ring, 4/ the initiation of actin filaments and, finally, 5/ their protrusion supported by the generation of negative membrane curvature (via Baiap factors). In order to test the central role of Cdc42 in the generation of CSF-cN actin protrusions, it is critical to knock it out only in CSF-cNs. A dominant-negative form under the control of the *pkd2l1* promoter seems to be optimal to avoid unspecific or secondary phenotypes. The generation and testing of such dominant negative form is currently on-going in the lab.

Does the initiation of CSF-cN microvilli follow the 'convergent elongation' model? In the line of the hypothesis that Cdc42 is the conductor of the initiation of microvilli, the actin nucleator responsible for the formation of new actin filaments would most likely be the Arp2/3 complex. Thus, it would be interesting to check the expression and localization of the Arp2/3 complex in CSF-cNs, especially at critical stages when actin protrusions arise from the ring of actin. According to our transcriptome dataset, all components showed high expression levels in CSF-cNs, but as in the reference population. Qualitative information about the localization of the complex in CSF-cNs, can be obtained by performing immunohistochemistry. Several commercial antibodies targeted against different subunits of the complex have been used in mouse and human tissues but, to our knowledge, never tested in zebrafish. An immunohistochemistry

protocol could be optimized to use these antibodies in order to detect proteins of the Arp2/3 complex in zebrafish at 24 hpf.
The Arp2/3 complex is best known to underlie the generation of branched actin networks and not parallel actin bundles as seen in microvilli and filopodia. However, a fine kinetic analysis of the formation of filopodia in culture cells showed that actin filaments could form parallel bundles from a branched network following a 'convergent elongation' model (Svitkina *et al.*, 2003) (see Chapter 1, III.A). In addition to testing the presence of the Arp2/3 complex, one could imagine a similar kinetic approach with high-resolution imaging to follow the organization of F-actin at early stages of CSF-cN morphogenesis.

Eventually, the better understanding of the molecular determinants underlying the morphogenesis of the CSF-cN apical extension should provide us with novel genes to manipulate its formation and investigate its role in the sensory functions of the cell. Altogether, these observations enabled us to associate specific candidate factors with each step of the formation of the CSF-cN apical extension leading to our current working model to explain the elaboration by the cells of their sensory organelle (Fig.21).

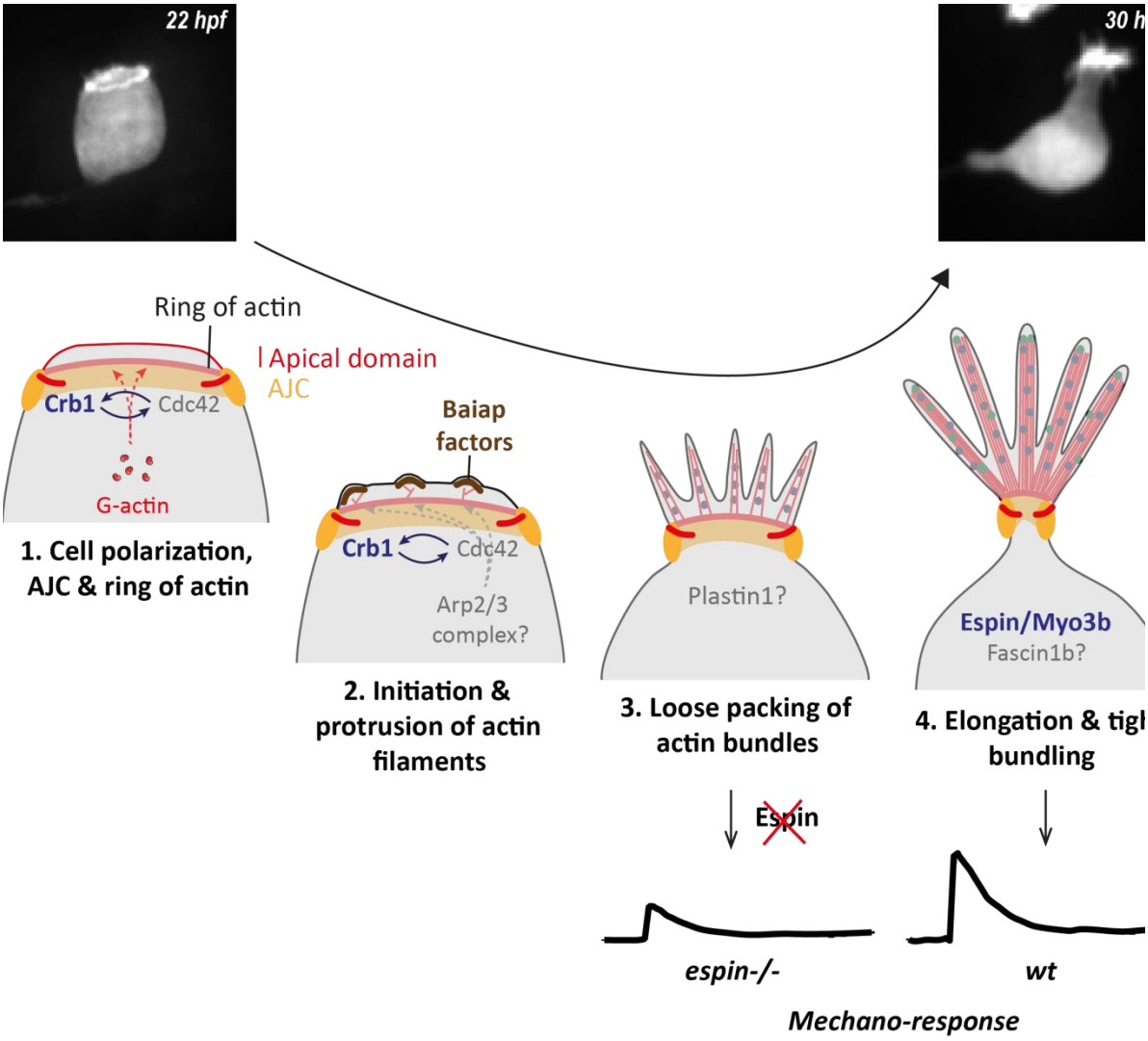

Figure 21. Mechanistic model of the formation of the microvilliated apical extension by CSF-cNs

We propose a sequential model to explain the formation of the microvilliated apical extension in CSF-cNs. (**1**) At the beginning of CSF-cN differentiation, the activity of polarity factors results in the establishment of several membrane domains. Crb1 is involved in the determination of the apical domain and the positioning of the junctional domain. Together with Cdc42, they participate to the formation of the apical junctional complexes (AJCs), adherens junctions and tight junctions, with the ring of actin. (**2**) Actin nucleation factors such as the Arp2/3 complex are recruited to the AJCs and the ring of actin possibly via Cdc42. Through the activity of the Arp2/3 complex, branched actin filaments are initiated from the initial network of F-actin constituted by the ring of actin. Recruitment of actin and membrane protruding are facilitated by the dual role of Baiap factors. (**3**) Branched actin filaments elongate and converge to form parallel actin bundles according to the 'convergent elongation' model. Bundles are short and loosely packed through the activity of an actin-bundling factor, maybe Villin. (**4**) Finally, Espin mediates the elongation, widening and tight packing of the bundles. Fascin2b could potentially be involved in the stabilization of the structure.

All the factors that we described to be expressed in CSF-cNs are indicated in bold dark blue and their functional analysis is on-going.

The factors indicated in grey are candidates that would be interesting to investigate in CSF-cNs to unravel the molecular mechanisms of morphogenesis.

In the absence of Espin in *espin*$^{icm26/icm26}$ mutant larvae, the shorter apical extension of CSF-cNs is associated with reduced mechano-response.

III. THE ROLE OF THE APICAL EXTENSION IN THE CSF-CN SENSORY FUNCTION

My results demonstrated that CSF-cNs with shorter apical extensions, as a result of the loss of Espin function, showed reduced sensory-mediated activity in response to passive tail-bending (Böhm *et al.*, 2016).

Does size matter? To analyze the consequences of the loss of Espin function on the sensory function of CSF-cNs, we took advantage of a previously described assay in the lab to test the mechanosensitivity of the cells (Böhm *et al.*, 2016). This previous work showed that CSF-cNs respond to mechanical stimuli produced by the tail bending of 4 to 5-dpf larvae. Subsequent work showed that isolated CSF-cNs are also mechanosensory *in vitro* (Sternberg *et al.*, 2018). Both works demonstrated that the CSF-cN mechanoresponse is Pkd2l1-dependent. In the analysis of the *espin* mutant, we found that CSF-cNs still displayed a response to mechanical stimulus but largely reduced compared to wild-type siblings. We correlated this impaired, but still present, activity to the shortening of the CSF-cN apical extension observed in our mutant. Detection of Pkd2l1 protein by immunohistochemistry showed that the channel was still expressed by mutant CSF-cNs at their apical extension, rejecting the hypothesis that the diminished response is due to Pkd2l1 mis-localization away from the apical extension. As there is a correlation between the size of the apical extension and the amplitude of the mechanosensory response, our current working hypothesis is that there is a direct link between the size of the apical extension and the sensory function. The surface presented by the apical extension could condition the number of channels present at the microvilli and therefore constitute a limiting factor. Further investigation is necessary to test these hypotheses and establish the underlying mechanisms. We will collaborate with Adeline Ort Del'Immagine in the team to perform electrophysiological recordings on the Pkd2l1 channel in CSF-cNs from *espin* mutant embryos and control siblings. If channel properties are not affected, Adeline can investigate the mechanosensory function of mutant cells *in vitro* by applying direct mechanical stimulation. Another possibility is that the structure of the apical extension itself is critical to enable the detection of the mechanical stimulus to its full extent, for example by deflection of the microvilli. In this case, the shortening of CSF-cN apical extension may have implications for their mechanosensory functions but not for their chemosensory ones.

Does the espin mutation impair the CSF-cN chemosensory functions? The assay we used to test CSF-cN function in the *espin* mutant only gave us access to the mechanosensory response of the cells. Work from our lab and other teams demonstrated that CSF-cNs also respond to pH and osmolarity changes (Orts-Del'Immagine *et al.*, 2012, 2016; Böhm, 2016; Jalalvand *et al.*, 2016). More investigation of the chemosensory response in

our *espin* mutant is needed to further complete the study of the functional consequences of the loss of Espin through the morphological defects observed in CSF-cNs. The optimal approach would be to measure CSF-cN responses upon pH or osmolarity changes *in vitro*, on cultured cells from *espin* mutant fish versus wild-type (Böhm, 2016; Sternberg *et al.*, 2018).

What is the role of the cilium in the sensory function? One interesting question is the role of the kinocilium in the sensory function of CSF-cNs. The primary cilium formed by CSF-cNs is motile and surrounded by the actin-based protrusion at the apical side of the cells (Böhm *et al.*, 2016). The role of cilia in sensory function constitutes a great field of investigation in the research area of sensory systems. Several types of sensory cells display a ciliated apical extension to collect sensory stimuli (Table 1) and some MSCs bear a cilium within their microvilliated apical extension. In iHCs, the kinocilium supports the elaboration and orientation of the staircase pattern of stereocilia during development before degenerating (see Chapter 1, II.B). In zebrafish nHCs, the kinocilium is retained at the apical side of the cells and was implicated in immature mechanosensory activity (Kindt, Finch and Nicolson, 2012). So far, the putative role of the CSF-cN motile cilium has not been studied. Across experiments during our analysis of CSF-cN morphology in the *espin* mutant, we frequently observed one membrane protrusion standing out of the shortened apical extension, which we assumed to be the cilium. We however never used a specific cilia marker and it would thus be interesting to verify its structure and motility in the *espin* mutant. This verification could be achieved by performing immunohistochemistry using the anti-α-acetylated tubulin antibody or anti-GFP in fixed *Tg(β-actin:arl13-GFP)* transgenic animals.
Eventually, to obtain a more complete picture of the sensory role of the different structures present at the apical side – microvilli and cilium – we need to build tools allowing distinguishing both. In the *espin* mutant, the actin-based protrusions are impacted but, *a priori*, not the cilium. The use of dominant negative forms or the generation of mutant lines targeting specific cilia factors, for example kinesins involved in the intraflagellar transport, should produce apical extensions bearing microvilli but no cilium.

IV. SO, HOW DO CSF-CNS COMPARE TO OTHER MICROVILLIATED SENSORY CELL TYPES?

A common cell factory to support the elaboration of a functional microvilliated sensory organelle. My work shed light on the basic principles underlying the formation of a functional sensory organelle by CSF-cNs. My results highlighted important similarities at the level of the molecular mechanisms underlying the establishment of the microvilliated sensory apical extension of CSF-cNs with the thoroughly studied HCs. Notably, my results converge to demonstrate that CSF-cNs similarly rely on the

interaction between Espin and Myo3b to ensure the proper lengthening of their actin-based protrusions. Furthermore, my observations as a whole indicate that the shape of the apical extension is as critical for the CSF-cN sensory function as mechanosensory transduction in HCs.
In the light of my results and our current understanding of the different MSC types, my hypothesis is that some of these basic principles are shared between MSCs constituting a common molecular factory underlying the making of a functional microvilliated apical sensory organ.

Revisiting the polymodality of MSCs with genome-wide analysis. Our genome-wide approach aiming at analyzing the transcriptome of two types of MSCs, CSF-cNs and nHCs, provided rich datasets that revealed the polymodality of the two cell types. CSF-cNs express Pkd2l1, a member of the transient receptor potential channel family, already known to be involved in various sensory modalities (Damann, Voets and Nilius, 2008). The transcriptome dataset of CSF-cNs revealed that CSF-cNs also express a great number of secreted peptides, receptors and channels involved in physiological functions as diverse as immunity, inflammation, and feeding. Interestingly, our analysis of the transcriptome of nHCs, long-known for their mechanosensory responses, confirmed expected mechanoreceptors and revealed putative novel chemosensory functions via the expression of numerous receptors for serotonin or commonly attributed to ORNs and TRCs. Functional analysis to test the response of nHCs to chemical cues are on-going in the lab, together with validation experiments to confirm the expression of the detected chemoreceptors by *in situ* hybridization. Detection of external chemical cues by neuromasts would provide zebrafish larvae with an additional sensor ideally located on the body to collect information from the environment.
The idea that MSCs might actually carry polymodal sensory functions is further documented by the example of solitary chemosensory cells. Solitary chemosensory cells are found scattered throughout epithelial tissues and were first related to the two main chemosensory systems, taste and olfaction (Sbarbati and Osculati, 2005). Recent work nicely demonstrated that SCCs could also serve as sentinels and alarm systems by detecting bacterial compounds in the lungs and respiratory tracts in mammals (Finger *et al.*, 2003; Lee *et al.*, 2017). Together, these results open the discussion to reconsider the generally admitted sensory functions attributed to specific MSCs.

Towards a theory where MSCs share a common polymodal ancestor. Revisiting polymodality in MSCs and discussing the existence of a shared factory to produce microvilliated sensory organelles, my hypothesis is that MSCs could have evolved from the same multifunctional ancestor cell. This common ancestor could have either been a bipolar protoneuron bearing microvilli and a primary cilium at its apical side, in which case sensory receptor cells such as HCs and TRCs would have lost the ability to grow an axon, or a cell resembling Choanoflagellates, in which case sensory neurons such as CSF-

cNs and vORNs would have later acquired neuronal properties (Arendt, 2008). In both cases, each MSC would have evolved to specialize towards one preferred sensory modality but retained abilities to perform others. According to this theory, MSCs would have inherited both the factory to build a microvilliated sensory organelle and a diversity of sensory functions from their common ancestor. The MSC polymodality would be the result of subsequent functional segregation (i.e. the distribution of functions among descendant cells) in parallel to functional divergence (the modification of the retained functions) and the acquisition of novel functions (Arendt, 2008).

Altogether, my results have provided critical insight into MSC polymodality and shared morphogenetic factory, favoring the theory that MSCs are evolutionarily related and provided means to address this question.

References

Arendt, D. (2008) 'The evolution of cell types in animals: Emerging principles from molecular studies', *Nature Reviews Genetics*, 9(11), pp. 868–882. doi: 10.1038/nrg2416.

Böhm, U. L. *et al.* (2016) 'CSF-contacting neurons regulate locomotion by relaying mechanical stimuli to spinal circuits', *Nature Communications*, 7:10866, pp. 1–8. doi: 10.1038/ncomms10866.

Böhm, U. L. (2016) *Physiological inputs to cerebrospinal fluid-contacting neurons*.

Campanale, J. P., Sun, T. Y. and Montell, D. J. (2017) 'Development and dynamics of cell polarity at a glance', *Journal of Cell Science*, 130(7), pp. 1201–1207. doi: 10.1242/jcs.188599.

Chen, B. *et al.* (1999) 'Espin contains an additional actin-binding site in its N terminus and is a major actin-bundling protein of the Sertoli cell-spermatid ectoplasmic specialization junctional plaque', *Molecular biology of the cell*, 10(12), pp. 4327–39. doi: 10.1091/mbc.10.12.4327.

Damann, N., Voets, T. and Nilius, B. (2008) 'TRPs in Our Senses', *Current Biology*, 18(18), pp. 880–889. doi: 10.1016/j.cub.2008.07.063.

Djenoune, L. *et al.* (2014) 'Investigation of spinal cerebrospinal fluid-contacting neurons expressing PKD2L1: evidence for a conserved system from fish to primates', *Frontiers in Neuroanatomy*, 8(26). doi: 10.3389/fnana.2014.00026.

Djenoune, L. *et al.* (2017) 'The dual developmental origin of spinal cerebrospinal fluid-contacting neurons gives rise to distinct functional subtypes', *Scientific Reports*. Springer US, 7(719). doi: 10.1038/s41598-017-00350-1.

Eisen, J. S. and Smith, J. C. (2008) 'Controlling morpholino experiments: don't stop making antisense', *Development*, 135(10), pp. 1735–1743. doi: 10.1242/dev.001115.

El-Brolosy, M. A. *et al.* (2018) 'Genetic compensation is triggered by mutant mRNA degradation', *bioRxiv*.

Fidelin, K. *et al.* (2015) 'State-Dependent Modulation of Locomotion by GABAergic Spinal Sensory Neurons', *Current Biology*. Elsevier, 25(23), pp. 3035–3047. doi: 10.1016/j.cub.2015.09.070.

Finger, T. E. *et al.* (2003) 'Solitary chemoreceptor cells in the nasal cavity serve as sentinels of respiration', *Proceedings of the National Academy of Sciences*, 100(15), pp. 8981–8986. doi: 10.1073/pnas.1531172100.

Hwang, W. Y. *et al.* (2013) 'Efficient genome editing in zebrafish using a CRISPR-Cas system', *Nature Biotechnology*. Nature Publishing Group, 31(3), pp. 227–229. doi: 10.1038/nbt.2501.

Jalalvand, E. *et al.* (2016) 'Ciliated neurons lining the central canal sense both fluid movement and pH through ASIC3', *Nature Communications*. doi: 10.1038/ncomms10002.

Kindt, K. S., Finch, G. and Nicolson, T. (2012) 'Kinocilia Mediate Mechanosensitivity in Developing Zebrafish Hair Cells', *Developmental Cell*, 23(2), pp. 329–341. doi: 10.1016/j.devcel.2012.05.022.

Kok, F. O. *et al.* (2015) 'Reverse genetic screening reveals poor correlation between morpholino-induced and mutant phenotypes in zebrafish', *Developmental Cell*, 32(1), pp. 97–108. doi: 10.7205/MILMED-D-14-00168.Long-chain.

Krugmann, S. *et al.* (2001) 'Cdc42 induces filopodia by promoting the formation of an IRSp53:Mena complex', *Current Biology*, 11(21), pp. 1645–1655. doi: 10.1016/S0960-9822(01)00506-1.

Lee, R. J. *et al.* (2017) 'Bacterial D-amino acids suppress sinonasal innate immunity through sweet taste receptors in solitary chemosensory cells', *Science Signaling*, 10(495), pp. 1–12. doi: 10.1126/scisignal.aam7703.

Li, J. *et al.* (2015) 'Intron targeting-mediated and endogenous gene integrity-maintaining knockin in zebrafish using the CRISPR/Cas9 system', *Cell Research*, 25(5), pp. 634–637. doi: 10.1038/cr.2015.43.

Liu, H. *et al.* (2016) 'Myosin III-mediated cross-linking and stimulation of actin bundling activity of Espin', *eLife*, (January).

Margolis, B. and Borg, J.-P. (2005) 'Apicobasal polarity complexes', *Journal of Cell Science*, 118(22), pp. 5157–5159. doi: 10.1242/jcs.02597.

Merritt, R. C. *et al.* (2012) 'Myosin IIIB uses an actin-binding motif in its espin-1 cargo to reach the tips of actin protrusions', *Current Biology*, 22(4), pp. 320–325. doi: 10.1109/TMI.2012.2196707.Separate.

Nasevicius, A. and Ekker, S. C. (2001) 'The zebrafish as a novel system for functional genomics and therapeutic development applications', *Curr Opin Mol Ther*, 3(3), pp. 224–228.

Orts-Del'Immagine, A. *et al.* (2012) 'Properties of subependymal cerebrospinal fluid contacting neurones in the dorsal vagal complex of the mouse brainstem', *Journal of Physiology*, 590(16), pp. 3719–3741. doi: 10.1113/jphysiol.2012.227959.

Orts-Del'Immagine, A. *et al.* (2016) 'A single polycystic kidney disease 2-like 1 channel opening acts as a spike generator in cerebrospinal fluid-contacting neurons of adult mouse brainstem', *Neuropharmacology*, 101, pp. 549–565. doi: 10.1016/j.neuropharm.2015.07.030.

Rossi, A. *et al.* (2015) 'Genetic compensation induced by deleterious mutations but not gene knockdowns', *Nature*, 524(7564), pp. 230–233. doi: 10.1038/nature14580.

Salles, F. T. *et al.* (2009) 'Myosin IIIa boosts elongation of stereocilia by transporting espin 1 to the plus ends of actin filaments', *Nature Cell Biology*, 11(4), pp. 443–450. doi: 10.1038/ncb1851.

Santos, F. *et al.* (2006) 'Lateral line hair cell maturation is a determinant of aminoglycoside susceptibility in zebrafish (Danio rerio)', *Hearing Research*, 213, pp. 25–33. doi: 10.1016/j.heares.2005.12.009.

Sbarbati, A. and Osculati, F. (2005) 'The taste cell-related diffuse chemosensory system', *Progress in Neurobiology*, 75(4), pp. 295–307. doi: 10.1016/j.pneurobio.2005.03.001.

Scita, G. *et al.* (2008) 'IRSp53: crossing the road of membrane and actin dynamics in the formation of membrane protrusions', *Trends in Cell Biology*, 18(2), pp. 52–60. doi: 10.1016/j.tcb.2007.12.002.

Sekerková, G. *et al.* (2003) 'Novel Espin Actin-bundling Proteins Are Localized to Purkinje Cell Dendritic Spines and Bind the SH3 Adapter Protein Insulin Receptor Substrate p53', *The Journal of Neuroscience*, 23(4), pp. 1310–1319. doi: 23/4/1310 [pii].

Sekerková, G. *et al.* (2006) 'Differential expression of espin isoforms during epithelial morphogenesis, stereociliogenesis and postnatal maturation in the developing inner ear', *Developmental Biology*, 291, pp. 83–95. doi: 10.1016/j.ydbio.2005.12.021.

Sekerková, G., Richter, C.-P. and Bartles, J. R. (2011) 'Roles of the Espin Actin-Bundling Proteins in the Morphogenesis and Stabilization of Hair Cell Stereocilia Revealed in CBA/CaJ Congenic Jerker Mice', *PLoS Genetics*, 7(3). doi: 10.1371/journal.pgen.1002032.

Shah, A. N. *et al.* (2015) 'Rapid reverse genetic screening using CRISPR in zebrafish', *Nature Methods*. Nature Publishing Group, 12(6), pp. 535–540. doi: 10.1038/nmeth.3360.

Steketee, M., Balazovich, K. and Tosney, K. W. (2001) 'Filopodial initiation and a novel filament-organizing center, the focal ring.', *Molecular biology of the cell*, 12(8), pp. 2378–95. doi: 10.1091/mbc.12.8.2378.

Sternberg, J. R. *et al.* (2018) 'Pkd2l1 is required for mechanoception in cerebrospinal fluid-contacting neurons and maintenance of spine curvature', *Nature Communications*, pp. 1–10. doi: 10.1038/s41467-018-06225-x.

Svitkina, T. M. *et al.* (2003) 'Mechanism of filopodia initiation by reorganization of a dendritic network', *Journal of Cell Biology*, 160(3), pp. 409–421. doi: 10.1083/jcb.200210174.

Zhao, H., Pykäläinen, A. and Lappalainen, P. (2011) 'I-BAR domain proteins: linking actin and plasma membrane dynamics', *Current Opinion in Cell Biology*, 23, pp. 14–21. doi: 10.1016/j.ceb.2010.10.005.

Zheng, L. *et al.* (2000) 'The Deaf Jerker Mouse Has a Mutation in the Gene Encoding the Espin Actin-Bundling Proteins of Hair Cell Stereocilia and Fails to Accumulate Espins', *Cell*, 102(3), pp. 377–385. doi: 10.1016/S0092-8674(00)00042-8.

ANNEX

SCIENTIFIC REPORTS

OPEN

The dual developmental origin of spinal cerebrospinal fluid-contacting neurons gives rise to distinct functional subtypes

Received: 11 October 2016
Accepted: 30 January 2017
Published online: 07 April 2017

Lydia Djenoune[1,2], Laura Desban[1], Johanna Gomez[1], Jenna R. Sternberg[1], Andrew Prendergast[1], Dominique Langui[1], Feng B. Quan[1,2], Hugo Marnas[1], Thomas O. Auer[3,4], Jean-Paul Rio[1], Filippo Del Bene[3], Pierre-Luc Bardet[1] & Claire Wyart[1]

Chemical and mechanical cues from the cerebrospinal fluid (CSF) can affect the development and function of the central nervous system (CNS). How such cues are detected and relayed to the CNS remains elusive. Cerebrospinal fluid-contacting neurons (CSF-cNs) situated at the interface between the CSF and the CNS are ideally located to convey such information to local networks. In the spinal cord, these GABAergic neurons expressing the PKD2L1 channel extend an apical extension into the CSF and an ascending axon in the spinal cord. In zebrafish and mouse spinal CSF-cNs originate from two distinct progenitor domains characterized by distinct cascades of transcription factors. Here we ask whether these neurons with different developmental origins differentiate into cells types with different functional properties. We show in zebrafish larva that the expression of specific markers, the morphology of the apical extension and axonal projections, as well as the neuronal targets contacted by CSF-cN axons, distinguish the two CSF-cN subtypes. Altogether our study demonstrates that the developmental origins of spinal CSF-cNs give rise to two distinct functional populations of sensory neurons. This work opens novel avenues to understand how these subtypes may carry distinct functions related to development of the spinal cord, locomotion and posture.

The cerebrospinal fluid (CSF) is a complex solution circulating around the central nervous system (CNS). It has classically been assumed that the CSF ensures the homeostasis of the CNS[1]. Multiple studies indicate that the CSF also conveys signals affecting the development and output functions of the CNS, such as feeding, sleep, and locomotion[2–6]. These observations suggest that chemical or mechanical cues from the CSF may act on neurons in the brain and spinal cord. Cerebrospinal fluid-contacting neurons (CSF-cNs) are precisely located at the interface between the CSF and the neuronal circuits[7,8]. In the vertebrate spinal cord, CSF-cNs reside around the central canal[9–15] and project an apical extension in contact with the CSF[8,16–18] and have a locally-projecting axon[14,19,20] that contacts other spinal neurons[12,15,21].

One essential step to understand spinal CSF-cN functions lies in identifying specific markers for these cells. In this regard, the polycystic kidney disease 2 like 1 (PKD2L1) channel also called TRPP3[22], which belongs to the Transient Potential Receptor (TRP) family, appears as a robust candidate to label CSF-cNs[11,13,23,24]. PKD2L1, originally identified as the sour taste receptor in the taste buds, has been found in the spinal CSF-cNs of mouse[11,13,25,26], zebrafish and macaques[13]. The opening of the PKD2L1 channel is modulated by variations in pH[27] and osmolarity[28]. Although the physiological variations of pH and osmolarity in the CSF are not well known, these observations suggest that CSF-cNs could be interoceptors modulated by chemical and/or mechanical cues from the CSF[23].

[1]Sorbonne Universités, UPMC Univ Paris 06, Inserm, CNRS, AP-HP, Institut du Cerveau et de la Moelle épinière (ICM) - Hôpital Pitié-Salpêtrière, Boulevard de l'hôpital, F-75013, Paris, France. [2]Muséum National d'Histoire Naturelle, Paris, 75005, France. [3]Institut Curie, Paris, 75005, France. [4]Present address: Thomas O Auer, Center for Integrative Genomics, Faculty of Biology and Medicine, University of Lausanne, Lausanne, Switzerland. Correspondence and requests for materials should be addressed to P.-L.B. (email: pierreluc.bardet@icm-institute.org) or C.W. (email: claire.wyart@icm-institute.org)

There is evidence that spinal CSF-cNs do not constitute a homogeneous population of neurons. In particular, these cells originate from distinct progenitor domains and are specified differentially by several cascades of transcription factors[26,29–32]. In zebrafish, CSF-cNs are subdivided into the ventral population, referred to as KA", originating from the progenitor domain p3 and a dorsal population, referred to as KA', originating from pMN[29,30]. In mouse, spinal CSF-cNs were recently shown to originate from the p3 and p2 progenitor domains[26]. In addition, some secreted compounds have been previously reported in a restricted number of spinal CSF-cNs, such as the somatostatin[33,34] or serotonin[35,36].

The zebrafish has emerged as an ideal model organism to study the development[13,29,30], the morphology and physiological roles of CSF-cNs *in vivo* due to its transparency at early stages[12,15,37]. Yet, few functional markers of CSF-cNs related to their sensory or secretory functions have been identified in this species. Here, we investigate whether the two types of spinal CSF-cNs defined by distinct developmental origins can be discriminated by morphology, projection on neuronal targets and expression of secreted compounds. Using a quantitative measure of cell shape, we show that ventral and dorsal CSF-cNs have differently shaped apical extensions as well as different axonal projections and consequently project onto distinct neuronal targets within the spinal cord. By electron microscopy (EM), we found that both populations of CSF-cNs exhibit large granular vesicles in accordance with secretory properties. We demonstrate that these two cell types express distinct modulators and peptides: while ventral CSF-cNs transiently express serotonin, dorsal CSF-cNs express the *sst1.1* somatostatin paralog. We observed that the Pkd2l1 channel is not required for the differentiation of CSF-cN axonal projections, for the expression of serotonin or somatostatin. Altogether, our results show that spinal CSF-cNs constitute two distinct functional cell types that differ in apical and axonal morphology, neuronal targets within the spinal cord as well as in the transient expression of secreted compounds.

Results

CSF-cNs are neurosecretory cells with an apical extension into the central canal. We characterized CSF-cN ultrastructure in transverse sections of the 2.5 days post fertilization (dpf) zebrafish spinal cord by transmission electron microscopy (TEM). Without specific markers, we observed cells around the central canal that bore an apical extension with microvilli (Supplemental Fig. 1). To demonstrate these cells were CSF-cNs, we transiently expressed the engineered genetically-encoded peroxidase APEX2 under the *pkd2l1* promoter (see Materials and Methods, Supplemental Fig. 2). In APEX2-TagRFP^{+} larvae, we performed diaminobenzidine (DAB) staining (see Material and Methods, and Supplemental Fig. 3). DAB was detected only within CSF-cNs in the spinal cord, making the cells appear darker (Supplemental Fig. 3b). The specific DAB staining (Figs 1 and 2) revealed that CSF-cNs were either round (Figs 1a and 2a-b) or pear-shaped (Fig. 1b). Ventral and dorsal CSF-cNs bear an apical extension with several microvilli directed toward the lumen of the central canal (Figs 1c and 2c). Among actin-based microvilli, we observed, as previously described in one cell[37], a single cilium directed toward the CSF (Fig. 1d, n = 12 ventral CSF-cNs, Fig. 2d, n = 3 dorsal CSF-cNs). This cilium bears two central microtubule singlets along the axoneme (Figs 1d and 2d-e), often seen in a kinocilium[38,39]. In APEX2^{+} CSF-cNs, we observed large granular vesicles (Figs 1e and 2f), suggesting that these cells either release or uptake peptides or neuromodulators into or from the CSF. Interestingly, we observed one axo-somatic symmetric synaptic contact at the basal pole of a CSF-cN (Fig. 1f), suggesting that CSF-cNs receive inhibitory synaptic inputs. Indeed, asymmetric synapses usually contain glutamate, are non-GABA immunoreactive and are therefore considered excitatory, while symmetric synapses contain GABA and are considered inhibitory[40–42]. Altogether, our TEM data show that both populations of CSF-cNs exhibit properties of sensory and secretory cells.

CSF-cNs display different shapes of apical extensions and axonal projections. As a quantitative analysis of CSF-cN morphology is difficult using serial EM, we turned to fluorescence for a quantitative comparison of the apical extension and the axonal projections of dorsal and ventral CSF-cNs. First, we tested whether these cells differ in the morphology of their apical extension. We investigated the shape of the CSF-cN apical extension by labeling the membrane of CSF-cNs in *Tg*(*pkd2l1*:*Gal4*;*UAS*:*TagRFPCAAX*;*cmlc2*:*eGFP*)*icm22* larvae or F-actin itself in *Tg*(*pkd2l1*:*Gal4*;*UAS*:*LifeAct-GFP*;*cryaa*:*V*)*icm28* larvae or larvae transiently expressing (*pkd2l1*:*Gal4*) and (*UAS*:*LifeAct-TagRFP*;*cryaa*:*C*). Using these different approaches, we found that the shape of the apical extension differs between ventral and dorsal CSF-cNs at 3 and 6 dpf (Fig. 3a,b and Material and Methods). The apical extension of dorsal CSF-cNs (Fig. 3a,b) was more extended along the border of the central canal than for ventral cells (Fig. 3a,b). The apical extension in ventral CSF-cNs was overall more compact with a small proportion displaying a more extended apical extension similar to dorsal CSF-cNs (13.3%, n = 6 out of 45 ventral CSF-cNs, Fig. 3a, empty arrow). Next, to assess whether ventral and dorsal CSF-cNs differ in their axonal projections, we injected the (*pkd2l1-TagRFP*) DNA construct to label single cells (Supplemental Fig. 4a) and reconstructed their axon (Fig. 3c, Supplemental Fig. 4b,c). All CSF-cN axonal projections were ventral, ipsilateral and ascending, yet they were heterogeneous along the rostrocaudal axis of the spinal cord (n = 54, Fig. 3c). We measured significant differences between the axonal projections of the two populations of CSF-cNs in terms of the area of the axonal arborization, the length of the axon, the dorso-ventral coverage within the spinal cord and the number of axonal branches (Fig. 3d). The larger axonal length, arborization and number of branches in ventral CSF-cNs compared to dorsal cells suggest these ventral cells possibly differentiate before dorsal ones. Nonetheless, the fact that the dorsal and ventral populations of CSF-cNs project on different domains along the dorso-ventral axis of the spinal cord suggests that these two populations may target different neuronal types within the ventral spinal cord.

Distinct neuronal targets for ventral and dorsal CSF-cNs within the spinal cord. Differences in the axonal projection of ventral and dorsal CSF-cNs suggest these cells may project onto distinct targets within the spinal cord. Our lab recently demonstrated that CSF-cNs project onto caudal primary (CaP) motor

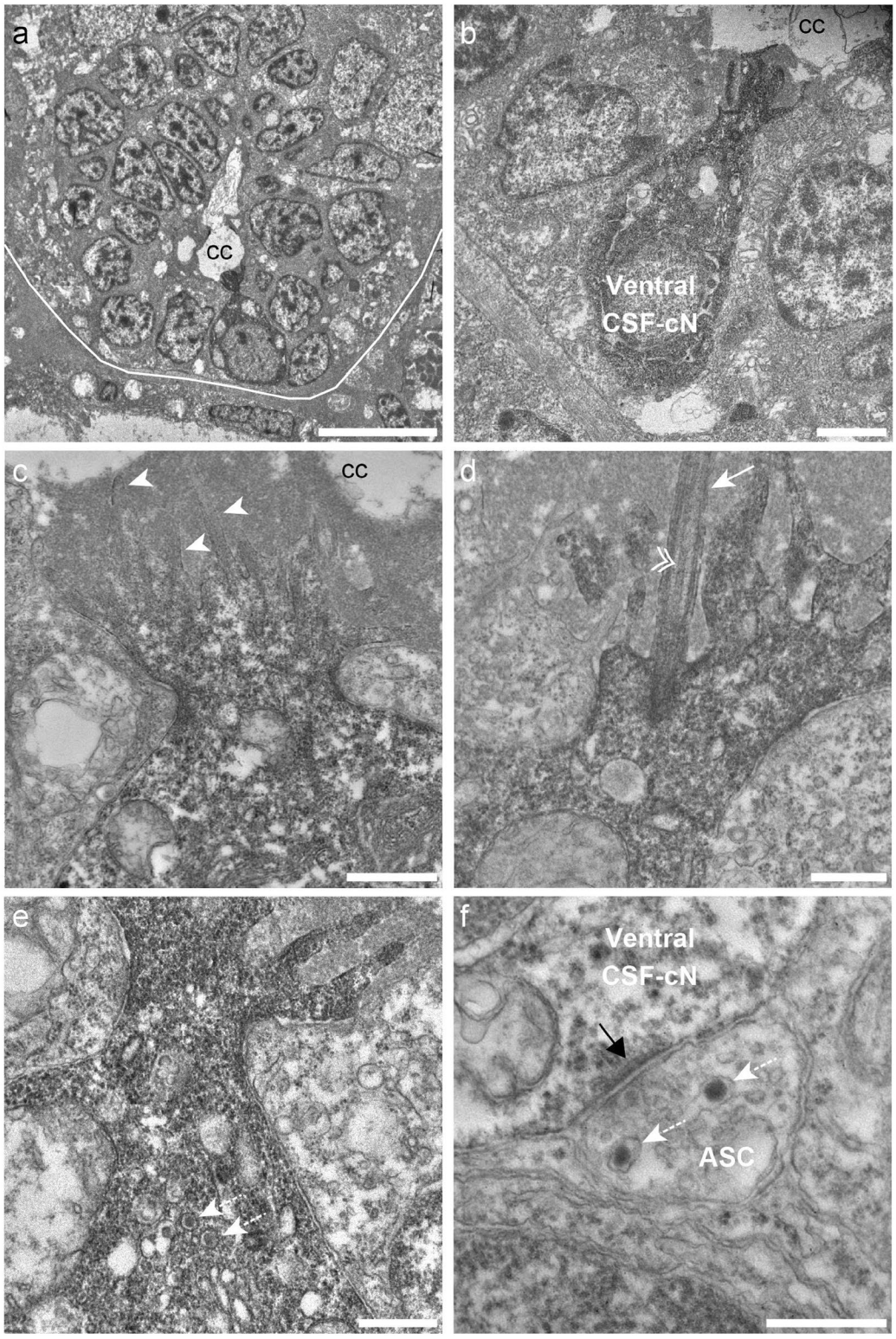

Figure 1. Ventral CSF-cNs exhibit an apical extension composed of microvilli and a kinocilium in the spinal cord. (**a**) Transverse section of the spinal cord showing restricted deposition of DAB in a ventral CSF-cN. (**b**) Overall view of a DAB^{+} ventral CSF-cN contacting the central canal (cc) and surrounded by ependymal cells. (**c**) Ventral CSF-cNs project at the apical pole an extension toward the central canal bearing several microvilli (arrowheads). (**d**) Within this extension is located a cilium (arrows) with two central microtubule along the axoneme (double arrowhead), suggesting a motile cilium. Large granular vesicles (LGV) are observed in the cytoplasm (**e**, dotted arrows) and axo-somatic synaptic contacts in the basal pole (**f**, ASC). Note the symmetry of the synaptic contact (black arrow) is reminiscent of an inhibitory synapse. Note the presence of LGV in the axon (**f**, dotted arrows). Scale bar = 10 μm (**a**), 2 μm (**b**), 1 μm (**c**), 500 nm (**d**,**e**) and 400 nm (**f**).

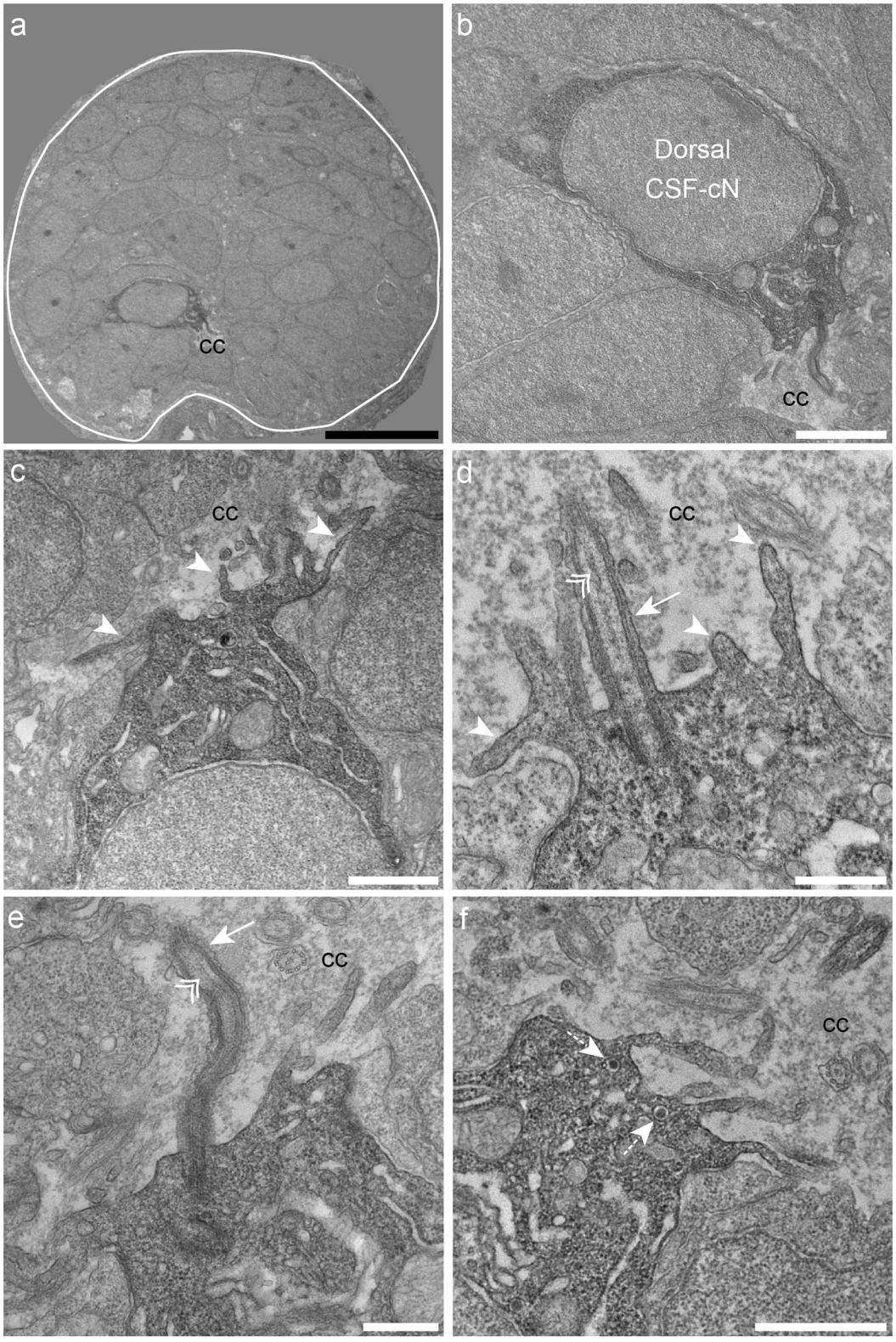

Figure 2. Dorsal spinal CSF-cNs also exhibit ultrastructural properties of sensory neurons. (**a**) Transverse section of the spinal cord showing restricted deposition of DAB in a dorsal CSF-cN. (**b**) Overall view of a DAB^{+} dorsal CSF-cN contacting the central canal (cc). (**c**,**d**) Dorsal CSF-cNs bear at the apical pole multiple microvilli (arrowheads). (**d**,**e**) In the apical pole is located a cilium (arrow) with two central microtubule singlets along the axoneme (double arrowhead), reminiscent of a motile cilium. (**f**) Dorsal CSF-cN also exhibit LGV distributed in the cytoplasm (dotted arrows). Scale bar = 10 μm (**a**), 2 μm (**b**), 1 μm (**c**,**f**) and 500 nm (**d**,**e**).

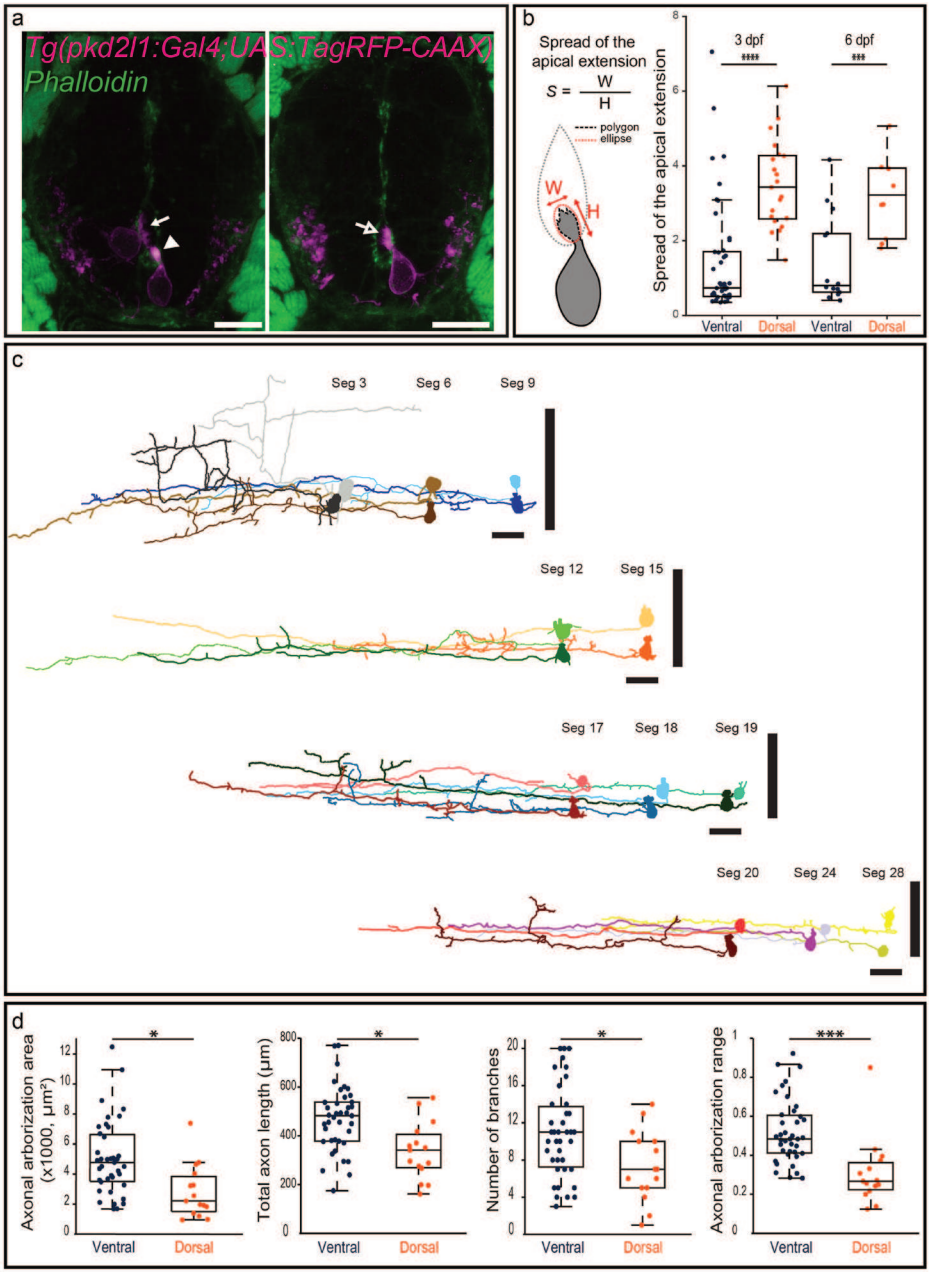

Figure 3. Morphological analysis of CSF-cNs reveals heterogeneous shapes of apical extension and axonal projections. (**a**) Transverse sections showing ventral and dorsal TagRFP-CAAX^{+} CSF-cNs (magenta) at 3 dpf reflecting the diversity of morphologies of the apical extension. The apical extension of all dorsal CSF-cNs spreads along the central canal border (arrow) while most ventral CSF-cNs (86.7%) form compact extensions (arrowhead). The small remaining subpopulation of ventral CSF-cNs exhibits the typical spread of dorsal apical extensions (arrow with empty head; Phalloidin staining, green). (**b**) Schematics of the analysis of the apical extension performed on each cell and statistical analysis comparing the size of the apical extension between ventral and dorsal CSF-cNs at 3 dpf ($n = 45$ versus 21) and 6 dpf ($n = 14$ versus 10). The apical extension of dorsal CSF-cNs extends more than for ventral CSF-cNs (two-sample t-tests, $p < 5 \cdot 10^{-7}$) and this difference persists at later stages (6 dpf, $p < 0.002$). (**c**) The reconstruction from dorsal (light shade) and ventral (dark shade) CSF-cNs from different segments (Seg) illustrates the diversity of axonal morphologies CSF-cNs between the two types along the spinal cord ($n = 11$ for each type). Vertical black bars represent the dorso-ventral limits of the spinal cord. Cells are positioned according to their dorso-ventral (D-V) position with dorsal edge set to 1 and ventral to 0. (**d**) Comparison of ventral and dorsal CSF-cNs for axonal arborization area, total axon length, number of branches and axonal arborization dorso-ventral range ($n = 39$ and 15 cells respectively). Ventral CSF-cNs have a wider axonal arborization ($p < 0.003$), a longer axon ($p = 0.0014$), reach more ventral domains of the spinal cord ($p < 9 \cdot 10^{-4}$), and cover a larger dorso-ventral (D-V) range ($p < 2 \cdot 10^{-4}$) with more axonal branches ($p < 0.02$). Two-sample t-tests were performed to compare the two populations. Scale bar = 10 µm (**a**) and 20 µm (**c**).

neurons and commissural primary ascending (CoPA) sensory interneurons within the escape circuit[43] as well as onto V0-v interneurons within the slow swimming circuit[15]. We investigated which CSF-cN type projects onto these targets using mosaic labeling in transgenic lines labeling CaP (*Tg*(*parg*^{mnet2}*-GFP*)[43,44]), V0-v (*Tg*(*vglut2a*:*lox*:*DsRed*:*lox*:*GFP*)[15,45]) or CoPA (*Tg*(*tbx16-GFP*)[43,46]). We observed that only ventral CSF-cNs form the stereotypical basket structure around the soma of CaP motor neurons (Fig. 4a, n = 7 out of 8 ventral CSF-cNs found projecting onto CaP and 0 out of 5 dorsal CSF-cNs). In contrast, we found only dorsal CSF-cNs contacting ventrolateral glutamatergic cells, putatively V0-v based on their location and our previous findings[15,47–49] (Fig. 4b, n = 3 out of 3 dorsal CSF-cNs and 0 out of 5 ventral CSF-cNs). Interestingly, we observed that both ventral and dorsal CSF-cNs project onto CoPA sensory interneurons (Fig. 4c,d, n = 4 dorsal and 5 ventral CSF-cNs). Altogether, our observations demonstrate a complex connectivity pattern from CSF-cNs onto their neuronal targets in the spinal cord. While some targets receive projections from both CSF-cN types (such as CoPA sensory interneurons), others seem to only receive inputs from either ventral (CaP motor neurons) or dorsal (ventrolateral glutamatergic neurons, most likely V0-v interneurons) CSF-cNs.

Investigation of secreted compounds expressed in dorsal and ventral CSF-cNs. We tested whether ventral and dorsal CSF-cNs differentially express secreted compounds previously reported in a restricted number of CSF-cNs, namely somatostatin[14,21,33,34] and serotonin[35,36]. By taking advantage of *pkd2l1* expression in CSF-cNs[13], we used the *Tg*(*pkd2l1*:*GCaMP5G*)*icm07* transgenic line to selectively target CSF-cNs[37]. We demonstrated the specificity of this line using fluorescent *in situ* hybridization (FISH) for *pkd2l1* mRNA coupled to GFP immunohistochemistry (IHC) to amplify the endogenous GCaMP5G signal from 24 hours post fertilization (hpf) to 5 dpf (Supplemental Fig. 5).

In zebrafish, somatostatin immunoreactivity has previously been reported[12], but 6 different paralogs exist (*sst1.1*, *sst1.2*, *sst2*, *sst3*, *sst5* and *sst6*)[50,51]. Testing the expression of all of them, we only detected expression of *sst1.1* in CSF-cNs. Expression of *sst1.1* was observed only in dorsal CSF-cNs (Fig. 5a,b, arrows) in the rostral part of the spinal cord, from segment 1 to 13 at 24, 48, 72 hpf and in the adult spinal cord (data *not shown*). Since *sst1.1* had been reported as expressed transiently in motor neurons from 19 hpf until 55 hpf[52], we showed using FISH for *sst1.1* with GFP IHC in 24 hpf *Tg*(*mnx1*:*GFP*) embryos[53] that *sst1.1* expression was excluded from motor neurons (Fig. 5c). Altogether, our results show that *sst1.1* is expressed in dorsal CSF-cNs and absent in ventral ones at early stages and restricted as well to a subpopulation of CSF-cNs in the adult. Next, we tested whether zebrafish CSF-cNs were serotoninergic by performing double IHC for 5-HT and GFP on *Tg*(*pkd2l1*:*GCaMP5G*)*icm07* embryos and larvae from 24 hpf to 72 hpf. At 24 hpf, no 5-HT immunostaining was detected in the zebrafish spinal cord (*data not shown*). At 48 hpf, we detected 5-HT in ventral CSF-cNs (Fig. 5d, arrowheads) in the rostral part of the spinal cord (from segment 1 to 24). This expression was restricted to a subset of ventral CSF-cNs (Fig. 5d). The proportion of 5-HT^{+} CSF-cNs at 48 hpf decreased along the rostrocaudal axis of the spinal cord (segments 3 to 6: 88.6 ± 16.0%, 96 cells; segments 10 to 13: 73.2 ± 27.3%, 100 cells; segments 23 to 26: 31.2 ± 33.3%, 94 cells). At 3 dpf, although 5-HT was still expressed along the entire spinal cord in other cells, the staining was absent in CSF-cNs in the rostral spinal cord (Fig. 5e). In conclusion, dorsal CSF-cNs express *sst1.1* while a subpopulation of ventral CSF-cNs population is transiently serotoninergic. Hence, these two populations originating from different progenitor pools differentiate into distinct cell types expressing specific secreted compounds.

***pkd2l1* null mutation does not impact on the differentiation of spinal CSF-cNs.** We previously showed that the PKD2L1 channel is expressed in spinal CSF-cNs across multiple vertebrate species[13] and that the channel appears necessary to mediate detection of spinal bending by CSF-cNs in the larva[37]. In *pkd2l1* mutants, we observed defects in locomotion that we interpreted as being caused by the lack of sensory responses in CSF-cNs[37]. To strengthen the conclusions of this previous study, we sought to precisely assess whether CSF-cNs develop properly in the *pkd2l1* mutants. We found that in mutants, CSF-cNs were still GABAergic, ventral ones were still serotoninergic, that the number of CSF-cNs was not impacted, and that the morphology of their axonal projections was not different from WT (Supplemental Fig. 6). We also wanted to determine whether the functional connection between ventral CSF-cNs and CaPs[43,54] was impacted and found that light-mediated activation of mutants CSF-cNs was still able to induce monosynaptic inhibitory postsynaptic currents in CaPs (Supplemental Fig. 7). Altogether, our results show that *pkd2l1* is not required for CSF-cN differentiation.

Discussion

Spinal CSF-cNs were previously shown to originate from distinct progenitor domains characterized by distinct pools of transcription factors in the embryo[26,29,30]. Here we demonstrate that these two domains give rise to two cell types of CSF-cNs with probably distinct functional properties at the larval stages (Supplemental Fig. 8). First, the morphology of these two cell types differs both at the apical extension level as well as at the axonal level. Furthermore, we show that these differences in axonal projections lead to differences in neuronal targets reached in the spinal cord. Second, our ultrastructure data indicate that both ventral and dorsal CSF-cNs bear dense granules under the apical extension, suggesting possible roles in release or uptake of compounds from the CSF. We show that ventral and dorsal populations express distinct secreted factors, in particular 5-HT and *sst1.1*, during development. Finally we show that Pkd2l1 is not necessary for the differentiation of CSF-cNs. Altogether, our results demonstrate that the two cell types of CSF-cNs previously identified with different developmental origins segregate into distinct populations bearing specific functional properties.

Due to their peculiar apical extension contacting the CSF, it had been hypothesized that CSF-cNs may release compounds into the CSF[7,55]. The presence of large granular vesicles (LGV) within CSF-cNs in our EM data, combined with expression of *sst1.1* and 5-HT for dorsal and ventral CSF-cNs respectively, reinforces this hypothesis.

Previous works have shown that CSF-cNs are chemosensory[11,24,56,57] as well as mechanosensory cells[37,43,58]. In zebrafish larvae, we previously showed that dorsal CSF-cNs respond to lateral bending of the spinal cord[37] while

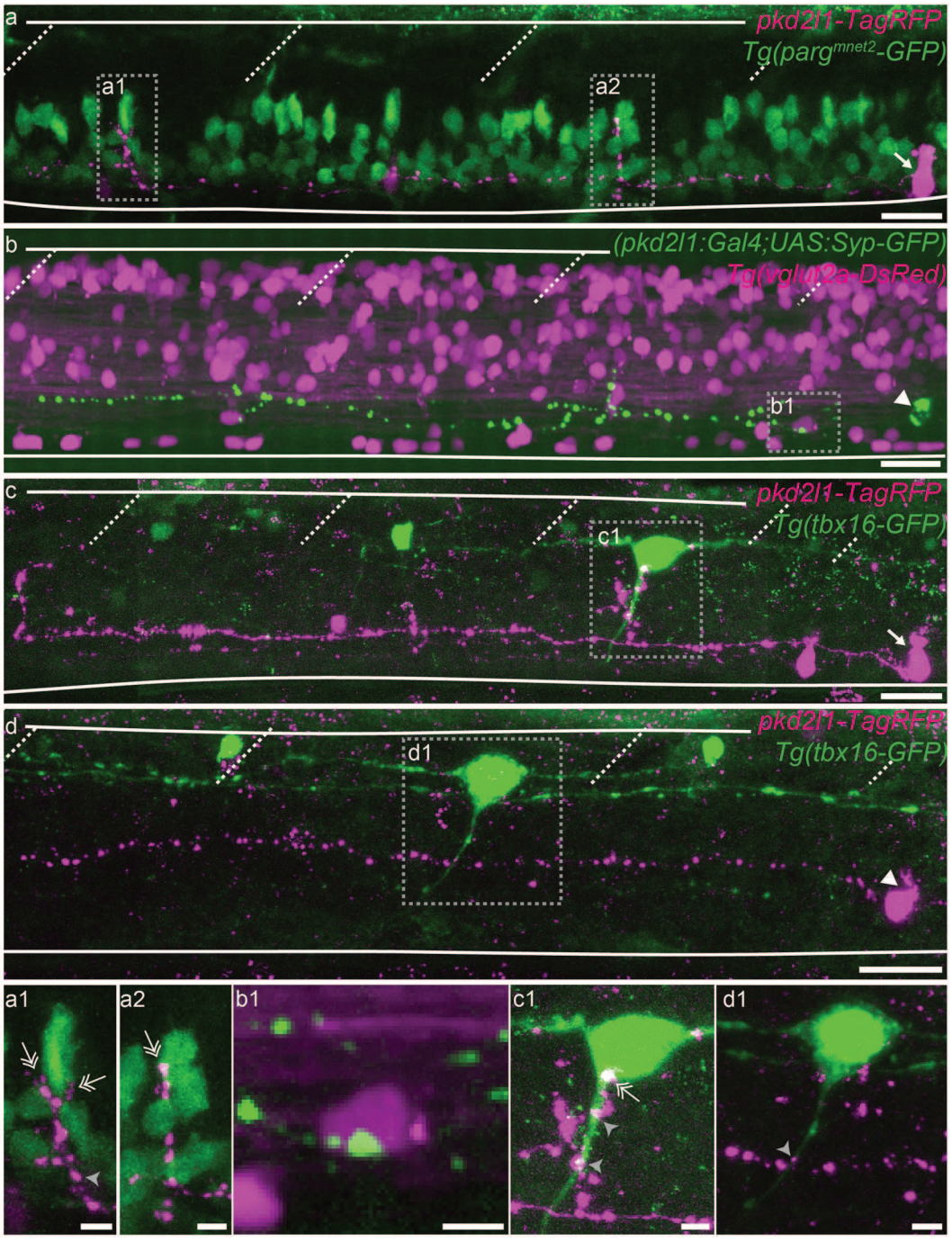

Figure 4. Ventral and dorsal CSF-cNs project onto distinct neuronal populations. (**a**–**d**) Z projection stacks showing contact from ventral and dorsal CSF-cNs onto different spinal targets. (**a**) Lateral view of a ventral CSF-cN (magenta, arrow) contacting 2 CaP motor neurons (identified based on their location within the segment) labelled in green in the *Tg*(*parg*^{mnet2}*-GFP*) transgenic line (**a1**,**a2**, double headed arrows). (**b**) Dorsal CSF-cN (green, arrowhead) contacting a putative V0-v interneuron (magenta, based on its dorso-ventral and lateral location) in the *Tg*(*vglut2a*:*DsRed*) transgenic line. (**c**,**d**) Ventral (**c**, arrow) and dorsal (**d**, arrowhead) CSF-cNs (magenta) contact CoPA sensory interneurons (green) labelled in the *Tg*(*tbx16-GFP*) transgenic line. Boxes with close-ups highlight contacts between the CSF-cN and its target. Scale bar = 20 μm (**a**–**d**) and 5 μm (**a1**–**d1**).

ventral CSF-cNs respond to longitudinal contractions[43]. The difference in shape of the apical extension between dorsal and ventral CSF-cNs may reflect a structural difference relevant for either their mechanosensory functions (direction of maximum sensitivity to bending of the tissue or CSF flow) or their secretory functions (with possibly larger surface area for dorsal CSF-cNs).

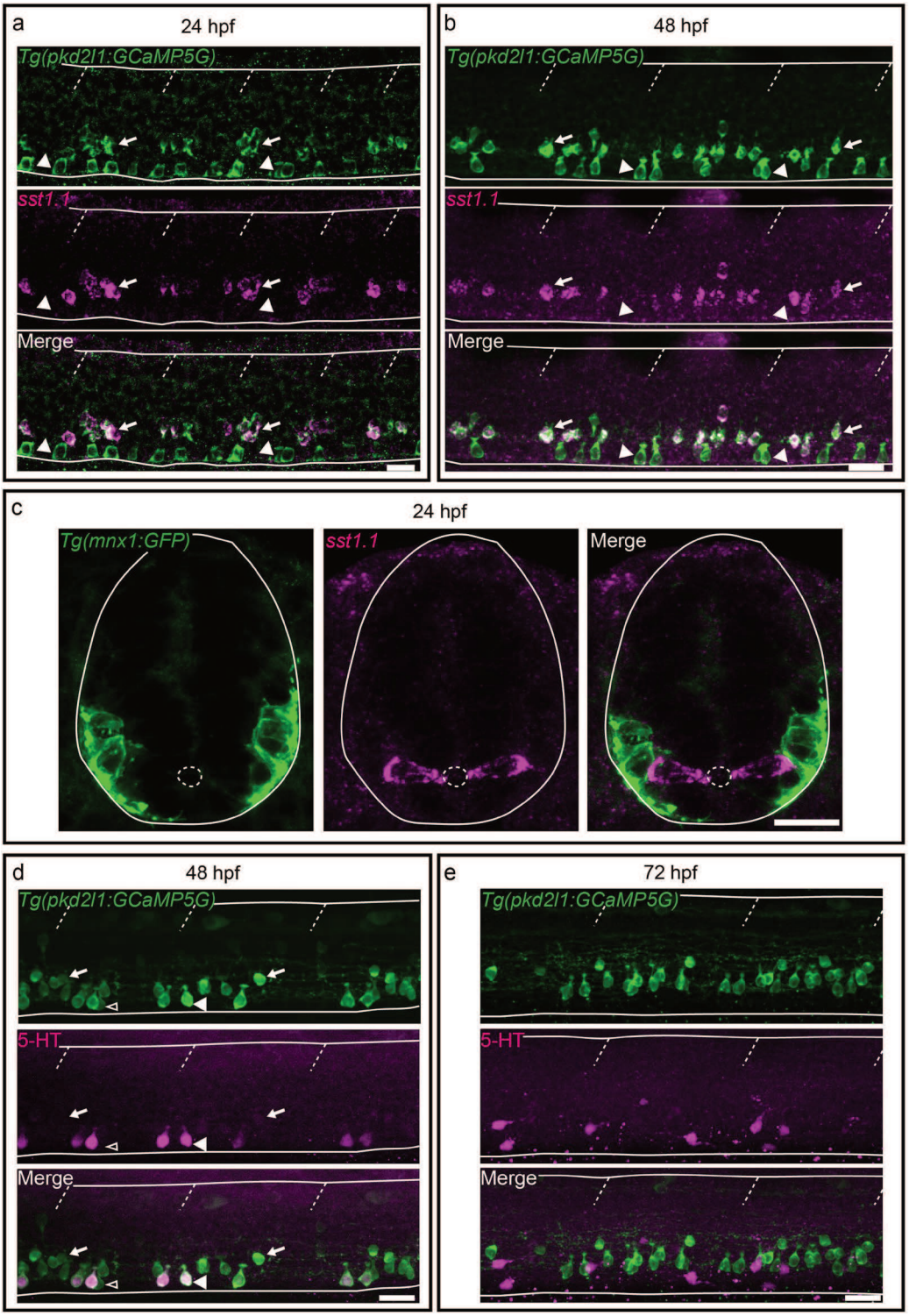

Figure 5. Secreted factors distinguish dorsal and ventral CSF-cNs: while dorsal express the somatostatin paralog *sst1.1*, ventral CSF-cNs express 5-HT. (**a**–**c**) Lateral views of the spinal cord show that *sst1.1* expression is restricted to dorsal CSF-cNs (arrows, FISH for *sst1.1* (magenta) coupled to GFP IHC (green) on *Tg*(*pkd2l1*:*GCaMP5G*)) (**a**,**b**) and *Tg*(*mnx1*:*GFP*) (**c**) embryos and larvae at 24 hpf (**a**,**c**) and 48 hpf (**b**). (**c**) Transverse sections show that *sst1.1* (magenta) is not expressed in motor neurons (green) as previously suggested (Devos *et al.*[52]). (**d**,**e**) IHC for 5-HT (magenta) and GFP (green) on *Tg*(*pkd2l1*:*GCaMP5G*) transgenic larvae at 48 hpf (**d**) and 72 hpf (**e**). (**d**) At 48 hpf, most ventral CSF-cNs express 5-HT (arrowhead, compared to negative cells shown with empty arrowhead). Note that dorsal CSF-cNs (arrows) are not labelled by 5-HT. (**e**) At 72 hpf, ventral CSF-cNs are not serotoninergic anymore in the rostral part of the spinal cord. Horizontal lines represent the limits of the spinal cord and slash dashed lines represent somite boundaries. Small dotted ellipses represent the limit of the central canal. Scale bars = 20 μm.

Transgenic/mutant	Labelling in the spinal cord	Original publication
Tg(pkd2l1:GCaMP5G)icm07	CSF-cNs	37
Tg(pkd2l1:GCaMP5G)icm07;pkd2l1^{icm02}	CSF-cNs	37
Tg(mnx1:GFP)	Motor neurons	53
Tg(pkd2l1:Gal4)icm10	CSF-cNs	15
Tg(UAS:TagRFP-CAAX;cmlc2:eGFP)icm22	Non applicable	This study
Tg(UAS:LifeAct-GFP;cryaa:V)icm28	Non applicable	This study
Tg(parg^{mnet2}*-GFP)*	Motor neurons	44
Tg(tbx16-GFP)	CoPAs	46
Tg(vglut2a:lox:DsRed:lox:GFP)	Glutamatergic interneurons	45

Table 1. Transgenic lines used in our study.

There are indications that spinal CSF-cNs harbor different morphologies in other species as well. In rat, spinal GABAergic CSF-cNs were first classified into three subtypes according to the shape of their soma[59]. Four morphological types of CSF-cNs were then described based on the shape of their soma, their axonal projection, and on the expression of the peptide Met-Enk-Arg-Gly-Leu[60]. These indications together with our data reveal a high level of heterogeneity among spinal CSF-cNs. Future studies will investigate the role of CSF-cN structural differences in sensory and secretory functions.

Using a single cell labelling approach, we show that ventral CSF-cNs have on average a longer and broader axonal arborization and cover a higher dorso-ventral spinal cord range with more axonal branches than dorsal CSF-cNs. These differences in axonal projections suggest the two CSF-cN populations might have distinct targets within the spinal cord. We had shown that CSF-cNs form active GABAergic synapses onto glutamatergic descending V0-v interneurons[15] as well as CaP primary motor neurons and CoPA sensory interneurons[43]. Here we show that only ventral CSF-cNs form the characteristic basket-like contact onto CaP soma while we only found dorsal CSF-cNs contacting ventrolateral glutamatergic neurons, most likely V0-v interneurons[47–49] previously shown to receive inputs from CSF-cNs[15]. Interestingly CoPA sensory interneurons received innervation from both dorsal and ventral CSF-cNs. Our results suggest that targets of the slow swimming circuits receive innervation from dorsal CSF-cNs while targets of the fast swimming circuit receive innervation from ventral CSF-cNs, and sensory interneurons involved in processing feedback receive innervation from both ventral and dorsal CSF-sNs. Further investigations will be necessary to establish whether other targets of the slow and fast swimming circuits follow the same dichotomy, receiving inputs from dorsal and ventral CSF-cNs respectively.

Multiple markers have been found in subsets of CSF-cNs across vertebrate species: somatostatin[12, 14, 21, 33, 34], dopamine[61–64] and serotonin[35, 36, 65]. The expression of most markers was reported in a restricted fraction of CSF-cNs. Here we tested whether some of these markers showed restricted expression patterns among CSF-cNs. We found that ventral CSF-cNs were at 48 hpf transiently serotoninergic as previously described in other species[35, 36, 65] in accordance with findings from Montgomery *et al.*[66], in zebrafish. In addition, we demonstrated that, even at 48 hpf, not all ventral CSF-cNs expressed 5-HT. This suggests that there may be different subtypes of ventral CSF-cNs based on 5-HT expression. Moreover, Montgomery *et al.*[66], also showed that the rate-limiting enzyme involved in 5-HT synthesis *tryptophan hydroxylase 1* a (*tph1a*)[67, 68] is expressed in the ventral spinal cord at 24 and 48 hpf suggesting that ventral CSF-cNs could constitute a transient source of serotonin at early stages. One possible explanation for the disappearance of 5-HT in ventral CSF-cNs at later stages could be the emergence of descending fibers from 5-HT^{+} neurons originating from the brainstem raphe nuclei from 48 hpf onwards[67]. 5-HT from descending fibers has been previously shown in mammals to suppress the monoaminergic expression of CSF-cNs[69–71]. The physiological relevance of the transient 5-HT expression among this ventral population of CSF-cNs remains to be elucidated.

Regarding the origin of somatostatin in zebrafish CSF-cNs, we found that among the six SST paralogs, *sst1.1* was the only one expressed. We demonstrated that the expression of this gene is specific and restricted to the dorsal population of CSF-cNs, identifying for the first time a specific marker of dorsal CSF-cNs. We also demonstrated that this peptide is excluded from motor neurons contrary to what previous studies suggested[52]. The physiological relevance of *sst1.1* expression by dorsal CSF-cNs is not known. In mammals and lamprey, it has been shown that somatostatin can reduce locomotor frequency[58, 72, 73]. The release of SST by dorsal CSF-cNs could impact the frequency of locomotor events along with the release of neuropeptides of the UII family, *urp1* and *urp2* by ventral CSF-cNs only[74] as previously suggested by the presence in coho salmon of a UII-like immunoreactive ventral population of CSF-cNs and a distinct somatostatinergic one[75]. Taken together, our results confirm that ventral and dorsal CSF-cNs express distinct peptides and neuromodulators. The transient nature of the expression of 5-HT suggest that it could have developmental roles to be further investigated.

Material and Methods

Animal care. Zebrafish (*Danio rerio*) adults and larvae were maintained and raised on a 14/10 hour light cycle. Fish lines used in this study are referenced in Table 1. Water was regulated at 28.5 °C, conductivity at 500 μS and pH at 7.4. All embryos and larvae under 6 dpf were anesthetized in 0.02% tricaine methane sulfonate (MS 222) (Sandoz, Levallois-Perret, France) and euthanized in 0.2% MS 222 prior to fixation. Experimental and animal protocols were approved by the Institut du Cerveau et de la Moelle Épinière in agreement with the French National Ethics Committee (Comité National de Réflexion Éthique sur l'Expérimentation Animale;

Ce5/2011/056) and European regulations.Genotype protocol for the *pkd2l1*^{icm02} mutants was described in ref. 37 (Böhm *et al*. 2016).

Generation of transgenic lines. In order to generate the *Tg*(*UAS*:*TagRFP-CAAX*;*cmlc2*:*eGFP*)*icm22* line, the TagRFP-CAAX sequence was amplified using a TagRFP-forward (5′-CCCGGGATCCACATGGTGTCTAAGGGCGAAG-3′) and reverse primer (5′-GATCGCGGCCGCTCAGGAGAGCACACACTTGCAGCTCATGCAGCCGGGGCCACTCTCATCAGGAGGGTTCAGCTTATTAAGTTTGTGCCC-3′) and inserted into the *pME-MCS* vector[76] via BamHI/NotI restriction digestion. The resulting *pME-TagRFP-CAAX* vector was recombined via a Gateway reaction (MultiSite Gateway Three-Fragment Vector Construction Kit) with *p5E-4nrUAS*[77], *p3E-pA* and *pDest-Tol2*; *cmlc2*:*eGFP*[76] resulting in (*p4nrUAS*:*TagRFP-CAAX-pA-Tol2*;*cmcl2*:*eGFP*). Using a similar approach, the *pME_LifeAct-GFP* plasmid was generated from the plasmid *pCS2_LifeAct-GFP* (kind gift from Nicolas David) using the SP6 promoter sequencing primer (5′-ATTTAGGTGACACTATAG-3′) and inserted into the pME_MCS vector via a BamHI/NotI restriction digestion. The final three-way gateway reaction used the *pME_LifeAct-GFP*, *pDest_cryaa*:*V* and *p5′E_polyA* plasmids to generate the (*UAS*:*LifeAct-GFP*;*cryaa*:*V*) construct. Microinjection of these plasmids was performed with Tol2 mRNA (25 ng/µl) following standard protocols. Transgenic founder fish *Tg*(*UAS*:*TagRFP-CAAX*;*cmlc2*:*eGFP*)*icm22* where screened based on GFP expression in the heart. These two lines were also screened based on transactivation of their respective transgene when crossed with various Gal4 lines.

Plasmid design. In order to investigate the CSF-cNs ultrastructure, we took advantage of the engineered peroxidase APEX2[78]. We generated a three-fragment Gateway recombining reaction (Invitrogen, Carlsbad, CA, USA) to design the (*UAS*:*APEX2-TagRFP*) construct. This plasmid was injected into single-cell stage *Tg*(*pkd2l1*:*Gal4*)*icm10* embryos at 60 ng/µl or co-injected with the (*pkd2l1*:*Gal4*)*icm10* construct into *Tg*(*pkd2l1*:*GaMP5G*)*icm07* singe-cell stage embryo. To generate the (*UAS*:*LifeAct-TagRFP*;*cryaa*:*C*) DNA construct, we extracted the coding sequence of the tagged protein LifeAct-TagRFP from the plasmid (*mTagRFP-T- LifeAct-7*) (Addgene #54586, kind gift from Michael Davidson) by PCR using a forward (5'-GGGGACAAGTTTGTACAAAAAAGCAGGCTAGATCTCTGCCACCATGGGCGTGGCCGACTTGATC-3') and a reverse (5'-GGGGACCACTTTGTACAAGAAAGCTGGGTACTAGTTTACTTGTACAGCTCGTCCATGCC-3') primer. LifeAct-TagRFP was then inserted into the plasmid *pDONR221* by a BP reaction to produce the *pME_LifeAct-TagRFP* plasmid and a three-way gateway reaction was performed using *pME_LifeAct-TagRFP*, *pDest_cryaa*:*C*, *p5′E_10XUAS* and *p3′E_polyA* plasmids to produce the (*UAS*:*LifeAct-TagRFP*;*cryaa*:*C*) construct.

Electron microscopy. To label CSF-cNs for electron microscopy, we followed the procedure described in refs 37, 78 and Supplemental Figs 2 and 3. 2.5 dpf larvae selected for TagRFP expression in CSF-cNs were primarily anaesthetized in 0.02% tricaine methane sulfonate (MS 222) then euthanized in 0.2% tricaine prior to fixation in 2% glutaraldehyde in 100 mM sodium cacodylate buffer pH 7.4 to which 2 mM of $CaCl_2$ was added for 45 min. Whole embryos were then rinsed in the same buffer 5 × 2 min each. Functional aldehyde excess was blocked by treating embryos for 5 min with 20 mM glycine in the sodium cacodylate buffer. Other rinses in buffer (5 × 2 min) were then carried out. The APEX2 peroxidase was further revealed in diaminobenzidine (DAB, 0.5 mg/ml) to which 10 mM hydrogen peroxide (30%) was added (see Lam *et al*.), in 100 mM cacodylate buffer. After 5 min, the reaction was stopped by rinsing embryos twice in cold buffer before post fixation in 2% osmium tetroxide (OsO_4) in the same buffer for 45 min. Embryos were then rinsed in cold distilled water, stained in 2% uranyl acetate in distilled water overnight in a cold chamber. Animals were returned to room temperature, rinsed in distilled water, then dehydrated in a graded series of ethanol, cleared in acetone, and embedded in epoxy resin (EMBed812, Electron Microscopy Science, France). Embryos were oriented coronally in resin molds cured at 60 °C for 48 hr. Whole embryos were imaged using a Leica DMRB microscope to assess the presence of DAB positive CSF-cNs and determine their location within the animals. Embryos were first cut in 1 µm semi-thin sections with an ultramicrotome (Ultracut E, Leica). Sections were picked up every µm, stained with toluidine blue. Semi-thin sectioning was performed until the first level of DAB^+ CSF-cN cell appears. Then, serial ultra-thin sections (~70 nm thick) were collected onto copper grids (about 8 sections per grid). 12 ventral CSF-cNs, and 3 dorsal CSF-cNs were analyzed. They were contrasted in urany-less solution (Delta Microscopies, France) for 1–2 min, rinsed in distilled water, dried for at least 1 hr. Observations were made with an Hitachi HT 7700 electron microscope operating at 70 kV. Electron micrographs from DAB^+ CSF-cNs were taken at low (×6200), medium (×22,000) and high (×53,000) magnifications, using an integrated AMT XR41-B camera (2048 × 2048 pixels). In all the images displayed, dorsal is up and rostral is left.

Analysis of the apical dendritic extension of CSF-cNs. To image the apical dendritic extension at a high resolution, we used different labeling strategies relying on transverse sections of the spinal cord. At 3 dpf, we used the stable *Tg*(*pkd2l1*:*Gal4*;*UAS*:*TagRFP-CAAX*;*cmlc2*:*eGFP*) transgenic line with membrane TagRFP and the transient expression of (*pkd2l1*:*Gal4*)[15] and (*UAS*:*LifeAct-TagRFP*;*cryaa*:*C*) DNA constructs injected into *Tg*(*pkd2l1*:*GCaMP5*)*icm07* eggs at the one cell stage to label F-actin with LifeAct[79]. At 6 dpf, we took advantage of the stable *Tg*(*pkd2l1*:*Gal4*;*UAS*:*LifeAct-GFP*;*cryaa*:*V*)*icm28* line. 3 and 6 dpf larvae were screened for expression in CSF-cNs and fixed using 4% paraformaldehyde (PFA) during 4 hours at 4 °C and immunostained as described below. We sliced 50 µm-thick transverse sections on larvae mounted in 3% low melting point agarose using a vibratome (HM 650 V Microtome, Thermo Scientific). For each cell, Z stacks (step size 0.25 µm) were acquired to image the entire apical extension and maximum projection was performed in Fiji[80]. The shape of the apical extension (S) was calculated as the ratio of the width (W, basal extension along the central canal) over the height (H, vertical extension within the central canal). W and H were extracted by drawing a polygon around the apical

extension using the polygon tool in Fiji and estimated by the parallel and perpendicular axis, respectively, of the best fitting ellipse (Fig. 4b).

Single cell labeling. To assess whether *pkd2l1* mutation led to a disruption of CSF-cN axonal refinement, we injected at 25 ng/µl the (*pkd2l1-TagRFP*) construct generated with a three-fragment Gateway recombineering reaction into single-cell stage embryos from *pkd2l1*$^{icm02/+}$ incrosses (see ref. 15). 3 dpf larvae selected for single CSF-cN expression were fixed with 4% PFA for 3 hours and immunostained following standard procedures. Genotyping of the larvae was performed after immunostaining. To assess the connectivity of ventral and dorsal CSF-cNs, the same procedure was followed when the (*pkd2l1-TagRFP*) construct has been injected in the *Tg*(*par g*^{mnet2}*-GFP*)[44] and *Tg*(*tbx16-GFP*)[46] *lines* and the (*pkd2l1*:*Gal4*) *with* (*UAS*:*synaptophysin-GFP*)[81] constructs in the *Tg*(*vglut2a.lox-DsRed-lox-GFP*)*line*[45]. Some of these animals have been imaged live.

Analysis of the axonal arborization of isolated CSF-cNs. To label and trace individual CSF-cNs, we followed the same procedure as described in ref. 15, in Supplemental Information and in Supplemental Fig. 4.

Fluorescent *in situ* (FISH). The *pkd2l1* ISH probe was generated as previously described[13]. The *sst1.1* plasmid originates from the Argenton lab, Padova, Italy[52, 82]. *pkd2l1* and *sst1.1* plasmids were respectively linearized with NotI and SalI. Digoxigenin (DIG)- and fluorescein (Fluo)-labeled probes were synthesized using SP6 RNA polymerase with the RNA Labeling Kit (Roche Applied Science, Basel, Switzerland) to generate both *pkd2l1* and *sst1.1* antisense probes. All probes were purified using the mini Quick Spin RNA Column (Roche, Basel, Switzerland). Whole-mount ISH were performed as previously described[13, 83] on embryos or larvae fixed in 4% PFA in phosphate buffered saline (PBS) overnight at 4 °C.

Immunohistochemistry (IHC). Procedures for IHC were described in Supplemental Information.

FISH coupled to IHC. Procedures were described in ref. 13. Briefly, *pkd2l1* and *sst1.1* FISH were performed prior to IHC of green fluorescent protein (GFP): embryos and larvae were washed and immunostained with the chicken anti-GFP antibody (1:500 dilution, Abcam ab13970, Cambridge, UK) overnight at 4 °C, and then incubated with the corresponding Alexa-conjugated secondary antibodies IgG (1:500, Invitrogen A11039, Carlsbad, CA, USA) combined with DAPI (2.5 µg/mL, Invitrogen D3571, Carlsbad, CA, USA).

Cell counting. To compare the density of markers investigated, we systematically imaged three regions along the rostrocaudal axis of the fish: segments 3–6 (referred as rostral), 10–13 (referred as middle and displayed in all Figures) and 23–26 (referred as caudal).

Imaging. Images were acquired using an Olympus FV1000 confocal microscope equipped with a 20 and 40x water and 60X oil immersion objectives using the 405, 473 and 543 nm laser lines or using an upright microscope (Examiner Z1, Zeiss) equipped with a spinning disk head (CSU-X1, Yokogawa) and a modular laser light source (LasterStack, 3i Intelligent Imaging Innovations). To determine the overlap of GFP in the *Tg*(*pkd2l1*:*GCaMP5G*)*icm07* transgenic embryos and larvae with *pkd2l1*, *sst1.1* FISH or GABA and 5-HT IHC, fish were mounted laterally in 1, 5% agarose covered of Vectashield Mounting Medium (Vectorlabs, CA, USA). To analyze apical extensions, slices were transferred into Vectashield mounting medium as well (Vectorlab, CA, USA).

Electrophysiology and optogenetic stimulation. Procedures for optogenetic stimulation of CSF-cNs and electrophysiological recordings of CaP motor neurons are described in Supplemental Information and Supplemental Fig. 7.

Statistics. We used Student's t-tests for the morphological comparison of ventral versus dorsal CSF-cNs in WT and *pkd2l1*$^{icm02/icm02}$ mutants and two-way ANOVAs to test the interaction between the genotypes and the cells investigated. The level of significance was $p < 0.05$ for all datasets. p values are represented as the following: (*)$p < 0.05$; (***)$p < 0.001$; (****)$p < 0.0001$.

References

1. Iliff, J. J. *et al.* A paravascular pathway facilitates CSF flow through the brain parenchyma and the clearance of interstitial solutes, including amyloid beta. *Sci Transl Med* **4**, 147ra111, doi:10.1126/scitranslmed.30037484/147/147ra111 (2012).
2. Pappenheimer, J. R., Miller, T. B. & Goodrich, C. A. Sleep-promoting effects of cerebrospinal fluid from sleep-deprived goats. *Proc Natl Acad Sci USA* **58**, 513–517 (1967).
3. Martin, F. H., Seoane, J. R. & Baile, C. A. Feeding in satiated sheep elicited by intraventricular injections of CSF from fasted sheep. *Life Sci* **13**, 177–184 (1973).
4. Lerner, R. A. *et al.* Cerebrodiene: a brain lipid isolated from sleep-deprived cats. *Proc Natl Acad Sci USA* **91**, 9505–9508 (1994).
5. Nishino, S. *et al.* Low cerebrospinal fluid hypocretin (Orexin) and altered energy homeostasis in human narcolepsy. *Ann Neurol* **50**, 381–388 (2001).
6. Xie, L. *et al.* Sleep drives metabolite clearance from the adult brain. *Science* **342**, 373–377, doi:10.1126/science.1241224342/6156/373 (2013).
7. Vigh, B., Vigh-Teichmann, I. & Aros, B. Special dendritic and axonal endings formed by the cerebrospinal fluid contacting neurons of the spinal cord. *Cell Tissue Res* **183**, 541–552 (1977).
8. Vigh, B. & Vigh-Teichmann, I. Actual problems of the cerebrospinal fluid-contacting neurons. *Microsc Res Tech* **41**, 57–83, doi:10.1002/(SICI)1097-0029(19980401)41:1<57::AID-JEMT6>3.0.CO;2-R (1998).
9. Kolmer, W. Das "Sagittalorgan" der Wirbeltiere. *Zeitschrift für Anatomie und Entwicklungsgeschichte* **60**, 652–717 (1921).
10. Agduhr, E. Über ein zentrales Sinnesorgan (?) bei den Vertebraten. *Zeitschrift für Anatomie und Entwicklungsgeschichte* **66**, 223–360 (1922).

11. Huang, A. L. *et al.* The cells and logic for mammalian sour taste detection. *Nature* **442**, 934–938, doi:10.1038/nature05084 (2006).
12. Wyart, C. *et al.* Optogenetic dissection of a behavioural module in the vertebrate spinal cord. *Nature* **461**, 407–410, doi:10.1038/nature08323nature08323 (2009).
13. Djenoune, L. *et al.* Investigation of spinal cerebrospinal fluid-contacting neurons expressing PKD2L1: evidence for a conserved system from fish to primates. *Front Neuroanat* **8**, 26, doi:10.3389/fnana.2014.00026 (2014).
14. Jalalvand, E., Robertson, B., Wallen, P., Hill, R. H. & Grillner, S. Laterally projecting cerebrospinal fluid-contacting cells in the lamprey spinal cord are of two distinct types. *J Comp Neurol* **522**, Spc1, doi:10.1002/cne.23584 (2014).
15. Fidelin, K. *et al.* State-Dependent Modulation of Locomotion by GABAergic Spinal Sensory Neurons. *Curr Biol* **25**, 3035–3047, doi:10.1016/j.cub.2015.09.070 (2015).
16. LaMotte, C. C. Vasoactive intestinal polypeptide cerebrospinal fluid-contacting neurons of the monkey and cat spinal central canal. *J Comp Neurol* **258**, 527–541, doi:10.1002/cne.902580405 (1987).
17. Stoeckel, M. E. *et al.* Cerebrospinal fluid-contacting neurons in the rat spinal cord, a gamma-aminobutyric acidergic system expressing the P2X2 subunit of purinergic receptors, PSA-NCAM, and GAP-43 immunoreactivities: light and electron microscopic study. *J Comp Neurol* **457**, 159–174, doi:10.1002/cne.10565 (2003).
18. Marichal, N., Garcia, G., Radmilovich, M., Trujillo-Cenoz, O. & Russo, R. E. Enigmatic central canal contacting cells: immature neurons in "standby mode"? *J Neurosci* **29**, 10010–10024, doi:10.1523/JNEUROSCI.6183-08.200929/32/10010 (2009).
19. Christenson, J., Bongianni, F., Grillner, S. & Hokfelt, T. Putative GABAergic input to axons of spinal interneurons and primary sensory neurons in the lamprey spinal cord as shown by intracellular Lucifer yellow and GABA immunohistochemistry. *Brain Res* **538**, 313–318 (1991).
20. Megias, M., Alvarez-Otero, R. & Pombal, M. A. Calbindin and calretinin immunoreactivities identify different types of neurons in the adult lamprey spinal cord. *J Comp Neurol* **455**, 72–85, doi:10.1002/cne.10473 (2003).
21. Christenson, J., Alford, S., Grillner, S. & Hokfelt, T. Co-localized GABA and somatostatin use different ionic mechanisms to hyperpolarize target neurons in the lamprey spinal cord. *Neurosci Lett* **134**, 93-97, doi:0304-3940(91)90516-V (1991).
22. Delmas, P. Polycystins: from mechanosensation to gene regulation. *Cell* **118**, 145–148, doi:10.1016/j.cell.2004.07.007S0092867404006671 (2004).
23. Orts-Del'immagine, A. *et al.* Properties of subependymal cerebrospinal fluid contacting neurones in the dorsal vagal complex of the mouse brainstem. *J Physiol* **590**, 3719–3741, doi:10.1113/jphysiol.2012.227959jphysiol.2012.227959 (2012).
24. Orts Del'Immagine, A. *et al.* A single polycystic kidney disease 2-like 1 channel opening acts as a spike generator in cerebrospinal fluid-contacting neurons of adult mouse brainstem. *Neuropharmacology*, doi:10.1016/j.neuropharm.2015.07.030 (2015).
25. Orts-Del'immagine, A. *et al.* Morphology, Distribution and Phenotype of Polycystin Kidney Disease 2-like 1-Positive Cerebrospinal Fluid Contacting Neurons in The Brainstem of Adult Mice. *PLoS One* **9**, e87748, doi:10.1371/journal.pone.0087748PONE-D-13-31038 (2014).
26. Petracca, Y. L. *et al.* The late and dual origin of cerebrospinal fluid-contacting neurons in the mouse spinal cord. *Development* **143**, 880–891, doi:10.1242/dev.129254 (2016).
27. Ishimaru, Y. *et al.* Transient receptor potential family members PKD1L3 and PKD2L1 form a candidate sour taste receptor. *Proc Natl Acad Sci USA* **103**, 12569–12574, doi:10.1073/pnas.0602702103 (2006).
28. Shimizu, T., Janssens, A., Voets, T. & Nilius, B. Regulation of the murine TRPP3 channel by voltage, pH, and changes in cell volume. *Pflugers Arch* **457**, 795–807, doi:10.1007/s00424-008-0558-6 (2009).
29. Park, H. C., Shin, J. & Appel, B. Spatial and temporal regulation of ventral spinal cord precursor specification by Hedgehog signaling. *Development* **131**, 5959–5969, doi:10.1242/dev.01456 (2004).
30. Yang, L., Rastegar, S. & Strahle, U. Regulatory interactions specifying Kolmer-Agduhr interneurons. *Development* **137**, 2713–2722, doi:10.1242/dev.048470dev.048470 (2010).
31. England, S., Batista, M. F., Mich, J. K., Chen, J. K. & Lewis, K. E. Roles of Hedgehog pathway components and retinoic acid signalling in specifying zebrafish ventral spinal cord neurons. *Development* **138**, 5121–5134, doi:10.1242/dev.066159138/23/5121 (2011).
32. Huang, P., Xiong, F., Megason, S. G. & Schier, A. F. Attenuation of Notch and Hedgehog signaling is required for fate specification in the spinal cord. *PLoS Genet* **8**, e1002762, doi:10.1371/journal.pgen.1002762PGENETICS-D-11-02695 (2012).
33. Buchanan, J. T., Brodin, L., Hokfelt, T., Van Dongen, P. A. & Grillner, S. Survey of neuropeptide-like immunoreactivity in the lamprey spinal cord. *Brain Res* **408**, 299–302, doi:0006-8993(87)90392-1 (1987).
34. Lopez, J. M. *et al.* Distribution of somatostatin-like immunoreactivity in the brain of the caecilian Dermophis mexicanus (Amphibia: Gymnophiona): comparative aspects in amphibians. *J Comp Neurol* **501**, 413–430, doi:10.1002/cne.21244 (2007).
35. Sims, T. J. The development of monamine-containing neurons in the brain and spinal cord of the salamander, Ambystoma mexicanum. *J Comp Neurol* **173**, 319–336, doi:10.1002/cne.901730208 (1977).
36. Chiba, A. & Oka, S. Serotonin-immunoreactive structures in the central nervous system of the garfish Lepisosteus productus (Semionotiformes, Osteichthyes). *Neurosci Lett* **261**, 73–76, doi:S0304-3940(98)01011-8 (1999).
37. Böhm, U. L. *et al.* CSF-contacting neurons regulate locomotion by relaying mechanical stimuli to spinal circuits. *Nat Commun* **7**, 10866, doi:10.1038/ncomms10866 (2016).
38. Flock, A. & Duvall, A. J. 3rd The Ultrastructure of the Kinocilium of the Sensory Cells in the Inner Ear and Lateral Line Organs. *J Cell Biol* **25**, 1–8 (1965).
39. Kindt, K. S., Finch, G. & Nicolson, T. Kinocilia mediate mechanosensitivity in developing zebrafish hair cells. *Dev Cell* **23**, 329–341, doi:10.1016/j.devcel.2012.05.022S1534-5807(12)00249-3 (2012).
40. DeFelipe, J. Types of neurons, synaptic connections and chemical characteristics of cells immunoreactive for calbindin-D28K, parvalbumin and calretinin in the neocortex. *J Chem Neuroanat* **14**, 1–19, doi:S0891061897100138 (1997).
41. Fiala, J. C., Feinberg, M., Popov, V. & Harris, K. M. Synaptogenesis via dendritic filopodia in developing hippocampal area CA1. *J Neurosci* **18**, 8900–8911 (1998).
42. Megias, M., Emri, Z., Freund, T. F. & Gulyas, A. I. Total number and distribution of inhibitory and excitatory synapses on hippocampal CA1 pyramidal cells. *Neuroscience* **102**, 527–540, doi:S0306-4522(00)00496-6 (2001).
43. Hubbard, J. M. *et al.* Intraspinal Sensory Neurons Provide Powerful Inhibition to Motor Circuits Ensuring Postural Control during Locomotion. *Curr Biol* **26**, 2841–2853, doi:10.1016/j.cub.2016.08.026 (2016).
44. Balciunas, D. *et al.* Enhancer trapping in zebrafish using the Sleeping Beauty transposon. *BMC Genomics* **5**, 62, doi:10.1186/1471-2164-5-62 (2004).
45. Koyama, M., Kinkhabwala, A., Satou, C., Higashijima, S. & Fetcho, J. Mapping a sensory-motor network onto a structural and functional ground plan in the hindbrain. *Proc Natl Acad Sci USA* **108**, 1170–1175, doi:10.1073/pnas.1012189108 (2011).
46. Wells, S., Nornes, S. & Lardelli, M. Transgenic zebrafish recapitulating tbx16 gene early developmental expression. *PLoS One* **6**, e21559, doi:10.1371/journal.pone.0021559 (2011).
47. Hale, M. E., Ritter, D. A. & Fetcho, J. R. A confocal study of spinal interneurons in living larval zebrafish. *J Comp Neurol* **437**, 1–16 (2001).
48. McLean, D. L., Fan, J., Higashijima, S., Hale, M. E. & Fetcho, J. R. A topographic map of recruitment in spinal cord. *Nature* **446**, 71–75, doi:10.1038/nature05588 (2007).
49. Satou, C., Kimura, Y. & Higashijima, S. Generation of multiple classes of V0 neurons in zebrafish spinal cord: progenitor heterogeneity and temporal control of neuronal diversity. *J Neurosci* **32**, 1771–1783, doi:10.1523/JNEUROSCI.5500-11.2012 (2012).

50. Tostivint, H., Lihrmann, I. & Vaudry, H. New insight into the molecular evolution of the somatostatin family. *Mol Cell Endocrinol* **286**, 5–17, doi:10.1016/j.mce.2008.02.029S0303-7207(08)00115-9 (2008).
51. Tostivint, H., Quan, F. B., Bougerol, M., Kenigfest, N. B. & Lihrmann, I. Impact of gene/genome duplications on the evolution of the urotensin II and somatostatin families. *Gen Comp Endocrinol* **188**, 110–117, doi:10.1016/j.ygcen.2012.12.015S0016-6480(13)00005-1 (2013).
52. Devos, N. *et al.* Differential expression of two somatostatin genes during zebrafish embryonic development. *Mech Dev* **115**, 133–137, doi:S0925477302000825 (2002).
53. Flanagan-Steet, H., Fox, M. A., Meyer, D. & Sanes, J. R. Neuromuscular synapses can form *in vivo* by incorporation of initially aneural postsynaptic specializations. *Development* **132**, 4471–4481, doi:10.1242/dev.02044 (2005).
54. Sternberg, J. R. *et al.* Optimization of a Neurotoxin to Investigate the Contribution of Excitatory Interneurons to Speed Modulation *In Vivo*. *Curr Biol* **26**, 2319–2328, doi:10.1016/j.cub.2016.06.037 (2016).
55. Vigh, B. & Vigh-Teichmann, I. Structure of the medullo-spinal liquor-contacting neuronal system. *Acta Biol Acad Sci Hung* **22**, 227–243 (1971).
56. Bushman, J. D., Ye, W. & Liman, E. R. A proton current associated with sour taste: distribution and functional properties. *FASEB J* **29**, 3014–3026, doi:10.1096/fj.14-265694fj.14-265694 (2015).
57. Jalalvand, E., Robertson, B., Tostivint, H., Wallen, P. & Grillner, S. The Spinal Cord Has an Intrinsic System for the Control of pH. *Curr Biol* **26**, 1346–1351, doi:10.1016/j.cub.2016.03.048 (2016).
58. Jalalvand, E., Robertson, B., Wallen, P. & Grillner, S. Ciliated neurons lining the central canal sense both fluid movement and pH through ASIC3. *Nat Commun* **7**, 10002, doi:10.1038/ncomms10002 (2016).
59. Barber, R. P., Vaughn, J. E. & Roberts, E. The cytoarchitecture of GABAergic neurons in rat spinal cord. *Brain Res* **238**, 305–328, doi:0006-8993(82)90107-X (1982).
60. Shimosegawa, T. *et al.* An immunohistochemical study of methionine-enkephalin-Arg6-Gly7-Leu8-like immunoreactivity-containing liquor-contacting neurons (LCNs) in the rat spinal cord. *Brain Res* **379**, 1–9, doi:0006-8993(86)90249-0 (1986).
61. Barreiro-Iglesias, A., Villar-Cervino, V., Anadon, R. & Rodicio, M. C. Descending brain-spinal cord projections in a primitive vertebrate, the lamprey: cerebrospinal fluid-contacting and dopaminergic neurons. *J Comp Neurol* **511**, 711–723, doi:10.1002/cne.21863 (2008).
62. Rodicio, M. C., Villar-Cervino, V., Barreiro-Iglesias, A. & Anadon, R. Colocalization of dopamine and GABA in spinal cord neurones in the sea lamprey. *Brain Res Bull* **76**, 45–49, doi:10.1016/j.brainresbull.2007.10.062S0361-9230(07)00399-1 (2008).
63. Roberts, B. L., Maslam, S., Scholten, G. & Smit, W. Dopaminergic and GABAergic cerebrospinal fluid-contacting neurons along the central canal of the spinal cord of the eel and trout. *J Comp Neurol* **354**, 423–437, doi:10.1002/cne.903540310 (1995).
64. Acerbo, M. J., Hellmann, B. & Gunturkun, O. Catecholaminergic and dopamine-containing neurons in the spinal cord of pigeons: an immunohistochemical study. *J Chem Neuroanat* **25**, 19–27, doi:S0891061802000728 (2003).
65. Parent, A. & Northcutt, R. G. The monoamine-containing neurons in the brain of the garfish, Lepisosteus osseus. *Brain Res Bull* **9**, 189–204 (1982).
66. Montgomery, J. E., Wiggin, T. D., Rivera-Perez, L. M., Lillesaar, C. & Masino, M. A. Intraspinal serotonergic neurons consist of two, temporally distinct populations in developing zebrafish. *Dev Neurobiol* **76**, 673–687, doi:10.1002/dneu.22352 (2016).
67. Bellipanni, G., Rink, E. & Bally-Cuif, L. Cloning of two tryptophan hydroxylase genes expressed in the diencephalon of the developing zebrafish brain. *Mech Dev* **119** Suppl 1, S215–220, doi:S0925477303001199 (2002).
68. Teraoka, H. *et al.* Hedgehog and Fgf signaling pathways regulate the development of tphR-expressing serotonergic raphe neurons in zebrafish embryos. *J Neurobiol* **60**, 275–288, doi:10.1002/neu.20023 (2004).
69. Branchereau, P., Chapron, J. & Meyrand, P. Descending 5-hydroxytryptamine raphe inputs repress the expression of serotonergic neurons and slow the maturation of inhibitory systems in mouse embryonic spinal cord. *J Neurosci* **22**, 2598–2606, doi:20026199 (2002).
70. Allain, A. E., Segu, L., Meyrand, P. & Branchereau, P. Serotonin controls the maturation of the GABA phenotype in the ventral spinal cord via 5-HT1b receptors. *Ann N Y Acad Sci* **1198**, 208–219, doi:10.1111/j.1749-6632.2010.05433.x (2010).
71. Wienecke, J. *et al.* Spinal cord injury enables aromatic L-amino acid decarboxylase cells to synthesize monoamines. *J Neurosci* **34**, 11984–12000, doi:10.1523/JNEUROSCI.3838-13.2014 (2014).
72. Barriere, G., Bertrand, S. & Cazalets, J. R. Peptidergic neuromodulation of the lumbar locomotor network in the neonatal rat spinal cord. *Peptides* **26**, 277–286, doi:10.1016/j.peptides.2004.09.002 (2005).
73. Miles, G. B. & Sillar, K. T. Neuromodulation of vertebrate locomotor control networks. *Physiology (Bethesda)* **26**, 393–411, doi:10.1152/physiol.00013.201126/6/393 (2011).
74. Quan, F. B. *et al.* Comparative distribution and *in vitro* activities of the urotensin II-related peptides URP1 and URP2 in zebrafish: evidence for their colocalization in spinal cerebrospinal fluid-contacting neurons. *PLoS One* **10**, e0119290, doi:10.1371/journal.pone.0119290PONE-D-14-36037 (2015).
75. Yulis, C. R. & Lederis, K. Relationship between urotensin II- and somatostatin-immunoreactive spinal cord neurons of Catostomus commersoni and Oncorhynchus kisutch (Teleostei). *Cell Tissue Res* **254**, 539–542 (1988).
76. Kwan, K. M. *et al.* The Tol2kit: a multisite gateway-based construction kit for Tol2 transposon transgenesis constructs. *Dev Dyn* **236**, 3088–3099, doi:10.1002/dvdy.21343 (2007).
77. Auer, T. O. *et al.* Deletion of a kinesin I motor unmasks a mechanism of homeostatic branching control by neurotrophin-3. *Elife* **4**, 10.7554/eLife.05061 (2015).
78. Lam, S. S. *et al.* Directed evolution of APEX2 for electron microscopy and proximity labeling. *Nat Methods* **12**, 51–54, doi:10.1038/nmeth.3179nmeth.3179 (2015).
79. Riedl, J. *et al.* Lifeact: a versatile marker to visualize F-actin. *Nat Methods* **5**, 605–607, doi:10.1038/nmeth.1220 (2008).
80. Schindelin, J. *et al.* Fiji: an open-source platform for biological-image analysis. *Nat Methods* **9**, 676–682, doi:10.1038/nmeth.2019nmeth.2019 (2012).
81. Meyer, M. P. & Smith, S. J. Evidence from *in vivo* imaging that synaptogenesis guides the growth and branching of axonal arbors by two distinct mechanisms. *J Neurosci* **26**, 3604–3614, doi:10.1523/JNEUROSCI.0223-06.2006 (2006).
82. Argenton, F., Zecchin, E. & Bortolussi, M. Early appearance of pancreatic hormone-expressing cells in the zebrafish embryo. *Mech Dev* **87**, 217–221, doi:S0925-4773(99)00151-3 (1999).
83. Parmentier, C. *et al.* Occurrence of two distinct urotensin II-related peptides in zebrafish provides new insight into the evolutionary history of the urotensin II gene family. *Endocrinology* **152**, 2330–2341, doi:10.1210/en.2010-1500en.2010-1500 (2011).

Acknowledgements

We thank Natalia Maties and Bogdan Buzurin from Animalliance for expert fish care. We thank Prof. Hervé Tostivint for precious feedback regarding the somatostatin experiments. We thank Déborah Delpeuch for help with genotyping and Sophie Nunes Figueiredo for technical assistance. We thank Peter Steenbergen, Dr Soojin Ryu, Freiburg University, Germany and Dr Heiko Loehr, University of Cologne, Germany for providing the *sst1.1* plasmid. We thank Vincent Guillemot from the ICM Biostatistics/Bioinformatics core facility for advices on statistics and the imaging facility PICPS from ICM. This work received support from the ERC starting grant

'Optoloco' #311673, the ATIP/Avenir program supported by the Fondation Bettencourt-Schueller, the Emergence program grant of the city of Paris and the HFSP research grant #RGP0063/2014. ICM facilities received support of the 'Investissements d'avenir' ANR-10-IAIHU-06.

Author Contributions

Lydia D. performed *in situ* hybridization, injected DNA constructs, performed IHCs, reconstructed cell morphology to complete the analysis of axonal projections with the help of J.G. and A.P., and the mapping of CSF-cN targets. Laura D. performed IHCs to complete the morphological analysis on CSF-cN apical extension. J.G. and J.R.S. performed the 5-HT and GABA IHC respectively. J.P.R. performed the EM analysis of CSF-cNs with the technical assistance of D.L., J.G. and Lydia D. F.B.Q. and H.M. performed additional *in situ* hybridization at later larval stages and in the adult zebrafish. Lydia D., J.G. and J.R.S. counted cells. J.R.S. performed the optogenetic stimulation of CSF-cNs and the electrophysiological recordings of CaPs. TOA generated the transgenic *icm22* line. C.W., P.L.B. and F.D.B. supervised research. Lydia D. and C.W. wrote the manuscript with feedback from all authors.

Additional Information

Supplementary information accompanies this paper at doi:10.1038/s41598-017-00350-1

Competing Interests: The authors declare that they have no competing interests.

Publisher's note: Springer Nature remains neutral with regard to jurisdictional claims in published maps and institutional affiliations.